# Cellular regulation of the dopamine transporter

Eriksen, Jacob

*Publication date:*
2010

*Document version*
Publisher's PDF, also known as Version of record

FACULTY OF HEALTH SCIENCES
UNIVERSITY OF COPENHAGEN

## PhD thesis

Jacob Eriksen

# Cellular Regulation of the Dopamine Transporter

Academic advisor: Ulrik Gether

Submitted: 09/12/09

# Preface

The present thesis is a presentation of the experimental work I have carried out during the last 3 years in the Molecular Neuropharmacology Group at the Department of Neuroscience and Pharmacology, University of Copenhagen.

All the experimental work presented in this thesis is related to aspects of cellular regulation of the dopamine transporter.

The thesis consists of a general introduction to the dopamine system and the dopamine transporter, which serves as a background for the experimental data presented. This is followed by a short presentation and a general discussion of the results presented in the thesis.

The full representation of the results is available in the following four papers (two published papers and two manuscripts) attached in the back of the thesis:

**Paper 1**: *Eriksen J, Rasmussen SGF, Rasmussen TN, Vægter CB, Cha JH, Zou MF, Newman AH, Gether U (2009) Visualization of Dopamine Transporter Trafficking in Live Neurons by Use of Fluorescent Cocaine Analogs. Journal of Neuroscience 29:6794-6808.*

**Paper 2**: *Eriksen J, Yoshimoto WEB, Jørgensen TN, Gether U (2009) Constitutively Internalized Dopamine Transporter is Primarily Sorted to a Late Endosomal/Lysosomal Pathway in both Dopaminergic Neurons and Cell Lines. Manuscript, ready for submission.*

**Paper 3**: *Madsen KL, Eriksen J, Milan-Lobo L, Han DS, Niv MY, Ammendrup-Johnsen I, Henriksen U, Bhatia VK, Stamou D, Sitte HH, McMahon HT, Weinstein H, Gether U (2008) Membrane localization is critical for activation of the PICK1 BAR domain. Traffic 9:1327-1343.*

**Paper 4**: *Eriksen J, Klewe IV, Egebjerg J, Christensen KV, Gether U (2009) The dopamine transporter impairs dopamine D2 receptor surface expression/ signalling and reveals promiscuous monoamine transporter/receptor interaction. Manuscript.*

Other related work carried out during my time as a PhD student is part of the following manuscripts, not included in the PhD thesis:

*Adkins EM, Samuvel DJ, Fog JU, Eriksen J, Jayanthi LD, Vaegter CB, Ramamoorthy S, Gether U (2007) Membrane Mobility and Microdomain Association of the Dopamine Transporter Studied with Fluorescence Correlation Spectroscopy and Fluorescence Recovery after Photobleaching. Biochemistry 46:10484-10497.*

*Eriksen J, Jørgensen TN, Gether U (2009) Regulation of dopamine transporter function by protein-protein interactions: challenges and new discoveries. Review. Manuscript submitted to Journal of Neurochemistry.*

I would like to thank my supervisor Ulrik Gether for always showing great interest in my projects/ideas and also providing ideas and advise.
Furthermore, I would like to thank all the people in the Molecular Neuropharmacology Group for their help and making it a pleasant environment.
A special thanks to Donna Czerny, Nabeela Khadim and Anette Dencker Kristensen for the invaluable technical assistance, and Trine Nygaard Jørgensen, Kenneth Lindegaard Madsen and Ib Vestergaard Klewe for the frutiful discussions and cooperations.
Finally, I would like to thank Anja for support and patience all the way, all the time.

December 2009

Jacob Eriksen

Cover illustration: Cultured rat dopaminergic neurons labeled with the fluorescent cocaine analog JHC 1-64 (chemical structure overlaid), which specifically binds the dopamine transporter.

## Summary

The dopamine transporter (DAT) mediates reuptake of dopamine from the synaptic cleft and is a target for widely abused psychostimulants such as cocaine and amphetamine. Nonetheless, little is known about the cellular distribution and trafficking of natively expressed DAT. DAT and its trafficking was visualized in cultured live midbrain dopaminergic (DA) neurons using novel fluorescently tagged cocaine analogs. The ligands enabled specific labelling and visualization of DAT in live neurons. In the DA neurons, DAT was uniformly distributed in the plasma membrane of the soma, the neuronal extensions, and varicosities along these extensions. Moreover, DAT was constitutively internalized into vesicular structures and the internalization was blocked by lentiviral-mediated expression of dominant-negative dynamin. DAT internalization and function was not affected by activation of protein kinase C (PKC) with phorbol-12-myristate-13-acetate (PMA) or by inhibition with staurosporine or GF109203X. These data are in contrast to findings for DAT in transfected heterologous cells and challenge the paradigm that trafficking and cellular distribution of endogenous DAT is subject to regulation by PKC.
To further characterize the intracellular pool of constitutively endocytosed DAT several strategies were employed in both cell lines and cultured DA neurons. First, to investigate the constitutive trafficking of heterologously expressed DAT we fused the N-terminus of DAT to the intracellular tail of the single-membrane spanning protein Tac, thereby creating an extracellular antibody epitope. Upon expression in HEK293 cells this TacDAT fusion protein displayed functional properties similar to the wild type transporter. In an ELISA based internalization assay, TacDAT intracellular accumulation was increased by inhibitors of lysosomal degradation and moreover TacDAT colocalized with the late endosomal marker Rab7. In the DA cell line 1Rb3An27 TacDAT also co-localized with EGFP-Rab7 and not with the recycling endosomal marker EGFP-Rab11. To assess whether sorting to late endosomes/lysosomes was a property also inherent to natively expressed transporter, DAT was visualized directly in cultured DA neurons using the fluorescent cocaine analog JHC 1-64. These data showed pronounced colocalization upon constitutive internalization with Lysotracker, a late endosomal/lysosomal marker; however only little co-lolization was observed with Alexa488-conjugated transferrin. Additionally, when expressing EGFP-Rab7 with lentivirus in cultured DA neurons a marked co-localization between JHC 1-64 and EGFP-Rab7 was observed. The data suggest that constitutively internalized DAT primarily is targeted to late endosomes and lysosomes both in heterologous cells and in cultured DA neurons.

DAT has been shown to be regulated by the dopamine D2 receptor (D2R), the primary target for anti-psychotics, through a direct interaction. D2R is among other places expressed as an autoreceptor in DA neurons. Transient over-expression of DAT with D2R in HEK293 cells reduced surface expression of D2R while DAT surface levels remained unaffected. Furthermore ß-Arrestin2 recruitment to D2R was compromised and D2R-mediated inhibition of cAMP accumulation was reduced as a consequence of the reduced surface level expression of D2R. The effects of DAT on D2R surface expression and signalling was not unique for DAT and D2R. Thus, transient co-expression of $ß_2$AR with DAT resulted in reduced surface levels of $ß_2$AR. In addition, co-expression of the serotonin transporter with D2R appeared to modulate the ß-Arrestin2 recruitment to D2R and the D2R-mediated inhibition of cAMP accumulation in a manner similar to co-expression of DAT. The data suggest that DAT affect D2R function and expression with no apparent specificity.

# Resumé (Danish)

Dopamintransporteren er ansvarlig for genoptag af dopamin fra den synaptiske kløft og er det primære mål for virkningen af udbredte psykostimulantia så som kokain og amfetamin. Selvom DAT spiller en central rolle for virkningen af psykostimulantia, så er viden om fordeling og 'trafficking' af DAT i endogene systemer begrænset. I nærværende studie har vi brugt fluorescensmærkede kokainanaloger med høj affinitet for DAT. Disse kokainanaloger muliggør visualisering af DAT i levende primærkulturer af dopaminerge kulturer.
I de dopaminerge nerveceller var DAT ensartet fordelt i plasma membranen både i soma og i nervecellens udløbere. FRAP (fluoresecens recovery after photobleaching) eksperimenter viste bidirektionel bevægelse af DAT, og desuden var der evidens for meget mobil DAT i både udløbere og varikositeter.
DAT udviste konstitutiv endocytose og blev ophobet i vesikulære strukturer, der muligvis repræsenterer en intracellulær pulje af DAT. Den konstitutive endocytose kunne blokeres af lentiviral medieret ekspression af dominant negativ dynamin 1, og konstitutiv internaliseret DAT co-lokaliserede til dels med både EGFP-Rab5 og transferrin receptoren. Overraskende var DAT internalisering ikke påvirket af protein kinase C (PKC) aktivitet i vores primærkulturer af dopaminerge nerveceller. Hverken stimulering af PKC med PMA eller ved at hæmme PKC med GF109203X påvirkede internaliseringen eller dopaminoptag. Disse resultater er forskellige fra observationer i cellelinier, som exogent udtrykker DAT og sætter spørgsmålstegn ved paradigmet om PKC-medieret regulering af DAT i dopaminerge nerveceller.
For yderligere at karakterisere den konstitutive internalisering, som vi observerede i de dopaminerge neuroner anvendte vi flere forskellige strategier til at detektere DAT i både cellelinier og dopaminerge nerveceller. For at undersøge internalisering af eksogent udtrykt DAT brugte vi et konstrukt med DAT N-terminalen fusioneret med den intracellulære del af enkelt transmembran domæne proteinet Tac for herved at skabe en ekstracellulær antistof-epitop. Når dette Tac-DAT fusionsprotein blev udtrykt i HEK293 celler udviste det funktionelle egenskaber svarende til vildtype transporteren og blev internaliseret i lighed med denne. I et ELISA eksperiment kunne vi kvantificere en konstitutiv tidsafhænigig DAT internaliserng i HEK293 og den medfølgende intracellulære akkumulering blev øget af leupeptin, en hæmmer af lysosomal degradering. Dette indikerer at Tac-DAT delvist blev sorteret til lysosomal degradering. For at videre undersøge denne hypotese udtrykte vi TacDAT i den dopaminerge cellelinie 1Rb3An27, og her undersøgte vi sorteringen af TacDAT v.h.a. co-udtryk af endosomale markører koblet til EGFP. Kvantificering viste at internaliseret TacDAT kolokaliserede med Rab7, som lokaliserer til sen endosomale vesikler, et forstadie til lysosomer. TacDAT kolokaliserede signifikant mere med Rab7 end Rab11, som lokaliserer til en anden type 'recycling' endosomer.
For at undersøge om dette også var gældende for konstitutivt internaliseret DAT enodgent, udtrykte vi EGFP-Rab markørerne v.h.a. lentivirus i primærkulturer med dopaminerge nerveceller. Ved hjælp af kokain-analogen, JHC 1-64 observerede vi at konstitutivt internaliseret DAT colokaliserede med Rab7 og ikke Rab11. Desuden var der en udpræget colokalisering mellem DAT og den lysosomale markør LysoTracker. Vi foreslår derfor at konstitutivt internaliseret DAT sorteres til degradering via rab7 positive vesikler til lysosomer både i cellelinier og primærkulturer med dopaminerge nerveceller, som udtrykker DAT endogent.
Samlet giver resultaterne et billede af en dynamisk opretholdelse DAT homøostase i dopaminerge nerveceller.

# Abbreviations

| | |
|---|---|
| a.a. | amino acid |
| ADHD | Attention-deficit hyperactivity disorder |
| BRET | Bioluminescence resonance energy transfer |
| CamKII | $Ca2^{+}$/calmodulin-dependent protein kinase II |
| CFP | Cyan fluorescent protein |
| CNS | Central nervous system |
| D2R | Dopamine D2 receptor |
| DA | Dopaminergic |
| DAT | Dopamine Transporter |
| EGFP | Enhanced green fluorescent protein |
| ELISA | Enzyme-linked immunosorbent assay |
| ER | Endoplasmatic reticulum |
| ERK | Extracellular signal-regulated kinase |
| ESCRT | Endosomal sorting complex required for transport |
| FRAP | Fluorescence recovery after photobleaching |
| FRET | Fluorescence resonance energy transfer |
| GABA | γ-aminobutyric acid |
| GAT1 | γ-aminobutyric acid transporter 1 |
| GPCR | G protein-coupled receptor |
| GluR2 | Glutamate receptor subunit 2 |
| HEK | Human embryonic kidney |
| KO | Knock out |
| LeuT | Leucine transporter |
| MAPK | Mitogen-activated protein kinase |
| NET | Norepinephrine transporter |
| NSS | Neurotransmitter:sodium symporter |
| PAE | Porcine aortic endothelial |
| PC-12 | Rat adrenal pheochromocytoma |
| PET | Positron emission tomography |
| PI3K | Phosphatidylinositol 3-kinase |
| PICK1 | Protein interacting with C-kinase 1 |
| PKC | Protein kinase C |
| PMA | Phorbol 12-myristate 13-acetate |
| SERT | Serotonin transporter |
| siRNA | small interfering RNA |
| SLC6 | Solute Carrier 6 |
| SN | Substantia nigra |
| Tac | T-cell activation |
| TM | Transmembrane domain |
| VMAT2 | Vesicular monoamine transporter 2 |
| VTA | Ventral tegmental area |
| YFP | Yellow fluorescent protein |

# Table of Contents

# INTRODUCTION

It is now more than 50 years ago that Carlsson and coworkers, with the findings that the akinetic effects of reserpine in rabbits could be reversed by the dopamine precursor L-dopa, discovered the role of dopamine as a neurotransmitter (Carlsson et al., 1957; Montagu, 1957; Carlsson et al., 1958), Since the seminal discoveries in 1957-58, a wealth of information has been obtained regarding the critical role of dopamine in regulating numerous different brain functions including control of locomotor activity, reward mechanisms, cognition and neuroendocrine systems. Moreover, it has been established how dysfunction of the dopamine system may be of central importance in a broad spectrum of neuropsychiatric disorders, such as Parkinson's disease, schizophrenia, Tourette's syndrome, attention-deficit hyperactivity disorder (ADHD) and drug addiction (Nestler, 2005; Albin and Mink, 2006; Iversen and Iversen, 2007). Consequently, major research resources have been dedicated to understanding the processes underlying these disorders together with the attempted development of drugs relieving patients from their devastating symptoms.

## Dopaminergic neurotransmission

Dopamine is synthesized in dopaminergic (DA) neurons from the amino acid tyrosine. Via the vesicular monoamine transporter 2 (VMAT2) dopamine is filled into synaptic vesicles from where it is released both from dendritic and axonal release sites upon neuronal excitatory activity (figure 1). DA neurons exhibit characteristic tonic and phasic firing patterns, where the tonic firing is dependent on an intrinsic pacemaker potential and the phasic firing is dependent on afferent input (Grace et al., 2007). Dopamine signals only through G-protein coupled receeptors (GPCRs), a

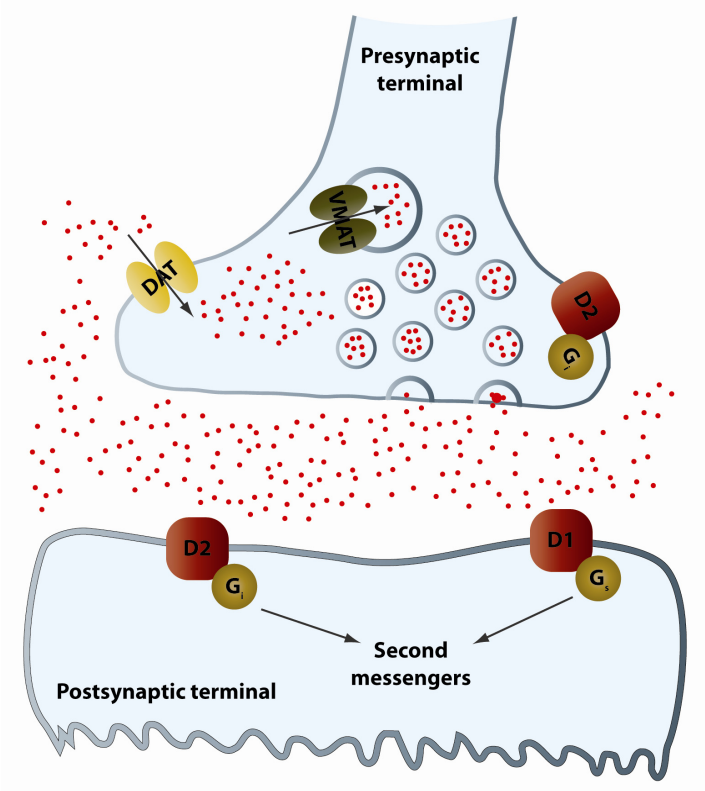


**Figure 1**: *Schematic representation of a dopaminergic synapse.*
*Cytosolic dopamine is filled into synaptic vesicles by the vesicular monoamine transporter 2 (VMAT). Dopamine is released into the synaptic cleft from presynaptic vesicles upon neuronal excitatory activity. Released dopamine reaches concentrations in the hundreds of micromolar range (Garris and Wightman, 1994) and binds pre- and postsynaptic dopamine receptors. The synaptic dopamine signal via D1-like and D2-like dopamine receptors result in a broad cascade of cellular responses mediated by second messengers. Termination of the signal is primarily accommodated by removal of the neurotransmitter by reuptake into the presynapse of the dopaminergic neuron facilitated by DAT.*

process often referred to as slow synaptic transmission (Greengard, 2001). Based on biochemical and pharmaceutical properties two main classes of dopamine receptors can be distinguished: D1-like (D1, D5) and D2-like (D2, D3, and D4) dopamine receptors (figure 1). Dopamine receptors are expressed in a variety of target neurons and signal to a wide range of membrane bound and intracellular effectors such as ion channels, secondary messenger systems and enzymes (Werkman et al., 2006).

The inactivation of neurotransmitters by reuptake into neurons was first discovered by Julius Axelrod and coworkers in the early 1960's, as they demonstrated that radiolabelled norepinephrine was accumulated in sympathetic nerve endings (Hertting et al., 1961; Wolfe et al., 1962) and subsequently released upon stimulation (Hertting and Axelrod, 1961) with the molecular properties being virtually unknown. However, with the cloning of neurotransmitter transporter such as the dopamine transporter (DAT) from various species in the beginning of the nineties (Kilty et al., 1991; Shimada et al., 1991; Usdin et al., 1991) the molecular identity of the proteins responsible for

the neurotransmitter reuptake was revealed. Later, the generation of the DAT knock out (KO) mouse showed that DAT was indeed essential for dopamine homeostasis and signalling in the brain (Giros et al., 1996). The disrupted clearance of released dopamine in the DAT KO mice resulted in about a 300-fold increase in the lifetime of dopamine in the extracellular space and a fivefold elevation in the basal extracellular dopamine levels (Gainetdinov et al., 1998; Jones et al., 1998). Even more strikingly, a profound depletion of intraneuronal dopamine stores (20-fold) and decreased amplitude of evoked dopamine release (4-fold) was found in DAT KO mice (Gainetdinov et al., 1998; Jones et al., 1998). These observations strongly suggest that in normal physiological situation, DAT is the principal inactivator of synaptic dopamine, and the major dopamine storage pools must be controlled by the DAT-mediated dopamine recycling (Jones et al., 1998; Gainetdinov and Caron, 2003).

## Dopaminergic projections

Despite its critical physiological and pathophysiological role, dopamine is only synthesized and released from a relatively discrete number of neuronal groups adding up to 40-45,000 neurons in rats and 400,000 to 600,000 neurons in humans. These are primarily located in the ventral tegmental area (VTA) and the substantia nigra (SN; > 70% of the DA neurons) of the midbrain (Bjorklund and Dunnett 2007). Although few in number the midbrain DA neuron afferents exhibit a high degree of arborisation with up to 300,000 branch points per axon (figure 2A). Therefore each neuron covers a large area and can broadcast a dopamine signal and exert strong influence over a large number of neurons in their target regions; including the forebrain and basal ganglia (Bjorklund and Dunnett, 2007; Matsuda et al., 2009).

The DA projections from the midbrain are classically divided in nigrostriatal, mesolimbic and mesocortical systems (figure 2B) (Lindvall et al., 1983; Bjorklund and Dunnett, 2007). The

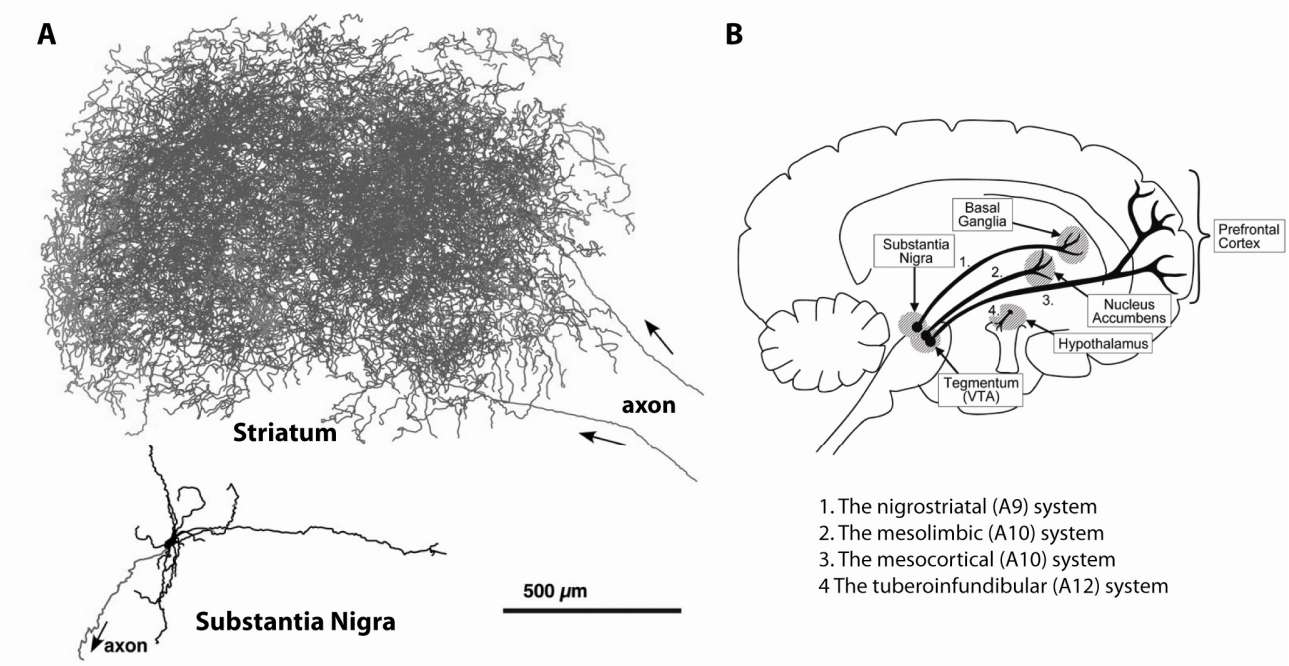


**Figure 2**: *Anatomy of a dopaminergic neuron and the major dopaminergic pathways in the human brain.*
***A)** 2D visualization of a dopaminergic neuron with its cell body and dendrites (**black**) in substantia nigra and its axonal afferents (**grey**) terminating in the striatum. Heavy axonal arborisation is evident in the striatum making one dopaminergic neurons capable of signalling to a large number of striatal neurons. Figure modified from (Matsuda et al., 2009). **B)** The major dopaminergic projections as described in the text. A9-A12 refers to the nomenclature introduced by Dahlström and Fuxe for the major dopaminergic cell groups characterized using catecholaminergic histofluorescence (Dahlstrom and Fuxe, 1964). Figure modified from (Leuner and Muller, 2006).*

nigrostriatal system projects from the substantia nigra (SN) to the dorsal striatum, and is involved in cognitive integration, habituation, sensorimotor coordination and initiation of movement. The mesolimbic system projects from the ventral tegmental area (VTA) to limbic structures such as nucleus accumbens, hippocampus, and amygdala. The mesocortical system projects from the VTA to several cortical regions. The mesolimbic and mesocortical systems are involved in regulation of motivation, attention and reward (Iversen and Iversen, 2007).

A fourth distinct dopamine pathway, the tuberoinfundibular system (figure 2B), is connected to the hormone secretory system of the pituitary gland. DA neurons project from the hypothalamus to the pituitary gland and regulate neuroendocrine function, particularly the release of prolactin (Leuner and Muller, 2006).

The role of DAT as a terminator of dopamine signaling differs markedly between these systems. DAT is expressed at high levels in the striatum and accounts for around 95% of the dopamine uptake, conversely the prefrontal cortex shows very low levels of DAT expression (Sesack et al., 1998) and the DAT accounts for only around 40% of dopamine uptake in the prefrontal cortex (Wayment et al., 2001).

## *The dopamine transporter*

### DAT structure

DAT belongs to the family of neurotransmitter:sodium symporters (NSS) (also referred to as the SLC6 [solute carrier 6] gene family) that in addition to DAT includes transporters for the neurotransmitters norepinephrine, serotonin, glycine and γ-aminobutyric acid (GABA). This class of transporters is characterized by co-transport of $Na^+$ and $Cl^-$. At the structural level, the transporters share a predicted structure with 12 transmembrane domains (TM), an intracellular N- and C-termini and a large extracellular loop 2 between TM3 and TM4 harbouring glycosylation sites (3 glycosylation sites in DAT) (Beuming *et al.* 2006; Chen *et al.* 2004; Gether *et al.* 2006; Torres and Amara 2007).

This predicted 12TM topology was supported by a high resolution crystal structure of a bacterial homologue, the Leucine transporter (LeuT) of the mammalian NSS family (Yamashita et al., 2005). LeuT shares an approximately 20% amino acid homology with the mammalian transporters with the highest homology in the TM regions and around the binding site (Beuming et al., 2006). The structure of the bacterial LeuT provided the first overview of the tertiary structure of SLC6 family members, and revealed an inverted repeat not elucidated in the primary structure, as TM 1-5 and

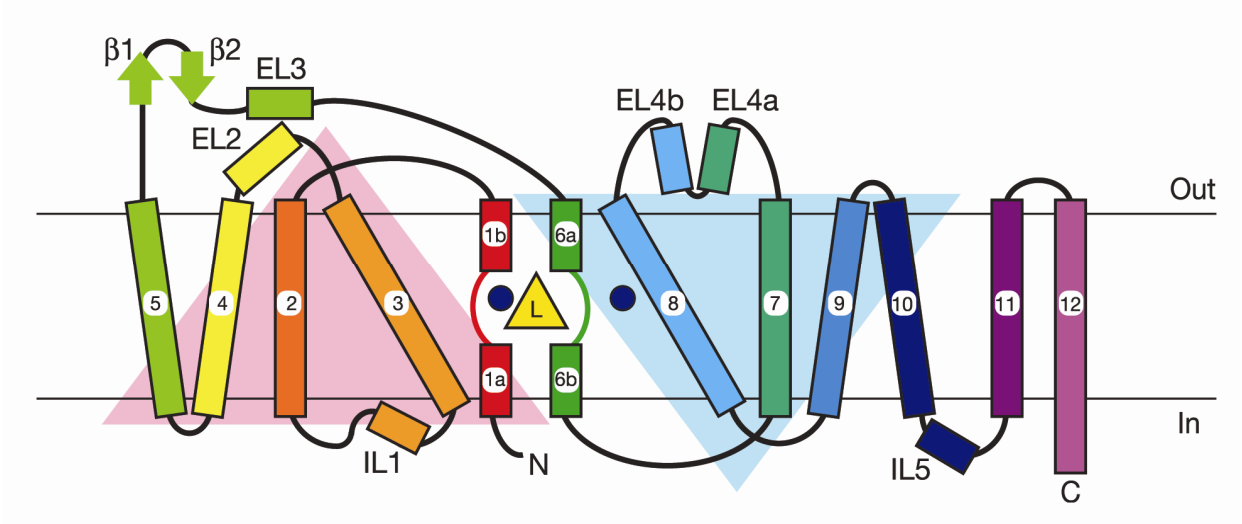


**Figure 3:** *Topology of the NSS family bacterial homolog LeuT.*
*The bacterial SLC6 gene family bacterial homolog LeuT has an internal structural repeat of a 5TM helical bundle. TM1-5 is related to TM6-10 by a twofold symmetry around an axis through the center of the membrane plane. The binding pocket is formed by TM1 TM3, TM6 and TM8 in the middle of the membrane plane (Yamashita et al., 2005).*

TM 6-10 are related by a twofold symmetry around an axis through the center of the membrane plane (figure 3). The partly unwound TM1 and TM6 together with TM3 and TM8 create the substrate binding site in the middle of the membrane plane (Yamashita et al., 2005). Interestingly the structural inverted symmetry is by no means unique to the SLC6 gene family. Recently several crystal stuctures from other bacterial transporter families have revealed a similar teritiary structure, suggesting a similar mechanism of transport for several transporters from various families and with different substrates (recently reviewed by (Abramson and Wright, 2009; Gouaux, 2009).

## Mechanism of transport

The transport of dopamine across the plasma membrane against its concentration gradient is coupled to co-transport of $Na^+$ and $Cl^-$. The driving force for this energetically unfavourable transport is the sodium gradient across the plasma membrane generated by the Na+/$K^+$-ATPase; also referred to as secondary active transport. DAT as other NSS family members is believed to

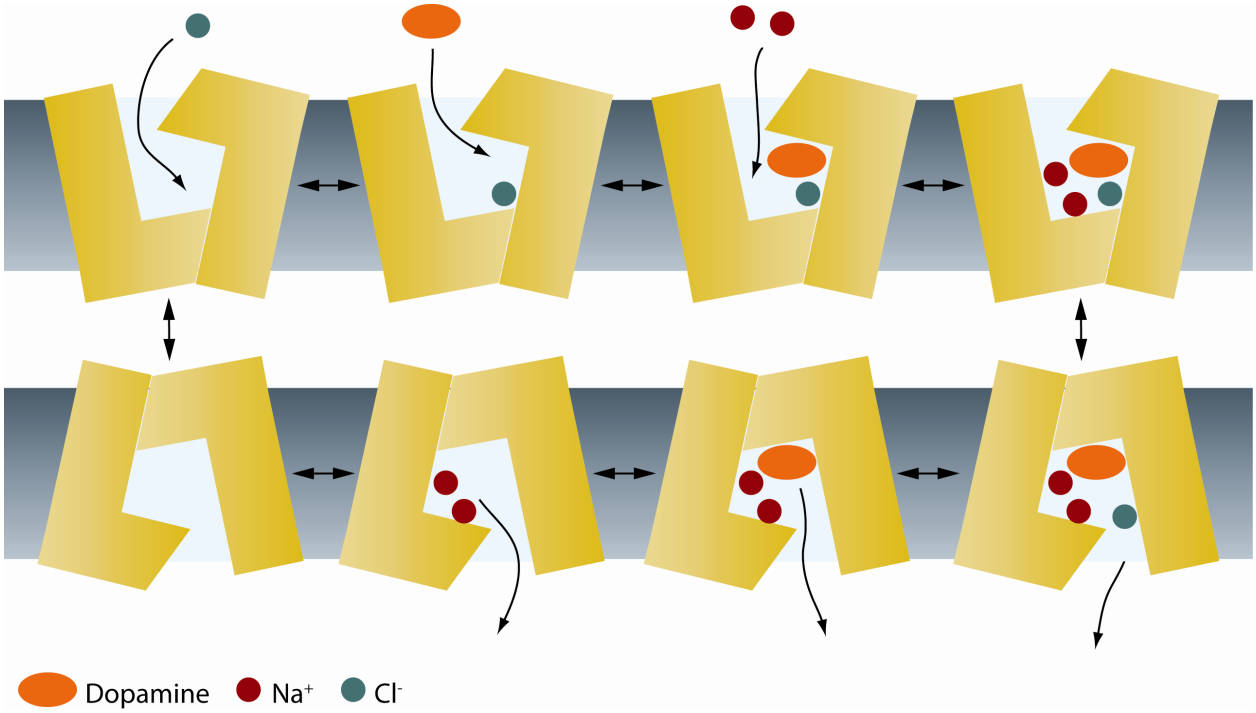


**Figure 4:** *DAT transport mechanism.*
*Orderly binding of ions and substrate is a prerequisite for the protein to undergo conformational changes that occlude the binding site from the extracellular space and exposes it to the intracellular site. Following release of ions and substrate, DAT returns to a conformation with the binding site exposed to the extracellular environment – ready to bind and transport a new dopamine molecule. Modified from (Rudnick, 2006).*

function by alternately exposing the substrate binding site to the extracellular and intracellular environment through conformational changes in DAT (figure 4). This alternating access model depends on a gating mechanism that shield the binding site from the extracellular environment by an external gate and the intracellular environment by an internal gate. Orderly binding of ions and substrate is a prerequisite for the protein to undergo conformational changes that occlude the binding site from the extracellular space and expose it to the intracellular site (Rudnick, 2006). Following release of ions and substrate DAT returns to a conformation with the binding site exposed to the extracellular environment – ready to bind and transport a new dopamine molecule (figure 4). The turnover rate of DAT has been estimated to be around 0.5 dopamine molecule / sec*transporter (Sonders et al., 1997; Prasad and Amara, 2001) suggesting that it takes around two seconds for DAT to go through the whole transport cycle.

It is predicted for DAT that two $Na^+$ and one $Cl^-$ are transported together with one positively charged dopamine molecule (Gu *et al.* 1994; Krueger 1990). Consequently, the transport process is electrogenic and can be analyzed by electrophysiology tools. However, electrophysiological experiments on *Xenopus* oocytes expressing DAT have revealed that the net movement of charges during substrate translocation is greater than the two positive charges expected for a transport cycle with a fixed stoichiometry (Meinild *et al.* 2004; Sonders *et al.* 1997). According to perforated-patch recordings in midbrain DA neurons (Ingram *et al.* 2002) these additional charges are likely due to an uncoupled $Cl^-$ flux that, together with the coupled current, is of a magnitude that can increase the firing rate of the DA neurons; hence, DAT mediated currents might play a role in modulating neuronal excitability (Ingram *et al.* 2002).

## DAT inhibitors and substrates

DAT forms together with the highly homologous norepinephrine transporter (NET) and serotonin transporter (SERT) the NSS subfamily of monoamine transporters. The monoamine transporters have received substantial attention as important targets for CNS drugs. The norepinephrine transporter (NET) and serotonin transporter (SERT) are the prime targets for antidepressants, with the selective SERT and NET inhibitors being effective against both depression and anxiety disorders (Iversen, 2006). Several classes of compounds interact with DAT, including transported substrates and different groups of inhibitors (figure 5) that are used for diagnostic, research and therapeutic purposes as well as being substances of abuse and neurotoxins (Chen et al., 2004).

The most well-known DAT interacting compounds are the psyhostimulants, cocaine and amphetamine. The term ‘psychostimulant’ generally refers to drugs that produce a variety of effects in humans including: increased energy, cardiovascular stimulation, elevated mood, and a decreased need for sleep. At higher doses, or after longer periods of use, psychostimulants can produce a

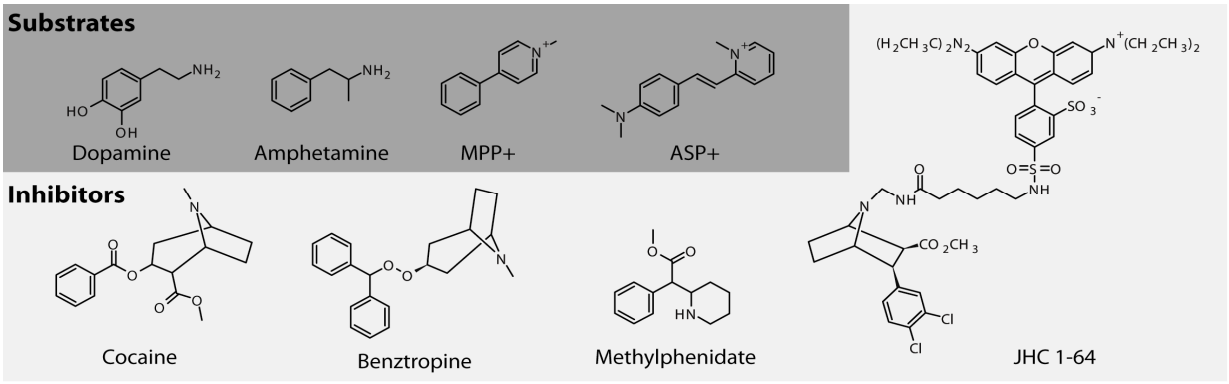


**Figure 5:** *Structure of selected DAT substrates and inhibitors*
*Amphetamine and cocaine are psychostimulants and drugs of abuse. Methylphenidate (Ritalin) is used in the treatment of ADHD. ASP+ (4-(4-(dimethylamino)styrl)-N-methyl-pyridinium) is DAT substrate structurally similar to the neurotoxin MPP+ (Schwartz et al., 2003). JHC 1-64 is a DAT inhibitor. It is a cocaine-derivative conjugated with rhodamine (Cha et al., 2005). Both ASP+ and JHC 1-64 are tool compounds used for repeated monitoring of DAT activity and trafficking, respectively, in live cells.*

range of disordered thought processes, including severe psychotic episodes. In animals, psychostimulants increase locomotor activity and are readily self-administered due to their powerful reinforcing properties (Rothman and Baumann, 2003).

Even though cocaine also inhibits the SERT and NET, DAT knock out (KO) mice show no stimulatory effects of cocaine suggesting that the psychostimulatory effects are mediated by DAT (Giros et al., 1996), and although DAT KO mice self-administers cocaine (Rocha et al., 1998), recent evidence from studies in a knock in mouse with a cocaine insensitive DAT suggest that both the main stimulatory and addictive effects of cocaine are mediated by DAT (Chen et al., 2006; Thomsen et al., 2009; Tilley et al., 2009). The same has been shown to be the case for the amphetamine effects (Giros et al., 1996; Fumagalli et al., 1998).

Amphetamine and cocaine exert their psychostimulatory effects by increasing the extracellular levels of dopamine thereby increasing the dopamine signalling. However, their mechanism of actions differs because cocaine is a competitive inhibitor and amphetamine is a substrate. Cocaine binds DAT in the substrate-binding site (Beuming et al., 2008) without being transported, thereby inhibiting transport and reuptake of released dopamine. Amphetamine is a substrate that is actively

transported by DAT (Wall et al., 1995; Sitte et al., 1998; Sulzer et al., 2005) and raise extracellular dopamine by several mechanism; hence, amphetamine does not only act as a competitive DAT substrate but also disrupts storage of vesicular dopamine and increases DAT mediated dopamine efflux (Sulzer et al., 2005).

## Amphetamine and DAT-mediated efflux

There is increasing evidence that the amphetamine induced DAT-mediated efflux is not directly coupled to uptake (Pifl and Singer, 1999; Scholze et al., 2002b; Meinild et al., 2004) and might even involve a channel-like mode of DAT (Sitte et al., 1998; Kahlig et al., 2005).

Several studies suggest that intracellular signalling via protein kinase C (PKC) is involved in amphetamine-mediated dopamine efflux (Browman et al., 1998; Kantor and Gnegy, 1998) and PKC activation alone might induce DAT-dependent dopamine efflux (Cowell et al., 2000). Gnegy and co-workers showed by use of specific PKC inhibitors that PKCß could be critical for amphetamine- and phorbol ester-induced dopamine efflux in rat striatal slices (Johnson et al., 2005b). Interestingly, it has been shown that phosphorylation of one or more serines in the distal DAT N-terminus shifts the transporter from a 'reluctant' to a 'willing' efflux state without interfering with inward transport (Khoshbouei et al., 2004). This phosphorylation may involve PKC; however, another study suggested that binding of $Ca^{2+}$/calmodulin-dependent protein kinase II (CaMKII) to the DAT C-terminus and CaMKIIα phosphorylation of the N-terminal serines stimulated amphetamine-mediated efflux (Fog et al., 2006). The effect was abolished in heterologous cells by mutation of five serines present in the distal DAT N-terminus. Similarly, chronoamperometry measurements in anesthetized mice exhibited reduced amphetamine-induced dopamine efflux in response to the CaMKII inhibitor KN93.

Amphetamine-induced dopamine efflux might also be regulated by syntaxin1A (Binda et al., 2008) previously shown to bind the DAT N-terminus (Lee et al., 2004). Perfusion of the patch pipette with the purified soluble cytosolic domain of syntaxin1A enabled amphetamine-induced dopamine efflux in a heterologous cell line as well as in midbrain DA neurons in culture at membrane potentials (resting neuronal membrane potential, -60 mV) normally not susceptible to amphetamine-induced dopamine efflux (Binda et al., 2008). Based on these findings, and the finding that amphetamine increased the interaction between DAT and syntaxin1A in a CaMKII-dependent manner, a mechanism is suggested in which amphetamine activation of CaMKII strengthens the DAT/syntaxin1A interaction, resulting in a mode of DAT in which efflux is possible (Binda et al., 2008).

## Localization of DAT in the dopaminergic neurons

Ultrastructural analyses of DAT localization in rat brain have been undertaken with immunoelectron microscopy. With gold-labelled antibodies against DAT, the transporter was shown to exclusively localize in neurons also expressing tyrosine hydroxylase, an enzyme necessary for dopamine synthesis (Nirenberg et al., 1996a; Hersch et al., 1997; Nirenberg et al., 1997). The concentration of DAT was highest in striatal axon terminals and DAT was mainly localized to the plasma membrane along the axons, and a bit surprising DAT was found to be excluded from the active zone of striatal synapses (Nirenberg et al., 1996a; Hersch et al., 1997; Sesack et al., 1998). Thus, it is believed that DAT transports dopamine back into the neurons as it diffuses out of the synapse.

DAT immunoreactivity was also observed in the nigral part of the nigrostriatal DA neurons. In the soma of the neuron DAT localized to the structures of the biosynthetic pathway, and DAT was also found in the distal parts of dendrites (Nirenberg et al., 1996a; Hersch et al., 1997). Some

localization within the endocytic pathway was also observed, as DAT was found in multivesicular bodies, which are precursors to lysosomes. No DAT immunoreactivity was observed within transport vesicles, but the explanation for this might be that the gold particles are larger than the transport vesicles and therefore mask them (Hersch et al., 1997).

The same subcellular distribution with DAT in the plasma membrane along distal dendritic processes and no DAT in the plasma membrane of the soma was observed in DA neurons of the ventral tegmental area (Nirenberg et al., 1997b). However, when comparing the DAT expression levels with immunoelectron microscopy in two different areas of the nucleus accumbens a difference is observed (Nirenberg et al., 1997a) indicating that the expression of DAT is dependent on cell specific factors.

## *Cellular regulation of dopamine transporter trafficking*

The mechanisms determining DAT distribution are largely unknown. Moreover, because of the sparse amount of DA neurons in the CNS and the general difficulties making biochemistry on neurons, most studies on DAT trafficking have been performed in heterologous expression systems. However, experiments in cell lines have identified both signalling pathways and protein interaction partners that regulate DAT function and availability.

### DAT in the biosynthetic pathway

The biosynthetic pathway consists of the endoplasmic reticulum (ER) and the Golgi apparatus and comprises the machinery for membrane protein synthesis and processing (Ellgaard and Helenius, 2003; Jackson, 2009). Several factors have been shown to influence the kinetics of passage through

the secretory pathway including folding and interactions with chaperones and coat complexes in the ER (Ellgaard and Helenius, 2003). ER export has been studied to varying degree in several members of the SLC6 family and especially two factors have been shown to influence the ER export in heterologous expression systems: 1) transporter oligomerization and 2) the cytoplasmic C-terminus.

Transporter oligomerization (reviewed in (Sitte et al., 2004)) has been reported for several of the members in the SLC6 gene family including DAT (Hastrup et al., 2001; Sorkina et al., 2003; Torres et al., 2003), SERT (Just et al., 2004), NET (Hahn et al., 2003), GABA transporter 1 (GAT1) (Scholze et al., 2002a) and recently Glycine transporter 1 and 2 (Bartholomaus et al., 2008), and several papers points towards oligomerization as a requirement for proper ER export.

DAT oligomerize already at an early stage in the secretory pathway (Sorkina et al., 2003) and evidence from the homologous GAT1 suggests that oligomerization is necessary for proper ER export (Scholze et al., 2002a). However, oligomerization alone is not sufficient for proper ER export. Mutational analysis in DAT have shown that oligomerization capable mutants and thus presumably folded mutants can be retained in the ER (Sorkina et al., 2003; Torres et al., 2003; Miranda et al., 2004). As several subtle mutations in the intracellular C-terminus has been shown to confer ER retention in DAT (Sorkina et al., 2003; Bjerggaard et al., 2004; Miranda et al., 2004) this suggests a necessity for an intact C-terminus for proper transporter ER-export even though an intact C-terminus is not required for oligomerization.

Studies from GAT1 have shown that the C-terminus binds Sec24D (Farhan et al., 2004) a component of the COPII coat complex that facilitates transport from ER to Golgi, and it was suggested that oligomerization somehow stabilize the coat formation (Farhan et al., 2004) thus linking the requirement of oligomerization and an intact C-terminus. The Sec24D binding motif is

conserved in the whole SLC6 family and, accordingly, both SERT and DAT ER export was impaired when co-expressed with a dominant negative Sec24D (Farhan et al., 2007).

## DAT endocytic trafficking

Several studies have investigated the dynamics of DAT residing in the plasma membrane, and results indicate that DAT internalizes both constitutively and in a regulated manner (Melikian, 2004). The endocytosis of a membrane protein is a well-described way of regulating the function of the protein at the membrane. Agonist-dependent internalization is a general mechanism for down-regulation of GPCRs and receptor tyrosine kinases at the plasma membrane (Kurten, 2003; Sorkin and von Zastrow, 2009).

The route followed by a membrane protein in the endocytic pathway is not unidirectional as for membrane proteins in the biosynthetic pathway destined for the plasma membrane. Several pathways have been described, but in the end the fate of an internalized membrane protein is either lysosomal degradation or recycling to the plasma membrane. Vesicles with internalized protein initially fuse with a compartment known as the early endosome. The early endosome sorts membrane proteins either for recycling or to late endosomes. The recycling pathway can either be direct from the early endosome back to the plasma membrane ('short loop recycling') or through an endocytic recycling compartment ('long loop recycling'). The early endosome matures into a late endosome and the pH drops through this maturation and in the late endosome yet another sorting event takes place. Some proteins are sorted into a trafficking pathway back to the *trans* Golgi network, and avoids degradation as the late endosome matures into a lysosome (Maxfield and McGraw, 2004). The endosomes are divided into subdomains that act as sorting regions for the incoming proteins, and Rab proteins, a group of small GTPases are important determinants of organelle subdomains in the endocytic pathway (Pfeffer and Aivazian, 2004; Stenmark, 2009).

The steady state DAT distribution in the enterochromaffin cell line, PC12, expressing the transporter has been shown to be 60% intracellularly and 40% on the cell surface in surface biotinylation experiments. Most of the intracellular DAT localized to a transferrin receptor positive compartment, likely to be the endocytic recycling compartment (Melikian and Buckley, 1999). Thus, constitutively internalized DAT was suggested to recycle through the endocytic recycling compartment as has been reported for the transferrin receptor. However the trafficking pathway observed was different from the route of the transferrin receptor (Loder and Melikian, 2003). Recent observations have supported constitutive recycling of DAT. Incubating porcine aortic endothelial (PAE) cells expressing yellow fluorescent protein (YFP) or cyan fluorescent protein (CFP) -tagged DAT with monensin to inhibit recycling, DAT surface expression decreased, when evaluated by both dopamine uptake and surface biotinylation (Sorkina et al., 2005). Knocking out either dynamin II or clathrin heavy chain with siRNAs, and thereby abolishing clathrin mediated internalization inhibited the effect of monensin. Thus, it was proposed that DAT is constitutively internalized in a clathrin-dependent manner and internalized DAT recycled back to the surface (Sorkina et al., 2005). A role for the intracellular DAT C-terminus in regulating DAT endocytosis has been suggested (Holton et al., 2005; Sorkina et al., 2005). The signal was defined in a 10 amino acid sequence (a.a. 587-597 in human DAT) and necessary for constitutive DAT internalization (Holton et al., 2005). Recently, an opposing signal was defined in the DAT N-terminus. It was shown that removal of the DAT N-terminus accelerated constitutive DAT internalization suggesting that the DAT N-terminus harbours an internalization braking mechanism (Sorkina et al., 2009). The relationship between these two signals remains to be elucidated.

## Protein Kinase C and DAT trafficking

Numerous studies have supported that DAT is subject to dynamic regulation in the plasma membrane thereby providing a mean of attenuating or increasing the strength of DA signalling. The most intensively studied mechanism is the regulatory effect of PKC activation. It has been demonstrated in several DAT transfected cell lines that activation of PKC by phorbol esters, such as phorbol 12-myristate 13-acetate (PMA), down-regulate dopamine transport (Zhu et al., 1997; Daniels and Amara, 1999; Melikian and Buckley, 1999; Chi and Reith, 2003; Sorkina et al., 2005; Eriksen et al., 2009). A similar down-regulation has also been reported using synaptosomal preparations (Copeland et al., 1996; Vaughan et al., 1997). The sustained DAT down-regulation in response to PKC activation results most likely from DAT endocytosis (Zhu et al., 1997; Daniels and Amara, 1999; Melikian and Buckley, 1999; Chi and Reith, 2003; Sorkina et al., 2005; Eriksen et al., 2009) although an initial rapid trafficking-independent inactivation of the transporter might occur at the plasma membrane (Mazei-Robison and Blakely, 2005) as also reported for the SERT (Jayanthi et al., 2005). Remarkably, the functional effect of PKC activation on DAT is not directly coupled to DAT phosphorylation (Granas et al., 2003; Cervinski et al., 2005) even though PKC phosphorylated serines in the DAT N-teminus at several positions (Foster et al., 2002; Granas et al., 2003; Gorentla et al., 2009); hence, it was shown that truncation of the distal N-terminus containing these serines, or mutation of the serines to alanines, did not affect DAT down-regulation in response to PMA (Granas et al., 2003).

It is, therefore, highly interesting that recent studies have suggested the involvement of another post-translational modification, ubiquitination, in PKC activated DAT down-regulation (Miranda et al., 2005; Sorkina et al., 2006; Miranda et al., 2007). Ubiquitination is a widespread post-translational modification regulating protein homeostasis in several ways. *Miranda et al.* showed that DAT was constitutively ubiquitinated and that this was augmented upon PMA stimulation

(Miranda et al., 2005). The ubiquitination was dependent on the presence of three lysines in the intracellular DAT N-terminus (Lys19, Lys27, Lys35) and concomitant mutation of these to arginines essentially abolished both ubiquitination and phorbol ester stimulated DAT down regulation (Miranda et al., 2007). Furthermore, fluorescence resonance energy transfer experiements (FRET) experiments with CFP-tagged DAT and YFP-tagged ubiquitin, demonstrated that ubiqutination was most prominent in endosomes supporting a role for ubiquitination as a signal for endocytosis (Miranda et al., 2005). In addition, an E3 ubiquitin ligase, NEDD4-2 was discovered in a small interfering RNA (siRNA) screen for proteins important for PKC-mediated DAT internalization in an endothelial cell line (Sorkina et al., 2006). Of note, knock-down of several other E3 ubiquitin ligases did not affect DAT endocytosis in the siRNA screen suggesting a specific requirement for NEDD4-2. In the siRNA screen, the ESCRT machinery-associated proteins epsin and Eps15/Eps15R were also identified as being important for PMA-mediated DAT endocytosis (Sorkina et al., 2006). Since DAT likewise colocalizes with overexpressed Hrs (Miranda et al., 2005), an endosomal sorting complex required for transport (ESCRT) 0 component, it is conceivable that ubiquitnated DAT is sorted by the ESCRT machinery. This is also in agreement with the fact that PKC-activation increased DAT degradation in HeLa and MDCK (Daniels and Amara, 1999; Miranda et al., 2005). It should be noted, however, that other studies have suggested that PMA-internalized DAT is recycled back to the plasma membrane (Melikian and Buckley, 1999; Sorkina et al., 2003; Sorkina et al., 2005). Of additional interest, Mortensen *et al.*, identified a mitogen-activated protein kinase phosphatase, MKP3, as an inhibitor of PKC mediated DAT internalization acting downstream of the DAT ubiquitination (Mortensen et al., 2008).

Melikian and co-workers have recently reported that the intracellular DAT C-terminal motif that appeared necessary constitutive was also necessary for PKC-mediated DAT internalization (Holton

et al., 2005). The motif is relatively well conserved among NSS proteins and mutating the motif in NET also resulted in impaired transporter internalization (Holton et al., 2005). Further studies showed that alanine substitutions of only residues 587-590 appeared sufficient to abolish PKC-mediated DAT down-regulation and accelerate constitutive DAT internalization (figure 6). Based on these results it was suggested that the four residue stretch is part of an endocytosis braking mechanism that is relieved upon PKC stimulation (Boudanova et al., 2008). It is noteworthy that the

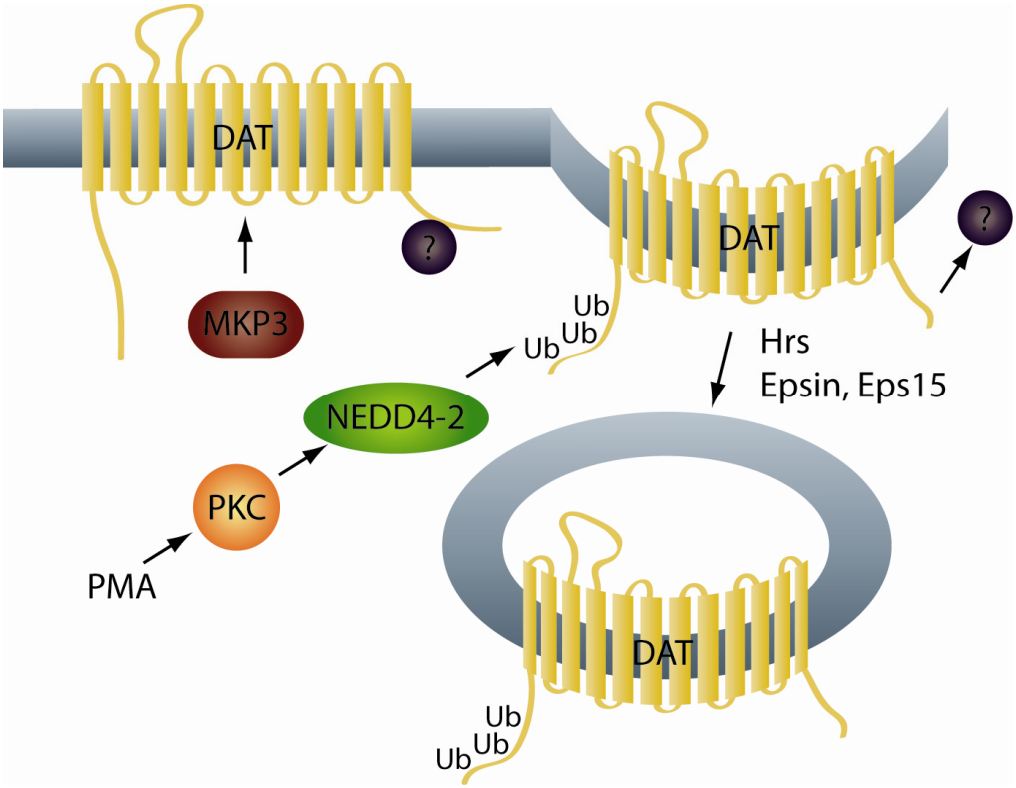


**Figure 6:** *Ubiquitination and interaction with the endocytic machinery orchestrate PKC-mediated DAT internalization.*
*According to (Sorkina et al. 2006), activation of PKC by phorbol esters (PMA) induces ubiquitination of the DAT N-terminus by the E3 ubiquitin ligase NEDD4-2. This results in endocytosis of DAT from the plasma membrane to endocytic compartments assisted by proteins in the endocytic machinery such as Eps15, Epsin and Hrs – possibly through interaction of these proteins with DAT. Additionally, activation of PKC has been hypothesized to mediate the release of an unknown protein factor (green with circle with ?) that interacts with a motif in the DAT C-terminus and in its bound state acts as an endocytic brake on the transporter (Boudanova et al. 2008). However, a possible relationship between the two mechanisms has not been elucidated. The phosphatise MKP3 is believed to antagonize PKC-mediated internalization by stabilizing DAT in the plasma membrane (Mortensen et al., 2008)*

same residues have been suggested to bind the COPII coat component, Sec24D in several members of the NSS family, suggesting a role of this region also in transporter folding and ER export (Farhan et al., 2007). Nevertheless, the relationship between this C-terminal motif and ubiquitination of the N-terminus in PKC mediated DAT endocytosis has not been clarified and awaits further investigations.

Additional kinase pathways have been shown to affect DAT surface expression. This includes downstream effectors of insulin signalling such as phosphatidylinositol 3-kinase (PI3K) and Akt. Inhibitors of both PI3K and Akt as well as overexpression of a dominant negative Akt mutant in heterologous cells decrease DAT surface levels (Carvelli et al., 2002; Garcia et al., 2005). An *in vivo* role of this pathway in regulating DAT levels was supported by studies of rats depleted of insulin by the diabetogenic agent streptozotocin. In these rats both Akt function and DAT surface expression was markedly reduced (Williams et al., 2007). There is also evidence that DAT is subject to regulation by mitogen-activated protein kinase (MAPK), i.e. MAPK inhibitors was shown to decrease dopamine uptake both in transfected HEK293 cells and in striatal synaptosomes. The effect may both involve alteration in DAT transport capacity and redistribution of DAT from the plasma membrane to the cytosol (Moron et al., 2003). DAT might moreover be subject to regulation by phosphatases, e.g. DAT has been proposed to exist in a complex with protein phosphatase 2A, similar to what have been suggested for SERT (Bauman et al., 2000).

## Regulation of DAT by substrates and inhibitors

As previously described, amphetamine increases extracellular dopamine both by acting as a competitive substrate and mediating reversal of transport. Another mechanism by which amphetamine increases extracellular dopamine is by inducing a redistribution of DAT away from

the cell surface (Saunders et al., 2000; Chi and Reith, 2003; Sorkina et al., 2003; Kahlig et al., 2006). The redistribution induced by amphetamine was blocked by cocaine (Saunders et al., 2000), however Kahlig et al. demonstrated that the presence of intracellular amphetamine, rather than the DAT transport cycle itself, was responsible for the effect (Kahlig et al., 2006). As it was observed for amphetamine-induced efflux, CaMKII activity was shown to be necessary for this amphetamine-induced redistribution (Wei et al., 2007). However, unlike amphetamine-induced efflux, the mechanism of amphetamine-induced redistribution does not involve N-terminal phosphorylation (Cervinski et al., 2005).

Recently, a biphasic effect of amphetamine on DAT trafficking was observed by Gnegy and co-workers (Johnson et al., 2005a; Chen et al., 2009; Furman et al., 2009b). Preceding the amphetamine-induced internalization of DAT just described, a rapid increase in surface expressed DAT was observed already after a 1 minute treatment of rat striatal synaptosomes with amphetamine (Johnson et al., 2005a). The increase in surface DAT was dependent on PKCβ activity (Furman et al., 2009b). Furthermore, disruption of the SNARE complex seems to abolish amphetamine-induced trafficking of DAT to the surface (Furman et al., 2009b).

In addition to amphetamine, the endogenous substrate dopamine has likewise been shown to induce DAT internalization in both DAT-expressing HEK293 cells and striatal synaptosomes (Saunders et al., 2000; Chi and Reith, 2003). On the other hand, the DAT blockers cocaine and methylphenidate have been demonstrated to increase DAT surface expression in cell line experiments and synaptosomes (Daws et al., 2002; Little et al., 2002). The apparent conclusion from these experiments is that substrates induce internalization whereas blockers modestly increase surface expression of DAT. This conclusion is supported by *in vivo* observations showing that users of the amphetamine derivative, methamphetamine, have less DAT in the striatum and that cocaine users

have an increased level of DAT (Little et al., 1993). The molecular mechanisms underlying substrate and blocker induced DAT surface regulation is still enigmatic, however a recently it has been suggested that an inward-facing conformation of DAT is more prone to internalization than an outward-facing conformation of DAT (Sorkina et al., 2009), thus the effect of the substrate might be to increase the probability of DAT being in an inward-facing conformation, and this might be part of the explanation for the substrate and blocker effect on DAT endocytosis.

## G protein coupled receptors and DAT

GPCRs constitute the largest family of membrane proteins in the human genome and are responsible for the majority of transmembrane signal transduction in response to hormones and neurotransmitters (Gether, 2000). As described above, several signalling pathways affect DAT function. Thus, it is not surprising that GPCRs and their downstream signalling cascades are involved in the regulation of DAT. Intriguingly; there is recent evidence suggesting also direct physical interaction between DAT and specific GPCRs. including the dopamine D2 receptor and possibly also the orphan receptor GPR37 (Marazziti et al., 2007).

The dopamine D2 receptor short (D2R) is expressed as a presynaptic autoinhibitory receptor in DA neurons and two studies have provided evidence that this receptor is likely to regulate DAT function (Bolan et al., 2007; Lee et al., 2007). Liu and co-workers provided evidence that D2R directly interacts with DAT with the interaction site depending on residues 1-33 in the DAT N-terminus and residues 311-344 in the D2Rs third intracellular loop (Lee et al., 2007). Overexpressing D2R in a cell line together with DAT increased dopamine uptake by 30-60% independently of the presence of D2R ligands and through an increased DAT surface expression. *In vivo* experiments with Tat-conjugated N-terminal DAT peptides decreased co-immunoprecipation of D2R with DAT as well as dopamine uptake in synaptosomes, and rats injected with the effector

peptides displayed increased locomotor activity (Lee et al., 2007). However, these peptides might interfere not only with D2R binding to the N-terminus but also with binding of other proteins such as syntaxin1A that was shown to bind to exactly the same region of DAT (Binda et al., 2008). It is nevertheless of interest that a correlation between schizophrenia and loss of DAT/D2R interaction recently has been reported. Co-immunoprecipitation of DAT with D2R was reduced to 60% in samples from the striatum of patients with schizophrenia compared to the control group, and in samples from patients with bipolar disease no difference was observed (Lee et al., 2009).

In contrast to what *Lee et al.* reported, *Bolan et al.*, observed in HEK293 cells co-expressing DAT and D2R that D2R activation increased dopamine uptake (up to 50%) via stimulation of a pertussis-toxin sensitive extracellular signal-regulated kinase (ERK) 1- and 2-dependent pathway. The increase in uptake was according to biotinylation experiments the result of an increase in DAT surface expression (Bolan et al., 2007). In the same study, co-immunoprecipitation experiments and BRET (bioluminescence resonance energy transfer) analyses indicated close proximity of DAT and D2R but no experimental evidence for a direct interaction was provided. Notably, an N-terminally truncated DAT was also co-immunoprecipitated, thus questioning the necessity for the DAT N-terminus in the interaction (Bolan et al., 2007). Taken together, there is strong evidence from two studies (Bolan et al., 2007; Lee et al., 2007) that D2R causes an increase in dopamine uptake through an increase in DAT surface expression. However, it seems unclear at this stage to what degree the effect is mediated directly via a physical interaction between the two proteins or via D2R activation of intracellular signalling cascades (figure 7). The sites in D2R and DAT that mediate the putative physical interaction are also not resolved. Of note, another D2-class receptor, the dopamine D3 receptor, was shown to up-regulate DAT surface expression in transfected HEK293 cells upon activation, however it was not investigated whether DAT and the D3 receptor interact (Zapata et al., 2007).

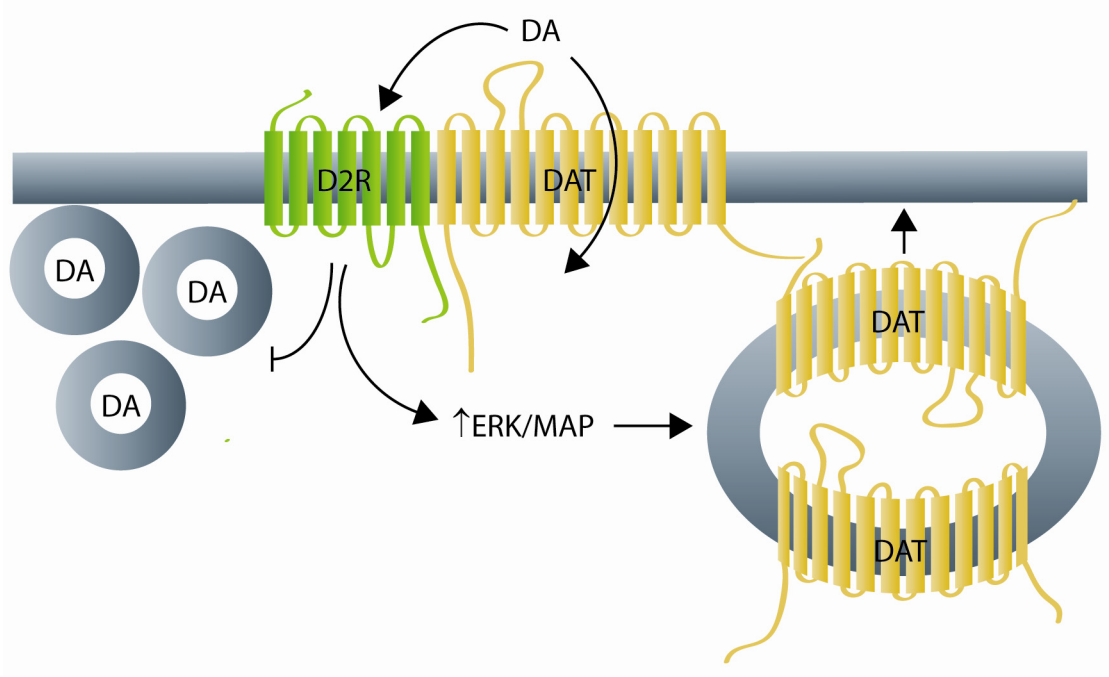


**Figure 7:** *The dopamine D2 receptor (D2Rs) regulates DAT function possibly via a direct interaction.*
*Results from recent studies suggest that the D2Rs increases DAT surface expression and thereby dopamine reuptake capacity either through a direct interaction with the transporter (Lee et al. 2007) or by receptor activation and subsequent stimulation of MAPK/ERK signalling pathway (Bolan et al. 2007). Through coupling to Gi, D2Rs exerts an autoinhibitory action on vesicular dopamine release. These effects both support a decrease of dopamine in the synaptic cleft.*

## Scaffolding of DAT

Protein scaffolding serves to organize proteins into supermolecular complexes to bring different molecular components in close proximity allowing them to work in concert thereby ensuring spatial and temporal control of cellular processes. Scaffolding proteins are characterized by the presence of often multiple protein interaction domains serving as assembly modules gluing together the proper interaction partners; i.e. by connecting membrane proteins to their downstream signalling partners or anchoring them in the right cellular microdomains. Little is known about DAT scaffolding and microdomain localization. As mentioned previously, electron microscopy studies of rat striatum indicated that DAT is restricted from the active zone of the presynapse but otherwise widely expressed along the axons (Hersch et al., 1997). Moreover, DAT was found to partially localize to

membrane rafts both in cell lines and synaptosomes (Foster et al., 2002; Adkins et al., 2007), and in cell lines DAT mobility appeared dependent on an intact actin cytoskeleton (Adkins et al., 2007).

A number of studies have investigated putative proteins and protein domains involved in DAT scaffolding. This includes PDZ domains that represent one of the most widespread protein recognition domains in cellular scaffolding processes, PDZ domains bind short linear consensus motifs mostly located at the C-terminus of their interaction partners and are often found in several copies in the same protein (Nourry et al., 2003; Kim and Sheng, 2004). DAT has a canonical PDZ-binding sequence at its C-terminus and in a yeast two-hybrid screen the dimeric PDZ domain protein PICK1 (protein interacting with C-kinase 1) was identified as a DAT interaction partner. This interaction, which was validated by co-immunoprecipitation experiments from brain tissue, was suggested to promote DAT surface expression and induce a clustering phenotype in transfected cells (Torres et al., 2001). However, Bjerggaard *et al.* later challenged these findings by showing that although PICK1 binds the extreme DAT C-terminus the interaction does not play a role in ER export and surface targeting of the transporter. Indeed DAT C-terminal residues were important for proper membrane targeting of DAT, but mutations in DAT were identified that specifically disrupted PDZ domain interactions without affecting surface targeting and mutations were identified that disrupted surface targeting without affecting PICK1 binding (Bjerggaard et al., 2004). Thus, the functional significance of the DAT PICK1 interaction remains to be settled. It is interesting to note that for other binding partners such as the glutamate receptor subunit 2 (GluR2) of the AMPA receptor and the acid sensing ion channel 2A it has been shown that PICK1 might affect endocytosis/recycling (Hanley and Henley, 2005; Lin and Huganir, 2007) or serve to recruit PKC to facilitate phosphorylation (Baron et al., 2002), respectively, but none of these effects have so far been shown for DAT.

An interaction between the C-terminus of DAT and the focal adhesion scaffolding protein Hic-5 was identified in a yeast two hybrid screen (Carneiro et al., 2002). Co-immunoprecipitation and GST pulldown studies demonstrated that the interaction was mediated by the membrane proximal part of the C-terminus of DAT and the multiple LIM domain-containing half of Hic-5. In HEK293 cells co-expressing Hic-5 and DAT, a decrease in dopamine uptake by 30% was observed. The decrease in transporter activity was attributed to a decrease in cell-surface level of DAT as demonstrated by cell surface biotinylation experiments (Carneiro et al., 2002). For SERT, which also can bind Hic-5, the interaction was suggested to promote translocation from a membrane-skeleton associated fraction to a cytoskeleton-associated fraction in platelets. This translocation was proposed to facilitate SERT internalization (Carneiro and Blakely, 2006).

Recently the synaptic vesicle protein synaptogyrin-3 was identified as yet another putative scaffolding protein interacting with DAT (Egana et al., 2009). It was demonstrated that the N-terminus of DAT also was capable of pulling down purified synaptic vesicles and in the catecholaminergic cell PC12 and MD9D cell lines, both containing VMAT-positive vesicles, overexpression of synaptogyrin-3 with DAT increased DAT uptake activity whereas synaptogyrin-3 siRNA reduced DAT activity. Likewise, DAT activity was reduced by 40% in the presence of the VMAT2 inhibitor reserpine in PC12 cells but not in HEK293 cells. Based on these findings, the authors suggest the challenging hypothesis that the interaction between synaptogyrin-3 and DAT couples DAT to synaptic vesicles and that this coupling leads to an increase in DAT activity and presumably a more efficient filling of synaptic vesicles (Egana et al., 2009). In addition it was recently shown that not only DAT localize in a complex with the synaptic vesicles but also the enzymes catalyzing the synthesis of dopamine suggesting a complete dopamine synthesis and transport scaffold on the synaptic vesicles (Cartier et al., 2009).

## Implications for a physiological role of dynamic DAT regulation

The majority of the abovementioned studies have been carried out in *ex vivo* systems and there are no studies directly showing that dynamic DAT regulation in the plasma membrane affects the overall function of the DA system. As already discussed, data from genetic mouse models support an essential role for DAT in regulating DA signalling, however as a model for dynamic regulation of the DAT in the plasma membrane the genetic models have some shortcomings since chronic alterations in DAT levels inevitably will lead to adaptations in the DA signalling machinery (Jones et al., 1998). Therefore, pharmacological studies might to some extent more appropriately describe a potential effect of cellular regulation of DAT in the plasma membrane. Several studies have been carried with focus on the effect of DAT inhibitor occupancy and physiological parameters both in humans and mouse. These studies have primarily been undertaken to study the paradox that some high-affinity DAT blocker produce a locomotor effect/have addictive properties whereas others display no behavioural effects (Desai et al., 2005a; Desai et al., 2005b). A relationship between DAT occupancy measured using positron emission tomography (PET) and the subjective feeling of high has been studied in cocaine users. The result was that DAT occupancy of approximately 50% was required to produce a feeling of high (Volkow et al., 1997). Similar results have been obtained in animals where a high DAT occupancy was required to produce any behavioural effects (Desai et al., 2005a). However, the occupancy alone is not the only parameter of DAT blockers that determines the behavioural effect. It also seems that the rate of occupancy is highly important for producing behavioural effects upon DAT blocking. As cocaine produces greater locomotor reponse than does benztropines which have a slower rate of occupancy, but same efficacy (Desai et al., 2005a).

Overall pharmacological and behavioural data suggest that acute blockade of DAT at a high level of DAT occupancy together with a fast rate of occupancy induce detectable physiological effects in

both animals and humans. This might be translatable into potential effects of cellular DAT down-regulation. Most effects changing DAT surface expression measured in cell systems are in the range of 10-50%. This would suggest that only maximal responses would generate measureable physiological responses according to the pharmacological data. However, as mentioned the rate of occupancy is also critical and, thus dynamic fast cellular down-regulation is likely to generate detectable effects on DA signalling that in turn might be detectable at the behavioural level.

# SUMMARY OF RESULTS

## *Study 1: Analyzing DAT trafficking in dopaminergic neurons*

**Paper 1: Visualization of Dopamine Transporter Trafficking in Live Neurons by Use of Fluorescent Cocaine Analogs**

**Motivation:** With the development of the fluorescent cocaine analogs from Dr. Amy H. Newman's laboratory at NIDA-IRS, National Institute of Health, it became a possibility to study dynamic trafficking aspects of DAT in a native system. Previously, the study of DAT dynamics in a native system has been hampered by the lack of tools to probe DAT, and accordingly most studies have been carried out in transfected cell lines that lack the complexity of DA neurons. By use of JHC 1-64 in combination with the establishment of lentiviral transduction we therefore set out to investigate DAT trafficking properties in primary cultures of DA midbrain neurons.

**Summary:** In HEK293 cells expressing DAT, the use of the cocaine analog, JHC 1-64, was verified as a tool for studying DAT trafficking. Several essential properties making JHC 1-64 a proper tool for studying DAT trafficking was observed: 1) JHC 1-64 binding is highly specific and binds DAT with a high affinity thereby providing a high signal-to-noise ratio; 2) JHC 1-64 does not permeate the plasma membrane, and therefore only labels surface DAT and 3) JHC 1-64 has an extremely slow off-rate, which is important for tracking DAT over en extended period of time..

In DA primary cultures JHC 1-64 specifically labelled neurons expressing obligate dopamine markers such as tyrosine hydroxylase, VMAT2, and DAT. The labelling was uniform in the DA

neurons and FRAP (fluorescence recovery after photobleaching) experiments showed a bidirectional movement of DAT in the neuronal extensions and a high DAT mobility.

We were unable to detect any PKC regulation of DAT in the DA neurons when probing DAT internalization and dopamine uptake, although we did detect PKC activity in the DA neurons and observed PKC-mediated DAT internalization in HEK293 cells. However, a notable constitutive DAT internalization was evident. We further characterized the constitutive DAT internalization to be dynamin-dependent and displayed a partial colocalization with the early endosomal marker Rab5 and the transferrin receptor.

## *Study 2: Sorting of constitutively internalized DAT*

**Paper 2: Constitutively Internalized Dopamine Transporter is Primarily Sorted to a Late Endosomal/Lysosomal Pathway in both Dopaminergic Neurons and Cell Lines**

**Motivation:** Based on the observations made in Paper 1 we wanted to further characterize the constitutive internalization of DAT in DA neurons. Previously, constitutive DAT internalization has been observed in cell lines, and it has been suggested that constitutively internalized DAT is sorted to recycling. We wanted to study the sorting fate of constitutively internalized DAT in the DA neurons together with a comparison of the DAT sorting pattern in cell lines. In this way we would be able to determine whether the constitutively internalized DAT is dependent on the cellular background as was the case for PKC-mediated internalization and whether constitutively internalized is sorted to degradation and/or recycling.

**Summary:** To study the constitutive DAT internalization in the two cell lines HEK293 and 1Rb3An27 we employed a new DAT construct, TacDAT. TacDAT is a fusion between the 1 TM

protein Tac and DAT, thus creating an extracellular N-terminal to which we added the high affinity FLAG antibody epitope. TacDAT displayed properties similar to wild-type DAT and enabled the quantification of transporter internalization in an ELISA assay and quantification of transporter sorting in a microscope-based assay. In HEK293 cells we show that both the inhibitor of lysomal proteases and the inhibitor of lysosomal degradation/recycling, monensin, increase the intracellular accumulation of DAT. Incubation of cells with monensin did not alter in the cell surface expression of DAT, and we conclude therefore that the monensin effect on intracellular TacDAT accumulation is not due to an inhibition of TacDAT recycling. Together with the observation that constitutively internalized TacDAT colocalized with the late endosomal marker EGFP-Rab7 we suggest that DAT is primarily sorted to a late endosomal/lysosomal pathway in HEK293. A similar pattern was observed in the DA cell line 1Rb27An3 where a quantification of colocalization between constitutively internalized TacDAT and the endosomal markers EGFP-Rab4, -Rab7, -Rab11, showed a significantly higher colocalization with Rab7 than with the recycling endosomal marker Rab11. This sorting pattern was distinct from the well described recycling protein, the $ß_2$-adrenergic receptor, which displayed a significantly higher colocalization with Rab11. Probing DAT internalization with JHC 1-64 in 1Rb3An27 also exhibited the highest colocalization with EGFP-Rab7. Finally, examining the sorting of constitutively internalized DAT in DA neurons using JHC 1-64 in cultures transduced with the EGFP-tagged endosomal markers DAT, again, displayed the highest degree of colocalization with EFGP-Rab7. Additionally, constitutively internalized DAT also colocalized with the lysosomal marker, LysoTracker Green. We conclude that constitutively internalized DAT sorts to a late endosomal/lysosomal pathway in both cell lines and cultured DA neurons.

## *Study 3: The DAT C-terminus activates PICK1*

**Paper 3: Membrane Localization is Critical for Activation of the PICK1 BAR domain**

**Motivation:** The DAT has previously been shown to bind the PDZ domain protein PICK1 in several systems (Torres et al., 2001; Bjerggaard et al., 2004; Madsen et al., 2005) via its extreme C-terminus. However, the function of the interaction remains unclear. Previously, it has been shown that co-expression of PICK1 and the interaction partner glutamate receptor subunit 2 (GluR2) causes a co-clustering of both proteins (Perez et al., 2001).

The aim of the present study was to understand the molecular determinants in PICK1 underlying this co-clustering phenotype. This was especially interesting in relation to the recently identified Bin/amphiphysin/Rvs (BAR) domain in the C-terminal half of PICK1. BAR domains are homodimeric modules that mediate curvature-dependent recognition and/or tubulation of lipid membranes (Peter et al., 2004; McMahon and Gallop, 2005). They are present in many proteins involved in cellular trafficking. The strongest evidence for a role of the BAR domain in PICK1 function is the demonstration that transfection of wild-type (wt) PICK1 into cerebellar Purkinje cells derived from PICK1 knock-out mice can restore LTD, which was not observed for a PICK1 mutant containing a mutant BAR domain deficient in lipid vesicle binding (Steinberg et al., 2006). Furthermore, understanding the molecular properties of the interaction between PICK1 and its binding partners might elucidate a role for the DAT/PICK1 interaction.

**Summary:** In COS7 cells, co-expression of PICK1 together with membrane proteins containing a C-terminal PICK1 binding sequence (including the DAT C-terminus fused to Tac) results in a co-clustering of both proteins that is not observed when each protein is expressed on its own. However, adding a PICK1 binding sequence to a cytosolic protein (eCFP) and coexpressing the protein with

PICK1 does not induce the clustering phenotype. This suggests that PICK1 needs to be recruited to the plasma membrane to induce the clustering phenotype which was supported by an experiment adding a myristoyl anchor to PICK1. This membrane localizing modification of PICK1 induced the clustering phenotype. Finally, it was shown that the co-clustering of PICK1 and the membrane protein ligand colocalized primarily with a Rab11 positive compartment. The data support altogether that in the absence of PDZ ligand, the PICK1 BAR domain is inhibited through a PDZ domain-dependent and linker-dependent mechanism. Moreover, they suggest that unmasking of the BAR domain's membranebinding capacity is not a consequence of ligand binding to the PDZ domain per se but results from, and coincides with, recruitment of PICK1 to a membrane compartment.

## *Study 4: Effects of DAT on D2R*

**Paper 4: The dopamine transporter impairs dopamine D2 receptor surface expression/ signalling and reveals promiscuous monoamine transporter/receptor interaction**

**Motivation:** Recent papers have described a direct interaction between DAT and the D2R, an interaction that displays functional effects on DAT (Bolan et al., 2007; Lee et al., 2007). Given that other membrane protein interaction partners have been shown to affect D2R signalling (Rashid et al., 2007) we hypothesized that DAT might influence D2R function.

**Summary:** Transient over-expressing DAT with D2R in HEK293 cells reduced surface expression of D2R while DAT surface levels remained unaffected. Furthermore ß-Arrestin2 recruitment to D2R was compromised and D2R-mediated inhibition of cAMP accumulation was reduced as a consequence of the reduced surface level expression of D2R. The effects of DAT on D2R surface

expression and signalling was not unique for DAT and D2R. Thus, transient co-expression of ß$_2$AR with DAT resulted in reduced surface levels of ß$_2$AR. In addition, co-expression of the SERT with D2R appeared to modulate the ß-Arrestin2 recruitment to D2R and the D2R-mediated inhibition of cAMP accumulation in a manner similar to co-expression of DAT.

# DISCUSSION

## The cellular environment determines properties of DAT trafficking

As already described in the introduction, the DA neuron is a highly complex cell type with a large axonal tree (figure 2). Therefore, it is important to take into account the native environment when studying the cellular regulation of proteins as different environment is likely to affect the properties of the behaviour of the protein. To the best of our knowledge, the use of the fluorescent cocaine analogues has for the first time allowed the direct visualization of DAT dynamics in a native environment. The distribution of DAT in the membrane when visualized with JHC 1-64 is uniform on the soma and along the neuronal extensions. This distribution is in agreement with studies of DAT in DA neurons in the brain. With immunoelectron microscopy DAT has been detected in the plasma membrane of DA neurons in both the midbrain and the target area (Nirenberg et al., 1996a; Hersch et al., 1997; Sesack et al., 1998). Using FRAP experiments we established that DAT exhibited bidirectional movement in the neuronal extensions; thus, we found no evidence of unidirectional targeting. Furthermore, the movement of DAT in the membrane was high with a diffusion constant of 0.5-1.1 $10^{-9}$ $cm^2$/sec and with a high mobile fraction (> 70%). This diffusion is consistent with a relatively freely diffusing membrane protein (Lippincott-Schwartz et al., 2001), although marginally faster than what has been observed for DAT in cell lines with a diffusion coefficiency around 0.3–0.4 × $10^{-9}$$cm^2$/sec (Adkins et al., 2007; Sorkina et al., 2009). However, it should be noted that the previously published FRAP experiments were all conducted on DAT tagged N-terminally with a fluorescent protein, and it cannot be excluded that the addition of a bulky fluorophore to DAT could affect the DAT diffusion rate. It might also represent biological difference, since variations in DAT mobility between cell lines (Adkins et al., 2007) and between

subcellular regions (Sorkina et al., 2009) has been observed, suggesting that the transporter mobility is subject to cellular regulation possibly through protein protein interactions.

The PKC regulated DAT endocytosis is the most well described DAT regulatory mechanism and therefore it was a surprise that we did not observe for the endogenous DAT in DA neurons. PKC activation was still detectable in the DA neurons as measured by the PKC activity FRET sensor CKAR. Thus, it is most likely not due to a decreased PKC activity in the neurons. To test whether the medium used for the neurons in some way could antagonize the effect of PKC activation, DAT-mediated dopamine uptake in our cultures were carried out after serum starvation and still we did not see any effect of PMA on uptake (figure 8). Previously PMA has been shown to decrease dopamine uptake (Vaughan et al., 1997; Chi and Reith, 2003) and decrease cell surface biotinylated DAT (Chi and Reith, 2003) in striatal synaptosomal preparations. However, the effects are observed at a concentration of 10 μM PMA. PMA is thought to activate PKC at a range from 1-100nM and structurally, phorbol esters resemble nonionic detergents, and to avoid nonspecific effects attributable to detergent properties, it is desirable to keep their concentrations low. PMA has nevertheless recently been reported to decrease the dopamine uptake by approximately 25% in another DA primary culture preparation. This was observed using a concentration of PMA as low as 100 nM (Hoover et al., 2007). The primary cultures used in this study were prepared from prenatal (E15) rats and cocultured with striatal

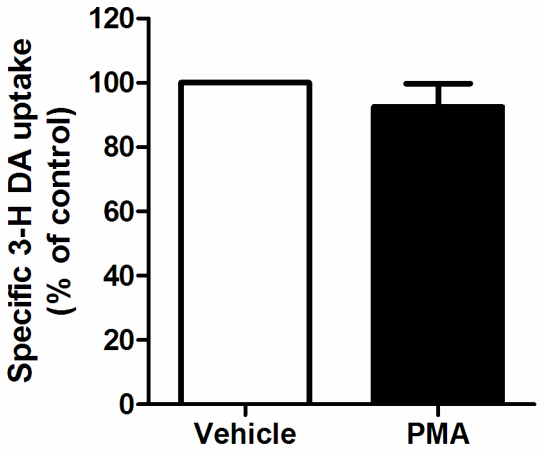


**Figure 8:** Dopamine uptake in serum starved dopaminergic neurons. Dopamine uptake was carried out as in figure 9, Paper 1 (Eriksen et al., 2009) with the exception that the neurons were preincubated in uptake buffer for 2 hours before 30 minustes incubation with PMA (1 μM) or vehicle (0.1% DMSO). PMA treatment did not affect dopamine uptake (p= 0.41, n=3, one sample t-test)

neurons. It is interesting to speculate that co-culturing with striatal neurons might provide an environment that confers PKC sensitivity to the DAT in the DA neurons. Our experiment were carried out in cultures from P1-P3 rats, thus the maturity of the neurons might be another factor that determines PMA sensitivity of the DAT. Recently, Amara and co-workers described that the MAP kinase phosphatase, MKP3, antagonizes PKC-mediated DAT down regulation (Mortensen et al., 2008). Interestingly MKP3 was differentially expressed in different cell lines, and it would highly interesting to see if knock-down of MKP3 would confer PKC sensitivity to the DA neurons.

## Sorting of DAT to a late endosomal/lysosomal pathway

Constitutive DAT internalization has been described in several cell lines (Chi and Reith, 2003; Loder and Melikian, 2003; Sorkina et al., 2005). However, in this study the constitutive internalization has been described for the first time for endogenous DAT in DA neurons. The constitutive DAT internalization in DA neurons was not sensitive to PKC inhibition or activation showing that it was a PKC independent phenomenon, and as opposed to the PKC-mediated internalization it was observed in both DA primary cultures and cell lines.

Curiously we were only able to observe internalization events in the soma and the proximal dendritic regions. When evaluating DAT in the distal extension, we did not observe any internalization events even though the neurite extensions represent the vast majority of DAT containing membrane in the preparations (figure 9). Thus, despite a profound DAT internalization in the soma, the amount internalized is small as compared to the extensive DAT/JHC 1-64 signal observed throughout the membrane of the DA neurons. The inability to detect DAT internalization in distal neuronal could be a matter of detection and resolution limitations in the confocal microscopy approach. Application of recently developed super-resolution microscopy techniques (Henriques and Mhlanga, 2009) could to help to resolve whether the lack of internalization in the

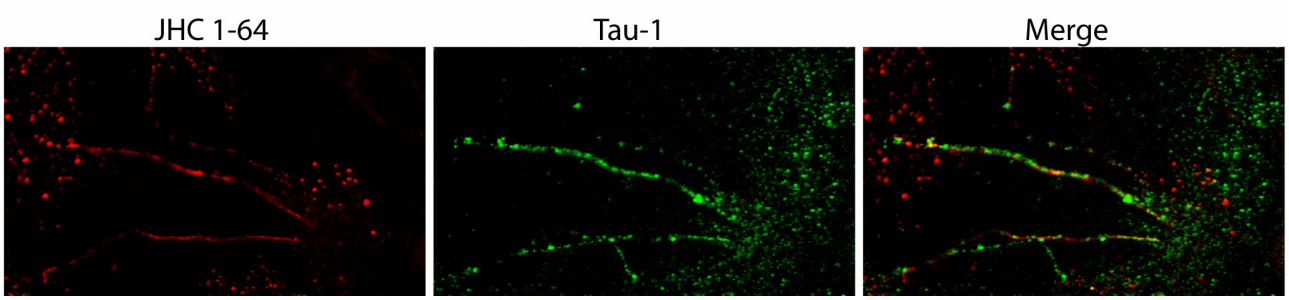


**Figure 9:** *JHC 1-64 labelling overlaps with the axonal marker Tau.*
*Dopaminergic cultures (as described in Paper 1) were incubated with 10 nM JHC 1-64 for 20 minutes at RT before fixation. Then the specimens were blocked and permeabilized and incubated with either mouse anti-Tau1 (1:500) and secondary detection was done with Alexa Fluor 488 goat anti-mouse or Alexa Fluor 488 goat anti-rabbit, respectively. Most narrow neuronal extensions labeled with JHC 1-64 co-stained also for Tau-1.*

extensions represents a true biological phenomenon. Interestingly immunoelectron microscopy studies have also described that the majority of DAT located to intracellular membranes was observed in the midbrain and in the soma and proximal dendrites of the neurons (Nirenberg et al., 1996b; Hersch et al., 1997; Nirenberg et al., 1997). Taken together, it is tempting to speculate that the soma of the DA neuron might represent an area primed for DAT internalization. This hypothesis is in agreement with an observation in cell lines, where a internalization-willing DAT mutant resided less in the cellular extrusions (Sorkina et al., 2009).

The sorting pattern of constitutively internalized DAT observed in HEK293 cells, 1Rb3An27 cells and DA neurons suggest that the internalized DAT is sorted primarily to degradation. The sorting pattern was determined using several different approaches to minimize the chances that a distinct sorting pattern was observed due to assay artifacts. The first approach used in HEK293 was to perturb the sorting pathways in HEK293 cells chemically. The inhibitor of lysososmal proteases, leupeptin was used to perturb lysosomal function and the sodium ionophore monensin was used as a general perturbation of endosomal maturation. Monensin is believed to function by dissipating the proton gradient across membrane either by being a proton ionophore or by having an indirect effect on the $Na^+/H^+$ exchanger (Mollenhauer et al., 1990). As endosomal maturation is dependent on a

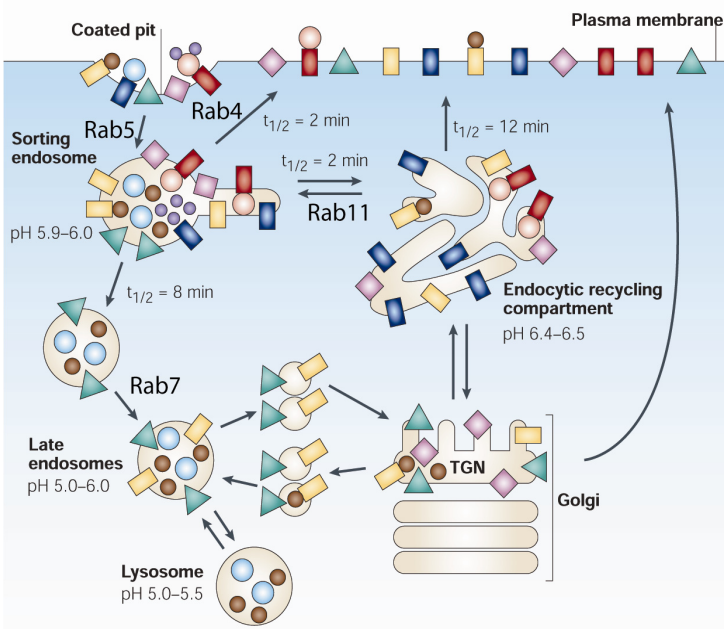


**Figure 10:** *The endocytic pathways. The figure shows the endocytic itineraries followed by various proteins. The sorting endosome is also known as the early endosome. The indicated $t_{½}$ are approximate values and cell-type dependent. The Rab GTPases (Rab 4, Rab5, Rab7, and Rab11) are located to their site of action (the figure is modified from: (Maxfield and McGraw, 2004)*

sequential lowering of pH (figure 10), monensin will affect sorting both to recycling and to lysosomal degradation (Maxfield and McGraw, 2004). Looking at the intracellular accumulation of TacDAT in HEK293 cells, we saw an effect of both leupeptin and monensin. However, when testing the effect of monensin on DAT surface expression we did not see any effect. We conclude accordingly that both the effect of leupetin and of monensin on intracellular TacDAT are due to a blockade in the degradative pathway. This was further supported when determining the sorting pattern of TacDAT, using EGFP-tagged Rab proteins, which act as molecular switches in coordinating vesicular trafficking. Rab proteins can be used to identify intracellular compartments as different Rabs locate to specific endosomal compartments (Stenmark, 2009). We used 4 different EGFP-tagged Rabs (figure 10): Rab4, a marker of early endosomes and involved in recycling from early endosomes (often referred to as 'short loop recycling'), Rab5 also a marker of early endosomes and involved in endocytosis, Rab7, a marker of late endosomes, and finally Rab11 a marker of recycling endosomes and involved in 'long loop recycling'.

In all systems tested DAT colocalized primarily with Rab7 and to some degree the early endosomal markers Rab4 and Rab5. This localization was independent of the way we probed DAT

internalization, i.e. using antibodies or JHC 1-64. Additionally, we observed a profound colocalization of internalized DAT with the lysosomal marker Lysotracker.

Altogether our data suggest that constitutively internalized DAT is sorted to degradation both in cell lines and in DA neurons.

Previously, observations regarding sorting of constitutively internalized DAT all suggest that DAT is sorted to a recycling pathway (Loder and Melikian, 2003; Sorkina et al., 2005; Furman et al., 2009a). In PC12 cells DAT has been suggested to have a fast constitutive recycling, however, when treating the cells with bafilomcyin, an inhibitor of vesicular proton pumps, no effect was seen on the surface expression of DAT, whereas a marked effect was seen on the well-known recycling membrane protein, the transferrin receptor. The conclusion that DAT recycled fast in PC12 cells was based on experiments at 18° C, which was supposed to inhibit exocytosis without interfering with endocytosis (Loder and Melikian, 2003), which is a simplification at best (Sorkin et al., 1991). A recent study has claimed that DAT recycles via a Rab11 dependent pathway as DAT plasma membrane DAT was increased upon co-expression of constitutively active Rab11, however, all experiments were steady state experiments and interestingly a dominant negative Rab11 did not exhibit any effect compared to a GFP control when quantifying DAT surface binding (Furman et al., 2009a).

Taken together, the data supporting a recycling of constitutively internalized DAT are open for discussion, however, it can not be excluded that recycling plays a role in some systems.

## Studying DAT trafficking with the silent partner Tac

In both paper 1 and 2, fusions between Tac and DAT are used to elucidate properties of DAT. Tac is a 1TM protein that has been used in several studies as a silent carrier used to determine trafficking signal in protein sequences studies (Mu et al., 2003; Lavezzari et al., 2004; Holton et al.,

2005; Lavezzari and Roche, 2007). In paper 2 we use a head to tail fusion of the DAT N-terminus to the Tac C-terminus and show that this TacDAT displays properties similar to DAT with regard to transport and trafficking. For future purposes it is interesting to note that a fully functional head to tail fusion between SERT and Tac has been made (Jørgensen and Gether, unpublished observations). With a collection of Tac/transporter fusion proteins it will be possible to screen transporters for similarities and differences in trafficking patterns.

Furthermore, as shown in paper 3, Tac can also be used to isolate DAT primary sequence signals. This is parallel to what been done before with DAT (Holton et al., 2005). By use of the TacDAT C24 (the distal 24 C-terminal amino acids in DAT fused to Tac) construct it was shown that this construct was able to cocluster PICK1 when the two proteins were expressed in COS7 cells. This phenotype is not observed for the full length DAT. When co-expressed with PICK1 DAT does not relocate to an intracellular compartment and cocluster with PICK1 (Bjerggaard et al., 2004). Based on these observations and the fact that PICK1 has been shown to exert trafficking effects on other interaction partners it is interesting to speculate that the DAT C-terminus by default is shielded in full length DAT and therefore is not influenced by co-expression of PICK1. Moreover, it is interesting to note that PICK1 in Paper 3 colocalizes primarily with Rab11 when co-expressed with its membrane protein ligands. This sorting pattern is different from what was observed and described for DAT in Paper 2. It is therefore also tempting to speculate that a regulatory mechanism could expose the DAT C-terminus and facilitate PICK1 binding and thereby divert DAT sorting to a Rab11 recycling pathway, sorting pattern is observed for the Tac constructs with a PICK1 binding sequence. Additionally the PICK1 binding has been shown to regulate the recycling of GluR2 another PICK1 binding partner (Lin and Huganir, 2007).

## Promiscous effects of DAT on D2R

The DAT/D2R interaction has previously been show to increase DAT function (Bolan et al., 2007; Lee et al., 2007). In the current study we show DAT also regulate D2R function. DAT exhibited a profound suppressive effect in HEK293 cells. An effect that was specific for DAT and D2R since DAT also suppressed the expression of the $ß_2$-adrenergic receptor. DAT affected both the G-protein coupled and ß-arrestin2-dependent signalling of D2R. Whereas the effect of G-protein signalling could be explained by the suppressive effects on D2R expression whereas the effect on the ß-Arrestin recruitment most likely was not an effect of the suppressed D2R expression.

It was not determined whether the functional effects were a consequence of the interaction, and with the presumably not very well-defined interaction sites it is potentially a difficult task to establish a link between the functional effects of DAT on D2R and the interaction. However, the data suggests that DAT is capable of regulating function of GPCR. This concept is not new since other GPCRs have previously been shown to regulate the function of D2R. Expressing D2R with the dopamine D1 receptor that in itself couples to Gs proteins results in a receptor complex that show enlarged Gq/11 mediated increase in intracellular calcium upon dopamine activation (Rashid et al., 2007). D2R can also directly interact with the Adenosine A2 receptor (Canals et al., 2003) and A2 agonist treatment of striatal membranes decreased agonist affinity for striatal D2R (Ferre et al., 1991). It will be interesting to see if DAT regulates D2R in DA neurons – whether a knockdown of DAT would increase the expression of D2R and modify its signalling properties. A chronic knock down of DAT as in a DAT KO mouse would not be a suitable model since the increased extracellular dopamine in the DAT KO mice causes a desensitization-mediated down-regulation of D2R (Giros et al., 1996).

## *Preliminary data and perspectives in the study of DAT trafficking*

### pHluorin-DAT: a probe for DAT membrane insertion

As our data per se does not exclude recycling and recycling might be a regulated feature in DAT, efforts were made to enable direct visualization of membrane insertion of DAT. For other membrane proteins, fusion with the fluorescent protein pHluorin has proven highly successful in detecting insertions in to the plasma membrane (Yudowski et al., 2006; Yudowski et al., 2007). pHluorin displays pH-sensitive fluorescence, i.e. when exposed to extracellular environment

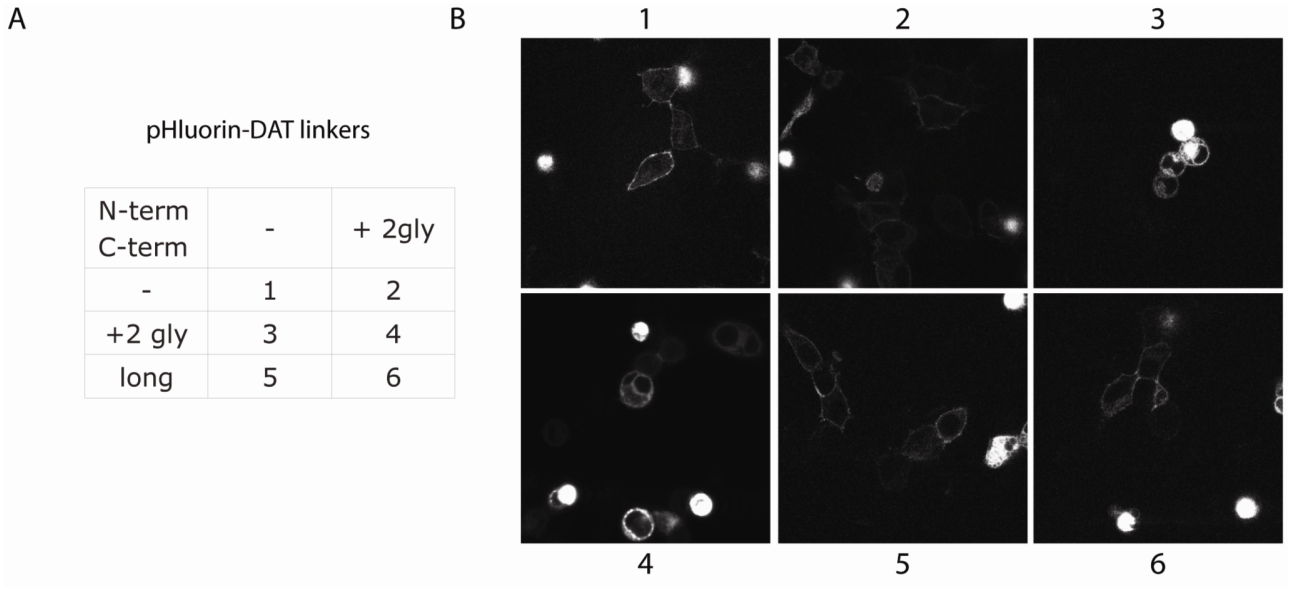


**Figure 11:** *Generation of a functional pHluorin-DAT.* ***A)*** *Six different pHluorin-DAT constructs were generated with two different N-terminal linker and thre different C-terminal linkers around the inserted pHluorin. -, no linker +2 gly denotes a two glycine linker, long linker. The constructs were generated by engineering BsrGI into the region encoding the extracellular loop 2 at position 198 in DAT in the pCDNA3 synDAT construct using a standard QuickChange protocol. pHluorin was amplified from a pHluorin-$\beta_2$-adrenergic construct (Yudowski et al., 2009) with different primer sets. Two sense primers, both with a BsiWI site and the one with an additional 2 glycine linker. Three antisense primers, all with a BsiWI site, and one with an additional 2 glycine linker. Combining these primers six versions of pHluorin was generated digested with BsiWI and inserted into BsrGI digested pcDNA3 synDAT with a BsrGI site. The sequences of the constructs were verified by sequencing.* ***B)*** *Expression of the six pHluorin-DAT constructs in HEK293 cells. : HEK293 cells or CAD cells transfected with pCDNA3 pHluorin-DAT 1-6 were seeded in 8 well LabTek chambers coated with poly-ornithine. The cells were used for experiments two days after transfection. The cells were imaged in HEPES buffered saline (25 mM HEPES, pH 7.4, with 130 mM NaCl, 5.4 mM KCl, 1.2 mM $CaCl_2$, 1.2 mM $MgSO_4$, 5 mM D-glucose). Imaging was performed as described in Paper 1.*

(pH~7.4), it is highly fluorescent. On the other hand, when exposed to the acidic environment in the lumen of endosomal compartments (pH<6.0), the fluorescence is rapidly and reversible quenched. Accordingly, fusion of pHluorin to the extracellular part of DAT will enable discrimination between transporters localized at the cell surface and transporters localized in intracellular compartments.

pHluorin-DAT constructs were made by inserting pHluorin into the second extracellular loop of hDAT. By combining 2 different C-terminal linkers and 3 different C-terminal linkers on pHluorin, six different constructs were made (figure 11A). When expressed in HEK293 cells, the 6 different pHluorin-DAT constructs had a maximum dopamine uptake that was 10% of wild type with none of the construct being significantly better than the other (data not shown), and when evaluating the expression by microscopy it was clear that a lot of cells displayed an intracellular accumulation of pHluorin-DAT (figure 11B). The intracellular accumulation likely represents ER retained pHluorin-DAT as the pH in ER is 7.4 (Wu et al., 2001) and therefore pHluorin-DAT will be visible in this intracellular compartment as opposed to other intracellular compartments with lower pH (figure 10). Although a lot of cells displayed ER retention, cells expressing low levels of pHluorin-DAT exhibited no intracellular fluorescence but only plasma membrane associated fluorescence. Therefore, it seems that high levels of pHluorin-DAT expression induce ER retention, most likely due to misfolding of the pHluorin-DAT construct. The misfolding phenotype was tried rescued by growing the cells at 30 °C with no effect (data not shown). However, since cells with low expression displayed a DAT distribution similar to wild type DAT and dopamine uptake was detectable, it was assumed that surface targeted DAT was functional.

Next the pHluorin-DAT #3 construct was expressed in the DA cell line CAD (Qi et al., 1997) to test the properties in a DA cell line. As in HEK293 cells, both cells with a distinct surface expression and cells with ER retained DAT were observed (figure 12A). Incubating the cells with an acidic ringer buffer (pH 5.3) quenched the pHluorin-DAT signal (figure 12A), and the signal could be

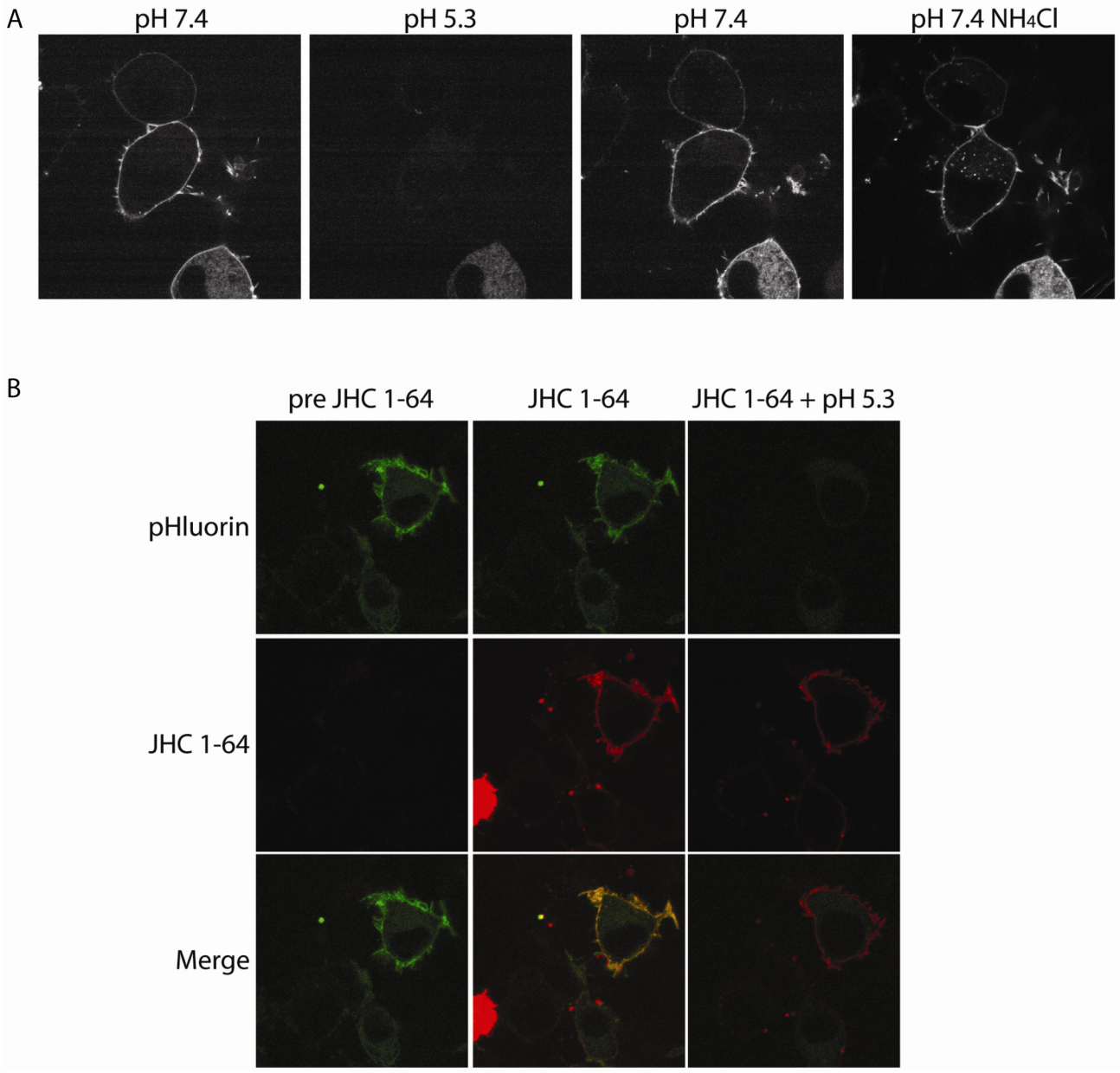


**Figure 12:** *Expression of a functional pHluorin-DAT in CAD cells.*
***A)*** *CAD cells transfected with pHluorin-DAT #3 were imaged as described in figure 11. The panel display the same cells first imaged in a neutral buffer, then in an acidic buffer that quenches the pHluorin signal. The signal is then rescued by applying a neutral buffer. Finally adding a buffer with ammonium chloride neutralizes the pH in the intracellular making pHluorin-DAT residing in vesicular compartments visible. Acidic solution (pH 5.3) was prepared by replacing HEPES in the imaging buffer with MES (pH 5.3), with all other components in the imaging buffer remaining unchanged. Ammonium chloride solution (pH 7.4) was prepared by substituting 50 mM NaCl in the imaging buffer with NH4Cl, with all other components remaining unchanged.* ***B)*** *For imaging with JHC 1-64 the cells were incubated with 5 nM JHC 1-64 for 20 minutes at room temperature and subsequently washed in buffer.*

rescued by adding a neutral ringer buffer (pH 7.4). Finally, adding ammonium chloride which neutralizes the pH in intracellular compartment made a distinct vesicular pHluorin-DAT signal

visible. This suggests that pHluorin-DAT has a cellular distribution like wild type DAT when expressed at low levels. We also tested binding of JHC 1-64 to pHluorin-DAT. JHC 1-64 fluorescence colocalized with the pHluorin signal (figure 12B), and the pHluorin signal was specific as it was sensitive to low pH (figure 12B) This further supports that the transporter on the cell surface is functional.

Even though pHluorin-DAT has a compromised expression it still seems functional and as it is possible to recognize and avoid cells with a compromised expression it seems feasible to undertake experiments with pHluorin-DAT. Using pHluorin-DAT, it might be possible to address fundamental questions regarding DAT insertion into the plasma membrane. E.g., what is the frequency and cellular location DAT membrane insertion and is this insertion of DAT regulated?

## Using the cocaine analogs as flow cytometry probes

As already shown, the fluorescent cocaine analogs have provided a tool for studying DAT in new and interesting ways. In addition, experiments have shown that the Oregon Green cocain analog, MFZ 9-18 can be used in flow cytometry experiments to describe a population profile of PMA-induced DAT down-regulation in HEK293 with average reduction of 31-35% of surface DAT (figure 13). The experiment is a proof of concept that the cocaine analogs can actually be used to probe changes in DAT surface expression using flow cytometry, and with this setup we intend to probe DAT surface expression in acute striatal synaptosomal preparations. Compared to uptake such an approach would not be sensitive to changes in membrane potential and thus more likely to represent a true quantitative readout of surface expression. The use of flow cytometry on striatal synaptosomes has been described previously (Wolf et al., 1991), and the with the setup it will be possible to detect changes in DAT surface expression upon acute *in vivo* or *ex vivo* stimulation with

e.g. insulin, which has previously been described to affect DAT surface expression in cell lines and in diabetogenized mice (Garcia et al., 2005; Williams et al., 2007). Furthermore, the setup would provide an elegant way of probing the PMA effect in striatal synaptosomes, providing information not available with either dopamine uptake or biotinylation experiments.

Another experimental possibility with the flow cytometry setup would be to purify DA neurons from a dissociated midbrain preparation

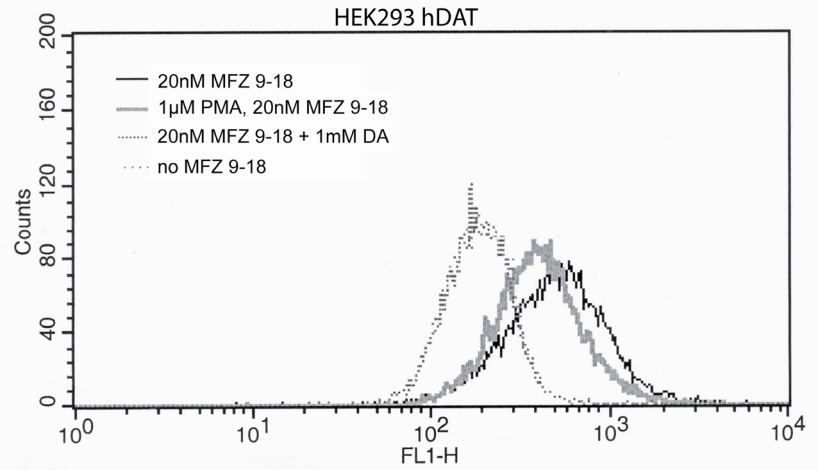


***Figure 13:*** *Flow cytometry was used to quantify DAT surface expression in HEK293 cells stably transfected with hDAT. The cells were seeded two days prior to experiments (3x106 in a 10 mm Petri dish). On the day of the experiment the cells were incubated in buffer 1 (+/- 1µM PMA) for 30 min at 37°C. After incubation, the cells were detached from plates using PBS with 5 mM EDTA, and the cells were collected and sedimented at 300 x g for 5 min. The cells were incubated with 20 nM MFZ 9-18 (+1 mM dopamine in the control for unspecific binding) in PBS with 1% BSA for 10 min at 4°C. Subsequently, the cells were washed 3 times in PBS + 1% BSA. Fluorescence intensity profiles of cell populations (10,000µtimes in PBS with 1% BSA each followed by sedimentation at 300 x g for 5 min, and the cells were then resuspended in 500 cells/sample) were measured using a FACS-Calibur instrument (BD Biosciences, Franklin Lakes, NJ). The reduction of DAT surface expression was between 31-35% in three independent experiments. The graph represents one of the experients.*

# REFERENCES


Abramson J, Wright EM (2009) Structure and function of Na(+)-symporters with inverted repeats. Curr Opin Struct Biol 19:425-432.

Adkins EM, Samuvel DJ, Fog JU, Eriksen J, Jayanthi LD, Vaegter CB, Ramamoorthy S, Gether U (2007) Membrane Mobility and Microdomain Association of the Dopamine Transporter Studied with Fluorescence Correlation Spectroscopy and Fluorescence Recovery after Photobleachingâ€ Biochemistry 46:10484-10497.

Albin RL, Mink JW (2006) Recent advances in Tourette syndrome research. Trends Neurosci 29:175-182.

Baron A, Deval E, Salinas M, Lingueglia E, Voilley N, Lazdunski M (2002) Protein kinase C stimulates the acid-sensing ion channel ASIC2a via the PDZ domain-containing protein PICK1. J Biol Chem 277:50463-50468.

Bartholomaus I, Milan-Lobo L, Nicke A, Dutertre S, Hastrup H, Jha A, Gether U, Sitte HH, Betz H, Eulenburg V (2008) Glycine Transporter Dimers: EVIDENCE FOR OCCURRENCE IN THE PLASMA MEMBRANE. J Biol Chem 283:10978-10991.

Bauman AL, Apparsundaram S, Ramamoorthy S, Wadzinski BE, Vaughan RA, Blakely RD (2000) Cocaine and antidepressant-sensitive biogenic amine transporters exist in regulated complexes with protein phosphatase 2A. Journal of Neuroscience 20:7571-7578.

Beuming T, Shi L, Javitch JA, Weinstein H (2006) A Comprehensive Structure-Based Alignment of Prokaryotic and Eukaryotic Neurotransmitter/Na+ Symporters (NSS) Aids in the Use of the LeuT Structure to Probe NSS Structure and Function. Molecular Pharmacology 70:1630-1642.

Beuming T, Kniazeff J, Bergmann ML, Shi L, Gracia L, Raniszewska K, Newman AH, Javitch JA, Weinstein H, Gether U, Loland CJ (2008) The binding sites for cocaine and dopamine in the dopamine transporter overlap. Nat Neurosci 11:780-789.

Binda F, Dipace C, Bowton E, Robertson SD, Lute BJ, Fog JU, Zhang M, Sen N, Colbran RJ, Gnegy ME, Gether U, Javitch JA, Erreger K, Galli A (2008) Syntaxin 1A interaction with the dopamine transporter promotes amphetamine-induced dopamine efflux. MolPharmacol 74:1101-1108.

Bjerggaard C, Fog JU, Hastrup H, Madsen K, Loland CJ, Javitch JA, Gether U (2004) Surface Targeting of the Dopamine Transporter Involves Discrete Epitopes in the Distal C Terminus But Does Not Require Canonical PDZ Domain Interactions. Journal of Neuroscience 24:7024-7036.

Bjorklund A, Dunnett SB (2007) Dopamine neuron systems in the brain: an update. Trends Neurosci 30:194-202.

Bolan EA, Kivell B, Jaligam V, Oz M, Jayanthi LD, Han Y, Sen N, Urizar E, Gomes I, Devi LA, Ramamoorthy S, Javitch JA, Zapata A, Shippenberg TS (2007) D2 receptors regulate dopamine transporter function via an extracellular signal-regulated kinases 1 and 2-dependent and phosphoinositide 3 kinase-independent mechanism. MolPharmacol 71:1222-1232.

Boudanova E, Navaroli DM, Stevens Z, Melikian HE (2008) Dopamine transporter endocytic determinants: Carboxy terminal residues critical for basal and PKC-stimulated internalization. Molecular and Cellular Neuroscience 39:211-217.

Browman KE, Kantor L, Richardson S, Badiani A, Robinson TE, Gnegy ME (1998) Injection of the protein kinase C inhibitor Ro31-8220 into the nucleus accumbens attenuates the acute response to amphetamine: tissue and behavioral studies. Brain Research 814:112-119.

Canals M, Marcellino D, Fanelli F, Ciruela F, de Benedetti P, Goldberg SR, Neve K, Fuxe K, Agnati LF, Woods AS, Ferre S, Lluis C, Bouvier M, Franco R (2003) Adenosine A2A-dopamine D2 receptor-receptor heteromerization: qualitative and quantitative assessment by fluorescence and bioluminescence energy transfer. J Biol Chem 278:46741-46749.

Carlsson A, Lindqvist M, Magnusson T (1957) 3,4-Dihydroxyphenylalanine and 5-hydroxytryptophan as reserpine antagonists. Nature 180:1200.

Carlsson A, Lindqvist M, Magnusson T, Waldeck B (1958) On the presence of 3-hydroxytyramine in brain. Science 127:471.

Carneiro AM, Blakely RD (2006) Serotonin-, protein kinase C-, and Hic-5-associated redistribution of the platelet serotonin transporter. Journal of Biological Chemistry 281:24769-24780.

Carneiro AM, Ingram SL, Beaulieu JM, Sweeney A, Amara SG, Thomas SM, Caron MG, Torres GE (2002) The multiple LIM domain-containing adaptor protein Hic-5 synaptically colocalizes and interacts with the dopamine transporter. Journal of Neuroscience 22:7045-7054.

Cartier EA, Parra LA, Baust TB, Quiroz M, Salazar G, Faundez V, Egana L, Torres GE (2009) A biochemical and functional protein complex involving dopamine synthesis and transport into synaptic vesicles. J Biol Chem.

Carvelli L, Moron JA, Kahlig KM, Ferrer JV, Sen N, Lechleiter JD, Leeb-Lundberg LM, Merrill G, Lafer EM, Ballou LM, Shippenberg TS, Javitch JA, Lin RZ, Galli A (2002) PI 3-kinase regulation of dopamine uptake. JNeurochem 81:859-869.

Cervinski MA, Foster JD, Vaughan RA (2005) Psychoactive Substrates Stimulate Dopamine Transporter Phosphorylation and Down-regulation by Cocaine-sensitive and Protein Kinase C-dependent Mechanisms. Journal of Biological Chemistry 280:40442-40449.

Cha JH, Zou MF, Adkins EM, Rasmussen SG, Loland CJ, Schoenenberger B, Gether U, Newman AH (2005) Rhodamine-labeled 2beta-carbomethoxy-3beta-(3,4-dichlorophenyl)tropane analogues as high-affinity fluorescent probes for the dopamine transporter. JMedChem 48:7513-7516.

Chen NH, Reith M, Quick M (2004) Synaptic uptake and beyond: the sodium- and chloride-dependent neurotransmitter transporter family SLC6. Pfl++gers Archiv European Journal of Physiology 447:519-531.

Chen R, Furman CA, Zhang M, Kim MN, Gereau RWt, Leitges M, Gnegy ME (2009) Protein kinase Cbeta is a critical regulator of dopamine transporter trafficking and regulates the behavioral response to amphetamine in mice. J Pharmacol Exp Ther 328:912-920.

Chen R, Tilley MR, Wei H, Zhou F, Zhou FM, Ching S, Quan N, Stephens RL, Hill ER, Nottoli T, Han DD, Gu HH (2006) Abolished cocaine reward in mice with a cocaine-insensitive dopamine transporter. Proc Natl Acad Sci U S A 103:9333-9338.

Chi L, Reith MEA (2003) Substrate-Induced Trafficking of the Dopamine Transporter in Heterologously Expressing Cells and in Rat Striatal Synaptosomal Preparations. Journal of Pharmacology And Experimental Therapeutics 307:729-736.

Copeland BJ, Vogelsberg V, Neff NH, Hadjiconstantinou M (1996) Protein kinase C activators decrease dopamine uptake into striatal synaptosomes. Journal of Pharmacology And Experimental Therapeutics 277:1527-1532.

Cowell RM, Kantor L, Hewlett GHK, Frey KA, Gnegy ME (2000) Dopamine transporter antagonists block phorbol ester-induced dopamine release and dopamine transporter phosphorylation in striatal synaptosomes. European Journal of Pharmacology 389:59-65.

Dahlstrom A, Fuxe K (1964) Localization of monoamines in the lower brain stem. Experientia 20:398-399.

Daniels GM, Amara SG (1999) Regulated Trafficking of the Human Dopamine Transporter. CLATHRIN-MEDIATED INTERNALIZATION AND LYSOSOMAL DEGRADATION IN RESPONSE TO PHORBOL ESTERS. Journal of Biological Chemistry 274:35794-35801.

Daws LC, Callaghan PD, Moron JA, Kahlig KM, Shippenberg TS, Javitch JA, Galli A (2002) Cocaine increases dopamine uptake and cell surface expression of dopamine transporters. BiochemBiophysResCommun 290:1545-1550.

Desai RI, Kopajtic TA, French D, Newman AH, Katz JL (2005a) Relationship between in vivo occupancy at the dopamine transporter and behavioral effects of cocaine, GBR 12909 [1-{2-[bis-(4-fluorophenyl)methoxy]ethyl}-4-(3-phenylpropyl)piperazine], and benztropine analogs. J Pharmacol Exp Ther 315:397-404.

Desai RI, Kopajtic TA, Koffarnus M, Newman AH, Katz JL (2005b) Identification of a Dopamine Transporter Ligand That Blocks the Stimulant Effects of Cocaine. J Neurosci 25:1889-1893.

Egana LA, Cuevas RA, Baust TB, Parra LA, Leak RK, Hochendoner S, Pena K, Quiroz M, Hong WC, Dorostkar MM, Janz R, Sitte HH, Torres GE (2009) Physical and functional interaction between the dopamine transporter and the synaptic vesicle protein synaptogyrin-3. Journal of Neuroscience 29:4592-4604.

Ellgaard L, Helenius A (2003) Quality control in the endoplasmic reticulum. Nat Rev Mol Cell Biol 4:181-191.

Eriksen J, Rasmussen SGF, Rasmussen TN, Vaegter CB, Cha JH, Zou MF, Newman AH, Gether U (2009) Visualization of Dopamine Transporter Trafficking in Live Neurons by Use of Fluorescent Cocaine Analogs. Journal of Neuroscience 29:6794-6808.

Farhan H, Reiterer V, Korkhov VM, Schmid JA, Freissmuth M, Sitte HH (2007) Concentrative export from the endoplasmic reticulum of the gamma-aminobutyric acid transporter 1 requires binding to SEC24D. J BiolChem 282:7679-7689.

Farhan H, Korkhov VM, Paulitschke V, Dorostkar MM, Scholze P, Kudlacek O, Freissmuth M, Sitte HH (2004) Two discontinuous segments in the carboxyl terminus are required for membrane targeting of the rat gamma-aminobutyric acid transporter-1 (GAT1). J BiolChem 279:28553-28563.

Ferre S, von Euler G, Johansson B, Fredholm BB, Fuxe K (1991) Stimulation of high-affinity adenosine A2 receptors decreases the affinity of dopamine D2 receptors in rat striatal membranes. Proc Natl Acad Sci U S A 88:7238-7241.

Fog JU, Khoshbouei H, Holy M, Owens WA, Vaegter CB, Sen N, Nikandrova Y, Bowton E, McMahon DG, Colbran RJ, Daws LC, Sitte HH, Javitch JA, Galli A, Gether U (2006) Calmodulin kinase II interacts with the dopamine transporter C terminus to regulate amphetamine-induced reverse transport. Neuron 51:417-429.
Foster JD, Pananusorn B, Vaughan RA (2002) Dopamine Transporters Are Phosphorylated on N-terminal Serines in Rat Striatum. Journal of Biological Chemistry 277:25178-25186.
Fumagalli F, Gainetdinov RR, Valenzano KJ, Caron MG (1998) Role of Dopamine Transporter in Methamphetamine-Induced Neurotoxicity: Evidence from Mice Lacking the Transporter. Journal of Neuroscience 18:4861-4869.
Furman CA, Lo CB, Stokes S, Esteban JA, Gnegy ME (2009a) Rab 11 regulates constitutive dopamine transporter trafficking and function in N2A neuroblastoma cells. Neurosci Lett 463:78-81.
Furman CA, Chen R, Guptaroy B, Zhang M, Holz RW, Gnegy M (2009b) Dopamine and Amphetamine Rapidly Increase Dopamine Transporter Trafficking to the Surface: Live-Cell Imaging Using Total Internal Reflection Fluorescence Microscopy. Journal of Neuroscience 29:3328-3336.
Gainetdinov RR, Caron MG (2003) MONOAMINE TRANSPORTERS: From Genes to Behavior. Annual Review of Pharmacology and Toxicology 43:261-284.
Gainetdinov RR, Jones SR, Fumagalli F, Wightman RM, Caron MG (1998) Re-evaluation of the role of the dopamine transporter in dopamine system homeostasis. Brain Res Brain Res Rev 26:148-153.
Garcia BG, Wei Y, Moron JA, Lin RZ, Javitch JA, Galli A (2005) Akt is essential for insulin modulation of amphetamine-induced human dopamine transporter cell-surface redistribution. MolPharmacol 68:102-109.
Garris P, Wightman R (1994) Different kinetics govern dopaminergic transmission in the amygdala, prefrontal cortex, and striatum: an in vivo voltammetric study. J Neurosci 14:442-450.
Gether U (2000) Uncovering molecular mechanisms involved in activation of G protein-coupled receptors. Endocr Rev 21:90-113.
Giros B, Jaber M, Jones SR, Wightman RM, Caron MG (1996) Hyperlocomotion and indifference to cocaine and amphetamine in mice lacking the dopamine transporter. Nature 379:606-612.
Gorentla BK, Moritz AE, Foster JD, Vaughan RA (2009) Proline-directed phosphorylation of the dopamine transporter N-terminal domain. Biochemistry 48:1067-1076.
Gouaux E (2009) Review. The molecular logic of sodium-coupled neurotransmitter transporters. Philos Trans R Soc Lond B Biol Sci 364:149-154.
Grace AA, Floresco SB, Goto Y, Lodge DJ (2007) Regulation of firing of dopaminergic neurons and control of goal-directed behaviors. Trends Neurosci 30:220-227.
Granas C, Ferrer J, Loland CJ, Javitch JA, Gether U (2003) N-terminal truncation of the dopamine transporter abolishes phorbol ester- and substance P receptor-stimulated phosphorylation without impairing transporter internalization. Journal of Biological Chemistry 278:4990-5000.
Greengard P (2001) The neurobiology of slow synaptic transmission. Science 294:1024-1030.
Hahn MK, Robertson D, Blakely RD (2003) A Mutation in the Human Norepinephrine Transporter Gene (SLC6A2) Associated with Orthostatic Intolerance Disrupts Surface Expression of Mutant and Wild-Type Transporters. J Neurosci 23:4470-4478.
Hanley JG, Henley JM (2005) PICK1 is a calcium-sensor for NMDA-induced AMPA receptor trafficking. EMBO J 24:3266-3278.
Hastrup H, Karlin A, Javitch JA (2001) Symmetrical dimer of the human dopamine transporter revealed by cross-linking Cys-306 at the extracellular end of the sixth transmembrane segment. ProcNatl AcadSci USA 98:10055-10060.
Henriques R, Mhlanga MM (2009) PALM and STORM: What hides beyond the Rayleigh limit? Biotechnology Journal 4:846-857.
Hersch SM, Yi H, Heilman CJ, Edwards RH, Levey AI (1997) Subcellular localization and molecular topology of the dopamine transporter in the striatum and substantia nigra. JComp Neurol 388:211-227.
Hertting G, Axelrod J (1961) Fate of tritiated noradrenaline at the sympathetic nerve-endings. Nature 192:172-173.
Hertting G, Axelrod J, Kopin IJ, Whitby LG (1961) Lack of uptake of catecholamines after chronic denervation of sympathetic nerves. Nature 189:66.
Holton KL, Loder MK, Melikian HE (2005) Nonclassical, distinct endocytic signals dictate constitutive and PKC-regulated neurotransmitter transporter internalization. Nat Neurosci 8:881-888.
Hoover BR, Everett CV, Sorkin A, Zahniser NR (2007) Rapid regulation of dopamine transporters by tyrosine kinases in rat neuronal preparations. Journal of Neurochemistry 101:1258-1271.
Iversen L (2006) Neurotransmitter transporters and their impact on the development of psychopharmacology. British Journal of Pharmacology 147:S82-S88.
Iversen SD, Iversen LL (2007) Dopamine: 50 years in perspective. Trends Neurosci 30:188-193.
Jackson CL (2009) Mechanisms of transport through the Golgi complex. J Cell Sci 122:443-452.

Jayanthi LD, Samuvel DJ, Blakely RD, Ramamoorthy S (2005) Evidence for Biphasic Effects of Protein Kinase C on Serotonin Transporter Function, Endocytosis, and Phosphorylation. Molecular Pharmacology 67:2077-2087.
Johnson LA, Furman CA, Zhang M, Guptaroy B, Gnegy ME (2005a) Rapid delivery of the dopamine transporter to the plasmalemmal membrane upon amphetamine stimulation. Neuropharmacology 49:750-758.
Johnson LAA, Guptaroy B, Lund D, Shamban S, Gnegy ME (2005b) Regulation of Amphetamine-stimulated Dopamine Efflux by Protein Kinase C {beta}. Journal of Biological Chemistry 280:10914-10919.
Jones SR, Gainetdinov RR, Jaber M, Giros B, Wightman RM, Caron MG (1998) Profound neuronal plasticity in response to inactivation of the dopamine transporter. Proc Natl Acad Sci U S A 95:4029-4034.
Just H, Sitte HH, Schmid JA, Freissmuth M, Kudlacek O (2004) Identification of an Additional Interaction Domain in Transmembrane Domains 11 and 12 That Supports Oligomer Formation in the Human Serotonin Transporter. J Biol Chem 279:6650-6657.
Kahlig KM, Binda F, Khoshbouei H, Blakely RD, McMahon DG, Javitch JA, Galli A (2005) Amphetamine induces dopamine efflux through a dopamine transporter channel. ProcNatlAcadSciUSA 102:3495-3500.
Kahlig KM, Lute BJ, Wei Y, Loland CJ, Gether U, Javitch JA, Galli A (2006) Regulation of dopamine transporter trafficking by intracellular amphetamine. Mol Pharmacol 70:542-548.
Kantor L, Gnegy ME (1998) Protein Kinase C Inhibitors Block Amphetamine-Mediated Dopamine Release in Rat Striatal Slices. Journal of Pharmacology And Experimental Therapeutics 284:592-598.
Khoshbouei H, Sen N, Guptaroy B, Johnson L, Lund D, Gnegy ME, Galli A, Javitch JA (2004) N-terminal phosphorylation of the dopamine transporter is required for amphetamine-induced efflux. PLoSBiol 2:E78.
Kilty JE, Lorang D, Amara SG (1991) Cloning and expression of a cocaine-sensitive rat dopamine transporter. Science 254:578-579.
Kim E, Sheng M (2004) PDZ domain proteins of synapses. NatRevNeurosci 5:771-781.
Kurten RC (2003) Sorting motifs in receptor trafficking. Adv Drug Deliv Rev 55:1405-1419.
Lavezzari G, Roche KW (2007) Constitutive endocytosis of the metabotropic glutamate receptor mGluR7 is clathrin-independent. Neuropharmacology 52:100-107.
Lavezzari G, McCallum J, Dewey CM, Roche KW (2004) Subunit-Specific Regulation of NMDA Receptor Endocytosis. J Neurosci 24:6383-6391.
Lee FJ, Pei L, Liu F (2009) Disruption of the dopamine transporter-dopamine D2 receptor interaction in schizophrenia. Synapse 63:710-712.
Lee FJ, Pei L, Moszczynska A, Vukusic B, Fletcher PJ, Liu F (2007) Dopamine transporter cell surface localization facilitated by a direct interaction with the dopamine D2 receptor. EMBO J 26:2127-2136.
Lee KH, Kim MY, Kim DH, Lee YS (2004) Syntaxin 1A and receptor for activated C kinase interact with the N-terminal region of human dopamine transporter. NeurochemRes 29:1405-1409.
Leuner K, Muller WE (2006) The complexity of the dopaminergic synapses and their modulation by antipsychotics. Pharmacopsychiatry 39 Suppl 1:S15-20.
Lin DT, Huganir RL (2007) PICK1 and Phosphorylation of the Glutamate Receptor 2 (GluR2) AMPA Receptor Subunit Regulates GluR2 Recycling after NMDA Receptor-Induced Internalization. Journal of Neuroscience 27:13903-13908.
Lindvall O, Bjorklund A, Skagerberg G (1983) Dopamine-containing neurons in the spinal cord: anatomy and some functional aspects. Ann Neurol 14:255-260.
Lippincott-Schwartz J, Snapp E, Kenworthy A (2001) Studying protein dynamics in living cells. Nat Rev Mol Cell Biol 2:444-456.
Little KY, Kirkman JA, Carroll FI, Clark TB, Duncan GE (1993) Cocaine use increases [3H]WIN 35428 binding sites in human striatum. Brain Res 628:17-25.
Little KY, Elmer LW, Zhong H, Scheys JO, Zhang L (2002) Cocaine induction of dopamine transporter trafficking to the plasma membrane. Mol Pharmacol 61:436-445.
Loder MK, Melikian HE (2003) The dopamine transporter constitutively internalizes and recycles in a protein kinase C-regulated manner in stably transfected PC12 cell lines. J BiolChem 278:22168-22174.
Madsen KL, Beuming T, Niv MY, Chang CW, Dev KK, Weinstein H, Gether U (2005) Molecular determinants for the complex binding specificity of the PDZ domain in PICK1. J BiolChem 280:20539-20548.
Madsen KL, Eriksen J, Milan-Lobo L, Han DS, Niv MY, Ammendrup-Johnsen I, Henriksen U, Bhatia VK, Stamou D, Sitte HH, McMahon HT, Weinstein H, Gether U (2008) Membrane localization is critical for activation of the PICK1 BAR domain. Traffic 9:1327-1343.
Marazziti D, Mandillo S, Di Pietro C, Golini E, Matteoni R, Tocchini-Valentini GP (2007) GPR37 associates with the dopamine transporter to modulate dopamine uptake and behavioral responses to dopaminergic drugs. Proceedings of the National Academy of Sciences 104:9846-9851.

Matsuda W, Furuta T, Nakamura KC, Hioki H, Fujiyama F, Arai R, Kaneko T (2009) Single Nigrostriatal Dopaminergic Neurons Form Widely Spread and Highly Dense Axonal Arborizations in the Neostriatum. J Neurosci 29:444-453.

Maxfield FR, McGraw TE (2004) Endocytic recycling. Nat Rev Mol Cell Biol 5:121-132.

Mazei-Robison MS, Blakely RD (2005) Expression studies of naturally occurring human dopamine transporter variants identifies a novel state of transporter inactivation associated with Val382Ala. Neuropharmacology 49:737-749.

McMahon HT, Gallop JL (2005) Membrane curvature and mechanisms of dynamic cell membrane remodelling. Nature 438:590-596.

Meinild AK, Sitte HH, Gether U (2004) Zinc potentiates an uncoupled anion conductance associated with the dopamine transporter. Journal of Biological Chemistry 279:49671-49679.

Melikian HE (2004) Neurotransmitter transporter trafficking: endocytosis, recycling, and regulation. Pharmacol Ther 104:17-27.

Melikian HE, Buckley KM (1999) Membrane trafficking regulates the activity of the human dopamine transporter. Journal of Neuroscience 19:7699-7710.

Miranda M, Dionne KR, Sorkina T, Sorkin A (2007) Three Ubiquitin Conjugation Sites in the Amino Terminus of the Dopamine Transporter Mediate Protein Kinase C-dependent Endocytosis of the Transporter. Molecular Biology of the Cell 18:313-323.

Miranda M, Sorkina T, Grammatopoulos TN, Zawada WM, Sorkin A (2004) Multiple Molecular Determinants in the Carboxyl Terminus Regulate Dopamine Transporter Export from Endoplasmic Reticulum. J Biol Chem 279:30760-30770.

Miranda M, Wu CC, Sorkina T, Korstjens DR, Sorkin A (2005) Enhanced ubiquitylation and accelerated degradation of the dopamine transporter mediated by protein kinase C. Journal of Biological Chemistry 280:35617-35624.

Mollenhauer HH, Morre DJ, Rowe LD (1990) Alteration of intracellular traffic by monensin; mechanism, specificity and relationship to toxicity. Biochim Biophys Acta 1031:225-246.

Montagu KA (1957) Catechol compounds in rat tissues and in brains of different animals. Nature 180:244-245.

Moron JA, Zakharova I, Ferrer JV, Merrill GA, Hope B, Lafer EM, Lin ZC, Wang JB, Javitch JA, Galli A, Shippenberg TS (2003) Mitogen-Activated Protein Kinase Regulates Dopamine Transporter Surface Expression and Dopamine Transport Capacity. Journal of Neuroscience 23:8480-8488.

Mortensen OV, Larsen MB, Prasad BM, Amara SG (2008) Genetic complementation screen identifies a mitogen-activated protein kinase phosphatase, MKP3, as a regulator of dopamine transporter trafficking. Mol Biol Cell 19:2818-2829.

Mu Y, Otsuka T, Horton AC, Scott DB, Ehlers MD (2003) Activity-dependent mRNA splicing controls ER export and synaptic delivery of NMDA receptors. Neuron 40:581-594.

Nestler EJ (2005) The neurobiology of cocaine addiction. Sci Pract Perspect 3:4-10.

Nirenberg MJ, Vaughan RA, Uhl GR, Kuhar MJ, Pickel VM (1996a) The dopamine transporter is localized to dendritic and axonal plasma membranes of nigrostriatal dopaminergic neurons. J Neurosci 16:436-447.

Nirenberg MJ, Chan J, Liu Y, Edwards RH, Pickel VM (1996b) Ultrastructural localization of the vesicular monoamine transporter-2 in midbrain dopaminergic neurons: potential sites for somatodendritic storage and release of dopamine. J Neurosci 16:4135-4145.

Nirenberg MJ, Chan J, Vaughan RA, Uhl GR, Kuhar MJ, Pickel VM (1997) Immunogold localization of the dopamine transporter: an ultrastructural study of the rat ventral tegmental area. J Neurosci 17:5255-5262.

Nourry C, Grant SGN, Borg JP (2003) PDZ Domain Proteins: Plug and Play! Science Signaling 2003:re7.

Perez JL, Khatri L, Chang C, Srivastava S, Osten P, Ziff EB (2001) PICK1 targets activated protein kinase Calpha to AMPA receptor clusters in spines of hippocampal neurons and reduces surface levels of the AMPA-type glutamate receptor subunit 2. J Neurosci 21:5417-5428.

Peter BJ, Kent HM, Mills IG, Vallis Y, Butler PJ, Evans PR, McMahon HT (2004) BAR domains as sensors of membrane curvature: the amphiphysin BAR structure. Science 303:495-499.

Pfeffer S, Aivazian D (2004) Targeting Rab GTPases to distinct membrane compartments. Nat Rev Mol Cell Biol 5:886-896.

Pifl C, Singer EA (1999) Ion dependence of carrier-mediated release in dopamine or norepinephrine transporter-transfected cells questions the hypothesis of facilitated exchange diffusion. MolPharmacol 56:1047-1054.

Prasad BM, Amara SG (2001) The Dopamine Transporter in Mesencephalic Cultures Is Refractory to Physiological Changes in Membrane Voltage. J Neurosci 21:7561-7567.

Qi Y, Wang JKT, McMillian M, Chikaraishi DM (1997) Characterization of a CNS Cell Line, CAD, in which Morphological Differentiation Is Initiated by Serum Deprivation. J Neurosci 17:1217-1225.

Rashid AJ, So CH, Kong MM, Furtak T, El-Ghundi M, Cheng R, O'Dowd BF, George SR (2007) D1-D2 dopamine receptor heterooligomers with unique pharmacology are coupled to rapid activation of Gq/11 in the striatum. Proc Natl Acad Sci U S A 104:654-659.

Rocha BA, Fumagalli F, Gainetdinov RR, Jones SR, Ator R, Giros B, Miller GW, Caron MG (1998) Cocaine self-administration in dopamine-transporter knockout mice. Nat Neurosci 1:132-137.

Rothman RB, Baumann MH (2003) Monoamine transporters and psychostimulant drugs. Eur J Pharmacol 479:23-40.

Rudnick G (2006) Structure/function relationships in serotonin transporter: new insights from the structure of a bacterial transporter. Handb Exp Pharmacol:59-73.

Saunders C, Ferrer JV, Shi L, Chen J, Merrill G, Lamb ME, Leeb-Lundberg LM, Carvelli L, Javitch JA, Galli A (2000) Amphetamine-induced loss of human dopamine transporter activity: an internalization-dependent and cocaine-sensitive mechanism. ProcNatlAcadSciUSA 97:6850-6855.

Scholze P, Freissmuth M, Sitte HH (2002a) Mutations within an Intramembrane Leucine Heptad Repeat Disrupt Oligomer Formation of the Rat GABA Transporter 1. J Biol Chem 277:43682-43690.

Scholze P, Norregaard L, Singer EA, Freissmuth M, Gether U, Sitte HH (2002b) The role of zinc ions in reverse transport mediated by monoamine transporters. Journal of Biological Chemistry 277:21505-21513.

Schwartz JW, Blakely RD, DeFelice LJ (2003) Binding and Transport in Norepinephrine Transporters. REAL-TIME, SPATIALLY RESOLVED ANALYSIS IN SINGLE CELLS USING A FLUORESCENT SUBSTRATE. Journal of Biological Chemistry 278:9768-9777.

Sesack SR, Hawrylak VA, Matus C, Guido MA, Levey AI (1998) Dopamine axon varicosities in the prelimbic division of the rat prefrontal cortex exhibit sparse immunoreactivity for the dopamine transporter. J Neurosci 18:2697-2708.

Shimada S, Kitayama S, Lin CL, Patel A, Nanthakumar E, Gregor P, Kuhar M, Uhl G (1991) Cloning and expression of a cocaine-sensitive dopamine transporter complementary DNA. Science 254:576-578.

Sitte HH, Farhan H, Javitch JA (2004) Sodium-Dependent Neurotransmitter TRANSPORTERS: OLIGOMERIZATION as a Determinant of Transporter Function and Trafficking. Mol Interv 4:38-47.

Sitte HH, Huck S, Reither H, Boehm S, Singer EA, Pifl C (1998) Carrier-mediated release, transport rates, and charge transfer induced by amphetamine, tyramine, and dopamine in mammalian cells transfected with the human dopamine transporter. J Neurochem 71:1289-1297.

Sonders MS, Zhu SJ, Zahniser NR, Kavanaugh MP, Amara SG (1997) Multiple ionic conductances of the human dopamine transporter: the actions of dopamine and psychostimulants. Journal of Neuroscience 17:960-974.

Sorkin A, von Zastrow M (2009) Endocytosis and signalling: intertwining molecular networks. Nat Rev Mol Cell Biol 10:609-622.

Sorkin A, Krolenko S, Kudrjavtceva N, Lazebnik J, Teslenko L, Soderquist AM, Nikolsky N (1991) Recycling of epidermal growth factor-receptor complexes in A431 cells: identification of dual pathways. J Cell Biol 112:55-63.

Sorkina T, Hoover BR, Zahniser NR, Sorkin A (2005) Constitutive and protein kinase C-induced internalization of the dopamine transporter is mediated by a clathrin-dependent mechanism. Traffic 6:157-170.

Sorkina T, Doolen S, Galperin E, Zahniser NR, Sorkin A (2003) Oligomerization of Dopamine Transporters Visualized in Living Cells by Fluorescence Resonance Energy Transfer Microscopy. Journal of Biological Chemistry 278:28274-28283.

Sorkina T, Richards TL, Rao A, Zahniser NR, Sorkin A (2009) Negative Regulation of Dopamine Transporter Endocytosis by Membrane-Proximal N-Terminal Residues. Journal of Neuroscience 29:1361-1374.

Sorkina T, Miranda M, Dionne KR, Hoover BR, Zahniser NR, Sorkin A (2006) RNA interference screen reveals an essential role of Nedd4-2 in dopamine transporter ubiquitination and endocytosis. Journal of Neuroscience 26:8195-8205.

Steinberg JP, Takamiya K, Shen Y, Xia J, Rubio ME, Yu S, Jin W, Thomas GM, Linden DJ, Huganir RL (2006) Targeted in vivo mutations of the AMPA receptor subunit GluR2 and its interacting protein PICK1 eliminate cerebellar long-term depression. Neuron 49:845-860.

Stenmark H (2009) Rab GTPases as coordinators of vesicle traffic. Nat Rev Mol Cell Biol 10:513-525.

Sulzer D, Sonders MS, Poulsen NW, Galli A (2005) Mechanisms of neurotransmitter release by amphetamines: A review. Progress in Neurobiology 75:406-433.

Thomsen M, Han DD, Gu HH, Caine SB (2009) Lack of cocaine self-administration in mice expressing a cocaine-insensitive dopamine transporter. J Pharmacol Exp Ther 331:204-211.

Tilley MR, O'Neill B, Han DD, Gu HH (2009) Cocaine does not produce reward in absence of dopamine transporter inhibition. Neuroreport 20:9-12.

Torres GE, Carneiro A, Seamans K, Fiorentini C, Sweeney A, Yao WD, Caron MG (2003) Oligomerization and Trafficking of the Human Dopamine Transporter. MUTATIONAL ANALYSIS IDENTIFIES CRITICAL DOMAINS IMPORTANT FOR THE FUNCTIONAL EXPRESSION OF THE TRANSPORTER. Journal of Biological Chemistry 278:2731-2739.

Torres GE, Yao WD, Mohn AR, Quan H, Kim KM, Levey AI, Staudinger J, Caron MG (2001) Functional interaction between monoamine plasma membrane transporters and the synaptic PDZ domain-containing protein PICK1. Neuron 30:121-134.

Usdin TB, Mezey E, Chen C, Brownstein MJ, Hoffman BJ (1991) Cloning of the cocaine-sensitive bovine dopamine transporter. Proc Natl Acad Sci U S A 88:11168-11171.

Vaughan RA, Huff RA, Uhl GR, Kuhar MJ (1997) Protein Kinase C-mediated Phosphorylation and Functional Regulation of Dopamine Transporters in Striatal Synaptosomes. Journal of Biological Chemistry 272:15541-15546.

Volkow ND, Wang GJ, Fischman MW, Foltin RW, Fowler JS, Abumrad NN, Vitkun S, Logan J, Gatley SJ, Pappas N, Hitzemann R, Shea CE (1997) Relationship between subjective effects of cocaine and dopamine transporter occupancy. Nature 386:827-830.

Wall SC, Gu H, Rudnick G (1995) Biogenic amine flux mediated by cloned transporters stably expressed in cultured cell lines: amphetamine specificity for inhibition and efflux. Molecular Pharmacology 47:544-550.

Wayment HK, Schenk JO, Sorg BA (2001) Characterization of extracellular dopamine clearance in the medial prefrontal cortex: role of monoamine uptake and monoamine oxidase inhibition. J Neurosci 21:35-44.

Wei Y, Williams JM, Dipace C, Sung U, Javitch JA, Galli A, Saunders C (2007) Dopamine transporter activity mediates amphetamine-induced inhibition of Akt through a Ca2+/calmodulin-dependent kinase II-dependent mechanism. MolPharmacol 71:835-842.

Werkman TR, Glennon JC, Wadman WJ, McCreary AC (2006) Dopamine receptor pharmacology: interactions with serotonin receptors and significance for the aetiology and treatment of schizophrenia. CNS Neurol Disord Drug Targets 5:3-23.

Williams JM, Owens WA, Turner GH, Saunders C, Dipace C, Blakely RD, France CP, Gore JC, Daws LC, Avison MJ, Galli A (2007) Hypoinsulinemia regulates amphetamine-induced reverse transport of dopamine. PLoS Biol 5:e274.

Wolf ME, Granneman JG, Kapatos G (1991) Characterization of the distribution of $G_{\alpha o}$ in rat striatal synaptosomes and its colocalization with tyrosine hydroxylase. Synapse 9:66-74.

Wolfe DE, Potter LT, Richardson KC, Axelrod J (1962) Localizing Tritiated Norepinephrine in Sympathetic Axons by Electron Microscopic Autoradiography. Science 138:440-442.

Wu MM, Grabe M, Adams S, Tsien RY, Moore HP, Machen TE (2001) Mechanisms of pH regulation in the regulated secretory pathway. J Biol Chem 276:33027-33035.

Yamashita A, Singh SK, Kawate T, Jin Y, Gouaux E (2005) Crystal structure of a bacterial homologue of Na+/Cl--dependent neurotransmitter transporters. Nature 437:215-223.

Yudowski GA, Puthenveedu MA, von Zastrow M (2006) Distinct modes of regulated receptor insertion to the somatodendritic plasma membrane. Nat Neurosci 9:622-627.

Yudowski GA, Puthenveedu MA, Henry AG, von Zastrow M (2009) Cargo-Mediated Regulation of a Rapid Rab4-Dependent Recycling Pathway. Mol Biol Cell 20:2774-2784.

Yudowski GA, Puthenveedu MA, Leonoudakis D, Panicker S, Thorn KS, Beattie EC, von Zastrow M (2007) Real-Time Imaging of Discrete Exocytic Events Mediating Surface Delivery of AMPA Receptors. J Neurosci 27:11112-11121.

Zapata A, Kivell B, Han Y, Javitch JA, Bolan EA, Kuraguntla D, Jaligam V, Oz M, Jayanthi LD, Samuvel DJ, Ramamoorthy S, Shippenberg TS (2007) Regulation of Dopamine Transporter Function and Cell Surface Expression by D3 Dopamine Receptors. Journal of Biological Chemistry 282:35842-35854.

Zhu SJ, Kavanaugh MP, Sonders MS, Amara SG, Zahniser NR (1997) Activation of Protein Kinase C Inhibits Uptake, Currents and Binding Associated with the Human Dopamine Transporter Expressed in Xenopus Oocytes. Journal of Pharmacology And Experimental Therapeutics 282:1358-1365.

# Paper 1

# Visualization of Dopamine Transporter Trafficking in Live Neurons by Use of Fluorescent Cocaine Analogs

Cellular/Molecular

# Visualization of Dopamine Transporter Trafficking in Live Neurons by Use of Fluorescent Cocaine Analogs

**Jacob Eriksen,[1]* Søren G. F. Rasmussen,[1]* Trine Nygaard Rasmussen,[1] Christian Bjerggaard Vaegter,[1] Joo Hwan Cha,[2] Mu-Fa Zou,[2] Amy Hauck Newman,[2] and Ulrik Gether[1]**

[1]Molecular Neuropharmacology Group and Center for Pharmacogenomics, Department of Neuroscience and Pharmacology, The Panum Institute, University of Copenhagen, DK-2200 Copenhagen N, Denmark, and [2]Medicinal Chemistry Section, National Institute on Drug Abuse–Intramural Research Program, National Institutes of Health, Baltimore, Maryland 21224

**The dopamine transporter (DAT) mediates reuptake of dopamine from the synaptic cleft and is a target for widely abused psychostimulants such as cocaine and amphetamine. Nonetheless, little is known about the cellular distribution and trafficking of natively expressed DAT. Here we use novel fluorescently tagged cocaine analogs to visualize DAT and DAT trafficking in cultured live midbrain dopaminergic neurons. The fluorescent tags were extended from the tropane N-position of 2$\beta$-carbomethoxy-3$\beta$-(3,4-dichlorophenyl)tropane using an ethylamino-linker. The rhodamine-, OR Green-, or Cy3-labeled ligands had high binding affinity for DAT and enabled specific labeling of DAT in live neurons and visualization by confocal imaging. In the dopaminergic neurons, DAT was uniformly distributed in the plasma membrane of the soma, the neuronal extensions, and varicosities along these extensions. FRAP (fluorescence recovery after photobleaching) experiments demonstrated bidirectional movement of DAT in the extensions and indicated that DAT is highly mobile both in the extensions and in the varicosities (immobile fraction less than ~30%). DAT was constitutively internalized into vesicular structures likely representing intracellular transporter pools. The internalization was blocked by lentiviral-mediated expression of dominant-negative dynamin and internalized DAT displayed partial colocalization with the early endosomal marker EGFP-Rab5 and with the transferrin receptor. DAT internalization and function was not affected by activation of protein kinase C (PKC) with phorbol-12-myristate-13-acetate (PMA) or by inhibition with staurosporine or GF109203X. These data are in contrast to findings for DAT in transfected heterologous cells and challenge the paradigm that trafficking and cellular distribution of endogenous DAT is subject to regulation by PKC.**

## Introduction

The dopamine transporter (DAT) mediates reuptake of dopamine from the synaptic cleft and in this way terminates dopaminergic signaling (Chen et al., 2004; Gether et al., 2006; Torres and Amara, 2007). Alteration in dopamine signaling and DAT function is coupled to neurological and psychiatric diseases including schizophrenia, bipolar disorder, ADHD (attention-deficit hyperactivity disorder), Tourette's syndrome, and Parkinson's disease (Gainetdinov and Caron, 2003; Torres et al., 2003; Gether et al., 2006). DAT is also the principle target for widely abused psychostimulants, such as cocaine and amphetamine (Chen et al., 2004; Gether et al., 2006; Torres and Amara, 2007). The transporter belongs to the family of neurotransmitter:sodium symporters (NSS) [also called the SLC6 (solute carrier 6) family or $Na^+/Cl^-$ coupled transporters] that in addition includes the transporters for norepinephrine, serotonin, glycine, and GABA. NSS proteins use the transmembrane $Na^+$ gradient as a driving force for transport of substrate and are characterized by additional cotransport of $Cl^-$ (Chen et al., 2004; Gether et al., 2006; Torres and Amara, 2007; Zomot et al., 2007).

It is assumed that DAT is subject to specific cellular regulation ensuring proper availability and activity of the transporter in the neuron. The most widely described regulatory mechanism involves redistribution of the transporter to an intracellular compartment in response to protein kinase C (PKC) activation (Daniels and Amara, 1999; Melikian and Buckley, 1999; Blakely and Bauman, 2000; Granas et al., 2003; Miranda et al., 2007). DAT trafficking might also be regulated by other protein kinases such as mitogen-activated protein kinase (MAPK) and Akt (Morón et al., 2003; Garcia et al., 2005) as well as being affected by substrates and inhibitors. Both dopamine and amphetamine have been shown to cause transporter internalization (Saunders et al., 2000; Chi and Reith, 2003), whereas cocaine was shown to acutely enhance DAT surface availability although the effect was relatively modest (Daws et al., 2002). A constitutive internalization signal in the DAT C terminus has recently been identified (Holton et al., 2005; Sorkina et al., 2005); however, it is not

Received Sept. 2, 2008; revised April 6, 2009; accepted April 15, 2009.

This work was supported in part by National Institutes of Health (NIH) Grant P01 DA 12408 (U.G.), the Lundbeck Foundation (U.G.), the Danish Medical Research Councils (U.G.), "Fabrikant Vilhelm Pedersen og Hustrus Mindelegat" (U.G.), and National Institute on Drug Abuse Intramural Research Program (NIDA-IRP), NIH (A.H.N.). We thank Dr. Erika Adkins for critical advice on the FRAP measurements and Dr. Alexandra Newton for providing the cDNA encoding CKAR. We thank Donna Czerny and Nabeela Khadim for excellent technical assistance. The MALDI-TOF spectra were obtained by Dr. Amina Woods, NIDA-IRP.

*J.E. and S.G.F.R. contributed equally to this work.

Correspondence should be addressed to Dr. Ulrik Gether, Molecular Neuropharmacology Group and Center for Pharmacogenomics, Department of Neuroscience and Pharmacology, The Panum Institute, University of Copenhagen, DK-2200 Copenhagen N, Denmark. E-mail: gether@sund.ku.dk.

DOI:10.1523/JNEUROSCI.4177-08.2009

 0270-6474/09/296794-15$15.00/0

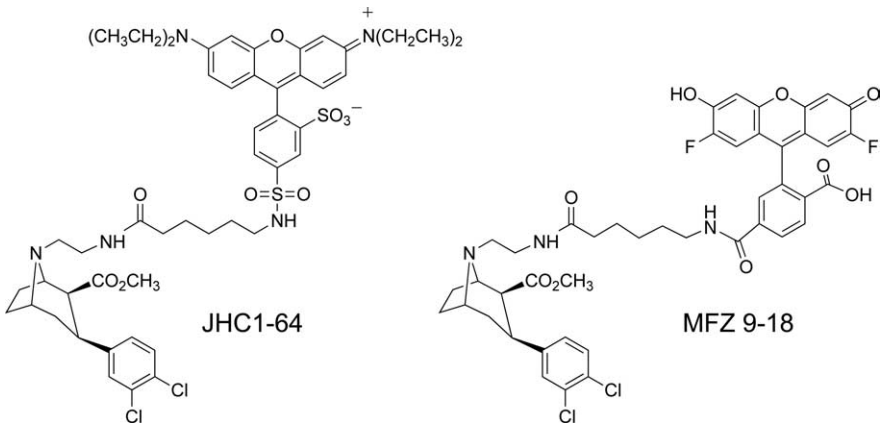


**Figure 1.** Structure of fluorescently labeled cocaine analogs. Left, The rhodamine conjugate JHC 1–64. Right, The Oregon Green conjugate MFZ 9–18. JHC 1–64 was synthesized as described previously (Cha et al., 2005). MFZ 9–18 was synthesized as described in Materials and Methods. For both compounds, the fluorescent tag was extended from the N-position of 2$\beta$-carbomethoxy-3$\beta$-(3,4-dichlorophenyl)tropane using an ethylamino-linker.

known whether this signal operates in the natively expressed transporter.

The vast majority of studies performed on DAT trafficking have been performed in non-neuronal and transfected heterologous expression systems and not on endogenously expressed transporter. One major problem is the relatively low number of dopaminergic and thereby DAT expressing neurons in the brain. As a consequence, it is generally difficult to obtain neuronal cultures containing a high fraction of dopaminergic neurons (di Porzio et al., 1987; Silva et al., 1988; Rayport et al., 1992; Ingram et al., 2002) making qualitative and quantitative studies of DAT regulation difficult. It has also appeared notoriously difficult to develop an efficient antibody against an extracellular epitope of the DAT and, thus, labeling of endogenous DAT in living cells has not been possible. To develop tools that might permit visualization of DAT in living cells, we recently synthesized a series of rhodamine-coupled fluorescent cocaine analogs (Cha et al., 2005). Here we use one of these ligands together with two new fluorescent cocaine analogs to visualize endogenously expressed DAT and its trafficking in primary cultures of rat midbrain dopaminergic neurons.

## Materials and Methods

*Synthesis of fluorescent ligands.* JHC 1–64 was synthesized as previously described (Cha et al., 2005). MFZ 9–17 was synthesized by adding diisopropylethylamine (6.0 mg, 47.0 $\mu$mol) to a solution of (−)-*N*-(2-aminoethyl)-2$\beta$-carbomethoxy-3$\beta$-(3.4-dichlorophenyl)-tropane (Cha et al., 2005) (6 mg, 16.85 $\mu$mol) and Cy3 *N*-hydroxysuccinimide ester (10 mg, 13.05 $\mu$mol) in DMF (2 ml) and the mixture was stirred overnight at 40–45°C. The solvent was then removed under reduced pressure and the resulting residue was purified directly by preparative thin-layer chromatography, eluting with $CHCl_3$-MeOH-28% $NH_4OH$ (70:30:1) to provide 13 mg (100%) of MFZ 9–17 as a red solid. MALDI-TOF MS calculated for $C_{48}H_{59}N_4Cl_2O_9S_2$ ($[M+H]^+$) was as follows: 969.31; found: 969.30. MFZ 9–18 was prepared from (−)-*N*-(2-aminoethyl)-2$\beta$-carbomethoxy-3$\beta$-(3.4-dichlorophenyl)-tropane (Cha et al., 2005) (10.3 mg, 28.9 $\mu$mol) and Oregon Green 488-X, *N*-succinimidyl ester (15 mg, 24.09 $\mu$mol) by the same procedure as described for MFZ 9–17 in quantitative yield as an orange solid. MALDI-TOF MS calculated for $C_{44}H_{41}N_3Cl_2F_2O_9$ ($[M+H]^+$) was as follows: 864.22; found: 864.23.

*Molecular biology.* A synthetic gene encoding the human DAT (hDAT) in the bicistronic vector pCIHygro and hDAT tagged at the N terminus with enhanced green fluorescent protein (EGFP-hDAT) were kindly provided by Dr. Jonathan A. Javitch, Columbia University (New York, NY) (Rees et al., 1996; Saunders et al., 2000). The cDNAs encoding dynamin and the dominant-negative dynamin mutant K44A in pFUGW-IRES-GFP were kind gifts from Dr. Rosalind A. Segal (Harvard Medical School, Boston, MA) (Zhou et al., 2007). pHsSynXW EGFP-Rab5a was generated by excising the cDNA encoding EGFP-Rab5A from pEGFP Rab5A (a kind gift from Dr. Katherine W. Roche, National Institute of Neurological Disorders and Stroke, Bethesda, MD) (Lavezzari et al., 2004) using Age1 and HpaI restriction sites followed by insertion into the lentiviral transfer vector pHsCXW (Leander Johansen et al., 2005). The CMV promoter was replaced with the promoter of synapsin to ensure selective neuronal expression (Dittgen et al., 2004).

*Cell culture and transfection.* Human embryonic kidney cells (HEK) 293 were grown in DMEM with GlutaMax (L-alanyl-L-glutamine), 10% fetal calf serum, and 0.01 mg/ml gentamicin (all reagents from Invitrogen) at 37°C in a humidified 5% $CO_2$ atmosphere. For stable expression of hDAT and EGFP-hDAT, HEK293 cells were seeded in 100 mm tissue culture plates, grown to ~30% confluence, and subsequently transfected with 2 $\mu$g of the pCIHygro constructs using Lipofectamine according to the instructions from the manufacturer (Invitrogen). A stably transfected pool was selected with 200 $\mu$g/ml hygromycin (Invitrogen) starting 2 d after transfection and continuing until control cells were dead, after which selection pressure were maintained with 100 $\mu$g/ml hygromycin. For transient expression of hDAT, HEK293 cells ($3 \times 10^6$ cells) were seeded in 75 $cm^2$ flasks. The cells were transfected the day after seeding with 3 $\mu$g of DNA and 9 $\mu$l of Lipofectamine 2000 reagent according to the manufacturer's instructions.

*Preparation and culturing of neurons.* Postnatally derived rat midbrain dopaminergic neurons were isolated and grown modified from (Rayport et al., 1992). Briefly, the cultures were obtained from the ventral midbrain of 1- to 3-d-old pups. The dissected tissue sample was digested in a papain solution for ~30 min at 37°C while slowly superfused with a mixture of 95% $O_2$ and 5% $CO_2$. The digested tissue was carefully triturated into single cells using increasingly smaller pipette tips. The cells were centrifuged at 500 × *g* for 5 min and resuspended in warm SF1C consisting of 50% MEM (Modified Eagle's Medium), 40% DMEM, and 10% F-12 Ham's nutrient mixture (all from Invitrogen) supplemented with bovine serum albumin (2.5 mg/ml), D-glucose (0.35%), glutamine (0.5 mM), 1% heat-inactivated calf serum (Invitrogen), kynurenic acid (5 mM), penicillin, streptomycin, liquid catalase (0.05%), and DiPorzio (di Porzio et al., 1980) (containing insulin, transferrin, superoxide dismutase, progesterone, cortisol, $Na_2SeO_3$, and T3). The neurons were plated on a monolayer of glial cells grown on coverslips. The cells were allowed to settle for ~2 h before addition of GDNF (Millipore Bioscience Research Reagents) (10 ng/ml). The next day 5-fluorodeoxyuridine was added to inhibit growth of glial cells. The cultures were used for experiments after 4–16 d *in vitro* (DIV).

*Lentivirus production and transduction.* Lentiviral vectors were produced according to procedures modified from Naldini et al. (1996b). HEK293T packaging cells (ATCC number CRL-11268) were plated on poly-ornithine-coated 175 $cm^2$ flasks and transiently triple transfected with the following: (1) 18 $\mu$g of a packaging plasmid encoding viral structure proteins (pBR$\Delta$8.91) (Zufferey et al., 1997); (2) 12 $\mu$g of an envelope plasmid encoding the envelope protein VSV-G (pMD.G) (Naldini et al., 1996a); and (3) 18 $\mu$g of the transfer plasmid containing the gene of interest (pFUGW-IRES-GFP Dynamin, pFUGW-IRES-GFP Dynamin K44A, pHsSynXW CKAR, or pHsSynXW EGFP-Rab5a). Transfection was performed in DMEM (Invitrogen) supplemented with 10% FBS (Invitrogen) using calcium phosphate precipitation. Medium was replaced with fresh medium after 5 h. Approximately 48 and 72 h after transfection, media containing lentivirus was collected, centrifuged at 900 × *g* for 5 min to remove cellular debris, filtered through a 0.45 $\mu$m filter, and concentrated by ultracentrifugation at 50,000 × *g* for 1.5 h at 4°C. The virus-containing pellet was resuspended in MEM (Sigma) at

1/280 of the original volume and stored in aliquots at −80°C. The neuronal cultures were incubated with concentrated lentivirus on days 2–3 *in vitro* and experiments were performed 6–8 d after infection.

*Immunocytochemistry.* Dopaminergic neurons, grown on a monolayer of glial cells on coverslips, were incubated with 10 nM JHC 1–64 in buffer 1 (25 mM HEPES, pH 7.4, with 130 mM NaCl, 5.4 mM KCl, 1.2 mM $CaCl_2$, 1.2 mM $MgSO_4$, 1 mM L-ascorbic acid, 5 mM D-glucose) for 20 min at room temperature (RT). Subsequently, the cells were washed and fixed in 3.7% formaldehyde in PBS for 20 min at 4°C before the specimen was permeabilized and blocked in blocking/permeabilization buffer (0.1% digitonin, 1% bovine serum albumin, and 5% goat serum in PBS). The neurons were stained with either a rat anti-DAT antibody (1:1000; MAB369; Millipore Bioscience Research Reagents), rabbit anti-VMAT2 (vesicular monoamine transporter 2) antibody (1:1000; Peel-Freez Biologicals), or a rabbit anti-TH (tyrosine hydroxylase) antibody (1:1000; Affinity Bioreagents) in blocking/permeabilization buffer for 1 h, washed 3 times in PBS, and incubated for 30 min with either Alexa Fluor 488 goat anti-rat or goat anti-rabbit antibody (1:500; Invitrogen). Finally, the specimens were mounted on glass slides with SlowFade Antifade (Invitrogen). The specimens were imaged using a Zeiss LSM 510 confocal laser-scanning station with an oil-immersion 63× 1.4 NA objective (Zeiss). JHC 1–64 was visualized using a 543 nm HeNe laser line and a 585 nm long-pass filter, whereas Alexa Fluor 488 was excited with the 488 nm laser line from an argon–krypton laser and the emitted light was detected using a 505–550 nm bandpass filter.

*Live cell imaging.* HEK293 cells stably expressing either hDAT or EGFP-tagged hDAT were grown in DMEM plus 10% FCS in poly-L-ornithine-treated 8-well LabTek Chambers. On the day of the experiment, the cells were incubated with the indicated fluorescent cocaine analogs in PBS with 5 mM glucose for designated time periods. After incubation, the living cells were imaged at RT using a Zeiss LSM 510 with a 63× NA 1.4 objective (Zeiss). The compounds JHC 1–64 and MFZ 9–17 were visualized using a 543 nm HeNe laser line and a 585 nm long-pass filter, whereas MFZ 9–18 and EGFP were detected with a 488 nm argon–krypton laser line and a 505–530 nm bandpass filter.

For imaging in dopaminergic neurons, ventral midbrain neurons grown in 2-well LabTek chambers on a glial monolayer for 4–16 DIV were used for all live neuron imaging studies. The neurons were incubated with 5 nM JHC 1–64 or 10 nM MFZ 9–18 in buffer 1 (25 mM HEPES, pH 7.4, with 130 mM NaCl, 5.4 mM KCl, 1.2 mM $CaCl_2$, 1.2 mM $MgSO_4$, 1 mM L-ascorbic acid, 5 mM D-glucose) for 20 min at room temperature. As controls for JHC 1–64's DAT specificity in neurons, the cultures were either preincubated with 1 mM dopamine, 1 $\mu$M mazindol, 10 $\mu$M desmethylimipramine, or 1 $\mu$M citalopram in uptake buffer for 15 min, before addition of 5 nM JHC 1–64 to the buffer and incubation for 20 min at RT. The cells were imaged as described for the HEK293 live cell experiments.

To detect internalization in midbrain dopaminergic neurons, the cultures were incubated with 5 nM JHC 1–64 for 30 min at 4°C, before the buffer was removed and replaced with 37°C warm uptake buffer (containing vehicle, 450 mM sucrose, or 1 $\mu$M PMA) and incubated for 30 or 60 min at 37°C (or 4°C for a temperature control). For the transferrin cointernalization experiments we used Alexa Fluor 488-conjugated transferrin (1:100; Invitrogen). After incubation the neurons were imaged at room temperature with same settings as described for the HEK293 cells and the distribution of JHC 1–64 on the neurons were analyzed with a *Z*-scan.

Time lapses were performed on midbrain dopaminergic neurons grown in LabTek chambers and incubated with 5 nM JHC 1–64 in buffer 1 for up to 1 h at 37°C to allow labeling of the DAT and subsequent constitutive internalization of the JHC 1–64/DAT complex. Next, the cells were washed once with buffer 1 and analyzed on the Zeiss LSM510 station with a heated stage kept at 37°C. The JHC 1–64/DAT complex was visualized by excitation with a 543 nm HeNe laser line. Pictures are an average of 2 line scans. Time series were obtained with 300 pictures in 20 min.

*Fluorescence recovery after photobleaching.* Cultures of midbrain dopaminergic neurons were labeled with 5 nM JHC 1–64 for 20 min followed by washing the cells in buffer 1. The neurons were subsequently kept in buffer with 10 $\mu$M RTI55 during the experiment to avoid any rebinding of JHC 1–64 to DAT. The fluorescence recovery after photobleaching (FRAP) measurements and calculations were performed essentially as described (Adkins et al., 2007). Spot photobleaching using circular regions of interest (ROIs) of 1–3 $\mu$m in diameter were placed on the neu-

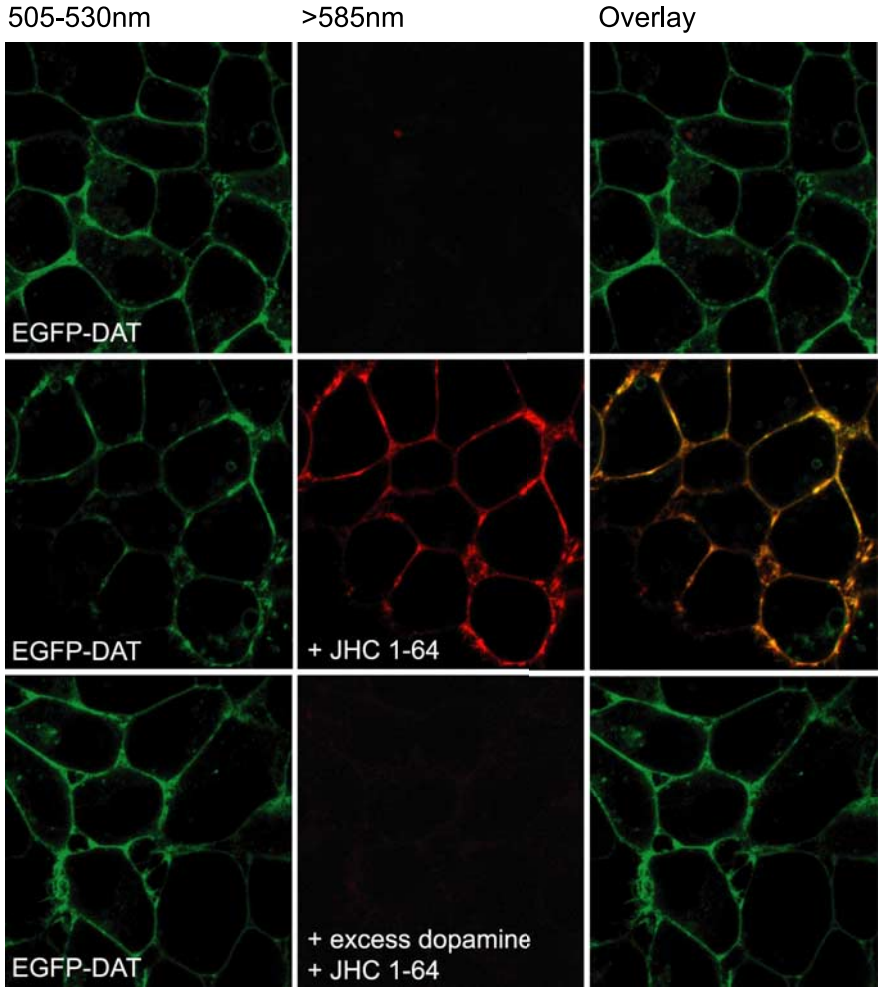


**Figure 2.** Specific labeling of EGFP-DAT with the fluorescent cocaine analog JHC 1–64. Top, Live HEK293 cells stably expressing EGFP-DAT without JHC 1–64 preincubation. Middle, Live HEK293 cells stably expressing EGFP-DAT preincubated with 5 nM JHC 1–64 for 20 min at RT. Bottom, Live HEK293 cells stably expressing EGFP-DAT preincubated with 1 mM dopamine for 15 min followed by 5 nM JHC 1–64 for 20 min at RT. EGFP fluorescence (left) was visualized using a 488 nm argon laser for excitation and a 505–530 nm bandpass filter for recording of fluorescence. For visualization of JHC 1–64 we used a 543 nm HeNe laser for excitation and a >585 nm long-pass filter for recording of fluorescence. The shown images are representative of at least five similar experiments with the same result.

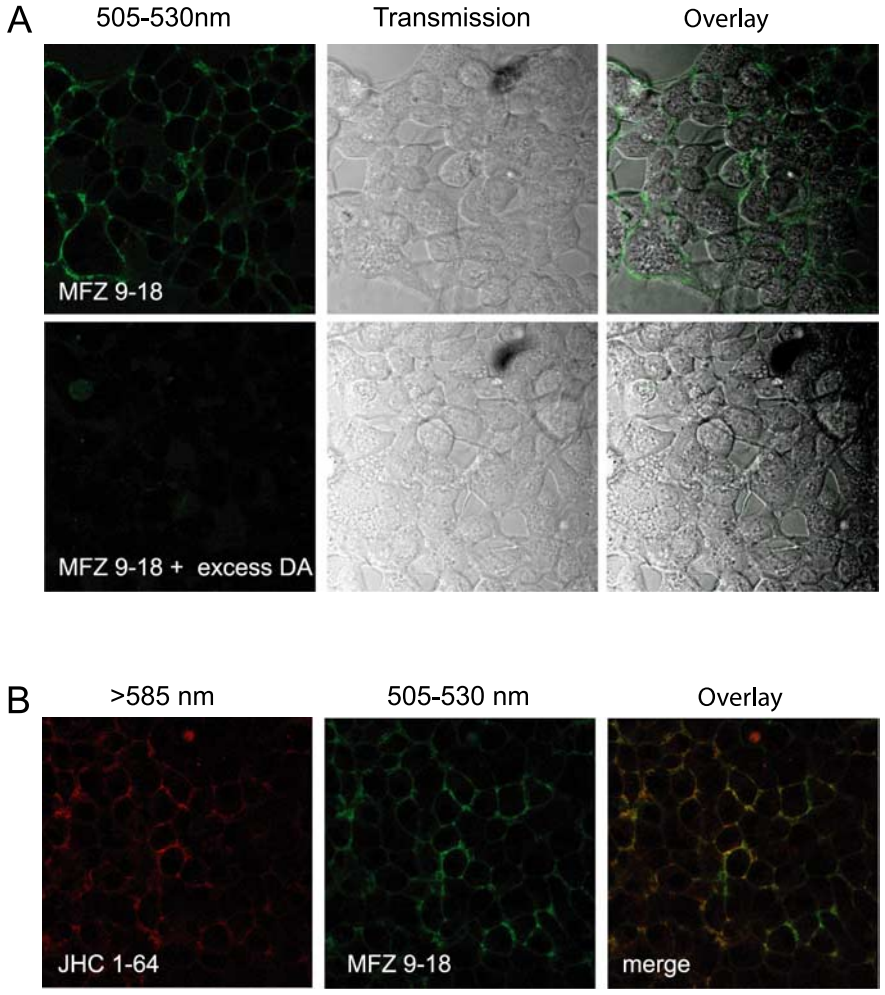


**Figure 3.** Specific labeling of DAT with the fluorescent cocaine analog MFZ 9–18. ***A***, Live HEK293 cells stably expressing DAT preincubated with 10 nM MFZ 9–18 for 20 min at RT (top) or with 1 mM dopamine for 15 min followed by 10 nM MFZ 9–18 for 20 min at RT (bottom). MFZ 9–18 was visualized using a 488 nm argon laser for excitation and a 505–530 nm bandpass filter for recording of fluorescence. ***B***, Live HEK293 cells stably expressing DAT preincubated with 10 nM MFZ 9–18 and 5 nM JHC 1–64 for 20 min at RT. The left panel shows fluorescence in the >585 nm channel, the middle panel shows fluorescence in the 505–530 nm channel, and the right panel shows overlay of the two channels. The shown images are representative of three similar experiments with the same result.

ronal extensions or boutons of the selected neurons, followed by bleaching of the region with the 488 nm laser line at 100% output for ~700 ms to obtain 30–70% bleaching compared with prebleach image. The pinhole was kept fully open to ensure complete bleaching through the cell. The transmission intensity was no higher than 1%, and the bleaching of the sample due to imaging was negligible according to experiments on fixed cells (data not shown). Images were obtained every 500 ms for an average of 1 min using the 543 nm laser line and a 585 nm long-pass filter. Measurements up to 5 min were also performed, with no change in diffusion time or mobile fraction observable after the first minute. Images were processed with Photoshop 6.0 (Adobe), and recovery curves were calculated using nonlinear least-squares fits in ORIGIN 5.0 (OriginLab) set to the general equation for FRAP as by (Yguerabide et al., 1982). The diffusion coefficient was determined using the following equation:

$$D = \omega_1^2/4\tau_D, \quad (1)$$

where $\omega$ is radius of the ROI set in the Zeiss program, and the $\tau_D$ is determined from the fit of the recovery curve. Because the thickness of the cell was less than the bleached volume in the $z$ direction, Equation 1 was used to determine diffusion coefficients. All measurements were performed at 22°C.

*Dopamine uptake in neurons.* The media was removed from midbrain neurons grown on a glial monolayer in 24-well plates (13–15 DIV) and buffer 1, containing 1 μM PMA, 1 μM staurosporine, 1 μM GF109203X, or vehicle was added before incubation for 30 min at 37°C. The incubation was terminated by aspirating the buffer followed by addition of 400 μl of buffer 1 containing 1 μM the catechol-*O*-methyltransferase inhibitor Ro 41–0960 (Sigma) and 100 μM pargyline (Sigma). Subsequently, 50 μl of vehicle or 10 μM cocaine (final concentration) for determination of nonspecific binding was added before addition of either ~100 nM [$^3$H]dopamine [2,5,6-($^3$H)-dopamine (7–21 Ci/mmol) (GE Healthcare)] or ~100 nM [$^3$H]dopamine plus 1 μM unlabeled in 50 μl of buffer 1. After 3 min of incubation at RT, the cells were washed twice with 500 μl of ice-cold buffer 1, lysed in 250 μl of 1% SDS, and left for 1 h at 37°C. Nonspecific binding was determined in the presence of 100 μM cocaine. All samples were subsequently transferred to 24-well counting plates (PerkinElmer Life Sciences) followed by addition of 500 μl of Opti-phase HiSafe 3 scintillation fluid (PerkinElmer Life Sciences). The samples were counted in a Wallac Tri-Lux β scintillation counter (PerkinElmer Life Sciences). All determinations were performed in triplicate. [$^3$H]dopamine uptake experiments in HEK293 cells transiently expressing the hDAT to determine inhibition constants for the fluorescent ligands were done as recently described (Cha et al., 2005).

## Results

### Synthesis of fluorescent cocaine ligands

We have recently synthesized fluorescent cocaine analogs containing rhodamine as the fluorescent moiety (Cha et al., 2005). Of these, JHC 1–64 showed the highest affinity for the human DAT (hDAT) (Cha et al., 2005). The fluorescent tag was extended from the N-position of 2β-carbomethoxy-3β-(3,4-dichlorophenyl)tropane using an ethylamino-linker (Fig. 1). To generate a ligand with a different fluorescent spectrum we coupled an Oregon Green moiety to the tropane nitrogen of the parent compound 2β-carbomethoxy-3β-(3,4-dichlorophenyl)tropane, using the ethylamino linker to give MFZ 9–18 (Fig. 1). Likewise, to generate a more photostable ligand than JHC 1–64, we coupled a Cy3 moiety to the ethylamino-linked tropane nitrogen of the parent compound to give MFZ 9–17 (supplemental Fig. S1, available at www.jneurosci.org as supplemental material). In this way, all three ligands possessed the identical pharmacophore and only differed in the fluorescent moiety extended from the tropane nitrogen (Fig. 1; supplemental Fig. S1, available at www.jneurosci.org as supplemental material).

To estimate the affinity of the two new ligands for the hDAT we determined the potency by which they inhibited [$^3$H]dopamine uptake into COS-7 cells transiently expressing the hDAT. The calculated $K_I$ values were 104 nM [SE interval (69.2;156 nM), $n = 3$] for MFZ 9–17 and 142 nM [SE interval (57.5;353 nM), $n = 3$] for MFZ 9–18. For JHC 1–64, we previously reported a $K_I$ value of 62 nM based on [$^3$H]dopamine uptake inhibition experiments and a value of 18 nM based on [$^3$H]CFT competition binding

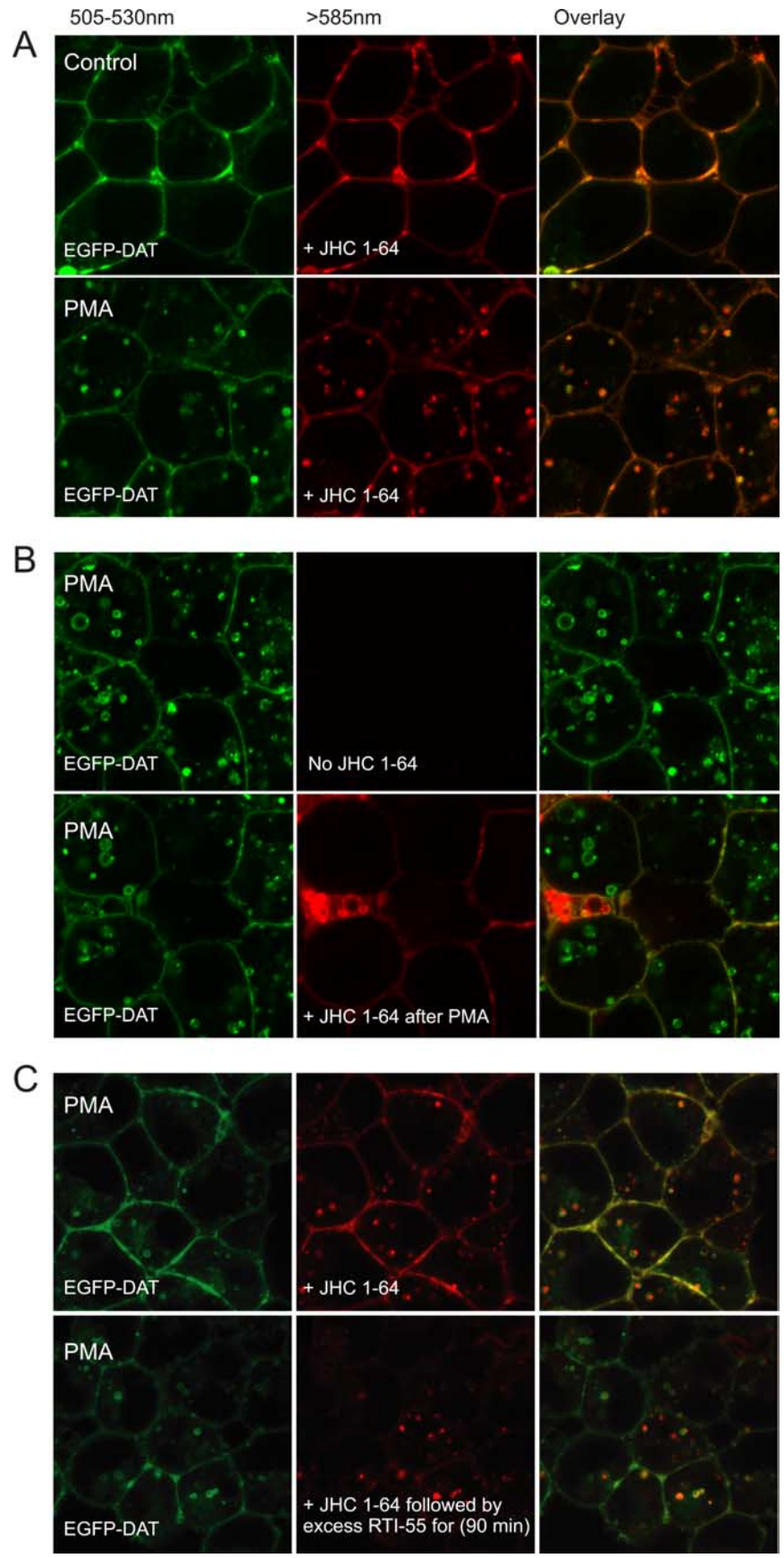


**Figure 4.** Visualization of DAT internalization in HEK293 cells expressing EGFP-DAT using the fluorescent cocaine analog JHC 1–64. ***A***, PMA promotes internalization of the EGFP-DAT/JHC 1–64 complex in live HEK293 cells stably expressing EGFP-DAT. The cells were incubated in the presence of 5 nM JHC 1–64 in PBS plus 5 mM glucose at RT for 20 min before incubation in the absence (top) or presence of 1 $\mu$M PMA (bottom) for 30 min at 37°C. ***B***, JHC 1–64 only labels EGFP-DAT in the plasma membrane and not internalized EGFP-DAT. HEK293 cells stably expressing EGFP-DAT was incubated for 30 min at 37°C in the presence of 1 $\mu$M PMA to obtain a fraction of internalized EGFP-DAT before labeling for 20 min in the absence (top) or presence of 5 nM JHC 1–64 at RT. ***C***, JHC 1–64 has a slow off-rate from EGFP-DAT and JHC 1–64 colocalizes with internalized DAT even after 90 min of incubation. HEK293 cells stably expressing EGFP-DAT was incubated with 5 nM JHC 1–64 for 20 min at RT before incubation for 30 min at 37°C. As in ***A***, this resulted in robust internalization of the DAT/JHC 1–64 complex (top). Subsequently, an excess of the high-affinity cocaine analog RTI-55 was added (10 $\mu$M) before incubation for up to 90 min at 37°C. JHC 1–64 only slowly dissociated from the cell surface and the dissociation was only visible after 90 min (bottom). However, even after 90 min of incubation, JHC 1–64 remained colocalized with EGFP-DAT, suggesting JHC 1–64 as a reliable marker for endocytosed DAT. Left panels show fluorescence in the 505–530 nm channel (EGFP), middle panels show fluorescence in the >585 nm channel (JHC 1–64), and right panels show overlay of the two channels. The shown images are representative of at least three similar experiments with the same results.

experiments (Cha et al., 2005). Thus, coupling of either Oregon Green or Cy3 instead of rhodamine to the parent compound 2$\beta$-carbomethoxy-3$\beta$-(3,4-dichlorophenyl)tropane was also well tolerated by the transporter resulting in two additional high affinity fluorescently tagged DAT ligands.

**Visualization of DAT in living HEK293 cells by the fluorescent cocaine analogs**

To demonstrate DAT labeling by JHC 1–64, we used HEK293 cells stably expressing hDAT with EGFP fused to the N terminus. The EGFP-hDAT cells were incubated for 20 min with vehicle, 5 nM JHC 1–64, or 5 nM JHC 1–64 plus 1 mM dopamine at RT. The cells were subsequently analyzed by confocal imaging. Recording from the EGFP channel (505–530 nm) showed that EGFP-hDAT was uniformly expressed in the plasma membrane (Fig. 2). An essentially identical pattern was observed in the JHC 1–64 channel (>585 nm) upon labeling with JHC 1–64 but no fluorescence was observed in the absence of JHC 1–64 and no fluorescence was observed when EGFP-hDAT was blocked with dopamine (Fig. 2). Specific labeling of DAT by JHC 1–64 is further supported by our previous observation that JHC 1–64 only labeled DAT transfected and not nontransfected HEK293 cells (Cha et al., 2005). Together, our data strongly suggest that JHC 1–64 labels DAT with high specificity and signal-to-noise ratio.

DAT could also be specifically labeled with MFZ 9–17 (supplemental Fig. S1,

available at www.jneurosci.org as supplemental material) and MFZ 9–18 (Fig. 3). The Oregon Green label in MFZ 9–18 was visualized with the same settings of the microscope as for EGFP (Fig. 3*A*), whereas the Cy3 label in MFZ 9–17 was visualized with the same settings as those used for JHC 1–64 (supplemental Fig. S1, available at www.jneurosci.org as supplemental material). For both ligands, we obtained a uniform labeling of the plasma membrane that was completely blocked by an excess of dopamine consistent with specific labeling of DAT. Additionally, simultaneous labeling with the spectrally distinct compounds JHC 1–64 and MFZ 9–18 revealed overlapping pattern as also would be expected if both ligands specifically bound the hDAT (Fig. 3*B*).

**Visualization of DAT internalization**

Activation of PKC by phorbol esters, such as PMA, is known to cause acute internalization of the DAT in heterologous cell systems (Daniels and Amara, 1999; Melikian and Buckley, 1999; Blakely and Bauman, 2000; Granas et al., 2003; Miranda et al., 2007). To investigate whether we could use the fluorescent cocaine analogs to visualize this internalization, we incubated HEK293 cells stably expressing the EGFP-hDAT with 5 nM JHC 1–64 for 20 min at RT followed by incubation for 30 min at 37°C in the presence or absence of 1 $\mu$M PMA. While no apparent change in distribution was observed with vehicle, PMA treatment led to the appearance of intracellular fluorescence in vesicular structures both in the EGFP and in the JHC 1–64 channel consistent with internalization of the transporter (Fig. 4*A*). In another experiment, we treated the cells with PMA before labeling with JHC 1–64. In the EGFP channel we observed, as expected, clear signs of internalization with significant intracellular fluorescence in vesicular structures; however, we did not observe any intracellular fluorescence from JHC 1–64 (Fig. 4*B*). This suggests that JHC 1–64 labels DAT at the surface and that in the time frame of the experiment, the compound does not pass the plasma membrane and label intracellularly localized DAT, to any measurable extent.

We also tested whether JHC 1–64 itself would influence DAT trafficking by use of HEK293 cells transfected with a modified hDAT containing an extracellular HA-tag in the second extracellular loop (HA-DAT) (Sorkina et al., 2006). Insertion of this extracellular tag permitted application of an ELISA-based assay to quantify surface expression as well as it permitted application of antibody feeding experiments to assess internalization. According to the ELISA assay, JHC 1–64 did not alter surface expression of HA-DAT (supplemental Fig. S2*A*, available at www.jneurosci.org as supplemental material). In the antibody feeding experiment, we performed confocal imaging after labeling with JHC 1–64 (supplemental Fig. S2*B*, available at www.jneurosci.org as supplemental material), anti-HA antibody (Alexa Fluor 488 conjugated HA.11) (supplemental Fig. S2*C*, available at www.jneurosci.org as supplemental material), or both JHC 1–64 and conjugated anti-HA antibody (supplemental Fig. S2*D*, available at www.jneurosci.org as supplemental material). After 60 min, we observed for all three conditions weak intracellular accumulation of JHC 1–64- and HA.11-positive vesicles (supplemental Fig. S2*B–D*, available at www.jneurosci.org as supplemental material). This represents most likely modest constitutive internalization of HA-DAT that is unaffected by JHC 1–64. Note that Chi and Reith (2003) also have reported constitutive internalization of DAT in HEK293 cells; however, they observed that close to 20% of surface expressed transporter was internalized over an hour, which appears much higher than indicated from our imaging experiments. Most likely, this apparent discrepancy results from the use of different methods and/or different expression levels.

**Labeling of DAT with JHC 1–64 is reversible but the off-rate is slow**

We also wanted to evaluate the reversibility of the DAT labeling. This was done first by using HEK293 EGFP-hDAT cells that were labeled with JHC 1–64 followed by treatment for 30 min at 37°C with 1 $\mu$M PMA. The cells were subsequently washed and incubated at 37°C in buffer containing 10 $\mu$M of the nonfluorescent cocaine analog RTI-55. The degree of JHC 1–64 labeling was followed over time and after 90 min of incubation the fluorescent labeling of the plasma membrane was reduced, consistent with dissociation of JHC 1–64 from the DAT binding pocket (Fig. 4*C*); however, the dissociation was slow, i.e., the dissociation was barely apparent after 45 min of incubation (data not shown). Importantly, labeling of internalized transporter was only slightly reduced as reflected by clear colocalization of EGFP and JHC 1–64 fluorescence even after 90 min of incubation, indicating that JHC 1–64 is a reliable reporter of endocytosed DAT (Fig. 4*C*).

To further verify that the slow loss of fluorescence was indeed a product of a slow off-rate for JHC 1–64 from DAT and not a nonspecific membrane partitioning, we measured the ability of JHC 1–64 to inhibit [$^3$H]dopamine uptake in DAT expressing HEK293 cells after washout at various time points to allow dissociation and prevent rebinding of JHC 1–64. The cells were labeled with 100 nM JHC 1–64, 500 nM JHC 1–64, or vehicle for 30 min before washing and incubation for 0, 20, 40, or 60 min at 37°C. [$^3$H]dopamine uptake was then assayed after two additional washes. After 60 min washout of either 100 or 500 nM JHC 1–64, [$^3$H]dopamine uptake was still markedly blocked and almost unchanged compared with 0 min washout (i.e., ~10% of vehicle treated for 100 nM JHC 1–64 and ~5% of vehicle treated for 500 nM JHC 1–64) with only a tendency toward loss of inhibition was seen (supplemental Fig. S3, available at www.jneurosci.org as supplemental material). These data strongly suggest very slow dissociation of JHC 1–64 from DAT and further support that JHC 1–64 can be used as a tool to track DAT molecules in live cells over even an extended period of time.

**Visualization of endogenous DAT in live neurons**

We wanted next to see whether we could use the ligands to visualize DAT endogenously expressed in neurons. We prepared postnatal cultures of rat midbrain neurons and assessed DAT expression by labeling with JHC 1–64. Incubation of the cultures with 5 nM JHC 1–64 for 15 min resulted in labeling of a fraction (~20%) but not all neurons in the culture (data not shown). No significant labeling was observed of the glial cell layer on which the postnatal neurons were grown (Fig. 5*A–C*). The labeling of the individual neurons indicated a widespread and generally uniform distribution of the DAT in the neurons with plasma membrane staining not only in the neuronal extensions and varicosities but also of the somas (Fig. 5*A–C*). Coincubation with either an excess of cocaine (10 $\mu$M) (data not shown), dopamine (1 mM), or the inhibitor mazindol (1 $\mu$M) blocked all staining except labeling of some irregular rounded structures that likely represented dead or dying cells (Fig. 5*A*,*B*). To validate that we indeed were visualizing endogenously expressed DAT and not SERT or NET, we coincubated with an excess of either the specific SERT inhibitor citalopram or the specific NET inhibitor desmethylimipramine of which neither affected JHC 1–64 staining (Fig. 5*B*). We also performed stainings with MFZ 9–18 (Fig. 5*D*), which revealed a labeling pattern very similar to that observed for JHC

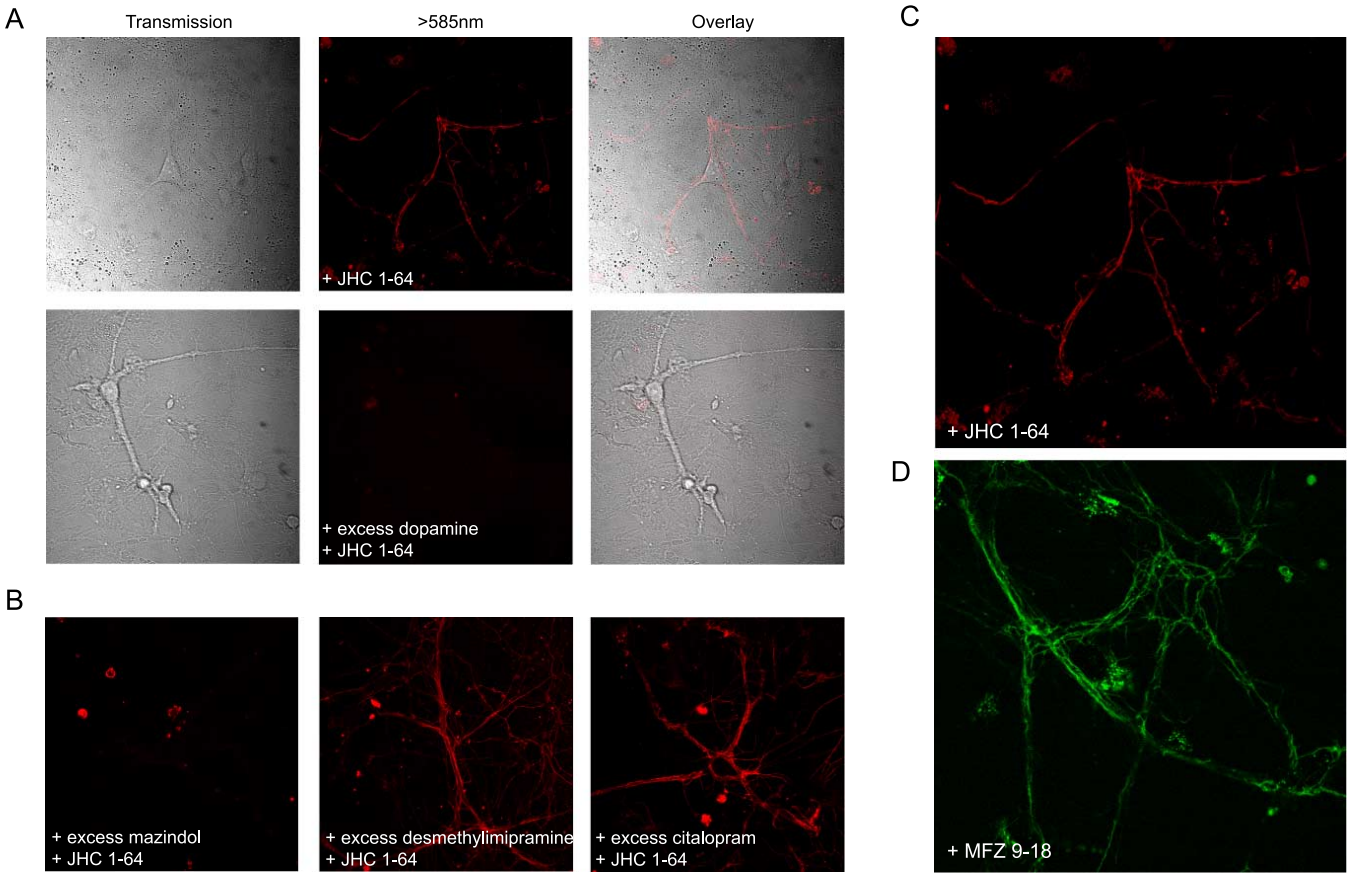


**Figure 5.** Visualization of endogenously expressed DAT in cultured postnatal midbrain neurons using fluorescent cocaine analogs. ***A***, Labeling with JHC 1–64 is blocked by dopamine. The neuronal cultures were incubated with 5 nM JHC 1–64 for 20 min (top) or preincubated with 1 mM dopamine for 15 min before incubation for 20 min with 5 nM JHC 1–64 (bottom). JHC 1–64 labeled ~20% of the neurons in the culture. Left panels show transmitted light, middle panels show JHC 1–64 fluorescence, and right panels show overlay. ***B***, JHC 1–64 labeling is blocked by the high-affinity DAT inhibitor mazindol but not by the selective SERT inhibitor citalopram or the selective NET inhibitor desmethylimipramine. The neuronal cultures were preincubated for 15 min with either 1 μM mazindol (left), 10 μM desmethylimipramine (middle), or 1 μM citalopram (right) before incubation with 5 nM JHC 1–64 for 20 min. ***C***, Enlarged picture of the JHC 1–64-labeled neuron shown in ***A***. The picture shows a wide and uniform distribution of JHC 1–64 labeling in the plasma membrane of both the soma and the neuronal extensions. ***D***, Visualization of endogenous DAT with MFZ 9–18. The neuronal cultures were incubated with 10 nM MFZ 9–18 for 20 min. Preincubation with dopamine abolished this labeling (data not shown). The labeling pattern for MFZ 9–18 strongly resembled that seen for JHC 1–64. JHC 1–64 was visualized by using a 543 nm HeNe laser for excitation and a >585 nm long-pass filter for recording of fluorescence, whereas MFZ 9–18 was visualized using a 488 nm argon laser for excitation and a 505–530 nm bandpass filter for recording of fluorescence. The experiments shown are representative of at least three similar experiments with the same results.

1–64 and like the JHC 1–64, labeling was blocked completely by preincubation with an excess of dopamine (data not shown). Note that when interpreting surface staining of somas and neuronal extensions it is important to be aware of fibers engaging other neurons. This cannot be excluded in, e.g., Figure 5*D*, whereas, e.g., the overlay of transmission and fluorescence in Figure 5*A* strongly suggests uniform labeling of the soma and proximal extensions. To address this question further and to enable correlation between labeling and neuronal morphology, the surface distribution of DAT was further studied by performing *Z*-scans through dopaminergic neurons labeled with JHC 1–64. The scans unraveled clear labeling of the soma and a large and uniformly labeled neurite tree (Fig. 6; supplemental Movie 1, available at www.jneurosci.org as supplemental material).

To investigate whether the neurons stained by our fluorescent cocaine analogs possessed the expected features of dopaminergic neurons, we performed a series of immunostainings with antibodies against DAT itself, tyrosine hydroxylase (TH), and the vesicular monoamine transporter-2 (VMAT2), all obligate markers of dopaminergic neurons (Rayport et al., 1992; Nirenberg et al., 1996). The immunostainings were performed subsequent to labeling of the cells with JHC 1–64 (10 nM) for 20 min. In the fixed and permeabilized cells JHC 1–64 staining of the neurons was markedly weaker than that seen in live cells; however, we still saw a similar labeling pattern with labeling of the plasma membrane of the soma, the neuronal extensions and varicosities along these extensions (Fig. 7). Importantly, the labeling was also under these conditions blocked by cocaine and dopamine (data not shown). As compared with live cells, the specific labeling appeared somewhat more punctuate/clustered, which is likely to represent an artifact of the fixation and permeabilization procedure (Fig. 7). Nonetheless, costaining with JHC 1–64 and DAT antibody (MAB369, directed against the intracellular N-terminal) showed almost perfect overlap in the neurons further supporting the specificity of JHC 1–64 labeling (Fig. 7*A*). Most neurons labeled by JHC 1–64 were also labeled with the antibodies against TH and VMAT2. The TH immunoreactivity was found in the cytoplasm of the soma as well as in the cytoplasm of discrete varicosities and along the neuronal extensions (Fig. 7*B*). As a result, the TH staining did not overlap directly with the plasma membrane staining observed for JHC 1–64 (Fig. 7*B*).

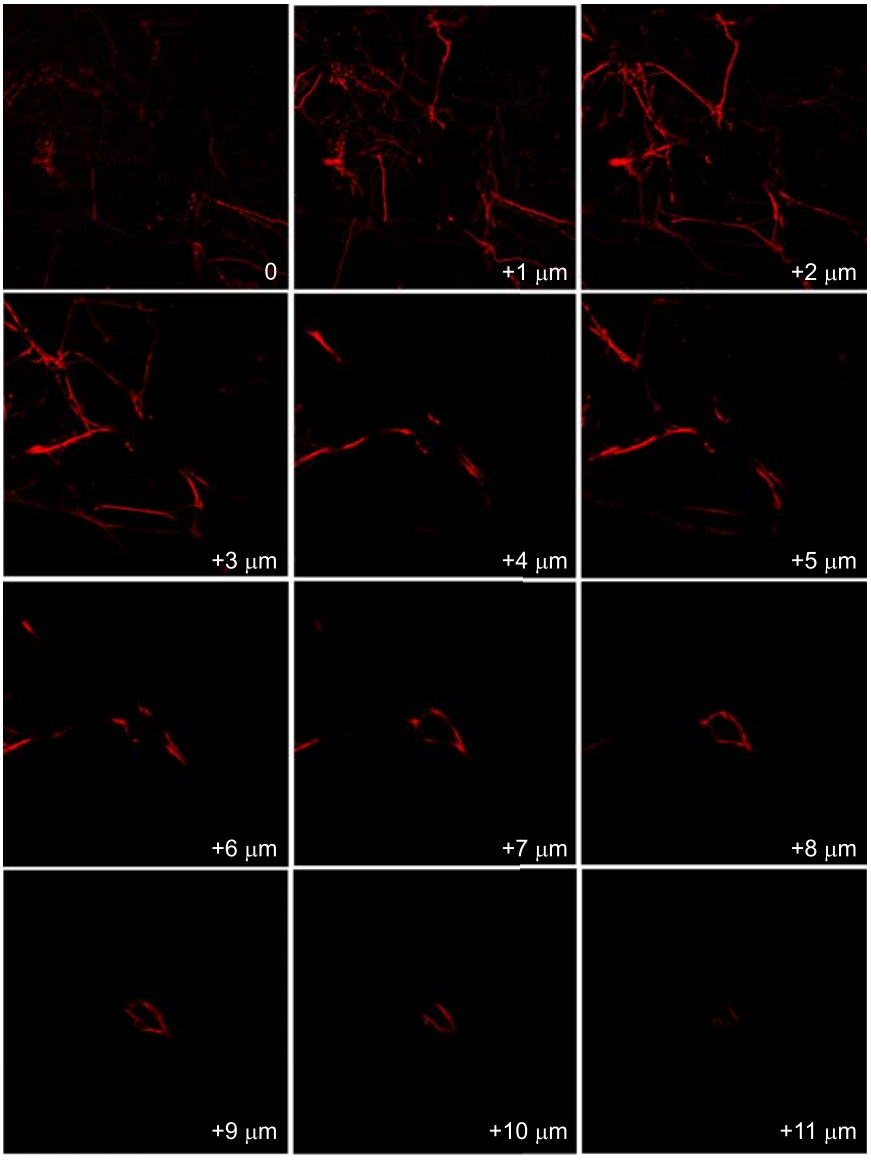


**Figure 6.** *Z*-scan of JHC 1–64-labeled dopaminergic neuron. The scan unravels labeling of the soma and a large and generally uniformly labeled neurite tree. The series of pictures shown represent as indicated 1 $\mu$m sections starting from the surface and ending 11 $\mu$m above the surface. The neuronal cultures were incubated with 5 nM JHC 1–64 for 20 min before the analysis was performed. JHC 1–64 was visualized using a 543 nm HeNe laser for excitation and a >585 nm long-pass filter for recording of fluorescence (see also supplemental Movie 1, available at www.jneurosci.org as supplemental material).

While JHC 1–64 staining, and thus DAT, was present not only in the varicosities but also along the neurites as well as in the plasma membrane of the soma, the VMAT2 staining was localized solely to the varicosities (Fig. 7*C*).

### Membrane mobility of the DAT assessed by FRAP

To assess lateral mobility of the DAT in the plasma membrane of live neurons we performed FRAP (fluorescence recovery after photobleaching) measurements after labeling for 20 min with 5 nM JHC 1–64. For the bleaching we used the 488 nm argon laser, a relatively short bleach period (700 ms), and a circular bleach spot with an average diameter of 1 $\mu$m. The pinhole was kept fully open to ensure complete bleaching through the cell and the bleaching was performed either at the edge of the varicosities or along the neuronal extensions (Fig. 8*A*). The resulting curves revealed fast recoveries and mobile fractions of larger than ~70% both in the varicosities and along the neuronal extensions (Fig. 8*A*) (mobile fraction, varicosities = 72.0 ± 10.2%; mobile fraction, extensions = 75.3 ± 7.3%, $n$ = 20–22). The calculated diffusion coefficients were $0.65 \pm 0.06 \times 10^{-9}$ cm$^2$/s in the extensions and $1.14 \pm 0.11 \times 10^{-9}$ cm$^2$/s, $n$ = 30–34). These values indicate that the JHC 1–64-occupied transporter is relatively freely moving in the membrane and that the lateral mobility might be even higher in the varicosities than in the extensions.

The mobility of DAT was further investigated by assessing whether DAT preferentially moved unidirectionally or bidirectionally in the neuronal extensions. The neurons were incubated for 20 min with 5 nM JHC 1–64, after which an extended piece of a neuronal extension (Fig. 8*B*, white box) was bleached with the 488 nm argon laser for several seconds followed by acquisition of images at appropriate time intervals. As shown in Figure 8*B*, we observed recovery of fluorescence from both sides reaching one another after ~40 s. The recovery appeared to occur with the same rate from either side. This is consistent with no directional movements of surface expressed DAT in the neuronal extensions of cultured dopaminergic neurons.

### Assessment of DAT internalization in dopaminergic neurons

Our data from the transfected HEK293 cells showed that we could assess internalization of the JHC 1–64-labeled transporter by live confocal imaging. To perform similar experiments in the dopaminergic neurons, we first preincubated the neurons with 5 nM JHC 1–64 at 4°C followed by incubation for up to 1 h at 37°C in the absence of any stimuli. During this period we observed a marked spontaneous redistribution of the JHC 1–64-labeled DAT, as indicated by the appearance of an increasing number of distinct JHC 1–64-positive intracellular vesicles in both the proximal neuronal extensions and in the soma (examples of vesicles indicated by arrows in Fig. 9*A*). Under control conditions at 4°C over the same time period we did not see any signs of redistribution but only staining of the plasma membrane (Fig. 9*A*). The redistribution of JHC 1–64-labeled DAT was also completely blocked by incubation with hypertonic sucrose, a crude and nonspecific inhibitor of clathrin-mediated endocytosis (Heuser and Anderson, 1989; Hansen et al., 1993) (Fig. 9*A*). Altogether, the data suggest that DAT undergoes marked constitutive internalization in dopaminergic neurons. Interestingly, in DAT expressing HEK293 cells we observed only modest constitutive redistribution upon incubation of the cells at 37°C up to 1 h (supplemental Fig. S4*A*, available at www.jneurosci.org as supplemental material), indicating a clear dif-

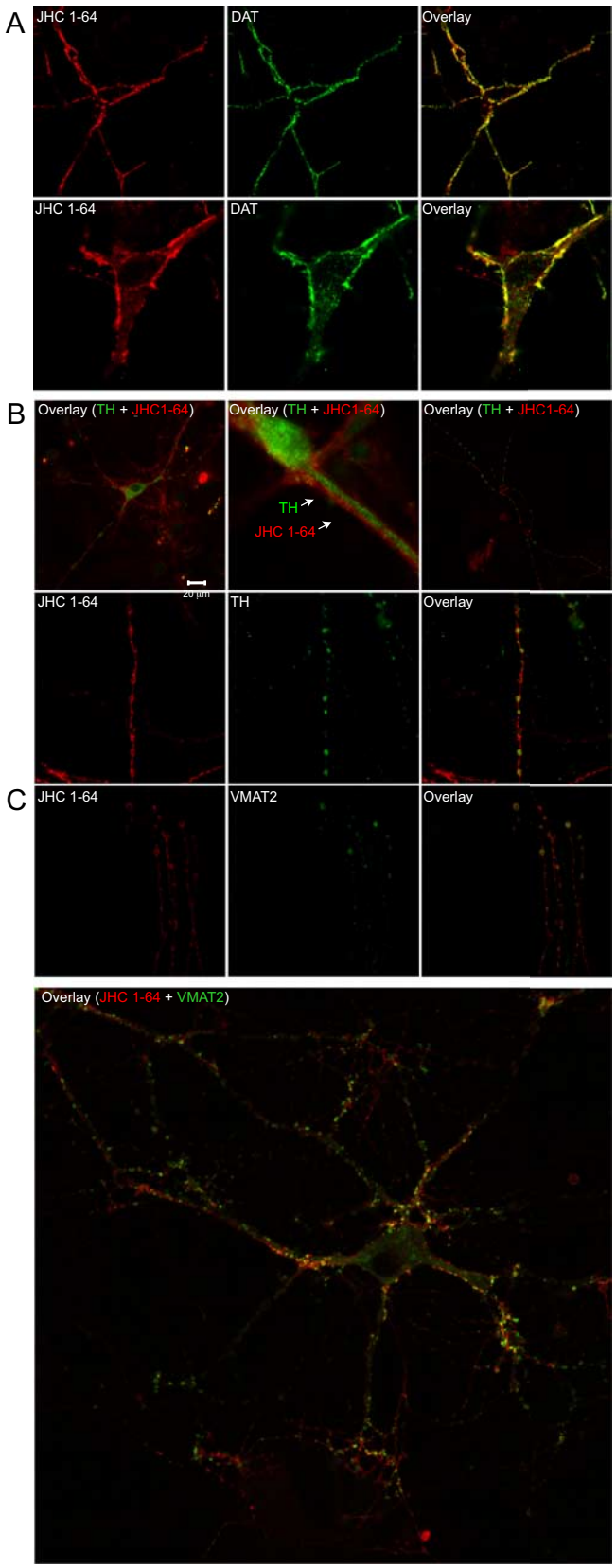


**Figure 7.** JHC 1–64 labels dopamine transporter (DAT)-positive, tyrosine hydroxylase (TH)-positive, and VMAT2-positive neurons. Cultured postnatal midbrain neurons were labeled with 10 nM JHC 1–64 for 20 min before they were fixed and stained for either DAT (***A***), TH (***B***), or VMAT2 (***C***). ***A***, Costaining of dopaminergic neuron with JHC 1–64 and rat anti-DAT antibody (MAB369) shown in two different magnifications. DAT immunoreactivity overlaps extensively in the extensions and in the plasma membrane of the soma. ***B***, Costaining of dopaminergic neuron with JHC 1–64 and anti-TH antibody. Top row, Three different overlays of JHC 1–64 and TH staining. Although present in the same neuron, the staining did not overlap, i.e., JHC 1–64 primarily stained the plasma membrane, whereas the TH staining appeared intracellular. The rounded strongly stained structure in the left picture is likely to represent a dead or dying cell and, thus, does not represent specific DAT staining by JHC 1–64. Similar rounded structures can also be seen when staining with JHC 1–64 in the presence of an excess of dopamine or inhibitor (Fig. 5*B*). Bottom row, JHC 1–64 labeling alone (left), TH staining alone (middle), and overlay (right) corresponding to a neuronal extension with characteristic varicosities. ***C***, Costaining of dopaminergic neuron with JHC 1–64 and anti-VMAT2 antibody. JHC 1–64 labeling alone (left), VMAT2 staining alone (middle), and overlay (right) corresponding to several neuronal extensions. Bottom, Overlay of JHC 1–64 and VMAT2 labeling of an entire dopaminergic neuron. The image illustrates the widespread presence of DAT and its colocalization with VMAT2. JHC 1–64 was visualized by using a 543 nm HeNe laser for excitation and a >585 nm long-pass filter for recording of fluorescence. DAT antibody, TH antibody, and VMAT2 antibody were visualized either using Alexa Fluor 488 goat anti-rat or anti-rabbit antibody. The experiments shown are representative of at least three similar experiments with the same results.

ference between natively expressed and heterologously expressed DAT.

We tested next whether PMA affected DAT internalization in the neurons; however, in contrast to our findings in HEK293 cells (supplemental Fig. S4, available at www.jneurosci.org as supplemental material), PMA had no observable effect on internalization of JHC 1–64-labeled DAT in the neurons, hence, JHC 1–64-positive intracellular vesicles appeared with a similar rate and to the same degree in the presence of PMA as in the absence of PMA (Fig. 9*A*). Careful examination of neuronal extensions and varicosities also did not reveal any signs of DAT redistribution in response to PMA. To assess whether the enhanced constitutive internalization seen in the neurons compared with HEK293 cells was the result of generally increased PKC activity, we incubated the cells with the PKC inhibitor staurosporine; however, also this treatment did not alter the observed constitutive DAT internalization (Fig. 9*A*) even though the same concentration of staurosporine was capable of blocking PMA-induced internalization in HEK293 cells (supplemental Fig. S4*B*, available at www.jneurosci.org as supplemental material). We tried in addition the more selective PKC inhibitor GF109203X but due to autofluorescence from this compound we were not able to obtain reliable imaging results (data not shown).

Together, the data suggest that endogenously expressed DAT is not subject to regulation by PKC in cultured dopaminergic neurons. This is not due to lack of PKC expression since staining with antibody directed against PKC suggested strong expression of the kinase in the DAT-positive neurons (supplemental Fig. S5*A*, available at www.jneurosci.org as supplemental material). To demonstrate that PKC is not only expressed in the DAT-positive neurons but also activated under the same experimental conditions used above, we took advantage of a genetically encoded fluorescence resonance energy transfer (FRET)-based reporter for PKC activity, C kinase activity reporter (CKAR) (Violin et al., 2003; Gallegos et al., 2006). CKAR consists of cyan fluorescent protein (CFP) and yellow fluorescent protein (YFP) tethered together by a substrate peptide specific for PKC and an FHA2 phosphopeptide-binding module. Phosphorylation of CKAR by PKC results in a decrease in the FRET signal between CFP and YFP, which can be measured as an increase in CFP/YFP emission ratio (Violin et al., 2003; Gallegos et al., 2006). First, we transiently expressed CKAR in HEK293 cells and measured the CFP/YFP emission ratio over time. PMA (1 $\mu$M) caused a rise in the CFP/YFP emission ratio, corresponding to a decrease in the FRET signal and consistent with PMA-mediated activation of PKC (supplemental

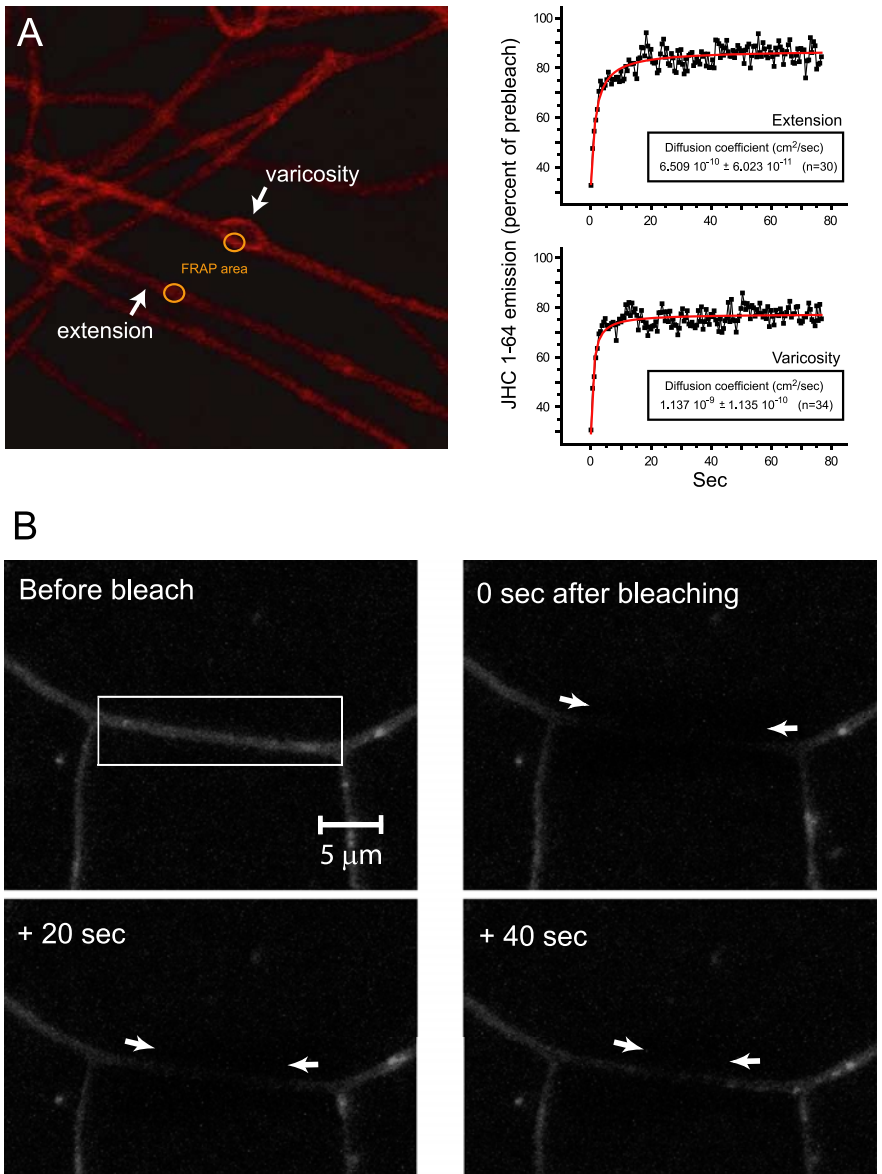


**Figure 8.** DAT is highly mobile in the plasma membrane of dopaminergic neurons. ***A***, FRAP measurements on JHC 1–64-labeled DAT in dopaminergic neurons in culture. The neurons were incubated with 5 nM JHC 1–64 for 20 min at RT, washed in buffer, and kept in buffer with 10 $\mu$M RTI55 during the experiment to avoid any potential rebinding of JHC 1–64 to DAT. Left, FRAP was measured at two anatomically distinct locations in the neurons: corresponding to the neuronal extensions and corresponding to the varicosities. Right, Representative FRAP measurements corresponding to an extension and a varicosity. The calculated average diffusion coefficients (*D*) are indicated. The mobile fractions constituted in the boutons 72.0 ± 10.2% and in the extensions = 75.3 ± 7.3% ($n$ = 20–22) of the labeled transporters. ***B***, Illustration of bidirectional lateral movements of DAT along the neuronal extensions. The neurons were labeled as described above with JHC 1–64 before bleaching the area indicated by the white box using the 488 nm laser line at 100% output for ~700 ms to obtain 30–70% bleaching compared with prebleach image. Subsequently, the bleached area was monitored and images taken with appropriate time intervals. The experiment shown is representative of at least three similar experiments.

Fig. S5*B*,*C*, available at www.jneurosci.org as supplemental material). Next, we expressed CKAR in our midbrain neuronal cultures using lentiviral transduction. The dopaminergic neurons expressing CKAR were identified with JHC 1–64. As shown in supplemental Figure S5*C* (available at www.jneurosci.org as supplemental material), stimulation with PMA resulted in a significant increase in the CFP/YFP emission ratio, demonstrating PMA-mediated activation of PKC in dopaminergic neurons similar to what was observed in HEK293 cells.

To obtain further support for the absence of PKC regulation in cultured DAT-positive neurons, as well as to obtain a quantitative measure, we analyzed the effect of PKC activation and inhibition on [$^3$H]dopamine uptake. Uptake was measured by incubating neurons in culture with ~100 nM [$^3$H]dopamine for 3 min, resulting in a specific uptake of 403 ± 58 pmol/min/well (mean ± SE, $n$ = 4, nonspecific uptake determined in the presence of 10 $\mu$M cocaine). As shown in Figure 9*B*, neither PKC activation with PMA nor PKC inhibition with staurosporine or GF109203 had any detectable effect on the measured uptake. Using a 10 times higher concentration of [$^3$H]dopamine did also not reveal any effect of PMA on uptake in the dopaminergic neurons (uptake in response to 1 $\mu$M PMA was 98.9 ± 3.9% of control uptake; mean ± SE, $n$ = 3).

To investigate further the constitutive internalization of JHC 1–64-labeled DAT, we used recombinant lentiviral vectors to mediate expression of the dominant-negative dynamin mutation K44A (van der Bliek et al., 1993; Robinson, 1994). To identify transduced cells the vector also encoded GFP separated from dynamin by an internal ribosome entry site (dynamin K44A IRES-GFP). Accordingly, GFP-positive cells indicated efficient lentiviral transduction. First, we performed experiments in DAT expressing HEK293 cells (supplemental Fig. S6, available at www.jneurosci.org as supplemental material). In these cells, transduction with lentivirus encoding dynamin K44A, but not wild-type dynamin, strongly inhibited PMA-induced internalization, in agreement with previous observations for heterologously expressed DAT in MDCK cells (Daniels and Amara, 1999) (supplemental Fig. S6, available at www.jneurosci.org as supplemental material). Next, we transduced our dopaminergic neurons and constitutive internalization of JHC 1–64-labeled DAT was assessed as described in Figure 9*A*. A substantial reduction in the amount of constitutively internalized JHC 1–64-labeled DAT was observed in the neurons expressing dynamin K44A, whereas this was not the case in neurons expressing dynamin wild type (Fig. 10*A*). This suggests that endogenously expressed DAT undergoes constitutive endocytosis via a dynamin-dependent pathway. Note that although the general transduction efficiency of neurons in the culture was high, only a relatively small fraction of the DAT-positive neurons was transduced and expressed the dynamin constructs, which underlines the general difficulty in achieving heterologous expression in this type of neurons.

To assess whether JHC 1–64-labeled DAT indeed was constitutively internalized to an endosomal compartment we trans-

duced the neuronal culture with lentivirus encoding the early endosomal marker Rab5A tagged with EGFP (EGFP-Rab5A) (Zerial and McBride, 2001; Deneka et al., 2003; Lavezzari et al., 2004). As for the dynamin constructs, we observed generally a high transduction efficiency in the culture with rather low transduction efficiency in the dopaminergic neurons. However, in all experiments we were able to identify a number of healthy DAT-positive neurons expressing EGFP-Rab5A. EGFP-Rab5A localized, as would be expected, to vesicular structures in the neurons as well as some nonvesicular cytosolic expression was apparent (Fig. 10*B*). In constitutive internalization experiments, performed as described in Figure 9*A*, we observed in the dopaminergic neurons after 60 min of incubation at 37°C several vesicles positive for both JHC 1–64/DAT and EGFP-Rab5A, supporting constitutive internalization into early endosomes (Fig. 10*B*). In some cases, we observed vesicles close to the plasma membrane likely reflecting recent endocytic events (Fig. 10*B*, right arrow).

We also performed constitutive internalization experiments upon labeling DAT with JHC 1–64 and the transferrin receptor with Alexa Fluor 488-conjugated transferrin. The transferrin receptor is internalized into early endosomes followed by sorting to recycling endosome (Blanpied et al., 2002). After 30 min, we observed modest JHC 1–64/DAT internalization and marked overlap with transferrin receptor-positive vesicles, again consistent with constitutive internalization of DAT into early endosomes. After 60 min, both JHC 1–64/DAT and transferrin receptor internalization were more pronounced; however, there was a tendency toward less colocalization of JHC 1–64 with transferrin-positive vesicles, which may be indicative of differential sorting of DAT and transferrin receptor (Fig. 10*C*).

We further explored the constitutively endocytosed JHC 1–64/DAT complex by confocal live imaging. We allowed constitutive internalization to occur by incubating JHC 1–64-labeled dopaminergic neurons for 1 h of incubation at 37°C and subsequently performed time laps with 300 pictures in 20 min at 37°C. A representative example of a movie resulting from this protocol is provided in the supplemental material (supplemental Movie 2, available at www.jneurosci.org). The acquired movies revealed multiple JHC 1–64/DAT-positive vesicles undergoing frequent "stepwise" movements. A careful analysis suggested that the vesicles could be divided into at least two major types depending on their mobility pattern. One type of vesicle was essentially immobilized during the observation period of 10 min (vesicles indicated by red arrows in Fig. 11). In contrast, other vesicles underwent often rapid movements over rather long distances during

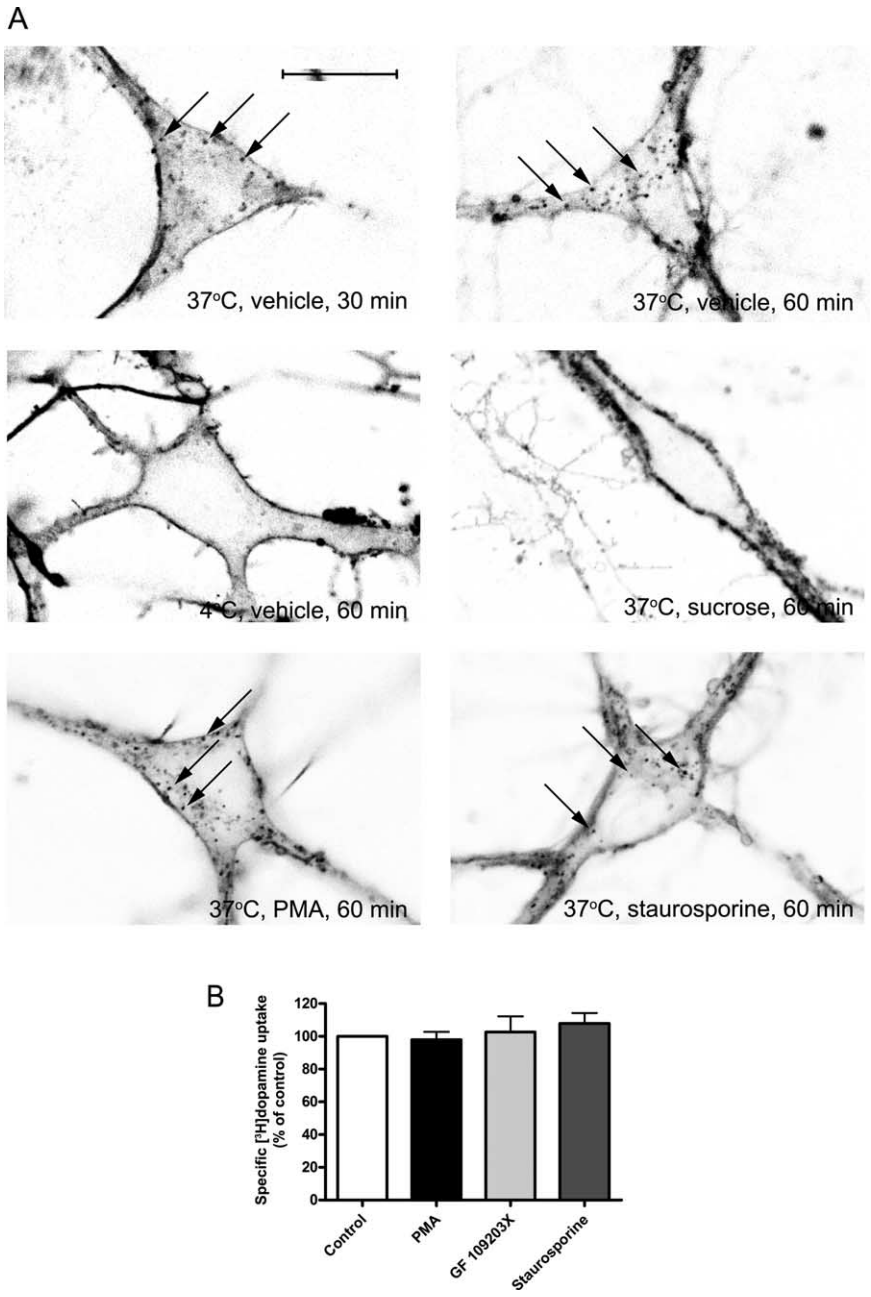


**Figure 9.** Visualization of constitutive DAT internalization in cultured midbrain dopaminergic neurons (7–10 DIV) using JHC 1–64. ***A***, Images of representative neurons incubated under indicated conditions. JHC 1–64 was visualized by using a 543 nm HeNe laser for excitation and a >585 nm long-pass filter for recording of fluorescence. The images show the fluorescence on a gray scale with darkest pixels representing the largest fluorescence. The neurons were first incubated with 5 nM JHC 1–64 for 30 min at 4°C to label surface DAT. Subsequently, the neurons were further incubated at 37°C for 30 min (top left), at 37°C for 60 min (top right), at 4°C for 60 min (middle left), at 37°C for 60 min in the presence of 450 mM sucrose (middle right), at 37°C for 60 min in the presence of 1 $\mu$M PMA (bottom left), and at 37°C for 60 min in the presence of 1 $\mu$M staurosporine (bottom right). The images suggest that the JHC 1–64/DAT complex undergoes temperature-dependent constitutive internalization that is blocked by sucrose. Moreover, and in contrast to what was observed in HEK293 cells, there is no effect on internalization in response to 1 $\mu$M PMA. Note that the sucrose treatment slightly alters the appearance of the neuron and makes the membrane looks thicker than in neurons that were not treated with sucrose. Scale bar, 20 $\mu$m. The experiments shown are representative of at least three similar experiments. ***B***, [$^3$H]dopamine uptake in cultured midbrain neurons was unaffected by PKC activation with 1 $\mu$M PMA and by PKC inhibition with staurosporine and GF109203X. [$^3$H]dopamine uptake under control conditions was 403 $\pm$ 58 pmol/min/well. Data are means $\pm$ SE, $n = 4$, $p = 0.68$, one-sample $t$ test.

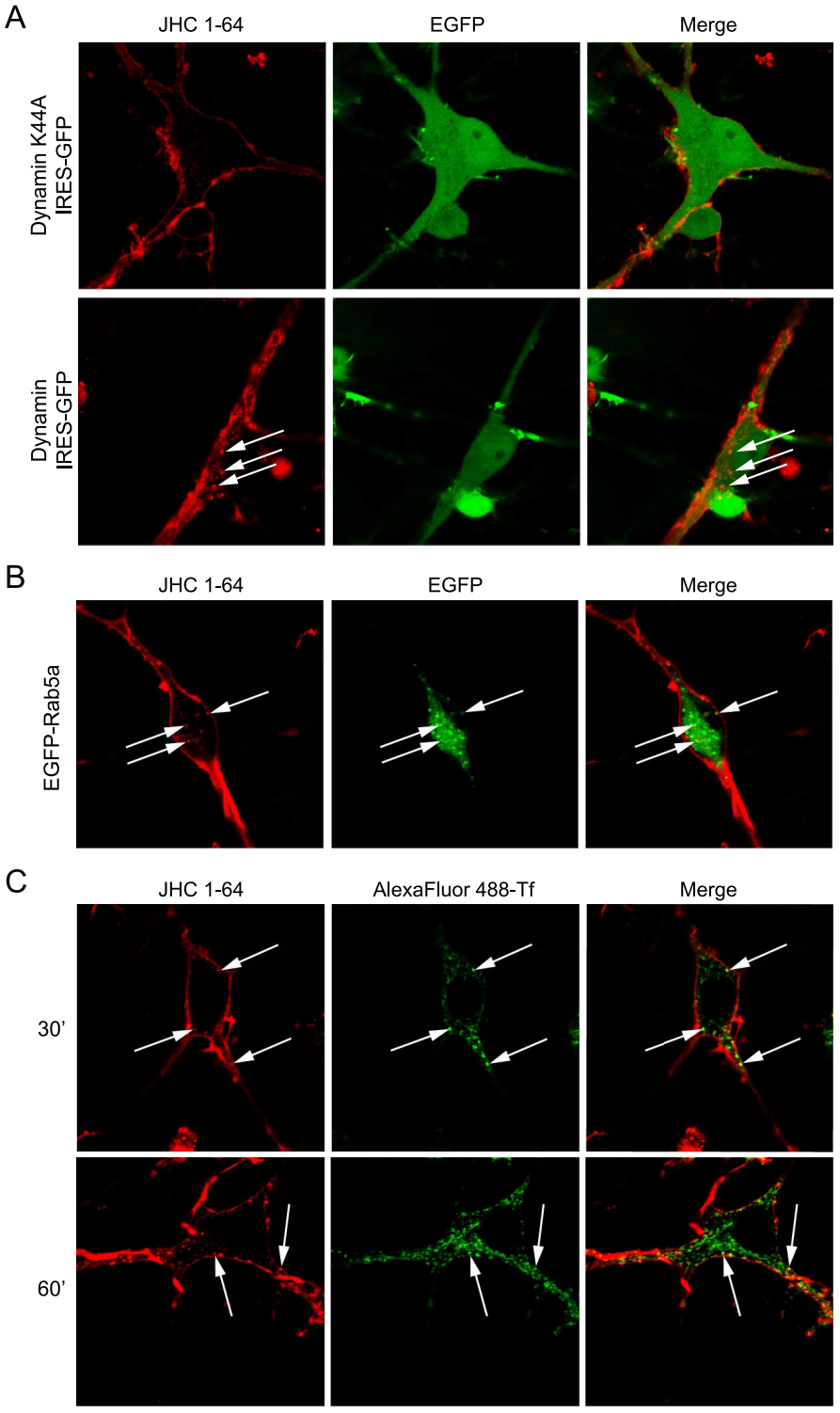


**Figure 10.** DAT internalizes in dopaminergic neurons into early endosomes in a dynamin-dependent manner. ***A***, Constitutive internalization is inhibited by overexpression of the dominant-negative dynamin mutation K44A. The neurons were transduced after 2–3 DIV with lentivirus encoding dominant-negative dynamin K44A or wild-type dynamin, both coupled to GFP expression. The analysis was performed after 8–10 DIV. The neurons were first incubated with 5 nM JHC 1–64 for 30 min at 4°C to label surface DAT. Subsequently, the neurons were further incubated for 60 min at 37°C to allow DAT internalization. In neurons expressing dynamin K44A, a substantial reduction in the amount of constitutively internalized DAT was observed, whereas overexpression of wild-type dynamin did not block internalization. In neurons overexpressing wild-type dynamin, selected internalized JHC 1–64-positive vesicles are indicated by arrows. ***B***, DAT internalizes into early endosomes. The neurons were transduced after 2–3 DIV with lentivirus encoding the early endosomal marker EGFP-Rab5A and analyzed after 8–10 DIV. Constitutive internalization was allowed as described above. In neurons expressing EGFP-tagged Rab5A, partial overlap between JHC 1–64- and EGFP-Rab5A-positive vesicles was seen. Selected costained vesicles are indicated by arrows. Some costained vesicles were localized close to the plasma membrane, probably indicating recent endocytic events. However, JHC 1–64-positive vesicles that were not EGFP-Rab5A-positive were also observed. Left panels show fluorescence in the >585 nm channel (JHC 1–64), middle panels fluorescence in the 505–530 nm channel (GFP or EGFP), and right panels show overlay of the two channels. The experiments shown are representative of 3–5 independent experiments. ***C***, Internalized DAT partially colocalizes with the transferrin receptor. Dopaminergic neurons at 8–10 DIV were incubated for 30 min at 4°C with 5 nM JHC 1–64 to label surface DAT and with AlexaFluor 488-conjugated transferrin to label the transferrin receptor. Subsequently, the neurons were further incubated for 30 (30′) and 60 (60′) min at 37°C to allow internalization. At 30 min, JHC 1–64/DAT internalization was modest but with marked overlap with transferrin-positive vesicles. After 60 min, a more pronounced JHC 1–64/DAT internalization was observed with partial colocalization with transferrin-positive vesicles. Selected costained vesicles are indicated by arrows. The experiment shown is representative of three independent experiments.

the observation period. The movements of these vesicles appeared to occur both toward and away from the soma (see supplemental Movie 2, available at www.jneurosci.org as supplemental material). In conclusion, the data support the existence of an intracellular transporter pool contained in vesicles with distinct mobility patterns, which can be visualized using fluorescently labeled cocaine ligands.

## Discussion

Despite the physiological importance of DAT and its role as drug target, little is known about trafficking of DAT in its native environment and how these processes are regulated. Due to the lack of appropriate tools, the majority of studies has been performed with epitope-tagged transporter in transfected, heterologous cells and, hence, the significance of many observations has not been evaluated in dopaminergic neurons where DAT is endogenously expressed. Here we have addressed this problem by using fluorescently tagged, high-affinity cocaine analogs that permitted direct visualization of endogenously expressed DAT in live dopaminergic neurons.

Previously, we demonstrated synthesis of rhodamine-coupled cocaine analogs with preserved high affinity for the DAT (Cha et al., 2005). Here we introduce two additional high-affinity analogs coupled to two different fluorescent labels, OR Green and Cy3, each with distinct spectral properties. To validate the usefulness of these analogs, we performed a series experiments in transfected HEK293 cells and, together, the data strongly support that the fluorescently tagged compounds label DAT with high specificity and can be used to track DAT in live cells. For JHC 1–64, we provide evidence for a very slow

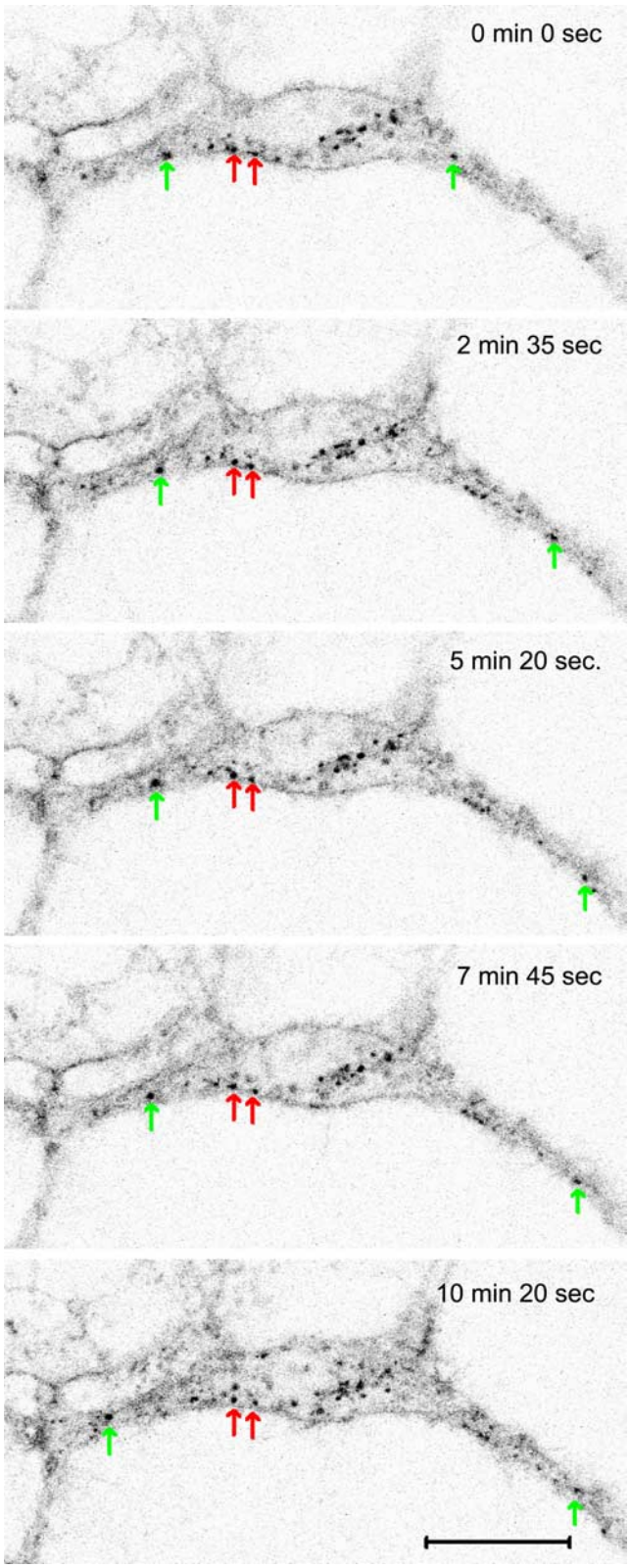


**Figure 11.** Tracking of internalized JHC 1–64/DAT-positive vesicles in cultured midbrain dopaminergic neurons. The neurons (6 DIV) were labeled with 5 nM JHC 1–64 at 37°C for 1 h to allow labeling and internalization of the DAT/JHC 1–64 complex. Subsequently, time laps were performed with 300 pictures in 20 min using a heated stage (37°C) on the LSM510 confocal microscope. JHC 1–64 was visualized by using a 543 nm HeNe laser for excitation and a >585 nm long-pass filter for recording of fluorescence. The images show the fluorescence on a gray scale with darkest pixels representing the largest fluorescence. A representative example of a movie resulting from this protocol is provided in the supplemental material (supplemental Movie 2, available at www.jneurosci.org). Selected images from this movie at indicated time points are shown. The larger fraction of the vesicles seemed to be stationary (exemplified by the 2 vesicles indicated by the red arrows), whereas a smaller fraction underwent often rapid movements over rather long distances during the observation period (vesicles indicated with green arrows). Scale bar, 20 $\mu$m.

dissociation-rate permitting tracking of DAT molecules in live cells over even an extended period of time.

It is a potential concern that by using the fluorescently tagged cocaine analogs we study an inhibitor-occupied transporter. Previously, it has been suggested that cocaine causes acute upregulation of DAT surface expression in transfected HEK293 cells (Daws et al., 2002). Thus, inhibitor binding might affect DAT trafficking; however, although the effect of cocaine on DAT trafficking was significant, the magnitude of the response was relatively modest (Daws et al., 2002). In addition, cocaine was found not to affect PMA-induced DAT internalization in GFP-expressing MDCK cells (Daniels and Amara, 1999). We were also unable to see any effect of JHC 1–64 on surface expression and constitutive trafficking of HA-tagged DAT in HEK293 cells; hence the effect of JHC 1–64 on endogenous DAT trafficking is likely to be absent or very minor.

Labeling of midbrain dopaminergic neurons with either JHC 1–64 or MFZ 9–18 revealed a uniform distribution of the DAT with labeling of somas, extensions, and varicosities. *Z*-stacking analysis allowed us to correlate staining with neuronal morphology and validate the widespread labeling of DAT in the individual neurons (Fig. 6). As expected, neurons that were stained with JHC 1–64 also displayed staining for VMAT2; however, whereas the VMAT2 staining localizes solely to varicosities along the extensions, JHC 1–64 staining, and thus DAT, was present not only in the varicosities but also along the extensions as well as in the plasma membrane of the soma. Of interest, the network of neuronal extensions in the DAT-positive neurons is likely to be mostly axonal as supported by costainings of our culture for DAT and for the dendritic marker MAP2 (supplemental Fig. S7, available at www.jneurosci.org as supplemental material).

Although the expression pattern in cultured neurons might not be identical to that found *in situ*, it is interesting to consider our observations in context of earlier EM studies in rat brain (Nirenberg et al., 1996, 1997; Hersch et al., 1997). These studies also provided evidence for widespread expression of DAT in axons as well as in dendrites. Moreover, they suggested perisynaptic/extrasynaptic localization of DAT challenging the classical paradigm of preferential presynaptic localization of DAT (Nirenberg et al., 1996, 1997; Hersch et al., 1997). Altogether, the present data add further support to the notion that DAT is not fulfilling its indispensable role in maintaining low extracellular levels of dopamine by being discretely expressed close to the dopamine release sites but rather by being present throughout the plasma membrane in the dopaminergic neurons.

This view is further supported by our FRAP measurements providing evidence that the JHC 1–64-labeled DAT in cultured dopaminergic neurons is highly mobile with mobile fractions constituting >70% of the JHC 1–64-labeled transporter molecules both in varicosities and in the neuronal extensions. The calculated diffusion coefficients ($0.5–1.1 \times 10^{-9}$ cm$^2$/s) were consistent with a relatively freely diffusing protein in the membrane (Lippincott-Schwartz et al., 2001). Of note, these values resembled more the values that we obtained previously for EGFP-tagged DAT in HEK293 cells ($\sim 0.4 \times 10^{-9}$ cm$^2$/s) than for EGFP-tagged DAT expressed in neuronally derived N2a cells

($\sim 0.1 \times 10^{-9}$ cm$^2$/s) (Adkins et al., 2007). Thus, DAT apparently displays less restricted diffusion in dopaminergic neurons and thereby in a native environment compared with a transfected neuronal cell line.

In heterologous cell lines, it is well established that activation of PKC by PMA leads to DAT internalization. The effect is not caused by direct phosphorylation of DAT (Granas et al., 2003) but more likely the result of ubiquitination of a cluster of lysines in the N terminus (Miranda et al., 2007). Although well established in heterologous cells, the effect on internalization has not yet been assessed for endogenously expressed DAT in cultured neurons. Interestingly, the current data strongly support that DAT is not subject to regulation by PKC in neurons as we were unable to see any difference compared with control after PMA stimulation or inhibition of PKC with staurosporine. Moreover, the lack of an effect in response to modulation of PKC activity was supported by dopamine uptake experiments showing no change in response to PMA and two different PKC inhibitors. The lack of an effect was also unlikely caused by enhanced tyrosine kinase activity, which was suggested to inhibit PMA-mediated redistribution of the GABA transporter-1 (Quick et al., 2004); hence, pretreatment with the tyrosine kinase inhibitor genistein did not uncover an effect of PMA on DAT in the neurons (data not shown). Of note, our findings agree with recent observations in cultured prenatal midbrain neurons that were transfected with epitope-tagged DAT and in which no visible effect of PMA was seen (Sorkina et al., 2006). However, PMA treatment of cocultures of midbrain and striatal neurons, as well as PMA treatment of striatal, synaptosomal preparations, was previously found to reduce DAT uptake activity (Vaughan et al., 1997; Chi and Reith, 2003; Hoover et al., 2007). Thus, although we were unable to see PKC-mediated regulation in cultured midbrain neurons we cannot exclude that under certain conditions endogenous DAT might be subject to regulation by this kinase.

While unable to observe an effect of PKC modulation, we observed constitutive, temperature-dependent intracellular accumulation of JHC 1–64-labeled transporter over time. We were only able to visualize the constitutive internalization in the soma and proximal neuronal extensions. This might suggest that the internalization only occurs here; however, we cannot exclude that we do not have sufficient resolution to see endocytosis in the thin neurites. Constitutive DAT internalization has been shown before in transfected heterologous cells (Holton et al., 2005; Sorkina et al., 2005) and a C-terminal motif has been suggested to mediate this constitutive internalization (Holton et al., 2005). In this study, we demonstrate that constitutive trafficking is indeed not restricted to heterologously expressed transporter but also is seen for DAT expressed in its native environment and that this internalization likely is mediated via a dynamin-dependent pathway. Dynamins have been identified as a key component and marker of clathrin-mediated endocytosis (van der Bliek et al., 1993; Robinson, 1994); hence, it is likely that constitutive endocytosis of endogenous DAT follows the same pathway as that suggested previously for heterologously expressed DAT (Sorkina et al., 2005; Rappoport, 2008). However, it is important to note that nonclathrin but dynamin-dependent pathways such as raft-mediated endocytosis also have been identified and may be responsible for or contribute to constitutive DAT endocytosis (Lajoie and Nabi, 2007). Of further interest, we obtained data suggesting that internalized JHC 1–64-labeled DAT colocalized in part with EGFP-Rab5A, a small GTPase localized to the early endocytic pathway (Zerial and McBride, 2001; Deneka et al., 2003; Lavezzari et al., 2004) and with the transferrin receptor, another marker of the early endocytic pathway (Blanpied et al., 2002). The colocalization was only partial, which is not surprising given that constitutive endocytosis is not a synchronized event elicited by a specific stimuli; hence, it would be expected that we after the incubation period also will see JHC 1–64-labeled DAT in other endosomal compartments along the endocytic pathway. For transferrin, the colocalization seemed to diminish over time possibly reflecting differential postendocytic sorting of DAT and the transferrin receptor.

The visualization of endocytosed JHC 1–64-labeled transporter suggests furthermore that cultured dopaminergic neurons contain a pool of intracellular transporter. Live imaging of the internalized transporter allowed us to follow movements of the intracellular vesicles. In this way, we identified JHC 1–64-positive vesicles that either were essentially immobilized or undergoing rapid movements during the observation period. Future studies are required to characterize the functional implications of these observations; however, it is tempting to speculate that the endocytosed JHC 1–64-labeled DAT unravel a recruitable pool of transporters that might permit rapid adaptation of the neuron to immediate changes in the need for neurotransmitter reuptake. Interestingly, a pool of intracellular transporters has before been suggested to exist for DAT (Buckley et al., 2000; Johnson et al., 2005) as well as for the homologous GABA transporter-1 (Wang and Quick, 2005).

## References


Adkins EM, Samuvel DJ, Fog JU, Eriksen J, Jayanthi LD, Vaegter CB, Ramamoorthy S, Gether U (2007) Membrane mobility and microdomain association of the dopamine transporter studied with fluorescence correlation spectroscopy and fluorescence recovery after photobleaching. Biochemistry 46:10484–10497.

Blakely RD, Bauman AL (2000) Biogenic amine transporters: regulation in flux. Curr Opin Neurobiol 10:328–336.

Blanpied TA, Scott DB, Ehlers MD (2002) Dynamics and regulation of clathrin coats at specialized endocytic zones of dendrites and spines. Neuron 36:435–449.

Buckley KM, Melikian HE, Provoda CJ, Waring MT (2000) Regulation of neuronal function by protein trafficking: a role for the endosomal pathway. J Physiol 525:11–19.

Cha JH, Zou MF, Adkins EM, Rasmussen SG, Loland CJ, Schoenenberger B, Gether U, Newman AH (2005) Rhodamine-labeled 2beta-carbomethoxy-3beta-(3,4-dichlorophenyl)tropane analogues as high-affinity fluorescent probes for the dopamine transporter. J Med Chem 48:7513–7516.

Chen NH, Reith ME, Quick MW (2004) Synaptic uptake and beyond: the sodium- and chloride-dependent neurotransmitter transporter family SLC6. Pflugers Arch 447:519–531.

Chi L, Reith ME (2003) Substrate-induced trafficking of the dopamine transporter in heterologously expressing cells and in rat striatal synaptosomal preparations. J Pharmacol Exp Ther 307:729–736.

Daniels GM, Amara SG (1999) Regulated trafficking of the human dopamine transporter. Clathrin-mediated internalization and lysosomal degradation in response to phorbol esters. J Biol Chem 274:35794–35801.

Daws LC, Callaghan PD, Morón JA, Kahlig KM, Shippenberg TS, Javitch JA, Galli A (2002) Cocaine increases dopamine uptake and cell surface expression of dopamine transporters. Biochem Biophys Res Commun 290:1545–1550.

Deneka M, Neeft M, van der Sluijs P (2003) Regulation of membrane transport by rab GTPases. Crit Rev Biochem Mol Biol 38:121–142.

di Porzio U, Daguet MC, Glowinski J, Prochiantz A (1980) Effect of striatal cells on in vitro maturation of mesencephalic dopaminergic neurones grown in serum-free conditions. Nature 288:370–373.

di Porzio U, Rougon G, Novotny EA, Barker JL (1987) Dopaminergic neurons from embryonic mouse mesencephalon are enriched in culture through immunoreaction with monoclonal antibody to neural specific protein 4 and flow cytometry. Proc Natl Acad Sci U S A 84:7334–7338.

Dittgen T, Nimmerjahn A, Komai S, Licznerski P, Waters J, Margrie TW, Helmchen F, Denk W, Brecht M, Osten P (2004) Lentivirus-based ge-

netic manipulations of cortical neurons and their optical and electrophysiological monitoring in vivo. Proc Natl Acad Sci U S A 101:18206–18211.
Gainetdinov RR, Caron MG (2003) Monoamine transporters: from genes to behavior. Annu Rev Pharmacol Toxicol 43:261–284.
Gallegos LL, Kunkel MT, Newton AC (2006) Targeting protein kinase C activity reporter to discrete intracellular regions reveals spatiotemporal differences in agonist-dependent signaling. J Biol Chem 281:30947–30956.
Garcia BG, Wei Y, Moron JA, Lin RZ, Javitch JA, Galli A (2005) Akt is essential for insulin modulation of amphetamine-induced human dopamine transporter cell-surface redistribution. Mol Pharmacol 68:102–109.
Gether U, Andersen PH, Larsson OM, Schousboe A (2006) Neurotransmitter transporters: molecular function of important drug targets. Trends Pharmacol Sci 27:375–383.
Granas C, Ferrer J, Loland CJ, Javitch JA, Gether U (2003) N-terminal truncation of the dopamine transporter abolishes phorbol ester- and substance P receptor-stimulated phosphorylation without impairing transporter internalization. J Biol Chem 278:4990–5000.
Hansen SH, Sandvig K, van Deurs B (1993) Clathrin and HA2 adaptors: effects of potassium depletion, hypertonic medium, and cytosol acidification. J Cell Biol 121:61–72.
Hersch SM, Yi H, Heilman CJ, Edwards RH, Levey AI (1997) Subcellular localization and molecular topology of the dopamine transporter in the striatum and substantia nigra. J Comp Neurol 388:211–227.
Heuser JE, Anderson RG (1989) Hypertonic media inhibit receptor-mediated endocytosis by blocking clathrin-coated pit formation. J Cell Biol 108:389–400.
Holton KL, Loder MK, Melikian HE (2005) Nonclassical, distinct endocytic signals dictate constitutive and PKC-regulated neurotransmitter transporter internalization. Nat Neurosci 8:881–888.
Hoover BR, Everett CV, Sorkin A, Zahniser NR (2007) Rapid regulation of dopamine transporters by tyrosine kinases in rat neuronal preparations. J Neurochem 101:1258–1271.
Ingram SL, Prasad BM, Amara SG (2002) Dopamine transporter-mediated conductances increase excitability of midbrain dopamine neurons. Nat Neurosci 5:971–978.
Johnson LA, Furman CA, Zhang M, Guptaroy B, Gnegy ME (2005) Rapid delivery of the dopamine transporter to the plasmalemmal membrane upon amphetamine stimulation. Neuropharmacology 49:750–758.
Lajoie P, Nabi IR (2007) Regulation of raft-dependent endocytosis. J Cell Mol Med 11:644–653.
Lavezzari G, McCallum J, Dewey CM, Roche KW (2004) Subunit-specific regulation of NMDA receptor endocytosis. J Neurosci 24:6383–6391.
Leander Johansen J, Dagø L, Tornøe J, Rosenblad C, Kusk P (2005) A new versatile and compact lentiviral vector. Mol Biotechnol 29:47–56.
Lippincott-Schwartz J, Snapp E, Kenworthy A (2001) Studying protein dynamics in living cells. Nat Rev Mol Cell Biol 2:444–456.
Melikian HE, Buckley KM (1999) Membrane trafficking regulates the activity of the human dopamine transporter. J Neurosci 19:7699–7710.
Miranda M, Dionne KR, Sorkina T, Sorkin A (2007) Three ubiquitin conjugation sites in the amino terminus of the dopamine transporter mediate protein kinase C-dependent endocytosis of the transporter. Mol Biol Cell 18:313–323.
Morón JA, Zakharova I, Ferrer JV, Merrill GA, Hope B, Lafer EM, Lin ZC, Wang JB, Javitch JA, Galli A, Shippenberg TS (2003) Mitogen-activated protein kinase regulates dopamine transporter surface expression and dopamine transport capacity. J Neurosci 23:8480–8488.
Naldini L, Blömer U, Gage FH, Trono D, Verma IM (1996a) Efficient transfer, integration, and sustained long-term expression of the transgene in adult rat brains injected with a lentiviral vector. Proc Natl Acad Sci U S A 93:11382–11388.
Naldini L, Blömer U, Gallay P, Ory D, Mulligan R, Gage FH, Verma IM, Trono D (1996b) In vivo gene delivery and stable transduction of nondividing cells by a lentiviral vector. Science 272:263–267.
Nirenberg MJ, Vaughan RA, Uhl GR, Kuhar MJ, Pickel VM (1996) The dopamine transporter is localized to dendritic and axonal plasma membranes of nigrostriatal dopaminergic neurons. J Neurosci 16:436–447.
Nirenberg MJ, Chan J, Vaughan RA, Uhl GR, Kuhar MJ, Pickel VM (1997) Immunogold localization of the dopamine transporter: an ultrastructural study of the rat ventral tegmental area. J Neurosci 17:5255–5262.
Quick MW, Hu J, Wang D, Zhang HY (2004) Regulation of a gamma-aminobutyric acid transporter by reciprocal tyrosine and serine phosphorylation. J Biol Chem 279:15961–15967.
Rappoport JZ (2008) Focusing on clathrin-mediated endocytosis. Biochem J 412:415–423.
Rayport S, Sulzer D, Shi WX, Sawasdikosol S, Monaco J, Batson D, Rajendran G (1992) Identified postnatal mesolimbic dopamine neurons in culture: morphology and electrophysiology. J Neurosci 12:4264–4280.
Rees S, Coote J, Stables J, Goodson S, Harris S, Lee MG (1996) Bicistronic vector for the creation of stable mammalian cell lines that predisposes all antibiotic-resistant cells to express recombinant protein. Biotechniques 20:102–104, 106, 108–110.
Robinson MS (1994) The role of clathrin, adaptors and dynamin in endocytosis. Curr Opin Cell Biol 6:538–544.
Saunders C, Ferrer JV, Shi L, Chen J, Merrill G, Lamb ME, Leeb-Lundberg LM, Carvelli L, Javitch JA, Galli A (2000) Amphetamine-induced loss of human dopamine transporter activity: an internalization-dependent and cocaine-sensitive mechanism. Proc Natl Acad Sci U S A 97:6850–6855.
Silva NL, Mariani AP, Harrison NL, Barker JL (1988) 5,7-Dihydroxytryptamine identifies living dopaminergic neurons in mesencephalic cultures. Proc Natl Acad Sci U S A 85:7346–7350.
Sorkina T, Hoover BR, Zahniser NR, Sorkin A (2005) Constitutive and protein kinase C-induced internalization of the dopamine transporter is mediated by a clathrin-dependent mechanism. Traffic 6:157–170.
Sorkina T, Miranda M, Dionne KR, Hoover BR, Zahniser NR, Sorkin A (2006) RNA interference screen reveals an essential role of Nedd4–2 in dopamine transporter ubiquitination and endocytosis. J Neurosci 26:8195–8205.
Torres GE, Amara SG (2007) Glutamate and monoamine transporters: new visions of form and function. Curr Opin Neurobiol 17:304–312.
Torres GE, Gainetdinov RR, Caron MG (2003) Plasma membrane monoamine transporters: structure, regulation and function. Nat Rev Neurosci 4:13–25.
van der Bliek AM, Redelmeier TE, Damke H, Tisdale EJ, Meyerowitz EM, Schmid SL (1993) Mutations in human dynamin block an intermediate stage in coated vesicle formation. J Cell Biol 122:553–563.
Vaughan RA, Huff RA, Uhl GR, Kuhar MJ (1997) Protein kinase C-mediated phosphorylation and functional regulation of dopamine transporters in striatal synaptosomes. J Biol Chem 272:15541–15546.
Violin JD, Zhang J, Tsien RY, Newton AC (2003) A genetically encoded fluorescent reporter reveals oscillatory phosphorylation by protein kinase C. J Cell Biol 161:899–909.
Wang D, Quick MW (2005) Trafficking of the plasma membrane gamma-aminobutyric acid transporter GAT1. Size and rates of an acutely recycling pool. J Biol Chem 280:18703–18709.
Yguerabide J, Schmidt JA, Yguerabide EE (1982) Lateral mobility in membranes as detected by fluorescence recovery after photobleaching. Biophys J 40:69–75.
Zerial M, McBride H (2001) Rab proteins as membrane organizers. Nat Rev Mol Cell Biol 2:107–117.
Zhou P, Porcionatto M, Pilapil M, Chen Y, Choi Y, Tolias KF, Bikoff JB, Hong EJ, Greenberg ME, Segal RA (2007) Polarized signaling endosomes coordinate BDNF-induced chemotaxis of cerebellar precursors. Neuron 55:53–68.
Zomot E, Bendahan A, Quick M, Zhao Y, Javitch JA, Kanner BI (2007) Mechanism of chloride interaction with neurotransmitter:sodium symporters. Nature 449:726–730.
Zufferey R, Nagy D, Mandel RJ, Naldini L, Trono D (1997) Multiply attenuated lentiviral vector achieves efficient gene delivery in vivo. Nat Biotechnol 15:871–875.

# *Supplementary Information*

## Visualization of dopamine transporter trafficking in live neurons by use of fluorescent cocaine analogues

Jacob Eriksen*[1], Søren G. F. Rasmussen*[1], Trine Nygaard Rasmussen[1], Christian Bjerggaard Vaegter[1], Joo Hwan Cha[2], Mu-Fa Zou[2], Amy Hauck Newman[2] and Ulrik Gether[1]

[1]Molecular Neuropharmacology Group and Center for Pharmacogenomics, Department of Neuroscience and Pharmacology, The Panum Institute, University of Copenhagen, DK-2200 Copenhagen, Denmark, and [2]Medicinal Chemistry Section, National Institute on Drug Abuse – Intramural Research Program, National Institutes of Health, 5500 Nathan Shock Drive, Baltimore, MD 21224,

*contributed equally to this work

---

Correspondence to:

Ulrik Gether, MD, Professor
Molecular Neuropharmacology Group and Center for Pharmacogenomics
Department of Neuroscience and Pharmacology, The Panum Institute
University of Copenhagen, DK-2200 Copenhagen N, Denmark
Tel: +45 3532 7548; Fax: +45 3532 7610; E-mail: gether@sund.ku.dk

***Supplementary Figure 1***

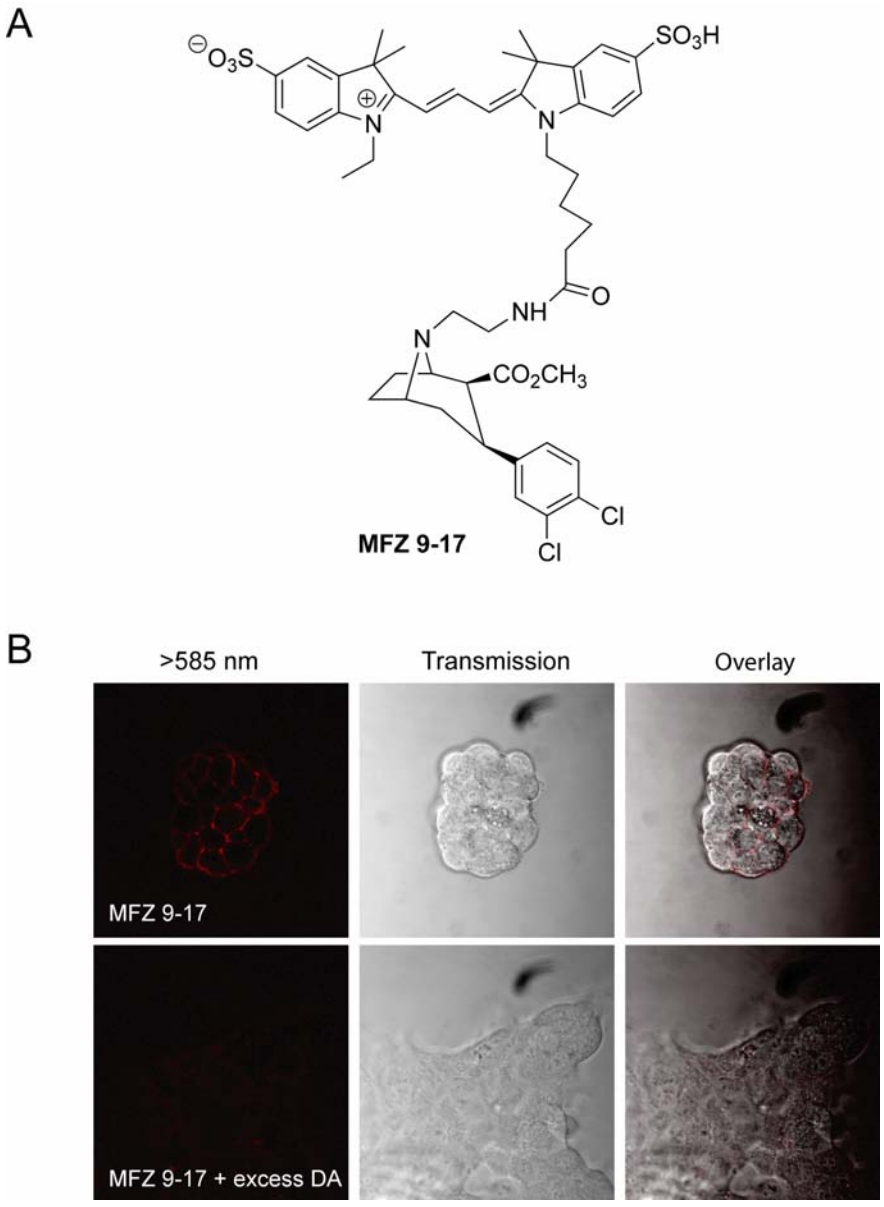


**Fig. S1. Specific labeling of DAT with the fluorescent cocaine analogue MFZ 9-17**. ***A***, Structure of the Cy3 conjugate MFZ 9-17. The compound was synthesized as described in *Experimental Procedures* by extending the fluorescent tag from the N- position of 2β-carbomethoxy-3β-(3,4-dichlorophenyl)tropane using an ethylamino-linker. ***B***, Live HEK293 cells stably expressing DAT preincubated with 10 nM MFZ 9-17 for 20 min at RT (*upper panels)* or with 1 mM dopamine for 15 min followed by 10 nM MFZ 9-17 for 20 min at RT (*lower panels*). MFZ 9-17 was visualized using a 543 nm HeNe laser for excitation and a >585 nm long pass filter for recording of fluorescence. Left panels show fluorescence in the >585 nm channel, middle panels transmitted light and right panels overlay of the two channels.

***Supplementary Figure 2***

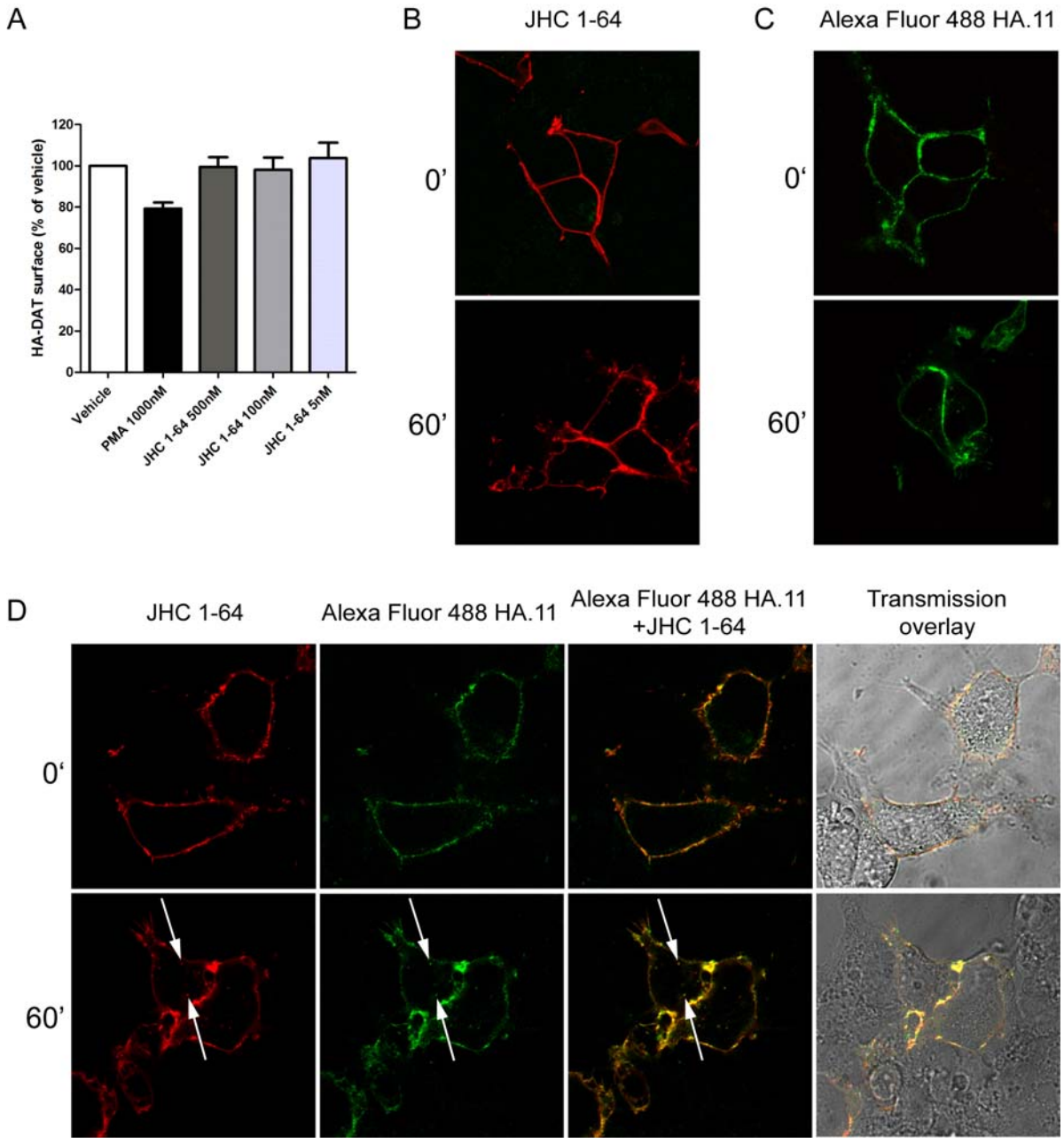


**Fig. S2. JHC 1-64 does not influence DAT surface expression or constitutive internalization in HEK293 cells.** ***A***, HEK293 cells transiently expressing DAT containing an HA tag in the second extracellular loop (HA-hDAT) (Sorkina et al., 2006) were incubated with PMA or indicated conentrations of JHC 1-64 for 1 hour before quantification of surface DAT by ELISA as described in Supplementary Material and Methods. None of the tested JHC 1-64 concentrations differed significantly from vehicle whereas PMA significantly downregulated HA-DAT surface expression ($P<0.05$, n=3, one sample t-test). Data are means ± SE. ***B***, ***C***, HEK293 cells expressing HA-hDAT were incubated with 5 nM JHC 1-64 (***B***) or 1 µg/ml Alexa Fluor 488-

conjugated HA.11 antibody (***C***) in buffer 1 for 20 minutes at RT to label HA-hDAT. Subsequently, the cells were either washed in buffer 1 and imaged (0') or incubated for 60 minutes at 37°C and then washed and imaged (60'). At time 0' no intracellular accumulation of either JHC 1-64 or HA.11 was visible. However, after 60 minutes of incubation at 37°C a weak intracellular accumulation of JHC 1-64 (***B***) and HA.11 (***C***) was observed (60'). This most likely represents modest constitutive internalization of HA-hDAT. (***D***) HEK293 cells expressing HA-hDAT were incubated with both 5 nM JHC 1-64 and 1 µg/ml Alexa Fluor 488-conjugated HA.11 antibody for 20 min at RT before the cells were either washed and imaged (0') or incubated for 60 minutes at 37°C and then washed and imaged (60'). In this experiment a similar pattern was observed indicating that constitutive DAT internalization does not seem to be affected by JHC 1-64. The overlays with transmission pictures confirm the specificity of JHC 1-64 as only cells labelled with HA.11 is labelled also with JHC 1-64 (***D***) showing that DAT is necessary for JHC 1-64 binding. Images are representative of three independent experiments.

***Supplementary Figure 3***

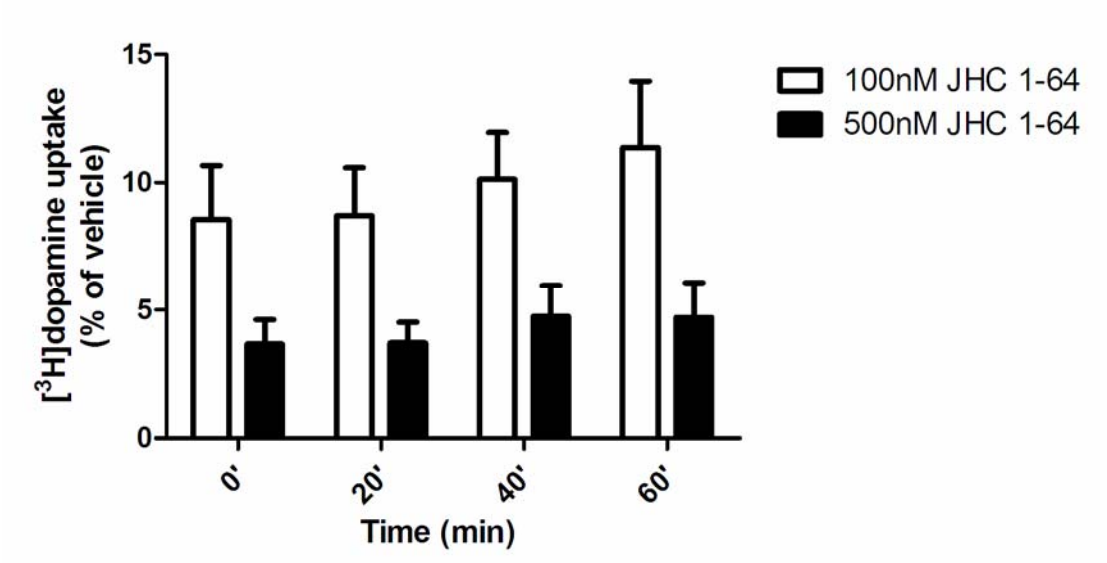


**Fig. S3. JHC 1-64 has a slow off-rate from DAT and inhibits DA uptake after prolonged wash-out.** HEK293 cells transiently transfected with DAT were incubated with either 100 nM JHC 1-64, 500 nM JHC 1-64 or vehicle (0.01% DMSO or 0.05% DMSO) for 30 minutes at RT. The cells were subsequently washed and incubated for 0, 20, 40, or 60 minutes at 37ºC. Following two additional washes [$^3$H]dopamine uptake was assayed. At all time points and at both concentrations, JHC 1-64 inhibited [$^3$H]dopamine uptake significantly. A tendency towards an increased uptake over time is seen. Data are means ± SE, n=3.

***Supplementary Figure 4***

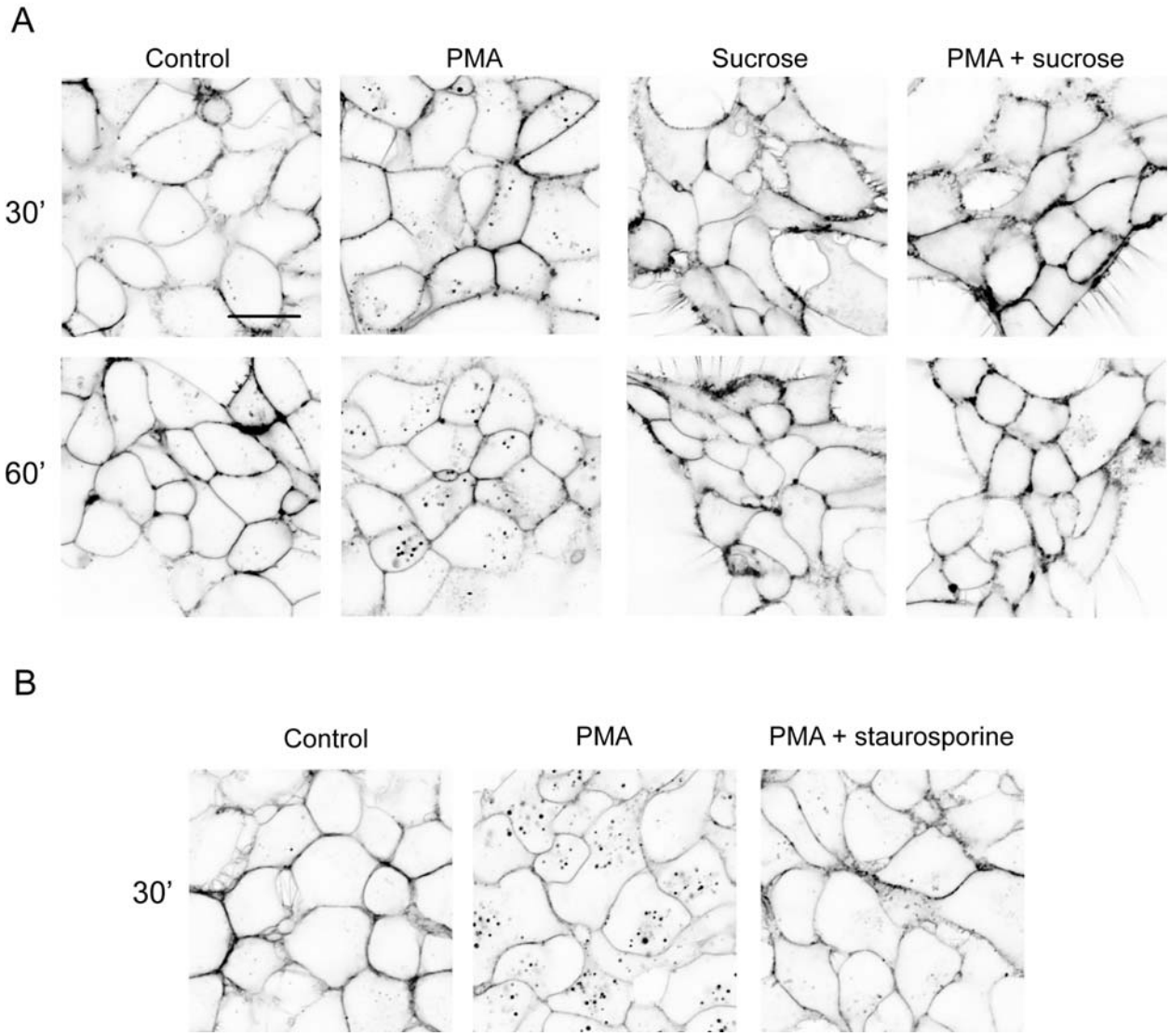


**Fig. S4. PMA-induced internalization of JHC 1-64 labeled DAT in HEK293 cells is blocked by sucrose and staurosporine.** **A**, HEK293 cells stably expressing wild type DAT were labeled with 5 nM JHC 1-64 at RT for 20 min before incubation for 30 min (*upper panels*) and 60 min (*lower panels*) at 37°C in the absence or presence of 1μM PMA with and without addition of 450 mM sucrose as indicated, or **B**, pre-incubated with 1 μM staurosporine as indicated. JHC 1-64 was visualized using a 543 nm HeNe laser for excitation and a >585 nm long pass filter for recording of fluorescence. The images show the fluorescence on a gray scale with darkest pixels representing the largest fluorescence. In the absence of PMA, there is hardly any redistribution of JHC 1-64 labeled DAT even after one hour of incubation. In the presence of PMA, intracellular fluorescence appeared in vesicular structures during the incubation period consistent with internalization of the transporter. This redistribution was completely blocked by sucrose in agreement with internalization through a clathrin-dependent pathway. Furthermore the PMA-induced internalization was blocked by the non-specific PKC inhibitor staurosporine. Scale bar 20 μm.

***Supplementary Figure 5***

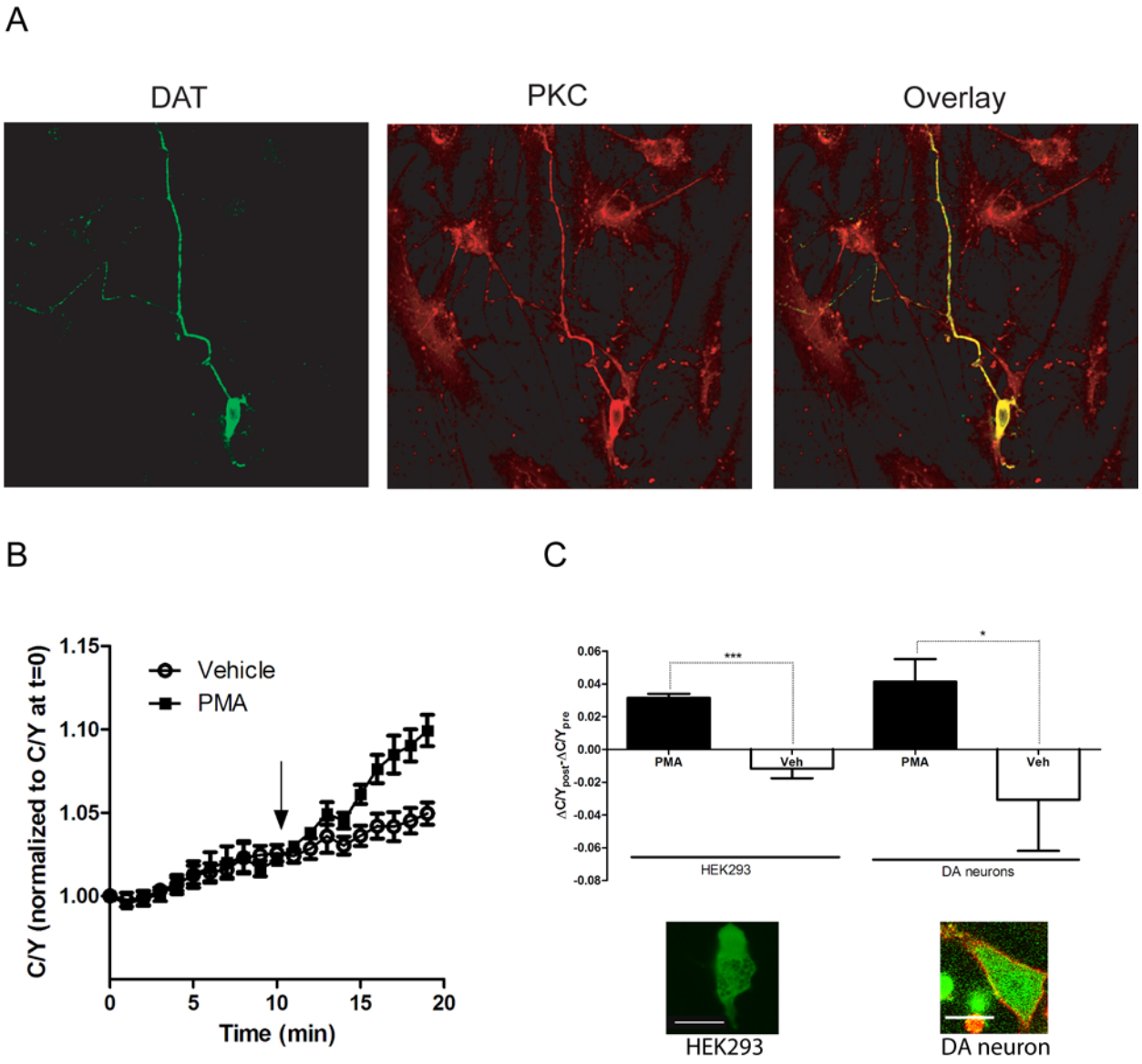


**Fig. S5. Protein kinase C is expressed and activated upon PMA stimulation in dopaminergic neurons.** ***A***, Midbrain neurons in primary culture were fixed, permeabilized and stained with a rat anti-DAT antibody (MAB369, 1:1000) and a rabbit PKC antibody (1:1000. Ac543-550, Calbiochem) recognizing a PKC consensus sequence. Secondary detection was obtained with Alexa Fluor 488 goat anti-rat and Alexa Fluor 568 goat anti-rabbit. DAT positive neurons also displayed substantial staining for PKC. As expected PKC staining was also seen in other neurons in the culture and in the glial cells. ***B***, The CKAR PKC FRET sensor was transiently expressed in HEK293 cells and a CFP (C) and FRET (Y) picture was acquired every minute for 20 minutes. After 10 minutes, 1 µM PMA or 0.1% DMSO was added to the cells (indicated by arrow), and a decrease in the FRET signal was observed (as indicated by the rise in the C/Y ratio). ***C***, CKAR was expressed in midbrain neuronal cultures by lentiviral

transduction and the dopaminergic neurons were identified by labelling with JHC 1-64 (see inset picture). The dopaminergic neurons were imaged and stimulated with PMA as described for HEK293 cells with the exception that images were only acquired every second minute to reduce bleaching. The effect of PMA was quantified as the difference between the slope after PMA/vehicle and the slope before PMA/vehicle. There was a significant difference between vehicle and PMA-treated cells in both HEK293 cells ($P<0.001$, n=22 cells per condition) and DA neurons ($P<0.5$, n=7 neurons for vehicle and n=8 neurons for PMA), indicating that PMA activates PKC in both HEK293 cells and DA neurons.

***Supplementary Figure 6***

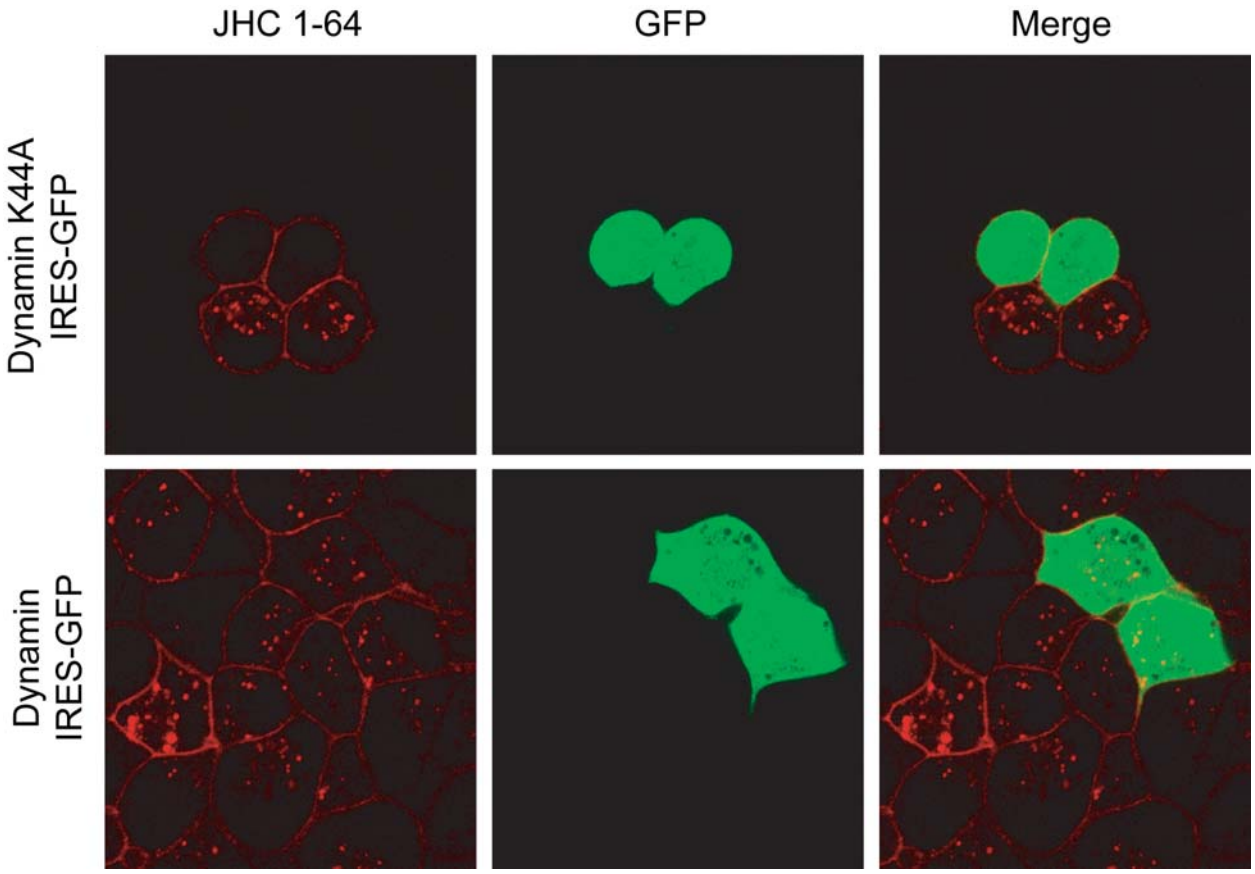


**Fig. S6. Dominant negative dynamin K44A blocks PMA-mediated JHC 1-64/DAT internalization in HEK293 cells.** HEK293 cells stably expressing hDAT were transduced with lentivirus encoding either dynamin K44A or dynamin wild type. To identify transduced cells the vector also encoded GFP separated from dynamin by an internal ribosome entry site (dynamin K44A IRES-GFP). Accordingly, GFP positive cells indicated efficient lentiviral transduction. Five days after transduction, the cells were labeled with 5 nM JHC 1-64 at RT for 20 min before incubation for 30 min at 37°C in the presence of 1μM PMA. Cells expressing dynamin K44A showed almost no PMA-induced internalization, whereas cells overexpressing dynamin wild type retained the PMA-induced DAT internalization.

***Supplementary Figure 7***

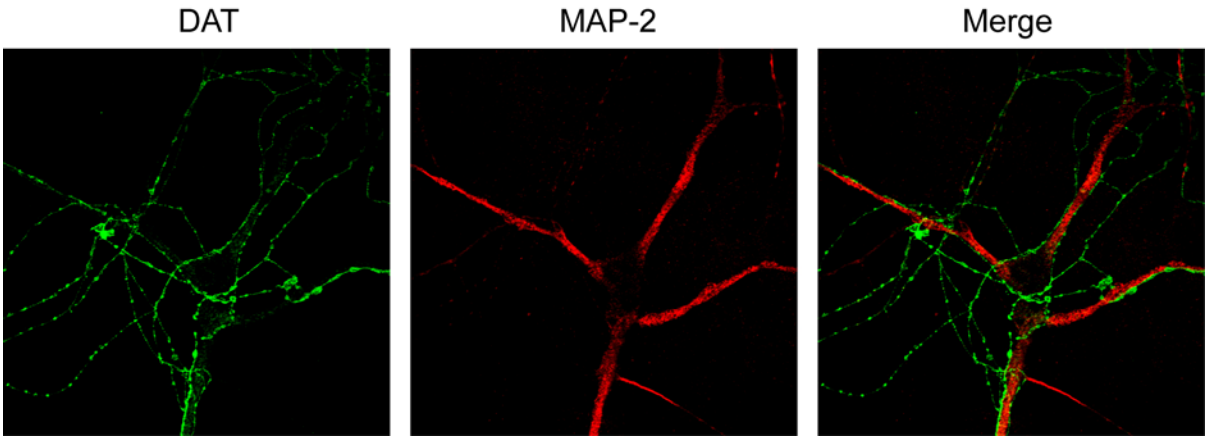


**Fig. S7. Little co-localization between DAT and the dendritic marker MAP2.** Midbrain neurons in culture were fixed, permeabilized and stained with rat anti-DAT antibody (MAB369, 1:1000) and rabbit anti-MAP2 (1:1000) antibody. Secondary detection was obtained with Alexa Fluor 488 goat anti-mouse or Alexa Fluor 488 goat anti-rabbit, respectively. Extensive networks of DAT positive fibers were observed in the culture; however, only little overlap was seen with MAP2. In the representative picture, a network of DAT positive fibers surrounds the MAP2 positive dendritic tree of another *non-dopaminergic* neuron.

## *Supplementary Materials and Methods*

*Molecular Biology*
pCDNA3.1 CKAR was a generous gift from Dr. Alexandra Newton, San Diego, CA. To clone CKAR into the lentiviral vector pHSynXW, CKAR was PCR amplified from the pCDNA3.1 vector with a 5' primer introducing a BsiWI site and a 3' primer recognizing a sequence 3' to the multiple cloning site in pCDNA3.1. The PCR fragment was digested with BsiWI and XbaI and ligated into pHSynXW digested with BsiWI and SpeI creating pHSynXW CKAR.

*HA-hDAT surface ELISA*
HEK293 cells transfected with hDAT with an extracellular HA epitope (HA-hDAT, as described in *Sorkina et al. 2006*) were seeded in 96 well plates (35,000 cells/well) the day before experiment. On the day of the experiment the cells were incubated with JHC 1-64 (500 nM, 100 nM and 5 nM), PMA (1µM) or DMSO (0.1%) for 1 hour at 37ºC. After incubation, the cells were fixed in 4% PFA in PBS for 20 minutes on ice, washed twice in PBS, blocked in PBS + 5% goat serum for 30 minutes and incubated with HA.11 antibody (1:1000; Covance, Princeton, NJ) in PBS + 5% goat serum for 60 minutes. Following 4 washes in PBS, the cells were then incubated with HRP-conjugated goat anti-mouse antibody (1:1000; Pierce) for 30 minutes and subsequently washed 4 additional times in PBS. The HRP activity was detected and quantified instantaneously by chemiluminescence using Supersignal ELISA femto maximum sensitivity substrate (Pierce) and a Wallac Victor$^2$ luminescence counter (PerkinElmer Life Science).

*JHC 1-64/HA.11 feeding experiment*
HEK293 cells, transiently transfected with HA-hDAT were grown in DMEM + 10% FCS and seeded in poly-L-ornithine treated 8-well LabTek Chambers (60,000 cells/well) the day before the experiment. On the day of the experiment, the cells were washed once in buffer 1, and then incubated with 5 nM JHC 1-64, 1µg/ml Alexa Fluor 488 conjugated HA.11 (Covance), or both for 20 minutes to allow labeling of the transporters with a minimum of trafficking occurring. Then the cells were either washed (0 minutes constitutive internalization) or incubated for 60 minutes at 37ºC (60 minutes constitutive internalization). Imaging was performed as described for EGFP-tagged DAT and JHC 1-64.

*JHC 1-64 off-rate experiment*
HEK293 cells transfected with pCDNA3 hDAT were seeded in 24 well plates (100,000 cells per well) the day before the experiment. On the day of the experiment, the cells were washed once in buffer 1, and then incubated with either 500 nM, 100 nM JHC 1-64 or vehicle (0.05% or 0.01% DMSO) for 30 minutes at RT. The solution was then aspirated and the cells washed once before incubation in buffer 1 for 0, 20, 40 or 60 minutes at 37°C. Subsequently the cells were washed twice and [$^3$H]dopamine uptake was assayed as described in Experimental Procedures.

*CKAR imaging*
HEK293 cells were transfected with pCDNA3.1 CKAR (encoding a fluorescence resonance energy transfer-based reporter for PKCactivity, C kinase activity reporter) and seeded in LabTek chambers as described above. On the day of the experiment the cells were washed once in buffer 1 and incubated for at least 20 minutes at RT before microscopy. The cells were imaged at RT on a Zeiss Axiovert 200 with a 63x NA1.4 oil objective, and a cooled charge-coupled device camera (Coolsnap, Photometrics) controlled by MetaMorph software (Meta Imaging, Universal Imaging Corporation, V. 4.6). CFP and FRET images were obtained with 436 nm excitation from a TILL xenon lamp light source through a CFP/YFP beam splitter (JP4PC,

Chroma) and two separate emission filters (a 480/40 nm filter for CFP and a 535/40 nm filter for FRET, both filters from Chroma Technologies) on a LUDL filter wheel allowing a rapid change of filters. A CFP and corresponding FRET image was acquired every 1 minute (40 ms exposure/image). After 10 minutes 1 μM PMA or 0.1% DMSO was added and pictures were collected for another 10 minutes.

Midbrain dopaminergic neurons were transduced with CKAR virus on day 2 *in vitro* and experiments were done after 7-9 DIV. The cells were washed once in buffer 1 and then incubated with 20 nM JHC 1-64 to help identify doapminergic neurons and left at RT for at least 20 minutes. The neurons were washed once in buffer 1 before imaging. CFP and FRET images were obtained every 2 minutes (80 ms exposure/image) and after 10 minutes 1 μM PMA or 0.1% DMSO was added and pictures were collected for another 10 minutes.

The data were analyzed using ImageJ (Rasband, W.S., ImageJ, U. S. National Institutes of Health, Bethesda, Maryland, USA, http://rsb.info.nih.gov/ij/, 1997-2008). The somas of the cells were outlined, the mean pixel intensity for each cell soma was obtained and the average image background pixel intensity was subtracted from each cell. The ratio between CFP and YFP for each cell at each time point was calculated as a measure for FRET as previously described (Violin et al., 2003). As a measure of the change in FRET after addition of either vehicle or PMA, the slope ΔC/Y(t) of the curve representing the 6 minutes before stimulus was calculated and subtracted from the slope ΔC/Y(t) 0-6 minutes after stimulus.

## *Supplementary references*

Violin JD, Zhang J, Tsien RY, Newton AC (2003) A genetically encoded fluorescent reporter reveals oscillatory phosphorylation by protein kinase C. J Cell Biol. 161(5):899-909.

Sorkina T, Miranda M, Dionne KR, Hoover BR, Zahniser NR, Sorkin A (2006) RNA interference screen reveals an essential role of Nedd4-2 in dopamine transporter ubiquitination and endocytosis. J Neurosci 26:8195-8205.

## Paper 2

# Constitutively Internalized Dopamine Transporter is Sorted Primarily to a Late Endosomal and Lysosomal Pathway in Cell Lines and Dopaminergic Neurons

**Constitutively Internalized Dopamine Transporter is Sorted Primarily to a Late Endosomal and Lysosomal Pathway in Cell Lines and Dopaminergic Neurons**

Jacob Eriksen, Trine Nygaard Jørgensen, Walden Bjørn Emil Yoshimoto and Ulrik Gether

Molecular Neuropharmacology Group and Center for Pharmacogenomics, Department of Neuroscience and Pharmacology, Faculty of Health Sciences, The Panum Institute, University of Copenhagen, DK-2200 Copenhagen, Denmark

**Running title:** Sorting of internalized dopamine transporter

**Corresponding author:**
Ulrik Gether, Molecular Neuropharmacology Group
Department of Neuroscience and Pharmacology
University of Copenhagen
The Panum Instutute 18.6, Blegdamsvej 3, DK-2200 Copenhagen N, Denmark
Tel: +45 35327548
Fax: +45 35327610
E-mail: gether@sund.ku.dk

**Abstract**

The dopamine transporter (DAT) mediates reuptake of dopamine from the synaptic cleft and is target for widely abused psychostimulants such as cocaine and amphetamine. DAT is known to undergo marked constitutive endocytosis but little is known about the fate and sorting of the endocytosed transporter. Here we show that DAT upon constitutive endocytosis is sorted primarily to late endosomes and lysosomes rather than into a recycling pathway. To study sorting in heterologous cells lines we fused the one-transmembrane segment protein Tac to DAT, thereby generating a transporter (TacDAT) with an extracellular N-terminal antibody epitope suited for trafficking studies. TacDAT was fully functional and endocytosed constitutively in HEK293 cells. The intracellular accumulation was increased by the lysosomal protease inhibitor leupeptin and by monensin, an inhibitor of lysosomal degradation and recycling. However, monensin did not affect TacDAT surface expression, and constitutively internalized TacDAT primarily colocalized with the late endosomal marker Rab7. In the dopaminergic cell line 1Rb3An27, TacDAT, also constitutively internalized, and co-localized primarily with Rab7 as compared to the marker of recycling endosomes, Rab11. This pattern was distinct from a bona fide recycling membrane protein, the $ß_2$-adrenergic receptor, which colocalized primarily with Rab11. Constitutively internalized wild type DAT probed with the fluorescently tagged cocaine analogue, JHC 1-64, also exhibited Rab7 colocalization in 1Rb3An27 cells. Finally, constitutively internalized DAT visualized with JHC 1-64 in cultured dopaminergic neurons colocalized both with Rab7 and the lysosomal marker, LysoTracker Green. We conclude that independent of cell type DAT is constitutively internalized and primarily sorted to a late endosomal/lysosomal pathway.

## Introduction

The dopamine transporter (DAT) mediates reuptake of dopamine from the synaptic cleft and terminates in this way dopaminergic signalling and mediates recycling of released dopamine (Chen et al., 2004, Gether et al., 2006, Torres and Amara, 2007). Alteration in dopamine signalling and DAT function is coupled to neurological and psychiatric diseases including schizophrenia, bipolar disorder, ADHD (Attention Deficit Hyperactivity Disorder), Tourette's syndrome and Parkinson's disease (Gainetdinov and Caron, 2003, Torres et al., 2003, Gether et al., 2006). DAT is also the principle target for widely abused psychostimulants, such as cocaine and amphetamine (Chen et al., 2004; Gether et al., 2006; Torres and Amara, 2007). The transporter belongs to the family of neurotransmitter:sodium symporters (NSS) (also called the SLC6 [solute carrier 6] family or $Na^+/Cl^-$ coupled transporters) that also includes the transporters for other neurotransmitters such as the norepinephrine, serotonin, glycine and GABA. NSS proteins utilize the transmembrane $Na^+$ gradient as a driving force for transport of substrate and are further characterized by additional co-transport of $Cl^-$ (Chi and Reith, 2003, Gether et al., 2006, Torres and Amara, 2007).

Numerous studies have supported that DAT is subject to dynamic regulation in the plasma membrane thereby providing a mean of attenuating or increasing the strength of dopaminergic signalling. The most intensively studied mechanism is the regulatory effect of protein kinase C (PKC) activation. It has been demonstrated in several DAT transfected heterologous cell lines as well as in synaptosomes that activation of PKC by phorbol esters, such as phorbol 12-myristate 13-acetate (PMA), down-regulates dopamine transport (Copeland et al., 1996, Vaughan et al., 1997, Zhu et al., 1997, Daniels and Amara, 1999, Melikian and Buckley, 1999, Chi and Reith, 2003, Sorkina et al., 2005, Eriksen et al., 2009). The sustained DAT down-regulation in response to PKC activation is believed mainly to be a result of DAT endocytosis through a clathrin-dependent mechanism (Daniels and Amara, 1999, Melikian and Buckley, 1999, Chi and Reith, 2003, Sorkina

et al., 2005). DAT trafficking is also regulated by other protein kinases such as mitogen-activated protein kinase (MAPK) and Akt (Moron et al., 2003, Garcia et al., 2005) as well as by substrates and inhibitors (Zahniser and Sorkin, 2009).

In addition, DAT undergoes a marked constitutive endocytosis, a property that first was described in heterologous cell lines (Chi and Reith, 2003, Loder and Melikian, 2003, Sorkina et al., 2005). Subsequent mutational analyses suggested that this constitutive internalization is promoted by a non-conventional trafficking motif in the DAT C-terminus (Holton et al., 2005, Sorkina et al., 2005) and possible negatively regulated by residues residing in the membrane proximal DAT N-terminus (Sorkina et al., 2009). Recently, we demonstrated by use of the fluorescent cocaine analogue JHC 1-64 as label that DAT endogenously expressed in cultured midbrain dopaminergic neurons also undergoes constitutive internalization that, however, was neither sensitive to activation or inhibition of PKC (Eriksen et al., 2009). The constitutive DAT internalization was dynamin-dependent and internalized transporter partially colocalized with the early endosomal markers Rab5 and partially with endocytosed transferrin (Eriksen et al., 2009).

A major question is the fate of the constitutively internalized transport protein. Previous studies in heterologous have indicated that DAT might be sorted to a recycling pathway (Loder and Melikian, 2003, Sorkina et al., 2005); however, postendocytic sorting of constitutively internalized DAT has not yet been analyzed in dopaminergic neurons as well as postendocytic sorting of constitutively internalized DAT in heterologous cells has not been analyzed in dynamic imaging experiments using co-expressed markers of distinct endocytic compartments. Here we investigate the postendocytic sorting of constitutively internalized DAT in both heterologous cells and cultured dopaminergic neurons. We take advantage of a fusion protein between the one-transmembrane segment protein Tac and DAT, which provides a transporter (TacDAT) with an extracellular N-terminal antibody epitope. In the absence of a DAT antibody directed towards an endogenous

extracellular epitope, TacDAT enables the application of antibody feeding experiments and implementation of ELISA-based trafficking assays. Moreover, by use of the fluorescent cocaine analogue JHC 1-64 we are able to analyze postendocytic sorting of DAT in cultured dopaminergic neurons. Taken together, our data suggest that constitutively internalized DAT is sorted to a late endosomal/lysosomal degradative pathway in both neurons and cell lines.

**Materials and Methods**

*Molecular biology*. TacDAT was generated by a two step PCR. First amplifying A) FLAG-Tac from pCDNA3 FLAG-Tac (Madsen et al., 2008) with primers generating an overhang identical to the N-terminal part of synDAT and B) amplifying part of synDAT from pCDNA3 synDAT with a 5' overhang identical to the C-terminal part of FLAG-Tac. Second, the products from the first round of PCR was used as template for generating a TacDAT fragment that was subsequently cloned into the pCDNA3 synDAT vector using *KpnI* and *BamHI*. pCDNA3.1 FLAG-ß$_2$-adrenergic receptor was a kind gift from Dr. Mark von Zastrow . pEGFP-Rab4 was a kind gift from Dr. Jose A. Esteban. pEGFP-Rab7 and pEGFP-Rab11 were kind gifts from Dr. Katherine W. Roche. pHsSynXW EGFP-Rab7 and -Rab11 was generated by PCR amplifying the cDNA encoding region EGFP-Rab7 and 11 from pEGFP-Rab4 and pEGFP-Rab11, respectively. After digestion with BsiWI + MluI fragments were ligated into the lentiviral transfer vector pHSynCXW (Eriksen et al., 2009). EGFP-Rab4 was cloned into pHsSynXW by excising EGFP-Rab4 from pEGFP-Rab4 with NheI and SalI and ligated into pHsSynXW digested with SpeI and SalI. The sequences of the cDNAs were verified by sequencing.

*Cell cultures and lentivirus production.* HEK293 cells and 1Rb3An27 cells were grown in Dulbecco's modified Eagle's medium (DMEM) with 10% fetal calf serum, and transfected using standard Lipo2000 protocols two days prior to the experiment. Dopaminergic neurons and lentivirus were prepared as previously described (Eriksen et al., 2009). Briefly, Postnatally derived rat midbrain dopaminergic neurons prepared using a protocol modified from (Rayport et al., 1992). Briefly, the cultures were obtained from the ventral midbrain of 1- to 3-d-old pups. The dissected tissue sample was digested in a papain solution for 30 min at 37°C while slowly superfused with a mixture of 95% $O_2$ and 5% $CO_2$. The digested tissue was carefully triturated into single cells using

increasingly smaller pipette tips. The cells were centrifuged at 500 x g for 5 min and resuspended in warm SF1C consisting of 50% MEM (Modified Eagle's Medium), 40% DMEM, and 10% F-12 Ham's nutrient mixture (all from Invitrogen) supplemented with bovine serum albumin (2.5 mg/ml), D-glucose (0.35%), glutamine (0.5mM), 1% heat-inactivated calf serum (Invitrogen), kynurenic acid (5 mM), penicillin, streptomycin, liquid catalase (0.05%), and diPorzio (di Porzio et al., 1980). The neurons were plated on a monolayer of glial cells grown in LabTek wells. The cells were allowed to settle for ~ 2 h before addition of GDNF (Millipore Bioscience Research Reagents) (10 ng/ml). The next day 5-fluorodeoxyuridine was added to inhibit growth of glial cells.

Lentiviral vectors were produced according to procedures modified from Naldini et al (Naldini et al., 1996). HEK293T packaging cells were transiently triple transfected with the following: (1) packaging plasmid encoding viral structure proteins (pBR8.91); (2) envelope plasmid encoding the envelope protein VSV-G (pMD.G); and (3) transfer plasmid containing the gene of interest (pHsSynXW EGFP-Rab4, -Rab7, -Rab11). Transfection was performed in DMEM (Invitrogen) supplemented with 10% FBS (Invitrogen) using calcium phosphate precipitation. Medium was replaced with fresh medium after 5 h. Approximately 48 and 72 h after transfection, media containing lentivirus was collected, centrifuged, filtered, and concentrated by ultracentrifugation at 50,000 x g for 1.5 h at 4°C. The virus-containing pellet was resuspended in MEM (Sigma) at 1/280 of the original volume and stored in aliquots at -80°C. The neuronal cultures were incubated with concentrated lentivirus on days 2–3 in vitro and experiments were performed 8–12 d after infection.

*[3H]Dopamine uptake experiments.* Uptake assays were carried out as described previously (Loland et al., 2004) using 2,5,6-[3H]dopamine (9–13 Ci/mmol, Amersham Pharmacia Biotech), and HEK293 cells transfected with equal amounts of pCDNA3 synDAT or 1µg pCDNA3 were plated in either 24-well ($10^5$ cells per well). The uptake assays were carried out 2 d after transfection for 3

min at room temperature (20–22 °C) in uptake buffer (25 mM HEPES, 130 mM NaCl, 5.4 mM KCl, 1.2 mM CaCl2, 1.2 mM MgSO4, 1 mM L-ascorbic acid, 5 mM D-glucose and 1 M of the catechol-O-methyltransferase inhibitor Ro 41-0960 (Sigma), pH 7.4).

*ELISA internalization assay.* HEK293 cells were transfected with Tac or TacDAT using Lipofectamine2000 at a 1:3 ratio to obtain similar surface expression and seeded in 96 well plates (35,000 cells/well) the next day. The experiment was performed 2 days after transfection. First, the cells were incubated with M1 (1μg/mL) in DMEM, 30 minutes at 4 °C, then media was replaced with 37 °C DMEM and placed at 37 °C (or 4 °C for surface quantification) for various periods with different compounds to drive internalization. To strip off surface M1, the cells were incubated with an acid strip buffer (0.5 M NaCl and 0.2 M acetic acid) for 5 minutes on ice, then washed twice with PBS and fixed in 4% paraformaldehyde in PBS and again washed twice in PBS. The cells were then blocked and permeabilized in PBS with 5% goat serum and 0.05% Triton X-100 for 30 minutes (background subtraction was done with cells that were not permeabilized). Then the cells were incubated with horseradish peroxidase-conjugated goat antimouse antibody (1:1000; Pierce) in PBS + 5% goat serum for 30 minutes, and washed two times in blocking buffer + two times in PBS. SuperSignal ELISA Femto Maximum Sensitivity Substrate (Pierce) was added to the wells and the luminescence was detected in a Wallac Victor2 after 2 minutes.

*Surface ELISA*. HEK293 cells transfected with HA-hDAT or TacDAT were seeded in 96 well plates (35,000 cells/well) the day before experiment. On the day of the experiment the cells were incubated with monensin (25 μM) or bafilomycin A (1 μM) for 1 hour at 37ºC. After incubation, the cells were fixed in 4% PFA in PBS for 20 minutes on ice, washed twice in PBS, blocked in PBS +

5% goat serum for 30 minutes and incubated with M1 (1:5000) or HA.11 antibody (1:1000; Covance, Princeton, NJ) in PBS + 5% goat serum for 60 minutes. Following 4 washes in PBS, the cells were then incubated with HRP-conjugated goat anti-mouse antibody for 30 minutes and subsequently washed 4 additional times in PBS. The HRP activity was described above.

*Immunofluorescence antibody internalization assays.* HEK293 cells or 1Rb27An3 cells were transfected with Lipofectamine2000 two days prior to experiment and seeded on coverslips treated with poly-ornithine the next day. The cells were incubated with M1 antibody (1μg/mL) in DMEM for 30 minutes at 4° C. The media was then replaced with 37° C DMEM and placed at 37° C for various periods to drive internalization. The internalization was stopped by washing with cold PBS followed by fixation in 4% paraformaldehyde in PBS, washed 3 times in PBS and permeabilized in PBS with 5% goat serum and 0.2% saponin. Alexa568 anti-mouse (1:500, Molecular Probes) against M1 in PBS + 5% goat serum was added for 30 minutes and then the specimens were washed 3 times in PBS prior to mounting.

For the colocalization experiments the cells were transfected with equal amounts of TacDAT or FLAG-tagged ß$_2$-adrenergic receptor and EGFP-Rab4, -Rab7 or -Rab11 and seeded on coverslips treated with poly-ornithine. On the day of the experiement the cells were incubated with Alexa568-conjugated M1 antibody for 30 minutes at 4° C, the media was then replaced with 37° C DMEM (+ 10 μM isoproterenol for experiments with the ß$_2$-adrenergic receptor) and placed at 37° C for 1hour to allow internalization. The cells were subsequently fixed in 4% PFA in PBS and mounted. The stained cells were visualized using a Zeiss LSM 510 confocal laser-scanning microscope using an oil immersion NA1.4 63x objective. EGFP was excited with the 488 nm laser line from an argon–krypton laser, and the emitted light was detected using a 505–550 nm bandpass filter, whereas the Alexa Fluor 568 dye was excited at 543 nm with a helium–neon laser, and the emitted light was

detected using a 585 nm long-pass filter. The resulting images were combined using IMAGEJ software.

*Colocalization quantification.* Quantification of colocalization with EGFP-tagged Rab4, Rab7 and Rab11 was done using the RG2B colocalization plug-in to IMAGEJ (RasbandW. S., ImageJ, U. S. National Institutes of Health, Bethesda, MD, USA, http://rsb.info.nih.gov/ij/, 1997–2006) as described (Chmelar and Nathanson, 2006, Madsen et al., 2008). Single cells were defined as regions of interest to avoid noise from untransfected cells and non-specific staining. A minimum threshold pixel intensity of 120 was set for each channel and the minimum ratio for pixel intensity between the two channels was set to 0.5. Results are displayed as percent colocalization as determined by dividing the area of colocalization pixels by the total area over the threshold of the M1 signal. 30-35 cells were used for quantification under each condition. Statistical significance was determined using a one way ANOVA with a Bonferroni multiple comparison test. Differences were considered significant when $p < 0.05$.

*DAT internalization with JHC 1-64.* 1Rb3An27 cells or dopaminergic neurons were grown in poly-L-ornithine treated LabTek Chambers. On the day of the experiment the cells were incubated with the indicated fluorescent cocaine analogues in uptake buffer with for designated time periods.
To detect internalization in midbrain dopaminergic neurons and 1Rn27An3 cells, the cultures were incubated with 5 nM JHC 1-64 in uptake buffer for 30 minutes at 4°C, before the buffer was removed and replaced with 37°C warm uptake buffer and incubated for 60 minutes at 37°C. For the Lysotracker co-localization experiment we used Lysotracker Green (100nM; Molecular Probes) in the last 10 minutes of incubation, and subsequently the cells were washed in uptake buffer. After incubation, the living cells were imaged at RT using a Zeiss LSM 510 with a 63x NA1.4 objective

(Zeiss, Jena, Germany). JHC 1-64 was visualized using a 543 nm HeNe laser line and a 585 nm long pass filter, EGFP were detected with a 488 nm argon-krypton laser line and a 505-550 nm band pass filter and the distribution of JHC 1-64 on the neurons were analyzed with a Z-scan.

**Results**

To enable the study of DAT trafficking with high specificity and to detect even small amounts of DAT endocytosis we generated a DAT construct with a high-affinity extracellular antibody epitope. To avoid disruption of the extracellular loops in the DAT, we decided to add an extra transmembrane segment to the N-terminus. This was done by making a head-to-tail fusion of the DAT and the single transmembrane segment protein Tac resulting in the fusion protein, TacDAT (Fig 1A). By fusing protein segments to the C-terminus of Tac, Tac fusion proteins has previously been used as a 'silent reporter' in several trafficking studies (Mu et al., 2003, Lavezzari et al., 2004, Holton et al., 2005, Lavezzari and Roche, 2007). At the Tac N-terminus, a FLAG epitope was introduced after the cleaved signal sequence (Madsen et al., 2008), which permitted the use of the mouse monoclonal M1 anti-FLAG antibody. Staining with M1 antibody of HEK293 cells expressing TacDAT demonstrated in the absence of permeabilization a clear surface staining, which confirmed that the N-terminal antibody epitope is exposed on the extracellular side of the plasma membrane and that the protein is expressed at the cell surface (Fig 1B). TacDAT was functionally analyzed in [$^3$H]dopamine uptake experiments in transiently transfected HEK293 cells (Fig. 1C). TacDAT mediated efficient uptake ($V_{max}$ = 511 ± 104 fmol/min/$10^5$, means ± SE, n=3) although the uptake was reduced as compared to DAT ($V_{max}$ = 2486 ± 236 fmol/min/$10^5$, means ± SE, n=3, p = 0.011, paired t-test). The $K_m$ value for TacDAT was not significantly different from DAT (p > 0.05), i.e. $K_m$ for TacDAT was 0.40 μM [0.36; 0.47 μM] (mean [SE interval] n=3) and 0.92 μM [SE interval (0.62 - 1.4 μM), n=3] for DAT. As our experiment would involve TacDAT with the M1 antibody bound, we made sure that M1 binding to TacDAT did not impair transporter function as determined by measuring [$^3$H]dopamine uptake in the presence of bound M1 antibody (Fig. 1D).

Previously, an HA-tag was successfully introduced into the second extracellular loop of DAT (Sorkina et al., 2006). We decided to compare this tag directly with the FLAG tag in Tac-DAT in a cell-surface ELISA assay by generating a TacDAT construct also harbouring the HA-tag. Interestingly, the signal from the FLAG epitope was almost 10-fold higher than the equimolar signal from the HA epitope (Fig. 1E), making TacDAT preferred for studying low abundant DAT trafficking events.

Next we wanted to test whether it was possible to detect previously proposed DAT trafficking properties using TacDAT in antibody based internalization assays. HEK293 cells transfected with TacDAT, or with Tac as a negative control, were incubated with M1 antibody at 4°C to label surface Tac or TacDAT. Subsequently, the cells were incubated at 37 °C to allow internalization for 30 minutes (Fig. 2A). After 30 minutes of internalization, a visible intracellular accumulation of TacDAT was seen, consistent with constitutive endocytosis as previously described for DAT (Loder and Melikian, 2003, Sorkina et al., 2005). No visible intracellular accumulation of Tac was observed (Fig 2B and C). To further investigate the trafficking properties of TacDAT, we stimulated TacDAT expressing HEK293 cells with phorbol-12-myristate-13-acetate (PMA). Addition of PMA (1 μM) during the 30 min internalization period increased substantially the amount of intracellular localized TacDAT (Fig. 2C), showing that TacDAT is internalized in response to PMA as is the case for DAT. Tac alone did not respond to PMA (data not shown).

Our data suggest that TacDAT not only is functional but also has retained the well-described trafficking properties of DAT in HEK293 cells. We decided, therefore, to use TacDAT in our further investigations. The presence of the efficient extracellular FLAG epitope allowed the use of a quantitative ELISA-based internalization assay. To perform the assay, TacDAT or Tac expressing cells were labelled with M1 antibody at 4 °C before internalization was allowed for 5-60 min with or without addition of PMA or the substrate amphetamine. Surface antibody was removed by acid

strip and intracellular transporter was measured by ELISA upon permeabilization of cells (Fig. 2D). Internalization was calculated as the amount of intracellularly accumulated TacDAT relative to initial TacDAT surface expression. In HEK293 cells transiently expressing TacDAT, a time-dependent and saturating internalization was observed (Fig. 2E). Incubation with either amphetamine (10 μM) or PMA (1 μM), increased TacDAT internalization over time (Fig. 2E), whereas in cells transfected with Tac no increase the internalization of Tac at any time point was observed for PMA or amphetamine as compared to untreated Tac (Fig. 2E). The largest effects of the treatments were seen after 60 minutes of incubation (Fig. 2F) with a tendency towards saturation for all conditions (Fig. 2E).

Next, we explored whether we could use the quantitative ELISA assay to investigate the fate of the constitutively internalized transporter (Fig. 2C and E). Specifically, we attempted to assess whether the internalized TacDAT was sorted to either lysosomal degradation or recycling by using compounds blocking either lysosomal degradation (the protease inhibitor leupeptin) or both recycling and lysosomal degradation (the proton ionophore, monensin). Leupeptin (100μg/ml, 1 hour) increased significantly the accumulated M1 antibody signal in HEK293 cells transiently expressing TacDAT whereas no significant effect was seen in cells transiently expressing Tac (Fig. 3A). An even more pronounced effect was observed for monensin on the intracellular accumulation of TacDAT (Fig. 3A). This effect could be the result of either inhbited lysosomal degradation or inhibited recycling. If it was the result of blocking recycling, a concomitant decrease in surface expression would be expected during the same period. We tested this using the surface ELISA assay; however, we observed no decrease in surface expression by incubating cells transiently expressing TacDAT for 60 min with monensin (Fig. 3B). We also tested the effect of bafilomycin A1, an $H^+$-ATPase inhibitor, which is known to blocks recycling of the transferrin receptor and thereby reduce transferrin receptor surface expression (Presley et al., 1997). However, similar to

what we observed for monensin, bafilomycin A1 did not affect TacDAT surface expression (Fig. 3B). We also tested the effect of bafilomycin A1 and monensin on HA-DAT in HEK293 cells and did not observe any effect the compounds on HA-DAT surface expression (Fig. S1)

Rab proteins are small GTPases that organize membrane protein trafficking (Stenmark, 2009) and it has been demonstrated that Rab4 and Rab11 are critical for recycling of membrane proteins from early endosomes ('short loop recycling') and recycling endosomes ('long loop recycling'), respectively (Jones et al., 2006). To assess whether constitutively endocytosed DAT recycled through any of these two pathways we co-expressed HA-DAT with dominant negative mutants (D.N.) of Rab4 (Rab4 D.N.) or Rab11 (Rab11 D.N.) (Yudowski et al., 2009); however, neither coexpression with Rab4 D.N. nor with Rab11 D.N. affected DAT steady state surface expression as compared to co-expression of Rab4 WT or Rab11 WT arguing further against a noteworthy continuous recycling of the transport protein in HEK293 cells (Fig. S2).

Rab proteins also represent widely used markers of distinct endosomal compartments. We therefore employed confocal imaging together with co-expression of TacDAT and Rab proteins tagged with enhanced green fluorescent protein (EGFP) in HEK293 cells. This included EGFP-Rab4 to visualize early endosomes and possibly the 'short loop recycling' pathway, EGFP-Rab7 to visualize late endosomes, or EGFP-Rab11 to visualize recycling endosomes and the 'long loop' recycling pathway (Jones et al., 2006, Stenmark, 2009). The internalization assay was carried out with 1 hour of internalization as described in Fig. 2A, except that we used a primary fluorophore-conjugated M1 antibody. This allowed us to visualize internalization without permeabilizing the cells, thereby keeping the cells intact and not disrupting any membranes or endosomal compartments. According to the resulting confocal images, TacDAT co-localized only to a limited degree with EGFP-Rab4 (Fig. 3C). Similarly, the co-localization of EGFP-Rab11 was limited with clearly distinct localization patterns for the M1 signal and the EGFP signal (Fig. 3C). In contrast,

the most prominent co-localization was observed for EGFP-Rab7 with multiple vesicular structures showing overlapping M1 and EGFP signals (Fig. 3C). In summary, our ELISA data (Fig. 3A, B) together with the colocalization data (Fig. 3C) support that in HEK293 cells constitutively internalized TacDAT is sorted primarily to a degradative pathway rather than to recycling.

To assess whether constitutive internalization and postendocytic sorting was dependent on cell type, TacDAT was expressed in the dopaminergic cell line 1Rb3An27 (Adams et al., 1996). Similar to our observations in the HEK293 cells, TacDAT internalized constitutively whereas no detectable constitutive internalization was observed in cells transfected with Tac (Fig. 4A). Since the 1Rb3An27 cells are difficult to transfect and because of poor cell adherence we were not able to obtain a sufficiently high specific signal to carry out the ELISA internalization assay. Instead we performed co-localization experiments like in the HEK293 cells. Similar to our observations in these cells, the confocal images indicated that TacDAT had the highest degree of colocalization with EGFP-Rab7, partial co-localization with EGFP-Rab4 and the lowest co-localization with EGFP-Rab11 (Fig. 4B) (Fig. 4B). Quantification of the colocalization supported this with EGFP-Rab7 colocalization being significantly higher than the colocalization with EGFP-Rab11 (one way ANOVA, $p < 0.01$, Bonferroni's Multiple Comparison Test) (Fig. 4D). The intermediate overlap with EGFP-Rab4 indicates that TacDAT is also found in an early endosomal compartment as expected since we have previously reported that is endycytosed through a dynamin-dependent mechanism to early endosomes (Eriksen et al., 2009).

To verify that the sorting pattern observed for TacDAT was indeed a specific property of the transporter and not a pattern that would be seen for any membrane protein, we did parallel experiments in which we transiently expressed a FLAG-tagged $ß_2$-adrenergic receptor (β2AR) in the 1Rb3An27 cells. The β2AR is internalized upon agonist treatment and the internalized receptor is efficiently recycled (Cong et al., 2001, Gage et al., 2001). In contrast to TacDAT, the β2AR

transiently expressed in 1Rb3An27 cells did not constitutively internalize to any detectable extent (data not shown); however, treatment of the cells with the agonist isopreteronol (10 μM) caused a marked time-dependent internalization (Fig. S3). Co-expression with the three EGFP-Rab proteins showed for the internalized receptor a pattern markedly different than that seen for internalized TacDAT. In the confocal images, the M1 antibody signal overlapped quite prominently with the signal from both EGFP-Rab4 and EGFP-Rab11 while rather little overlap was seen with the signal from EGFP-Rab7 (Fig. 4D). Quantification of the signals confirmed this by showing significantly higher colocalization of the internalized β2AR with EGFP-Rab4 and EGFP-Rab11 than with EGFP-Rab7 (One way ANOVA, $p < 0.001$, Bonferroni's Multiple Comparison Test). This pattern of co-localization is consistent with postendocytic sorting of the β2AR to recyling pathways rather then to degradation. Note that the association of the β2AR with both the Rab4 pathway (Yudowski et al., 2009) and the Rab 11 pathway (Moore et al., 2004) has been described previously.

To exclude that TacDAT did not display altered postendocytic sorting as compared to DAT without Tac fused to the N-terminus, we performed experiments in 1Rb3An27 cells on non-tagged DAT using our previously described rhodamine-coupled cocaine analogue, JHC 1-64. This analogue enables fluorescent labelling of surface DAT in live cells with high specificity and was recently used to demonstrate constitutive internalization of endogenous DAT in dopaminergic neurons (Eriksen et al., 2009). Cells transiently co-expressing DAT and EGFP-tagged Rab4, Rab7 or 11 were labelled with JHC 1-64 and analyzed by confocal imaging after 1 hour of internalization. Again we observed the most pronounced colocalization with EGFP-Rab7 and rather limited co-localization with EGFP-Rab4 and EGFP-Rab11 (Fig. 5). We also carried out time series experiments in the 1Rb3An27 cells expressing both DAT and EGFP-Rab7 showing that DAT positive vesicles and EGFP-Rab7 positive vesicles were indeed identical as they co-migrated over time (Fig. S4). Moreover, DAT Internalization in cells co-expressing HA-DAT and EGFP-tagged

Rab4, Rab7 or 11 was probed with the HA.11 antibody and once again we saw a higher degree of colocalization between HA-DAT and EGFP-Rab7 than between HA-DAT and GFP-Rab11 (Fig. S5).

Finally, we tested whether the same postendocytic sorting pattern was observed for endogenous DAT in dopaminergic neurons. As mentioned, we recently demonstrated a marked constitutive internalization of DAT in these neurons by labelling DAT with the fluorescent cocaine analogue JHC 1-64. To determine the sorting of this constitutively internalized DAT, the dopaminergic cultures were transduced at 2-3 DIV (days in vitro) with lentivirus encoding EGFP-Rab4, -Rab7, or -Rab11. After 10-14 DIV the constitutive DAT internalization was analyzed using JHC 1-64 (1 hour of internalization). As in the non-transduced neurons (Eriksen et al., 2009), we observed clear constitutive DAT internalization (Fig 6A), and as seen in both tested cell lines the most evident co-localization was seen between EGFP-Rab7 and DAT/JHC 1-64 with less apparent co-localization between DAT and both EGFP-Rab4 and EGFP-Rab11 (Fig. 6A). To further study whether the co-localization of DAT with the late enodosomal marker Rab7 is a reflection of constitutively DAT being sorted to a lysosomal degradation pathway, we looked at the constitutive DAT internalization in dopaminergic neurons together with the lysosomal marker, Lysotracker Green. Substantial colocalization between internalized DAT and the Lysotracker was observed (Fig. 6B) supporting that constitutively internalized DAT is sorted to a lysosomal degradative pathway.

**Discussion**

It is well established that DAT undergoes constitutive endocytosis in transfected heterologous cells (Chi and Reith, 2003, Loder and Melikian, 2003, Sorkina et al., 2005) and recently it was demonstrated that also DAT endogenously expressed in dopaminergic neurons is constitutively internalized (Eriksen et al., 2009). However, the postendocytic sorting and fate of the internalized transporter has remained uncertain. In the current study, we address this question in both cell lines and dopaminergic neurons using a series of different complementary approaches. The predominant observation was that constitutively internalized DAT was primarily sorted to a lysosomal/degradative pathway.

DAT sorting was first studied using a new DAT fusion protein with an extra transmembrane segment. This TacDAT construct was made by fusing the single transmembrane protein Tac to DAT. Tac itself seems to be rather inert in its trafficking properties and several studies have used Tac fusion proteins to define trafficking signals in cytosolic domains of membrane proteins including DAT (Holton et al., 2005) and other transporters (Kalandadze et al., 2004, Colgan et al., 2007). However, to our knowledge this is the first time Tac has been used as a 'silent reporter' for an entire membrane protein. Importantly, TacDAT displayed functional properties similar to DAT although maximum uptake was reduced (Fig 1C). Furthermore TacDAT was constitutively internalized as well as it internalized in response to PMA and amphetamine stimuli in HEK293 cells (Fig. 2C and E) as previously described for DAT in this cell line (Chi and Reith, 2003, Kahlig et al., 2006, Eriksen et al., 2009) and other systems (Melikian and Buckley, 1999, Sorkina et al., 2003, Sorkina et al., 2005). The observed trafficking properties for TacDAT must be related to the DAT part of TacDAT since Tac alone, in agreement with previous observations (Holton et al., 2005), did not internalize to any detectable degree, neither constitutively nor response to PMA, according to microscopic assays (Fig. 2C).

Antibodies recognizing extracellular epitopes in membrane proteins are highly desirable for dynamic studies of their trafficking properties; however, it has proven notoriously difficult to develop an efficient antibody against an endogenous extracellular epitope of the DAT, and with the N- and C-termini located intracellularly it has even been difficult to introduce extracellular antibody tags in the extracellular domains of the transporter. Nevertheless, Sorkin and coworkers were capable of introducing a hemagglutinin tag (HA-tag) in the large second extracellular loop (ECL2) and maintain transport activity and wild type expression upon transfection (Sorkina et al., 2006). Use of the epitope has already allowed interesting new insight into DAT trafficking using both heterologous cells and transfected dopaminergic neurons in culture (Sorkina et al., 2006, Miranda et al., 2007, Sorkina et al., 2009). The present TacDAT construct represents an alternative way of generating an extracellular antibody epitope and carries several properties that complement already existing approaches for studying DAT trafficking. Most importantly, the M1 FLAG antibody epitope at the Tac N-terminus harbours several desirable features: 1) It is outside the DAT primary sequence and thus unlikely to interfere with DAT function. 2) The M1 antibody bound to the FLAG epitope displays an almost 10 times higher signal/DAT molecule than the HA.11 antibody on the HA epitope in extracellular loop 2 (Fig. 1E), which makes the FLAG epitope applicable to studies of low abundant internalization events. 3) The M1 antibody can be stripped off from the FLAG eptitope, which is essential for the quantitative ELISA internalization assays (Fig. 2E) and not possible for the HA.11 antibody bound to HA-DAT (Sorkina et al., 2006). 4) Labeling of the FLAG-epitope with M1 antibody can be done at 4 °C and thus at a truly trafficking-restricted temperature. This is not the case for labeling of HA-DAT with HA.11, which is only possible at 18°C or higher (Sorkina et al., 2006). Finally, it interesting to consider extending the use of Tac fusion constructs to other transporters in the family. Importantly, fusing SERT and Tac head-to-tail results in a TacSERT construct that upon expression in HEK293 cells retains the function and

trafficking properties of wild type SERT (Jørgensen and Gether, unpublished observations). Thus, it might be possible to use Tac fusion constructs as a general means of tagging transporters thereby allowing direct comparisons of trafficking properties between different transporters as well as dissection of distinct trafficking signals.

Using a quantitative ELISA based internalization assay in HEK293 cells expressing TacDAT, we showed that the apparent constitutive intracellular accumulation of TacDAT was increased by both inhibitor of lysosomal proteases (leupeptin) and the recycling/degradation inhibitor monensin (Fig. 3A). Monensin is a cationophore believed to exert its role on membrane protein trafficking by dissipating the pH gradient across the intracellular membranes thereby bringing trafficking between intracellular compartments to a hold as this is dependent on differences in pH gradients (Mollenhauer et al., 1990). The apparent increase in intracellular accumulation in response monensin might accordingly both be an effect of inhibiting sorting to lysosomal degradation and of inhibiting recycling back to the plasma membrane. However, according to a surface ELISA assay monensin did not affect TacDAT surface expression, which essentially rules out that the increased TacDAT accumulation is due to an inhibition of recycling. TacDAT surface expression was also not affected by bafilomycin A1, a $H^+$-ATPase inhibitor that also disrupts vesicular pH-gradients (Johnson et al., 1993) (Fig. 3B). Furthermore no effect of monensin or bafilomycin A1 was seen on the surface expression of HA-DAT in HEK293 cells (Fig. S1). Previously, it was likewise found in DAT expressing PC12 cells that bafilomycin did not affect DAT surface expression (Loder and Melikian, 2003). Conversely, the transferrin receptor, a well studied constitutively recycling membrane protein, was shown to decrease its surface expression upon bafilomycin A1 treatment (Loder and Melikian, 2003). In another study using transfected PAE cells, DAT surface expression and function was reduced by monensin as assessed by surface biotinylation and dopamine uptake experiments (Sorkina et al., 2005). This might reflect interruption of DAT recycling; however,

regarding the uptake experiments it is a caveat, as also noted by the authors, that monensin as a sodium ionophore most likely would affect the sodium plasma membrane sodium gradient, which is the driving force for dopamine transport, i.e. a reduction in dopamine uptake in response to monensin cannot necessarily be attributed to reduced surface expression (Sorkina et al., 2005).

In our further strategy to investigate DAT postendocytic sorting, we used Rab proteins fused to EGFP in combination with confocal imaging. Co-expression of TacDAT in HEK293 cells with EGFP-tagged versions of the endosomal markers Rab4 (early endosomes/recycling), Rab7 (late endosomes) or Rab11 (long loop recycling) showed the most pronounced colocalization in a vesicular pattern with the late endosomal marker Rab7 (Fig. 3C), whereas little colocalization was observed with Rab4 and Rab11. Similarly, in the the dopaminergic cell line 1Rb3An27, we observed clear constitutive internalization and when probing the colocalization with the EGFP-tagged Rab proteins in a quantitative manner, the highest colocalization was observed with Rab7, which was significantly higher than with Rab11, but not Rab4 (Fig. 4D). The sorting pattern observed was most likely not an artefact of the assay since only cells expressing TacDAT internalized M1 antibody (data not shown). In addition, parallel experiments in the 1Rb3An27 cells with the ß$_2$-adrenergic receptor exhibited a different colocalization pattern characterized by highest colocalization with Rab4 and Rab11 (Fig. 4E), as expected for protein well-known to undergo efficient recycling and verifying that the quantification does indeed reflect properties of the analysed protein. Furthermore, we observed the same co-localization pattern as for TacDAT when using our previously described fluorescent cocaine analogue JHC 1-64 as label to follow postendocytic sorting of non-tagged DAT. Finally, we studied sorting of the internalized endogenous DAT in dopaminergic primary cultures that were transduced with lentivirus encoding EGFP-tagged Rab4, Rab7 or Rab11. Constitutive internalization of endogenous DAT was visualized using the cocaine analog JHC 1-64 and, as in the cell lines, DAT primarily colocalized

with Rab7 (Fig. 6A). Additionally, we observed a profound colocalization between DAT and lysosomal marker Lysotracker further supporting that constitutively internalized DAT is sorted to late endosome/degradation in dopaminergic neurons (Fig. 6B).

We should note that the quantified co-localization in 1Rb3An27 cells of EGFP-Rab4 indicated relatively high co-localization with both internalized TacDAT and $ß_2$-adrenergic receptor. However, qualitative differences became apparent by examination of individual images. Only relatively few TacDAT positive vesicles showed direct overlap with EGFP-Rab4 whereas examination of images of internalized $ß_2$-adrenergic receptor gave the impression of a much higher degree of co-localization with EGFP-Rab4, i.e. in regions with enriched EGFP signal we observed a corresponding marked enrichment in M1 signal, which was never seen for TacDAT (Fig. 4B and C). Together with our data in HEK293 cells, which argue strongly against any major recycling, we find it therefore unlikely that TacDAT to any significant extend follows a Rab4 'short loop' recycling pathway in the 1Rb3An27 cells. Rather, we find it likely that co-localization with EGFP-Rab4 simply might reflect presence of TacDAT in early endosomes (Stenmark, 2009).

Previous reports have proposed that constitutively internalized DAT is sorted to a recycling pathway (Loder and Melikian, 2003, Sorkina et al., 2005, Furman et al., 2009). These previous studies were carried out in other cell types than those used in this study and different methodological approaches were undertaken but otherwise we have no immediate explanation for the apparent discrepancy with the present data. Of note, DAT was suggested to undergo fast constitutive recycling in transfected PC12 cells; nonetheless, when treating the cells with bafilomcyin no effect was seen on DAT surface expression, whereas a marked effect was seen on the well-known recycling membrane protein, the transferrin receptor (Loder and Melikian, 2003). Moreover, the conclusion was based on experiments performed 18° C, which was supposed to inhibit exocytosis without interfering with endocytosis (Loder and Melikian, 2003); however, this

might represent a simplification (Sorkin et al., 1991). In a recent study, it was proposed that DAT recycles via a Rab11 dependent pathway because the level of DAT in the plasma membrane DAT was increased upon co-expression of constitutively active Rab11 but all experiments were steady state experiments and a dominant negative Rab11 mutant did not exhibit any effect compared to a GFP control when quantifying DAT surface binding (Furman et al., 2009).

Summarized, our data suggest that constitutively internalized DAT is sorted to late endosomes/lysosomes both in cell lines and dopaminergic neurons. The fact that the sorting pattern is the same in three different cellular systems (HEK293 cells, 1Rb3An27 cells and cultured dopaminergic neurons) suggest that the constitutive internalization depends on general cellular factors as opposed to the PKC-mediated DAT internalization where the cellular environment seems to affect the PKC stimulation to a high degree (Mortensen et al., 2008, Eriksen et al., 2009). The sorting of DAT directly to degradation rather than to recycling challenges previous suggestions of a continuously cycling intracellular pool of transporter that might be rapidly recruited to meet immediate changes in the need for neurotransmitter reuptake from the extracellular space (Melikian and Buckley, 1999, Johnson et al., 2005). In the future it should therefore be highly interesting to investigate to what degree postendocytic sorting might be subject to regulation and redirection by yet unknown mechanisms with putative impact on the overall regulation of dopaminergic signalling.

**References**


Adams F, La Rosa F, Kumar S, Edwards-Prasad J, Kentroti S, Vernadakis A, Freed C, Prasad K (Characterization and transplantation of two neuronal cell lines with dopaminergic properties. Neurochemical Research 21:619-627.1996).

Chen NH, Reith M, Quick M (Synaptic uptake and beyond: the sodium- and chloride-dependent neurotransmitter transporter family SLC6. Pfl++gers Archiv European Journal of Physiology 447:519-531.2004).

Chi L, Reith MEA (Substrate-Induced Trafficking of the Dopamine Transporter in Heterologously Expressing Cells and in Rat Striatal Synaptosomal Preparations. Journal of Pharmacology And Experimental Therapeutics 307:729-736.2003).

Chmelar RS, Nathanson NM (Identification of a novel apical sorting motif and mechanism of targeting of the M2 muscarinic acetylcholine receptor. J Biol Chem 281:35381-35396.2006).

Colgan L, Liu H, Huang SY, Liu Y-J (Dileucine Motif Is Sufficient for Internalization and Synaptic Vesicle Targeting of Vesicular Acetylcholine Transporter. Traffic 8:512-522.2007).

Cong M, Perry SJ, Hu LA, Hanson PI, Claing A, Lefkowitz RJ (Binding of the beta2 adrenergic receptor to N-ethylmaleimide-sensitive factor regulates receptor recycling. J Biol Chem 276:45145-45152.2001).

Copeland BJ, Vogelsberg V, Neff NH, Hadjiconstantinou M (Protein kinase C activators decrease dopamine uptake into striatal synaptosomes. Journal of Pharmacology And Experimental Therapeutics 277:1527-1532.1996).

Daniels GM, Amara SG (Regulated Trafficking of the Human Dopamine Transporter. CLATHRIN-MEDIATED INTERNALIZATION AND LYSOSOMAL DEGRADATION IN RESPONSE TO PHORBOL ESTERS. Journal of Biological Chemistry 274:35794-35801.1999).

di Porzio U, Daguet MC, Glowinski J, Prochiantz A (Effect of striatal cells on in vitro maturation of mesencephalic dopaminergic neurones grown in serum-free conditions. Nature 288:370-373.1980).

Eriksen J, Rasmussen SGF, Rasmussen TN, Vaegter CB, Cha JH, Zou MF, Newman AH, Gether U (Visualization of Dopamine Transporter Trafficking in Live Neurons by Use of Fluorescent Cocaine Analogs. Journal of Neuroscience 29:6794-6808.2009).

Furman CA, Lo CB, Stokes S, Esteban JA, Gnegy ME (Rab 11 regulates constitutive dopamine transporter trafficking and function in N2A neuroblastoma cells. Neurosci Lett 463:78-81.2009).

Gage RM, Kim KA, Cao TT, von Zastrow M (A transplantable sorting signal that is sufficient to mediate rapid recycling of G protein-coupled receptors. J Biol Chem 276:44712-44720.2001).

Gainetdinov RR, Caron MG (MONOAMINE TRANSPORTERS: From Genes to Behavior. Annual Review of Pharmacology and Toxicology 43:261-284.2003).

Garcia BG, Wei Y, Moron JA, Lin RZ, Javitch JA, Galli A (Akt is essential for insulin modulation of amphetamine-induced human dopamine transporter cell-surface redistribution. MolPharmacol 68:102-109.2005).

Gether U, Andersen PH, Larsson OM, Schousboe A (Neurotransmitter transporters: molecular function of important drug targets. Trends in Pharmacological Sciences 27:375-383.2006).

Holton KL, Loder MK, Melikian HE (Nonclassical, distinct endocytic signals dictate constitutive and PKC-regulated neurotransmitter transporter internalization. Nat Neurosci 8:881-888.2005).

Johnson L, Dunn K, Pytowski B, McGraw T (Endosome acidification and receptor trafficking: bafilomycin A1 slows receptor externalization by a mechanism involving the receptor's internalization motif. Mol Biol Cell 4:1251-1266.1993).

Johnson LA, Furman CA, Zhang M, Guptaroy B, Gnegy ME (Rapid delivery of the dopamine transporter to the plasmalemmal membrane upon amphetamine stimulation. Neuropharmacology 49:750-758.2005).

Jones MC, Caswell PT, Norman JC (Endocytic recycling pathways: emerging regulators of cell migration. Current Opinion in Cell Biology 18:549-557.2006).

Kahlig KM, Lute BJ, Wei Y, Loland CJ, Gether U, Javitch JA, Galli A (Regulation of dopamine transporter trafficking by intracellular amphetamine. Mol Pharmacol 70:542-548.2006).

Kalandadze A, Wu Y, Fournier K, Robinson MB (Identification of Motifs Involved in Endoplasmic Reticulum Retention-Forward Trafficking of the GLT-1 Subtype of Glutamate Transporter. Journal of Neuroscience 24:5183-5192.2004).

Lavezzari G, McCallum J, Dewey CM, Roche KW (Subunit-Specific Regulation of NMDA Receptor Endocytosis. J Neurosci 24:6383-6391.2004).

Lavezzari G, Roche KW (Constitutive endocytosis of the metabotropic glutamate receptor mGluR7 is clathrin-independent. Neuropharmacology 52:100-107.2007).

Loder MK, Melikian HE (The dopamine transporter constitutively internalizes and recycles in a protein kinase C-regulated manner in stably transfected PC12 cell lines. J BiolChem 278:22168-22174.2003).

Loland CJ, Granas C, Javitch JA, Gether U (Identification of intracellular residues in the dopamine transporter critical for regulation of transporter conformation and cocaine binding. J Biol Chem 279:3228-3238.2004).

Madsen KL, Eriksen J, Milan-Lobo L, Han DS, Niv MY, Ammendrup-Johnsen I, Henriksen U, Bhatia VK, Stamou D, Sitte HH, McMahon HT, Weinstein H, Gether U (Membrane localization is critical for activation of the PICK1 BAR domain. Traffic 9:1327-1343.2008).

Melikian HE, Buckley KM (Membrane trafficking regulates the activity of the human dopamine transporter. Journal of Neuroscience 19:7699-7710.1999).

Miranda M, Dionne KR, Sorkina T, Sorkin A (Three Ubiquitin Conjugation Sites in the Amino Terminus of the Dopamine Transporter Mediate Protein Kinase C-dependent Endocytosis of the Transporter. Molecular Biology of the Cell 18:313-323.2007).

Mollenhauer HH, Morre DJ, Rowe LD (Alteration of intracellular traffic by monensin; mechanism, specificity and relationship to toxicity. Biochim Biophys Acta 1031:225-246.1990).

Moore RH, Millman EE, Alpizar-Foster E, Dai W, Knoll BJ (Rab11 regulates the recycling and lysosome targeting of beta2-adrenergic receptors. J Cell Sci 117:3107-3117.2004).

Moron JA, Zakharova I, Ferrer JV, Merrill GA, Hope B, Lafer EM, Lin ZC, Wang JB, Javitch JA, Galli A, Shippenberg TS (Mitogen-Activated Protein Kinase Regulates Dopamine Transporter Surface Expression and Dopamine Transport Capacity. Journal of Neuroscience 23:8480-8488.2003).

Mortensen OV, Larsen MB, Prasad BM, Amara SG (Genetic complementation screen identifies a mitogen-activated protein kinase phosphatase, MKP3, as a regulator of dopamine transporter trafficking. Mol Biol Cell 19:2818-2829.2008).

Mu Y, Otsuka T, Horton AC, Scott DB, Ehlers MD (Activity-dependent mRNA splicing controls ER export and synaptic delivery of NMDA receptors. Neuron 40:581-594.2003).

Naldini L, Blomer U, Gallay P, Ory D, Mulligan R, Gage FH, Verma IM, Trono D (In vivo gene delivery and stable transduction of nondividing cells by a lentiviral vector. Science 272:263-267.1996).

Presley JF, Mayor S, McGraw TE, Dunn KW, Maxfield FR (Bafilomycin A1 treatment retards transferrin receptor recycling more than bulk membrane recycling. J Biol Chem 272:13929-13936.1997).

Rayport S, Sulzer D, Shi WX, Sawasdikosol S, Monaco J, Batson D, Rajendran G (Identified postnatal mesolimbic dopamine neurons in culture: morphology and electrophysiology. Journal of Neuroscience 12:4264-4280.1992).

Sorkin A, Krolenko S, Kudrjavtceva N, Lazebnik J, Teslenko L, Soderquist AM, Nikolsky N (Recycling of epidermal growth factor-receptor complexes in A431 cells: identification of dual pathways. J Cell Biol 112:55-63.1991).

Sorkina T, Doolen S, Galperin E, Zahniser NR, Sorkin A (Oligomerization of Dopamine Transporters Visualized in Living Cells by Fluorescence Resonance Energy Transfer Microscopy. Journal of Biological Chemistry 278:28274-28283.2003).

Sorkina T, Hoover BR, Zahniser NR, Sorkin A (Constitutive and protein kinase C-induced internalization of the dopamine transporter is mediated by a clathrin-dependent mechanism. Traffic 6:157-170.2005).

Sorkina T, Miranda M, Dionne KR, Hoover BR, Zahniser NR, Sorkin A (RNA interference screen reveals an essential role of Nedd4-2 in dopamine transporter ubiquitination and endocytosis. Journal of Neuroscience 26:8195-8205.2006).

Sorkina T, Richards TL, Rao A, Zahniser NR, Sorkin A (Negative Regulation of Dopamine Transporter Endocytosis by Membrane-Proximal N-Terminal Residues. Journal of Neuroscience 29:1361-1374.2009).

Stenmark H (Rab GTPases as coordinators of vesicle traffic. Nat Rev Mol Cell Biol 10:513-525.2009).

Torres GE, Amara SG (Glutamate and monoamine transporters: new visions of form and function. Current Opinion in Neurobiology 17:304-312.2007).

Torres GE, Gainetdinov RR, Caron MG (Plasma membrane monoamine transporters: structure, regulation and function. Nat Rev Neurosci 4:13-25.2003).

Vaughan RA, Huff RA, Uhl GR, Kuhar MJ (Protein Kinase C-mediated Phosphorylation and Functional Regulation of Dopamine Transporters in Striatal Synaptosomes. Journal of Biological Chemistry 272:15541-15546.1997).

Yudowski GA, Puthenveedu MA, Henry AG, von Zastrow M (Cargo-Mediated Regulation of a Rapid Rab4-Dependent Recycling Pathway. Mol Biol Cell 20:2774-2784.2009).

Zahniser NR, Sorkin A (Trafficking of dopamine transporters in psychostimulant actions. Semin Cell Dev Biol 20:411-417.2009).

Zhu SJ, Kavanaugh MP, Sonders MS, Amara SG, Zahniser NR (Activation of Protein Kinase C Inhibits Uptake, Currents and Binding Associated with the Human Dopamine Transporter Expressed in Xenopus Oocytes. Journal of Pharmacology And Experimental Therapeutics 282:1358-1365.1997).

**Figure Legends**

**Figure 1:** TacDAT is a 13 transmembrane segment fusion protein with a high-affinity FLAG epitope and that is functionally expressed at the plasma membrane in HEK293 cells. A) TacDAT is a head-to-tail fusion of hDAT (blue) and Tac (green) with an N-terminal FLAG-epitope, DYKDDDDK. B) Non-permeabilizing immunostaining of HEK293 cells transfected with TacDAT using an M1 antibody recognizing the FLAG-epitope reveals that TacDAT is expressed at the plasma membrane of HEK293 cells and that the FLAG-epitope is exposed on the extracellular side of the plasma membrane. Scale bar is 10 μm. C) Dopamine uptake in HEK293 cells transfected with TacDAT or hDAT shows that TacDAT is functional at the plasma membrane with a Km 0.40 μM [SE interval (0.36 - 0.47 μM), n=3] similar to hDAT 0.92 μM [SE interval (0.62 - 1.4 μM), n=3], ($p>0.05$, student's t-test n=3). However the $V_{max}$ of TacDAT; 511 +/- 104 fmol/min/$10^5$ cells was significantly lower than the $V_{max}$ of DAT, 2486 +/- 236 fmol/min/$10^5$ cells ($p = 0.011$, paired t-test n=3). D) Preincubating HEK293 cells expressing TacDAT or hDAT for 30 mins at 4° C with M1 antibody does not impair dopamine uptake suggesting that antibody binding does not affect TacDAT function. E) The surface ELISA signal from the M1 antibody of cells expressing TacDAT with an HA-tag in the extracellular loop 2 was almost 10-fold higher pr molecule than the signal from the HA.11 antibody.

**Figure 2:** Visualizing TacDAT internalization using an M1 antibody-based internalization assay. A) To be able to detect TacDAT internalization we set up a conventional antibody internalization assay, in which we first labelled the cells with M1 at 4 °C, to label surface TacDAT at a trafficking blocked temperature. Then the cells were incubated at 37 °C in new media to allow internalization of TacDAT, followed by a fixation to stop the process. Finally the cells were permeabilized and

incubated with a secondary fluorophore-conjugated antibody that recognizes M1 as a preparation for immuno-fluorescence microscopy. B) Confocal images of HEK293 cells expressing Tac assayed as just described. Only surface staining was observed whether the internalization was carried out at 4 °C or 37 °C indicating that Tac resides in the plasma membrane and does not undergo any visible internalization within 30 minutes. C) The same assay with HEK293 cells expressing TacDAT. No intracellular accumulation is observed when internalizing at 4 °C, however at 37 °C an intracellular accumulation of TacDAT is observed suggesting a constitutive internalization of TacDAT, and the internalization is intensified when incubating with the PKC activator PMA (1 μM). D) Brief description of the ELISA-based internalization assay. The analysed cells were first labeled with M1 at 4 °C and then either incubated at 4° C for surface detection or incubated at 37° C for various periods to allow internalization. After the internalization period the cells were placed on ice and the surface antibody was stripped off using an acid strip buffer. After fixation the cells were permeabilized and the intracellular accumulated antibody was detected with a horseradish peroxidase-conjugated secondary antibody. The internalization signal was expressed as the proportion of the start surface signal. E) Using the cell-based ELISA assay it was possible to quantify the amount of internalized Tac and TacDAT relative to the surface fraction in HEK293 cells. A time dependent intracellular accumulation of TacDAT was observed and this internalization was significantly larger than for Tac. TacDAT internalization was further accelerated when stimulating with PMA (1μM) or amphetamine (10μM). F) Amphetamine and PMA had no significant effect on Tac after 1h of internalization whereas a significant effect was seen on TacDAT for both compounds and TacDAT control was significantly higher than Tac (One way ANOVA with Bonferroni's Multiple Comparison Test, ** $p < 0.01$ and *** $p < 0.001$).

**Figure 3:** Monensin and leupetin increase intracellular TacDAT accumulation and TacDAT colocalize with the late endosomal marker Rab7 in HEK293 cells. A) In HEK293 cells transfected with TacDAT the intracellular accumulation of TacDAT after 1 hour of internalization was increased significantly upon incubation with either the protease inhibitor leupeptin (100 μg/ml) or the recycling inhibitor monensin (25 μM) (One way ANOVA, Dunnett's Multiple Comparison test, * $p < 0.05$, ** $p < 0.01$, n=4). B) TacDAT surface expression after treatment with monensin (25 μM) or bafilomycin (XXXX) for 1 hour was determined in an ELISA assay. Neither monensin ($p > 0.05$, paired t-test, n=5) nor bafilomycin ($p > 0.05$, paired t-test, n=3) had any significant effect on TacDAT surface expression. C) Confocal microscopy images of colocalization between TacDAT and EGFP-tagged Rab4, Rab7 and Rab11 after 1 hour of AlexaFluor 568-conjugated M1 antibody internalization in HEK293 cells. TacDAT exhibited the most prominent colocalization with the late endosomal marker Rab7. Data are representative of at least three independent experiments. Scale bar 10 μm.

**Figure 4:** TacDAT is constitutively internalized in the dopaminergic cell line 1Rb3An27 and colocalize primarily with EGFP-Rab7. A) Experiment as in Fig. 2A. No detectable constitutive internalization was observed after 1 hour in 1Rb3An27 cells expressing Tac, whereas in cells expressing TacDAT, internalization was evident as analyzed by confocal microscopy. Pictures are representative of several experiments. B) Quantification of fluorescence colocalization between internalized TacDAT and the EGFP-tagged endosomal markers Rab4, Rab7 and Rab11 after 1 hour of M1 internalization. TacDAT exhibited the highest level of colocalization with EGFP-Rab7 which was significantly different from colocalization with the 'long loop' recycling marker EGFP-Rab11 ($p < 0.01$, One way ANOVA, Bonferroni's Multiple Comparison Test). The colocalization with the 'short loop' recycling marker Rab4 was intermediate and did not differ significantly from either

Rab7 or Rab11. C) Colocalization quantification of a FLAG-tagged ß$_2$-adrenergic receptor (ß$_2$AR) with EGFP-Rab4, 7 and 11 after 1 hour of isoproterenol (10 μM) stimulation was carried out as a control for specificity of the sorting pattern found in B). As expected the ß$_2$-adrenergic receptor, a bona fide recycling membrane protein, showed a higher degree of colocalization with the recycling markers Rab4 and Rab11 than with the late endosomal marker Rab7 (One way ANOVA, $p < 0.001$, Bonferroni's Multiple Comparison Test). Representative pictures from the colocalization analysis are shown for TacDAT (D) the ß$_2$-adrenergic receptor (E). Colocalization data was analysed from 30 images from each condition. Scale bars 10μm.

**Figure 5:** Visualization of constitutive DAT internalization in live 1Rb3An27 cells with the cocaine analog, JHC 1-64, reveals a predominant colocalization with EGFP-Rab7. 1Rb3An27 cells expressing DAT together with EGFP-Rab4, -Rab7 or -Rab11 were incubated with the cocaine analog JHC 1-64 (5 nM) at 4 °C to label surface DAT and subsequently incubated at 37 °C to drive internalization of DAT. After internalization the live cells were imaged using confocal microscopy, and a predominant colocalization with the late endosomal marker EGFP-Rab7 was observed. Images are representative of three independent experiments.

**Figure 6:** Constitutive DAT internalization in cultured dopaminergic neurons is sorted to a late endosomal/lysosomal pathway. A) Postnatal mesencephalic primary cultures from rat pups were transduced with lentivirus encoding EGFP-Rab4, -Rab7 or –Rab11 at day 2-3 in vitro. At day 10-14 in vitro the cultures were used for constitutive DAT sorting experiments by incubating the cultures with 5 nM JHC 1-64 at 4 °C to label surface DAT then the cells were incubated at 37 °C for 1 hour to drive the constitutive internalization. Subsequently the live cells were imaged at room temperature using confocal microscopy. As for the cell lines the most apparent colocalization was

observed between DAT/JHC 1-64 and the late endosomal marker EGFP-Rab7 in the soma of the dopaminergic neurons, whereas for Rab 4 and Rab 11 the colocalization was not noticeable. B) With an experiment parallel to A) we observed a prominent colocalization between the lysosomal marker lysotracker and constitutive internalized DAT in the dopaminergic neurons. Lysotracker Green (100 nM) was added in the last 10 minutes of incubation before imaging. Images are representative of at least 3 batches of neuronal cultures and three transductions. Scale bar 10 μm.

Figure 1

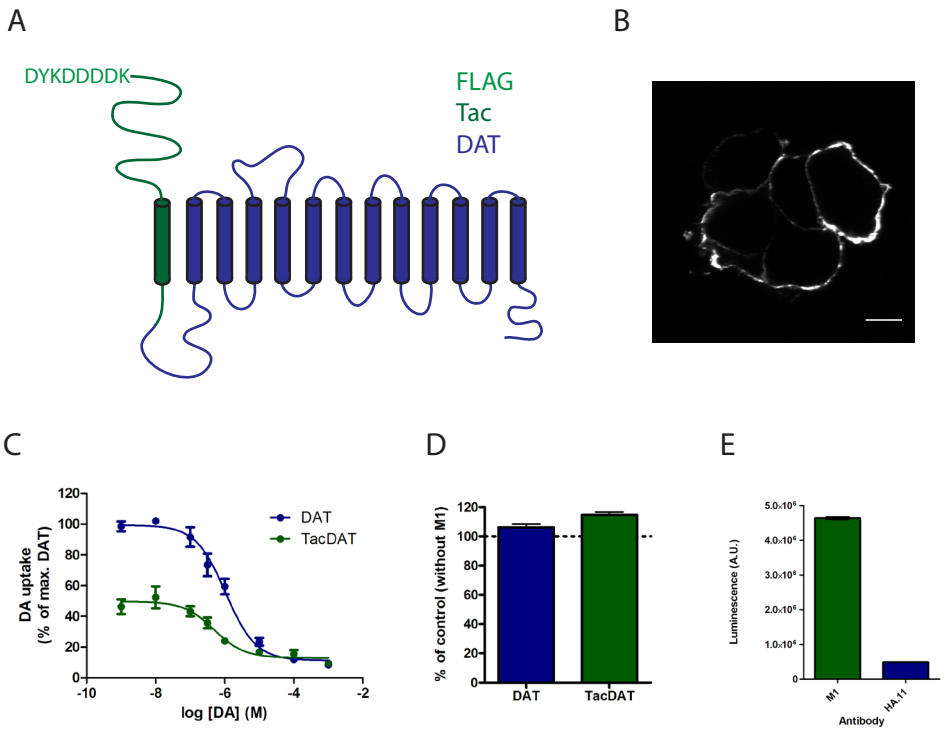
A
DYKDDDDK
FLAG
Tac
DAT
B
C
DA uptake
(% of max. DAT)
DAT
TacDAT
log [DA] (M)
D
% of control (without M1)
DAT
TacDAT
E
Luminescence (A.U.)
M1
HA.11
Antibody

Figure 2

A

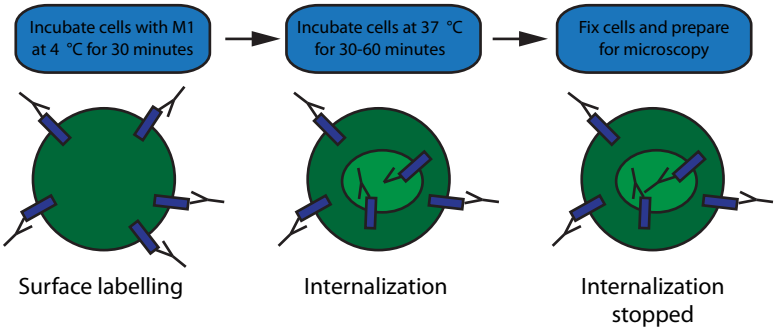


B

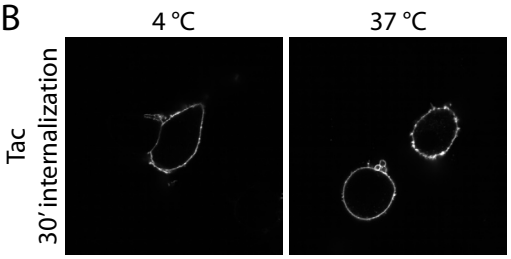


C

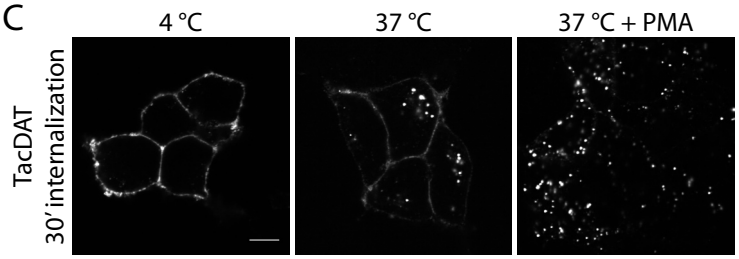


D

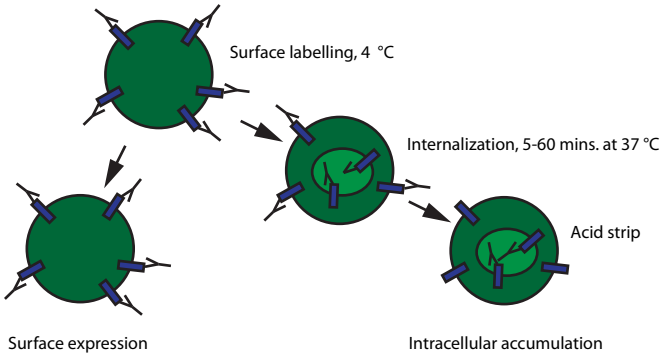


$$\text{Internalization} = \frac{\text{Intracellular accumulation}}{\text{Surface expression}}$$

E

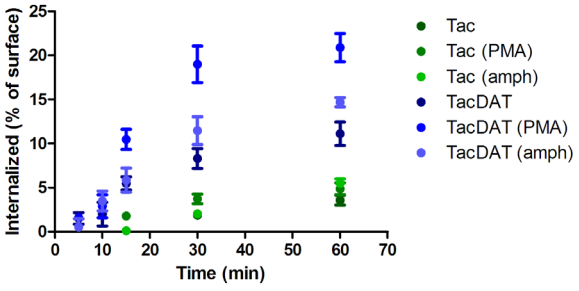


F

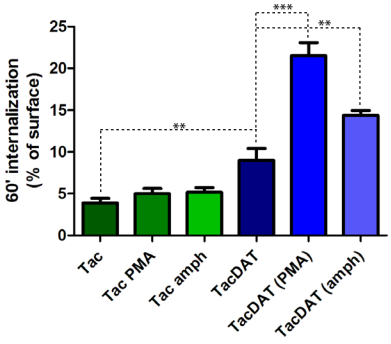

Figure 3

A

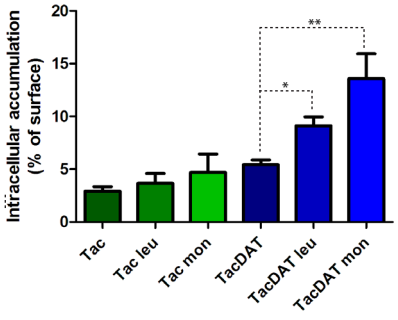
Intracellular accumulation
(% of surface)
20
15
10
5
0
**
*
Tac
Tac leu
Tac mon
TacDAT
TacDAT leu
TacDAT mon

B

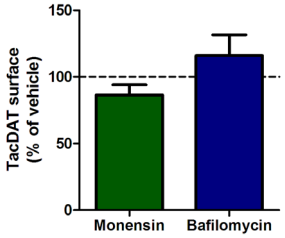
TacDAT surface
(% of vehicle)
150
100
50
0
Monensin
Bafilomycin

C

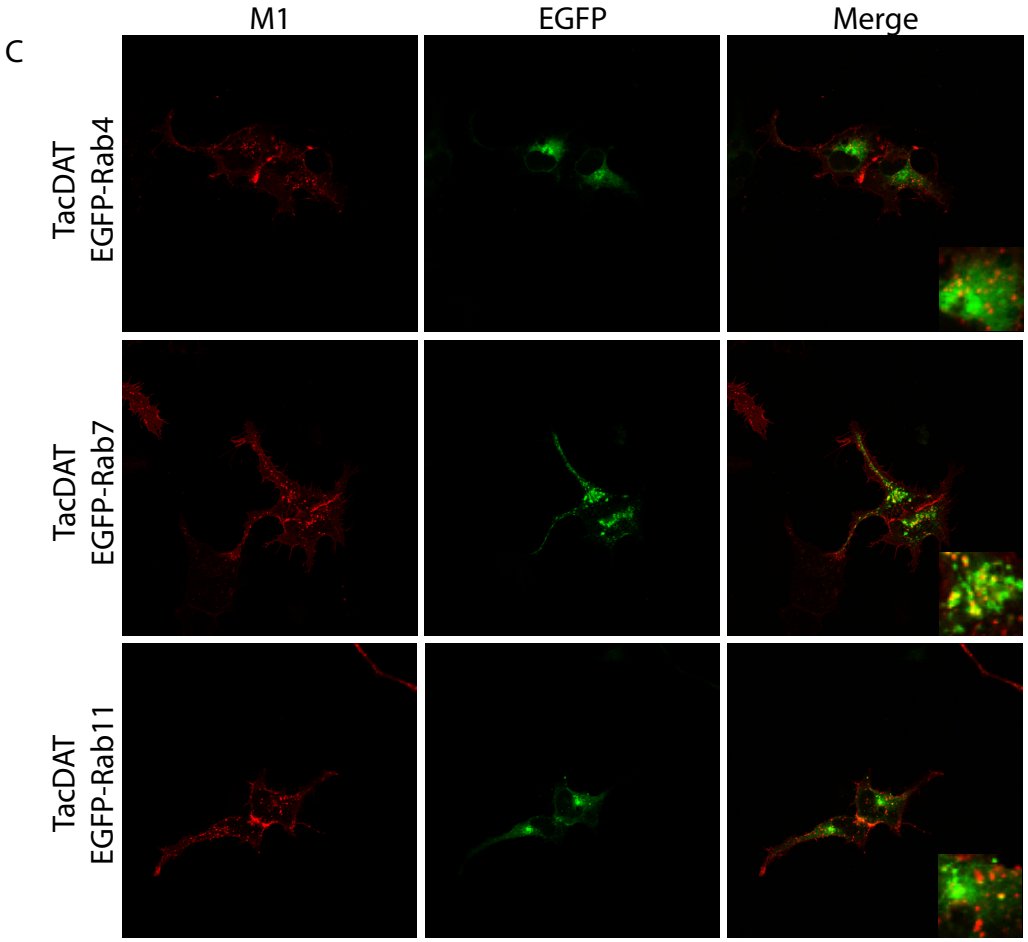
M1
EGFP
Merge
TacDAT
EGFP-Rab4
TacDAT
EGFP-Rab7
TacDAT
EGFP-Rab11

Figure 4

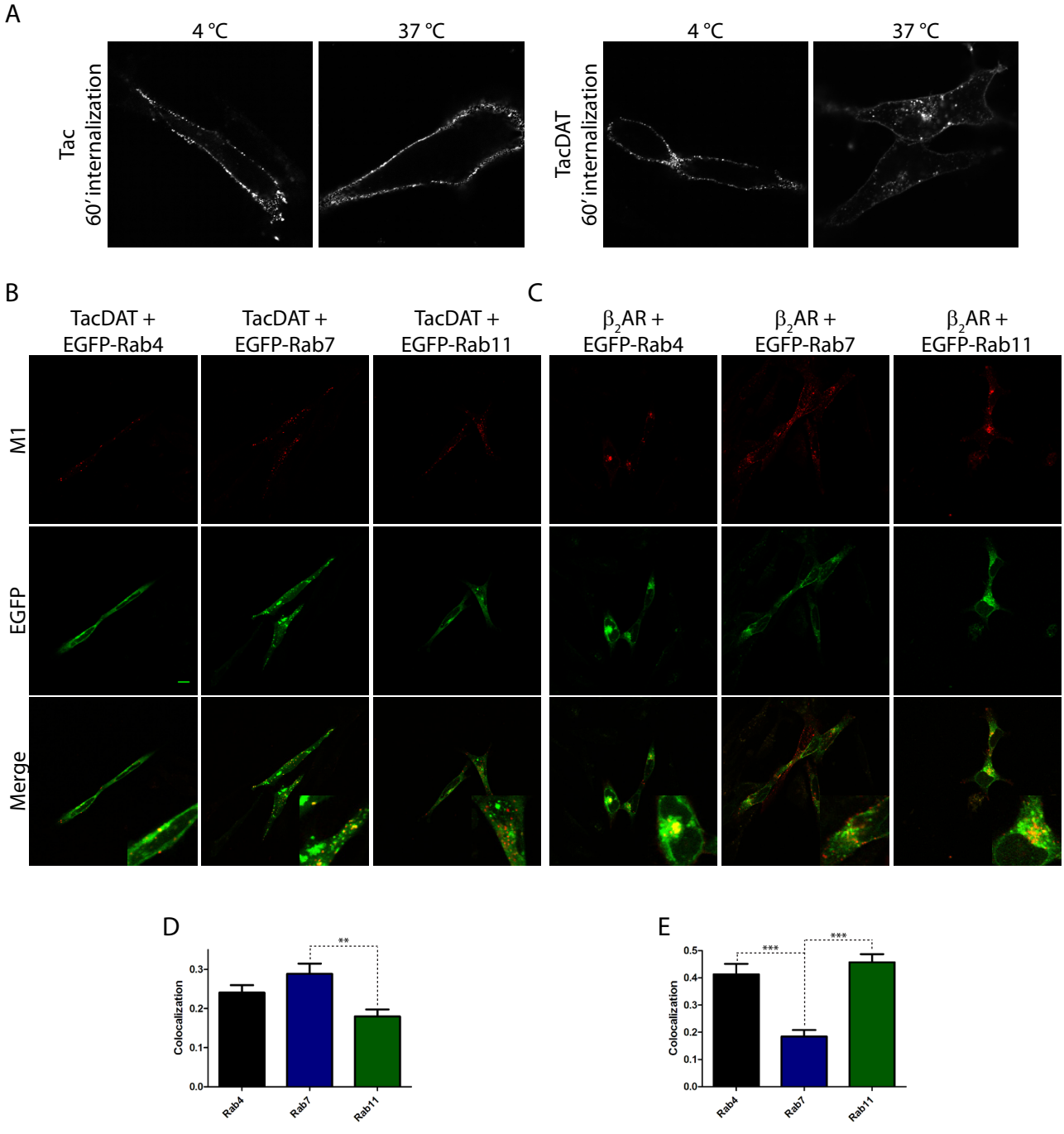
A
4 °C
37 °C
Tac
60' internalization
4 °C
37 °C
TacDAT
60' internalization
B
TacDAT + EGFP-Rab4
TacDAT + EGFP-Rab7
TacDAT + EGFP-Rab11
C
β2AR + EGFP-Rab4
β2AR + EGFP-Rab7
β2AR + EGFP-Rab11
M1
EGFP
Merge
D
Colocalization
0.0
0.1
0.2
0.3
**
Rab4
Rab7
Rab11
E
Colocalization
0.0
0.1
0.2
0.3
0.4
0.5
***
***
Rab4
Rab7
Rab11

Figure 5

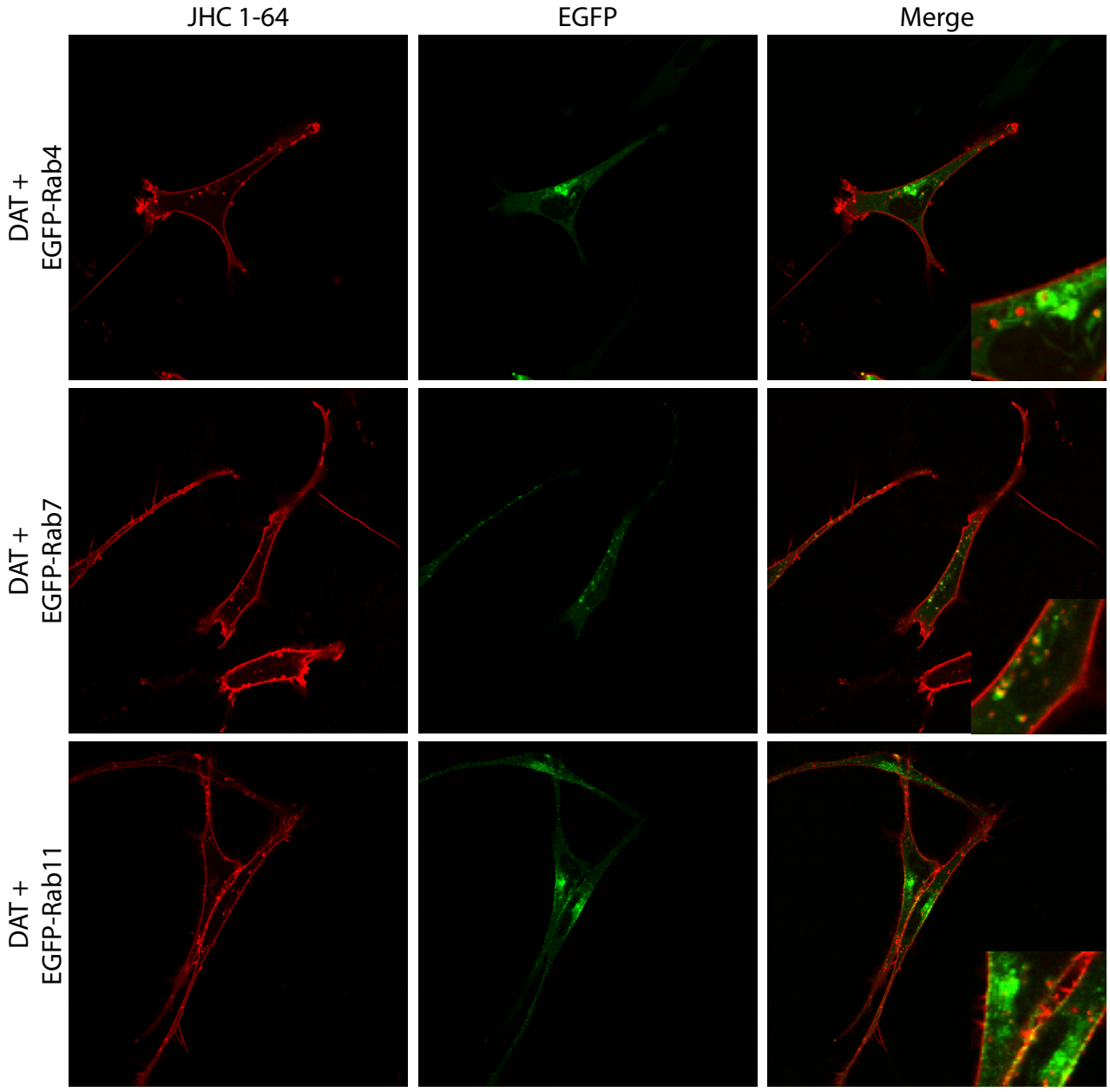

Figure 6

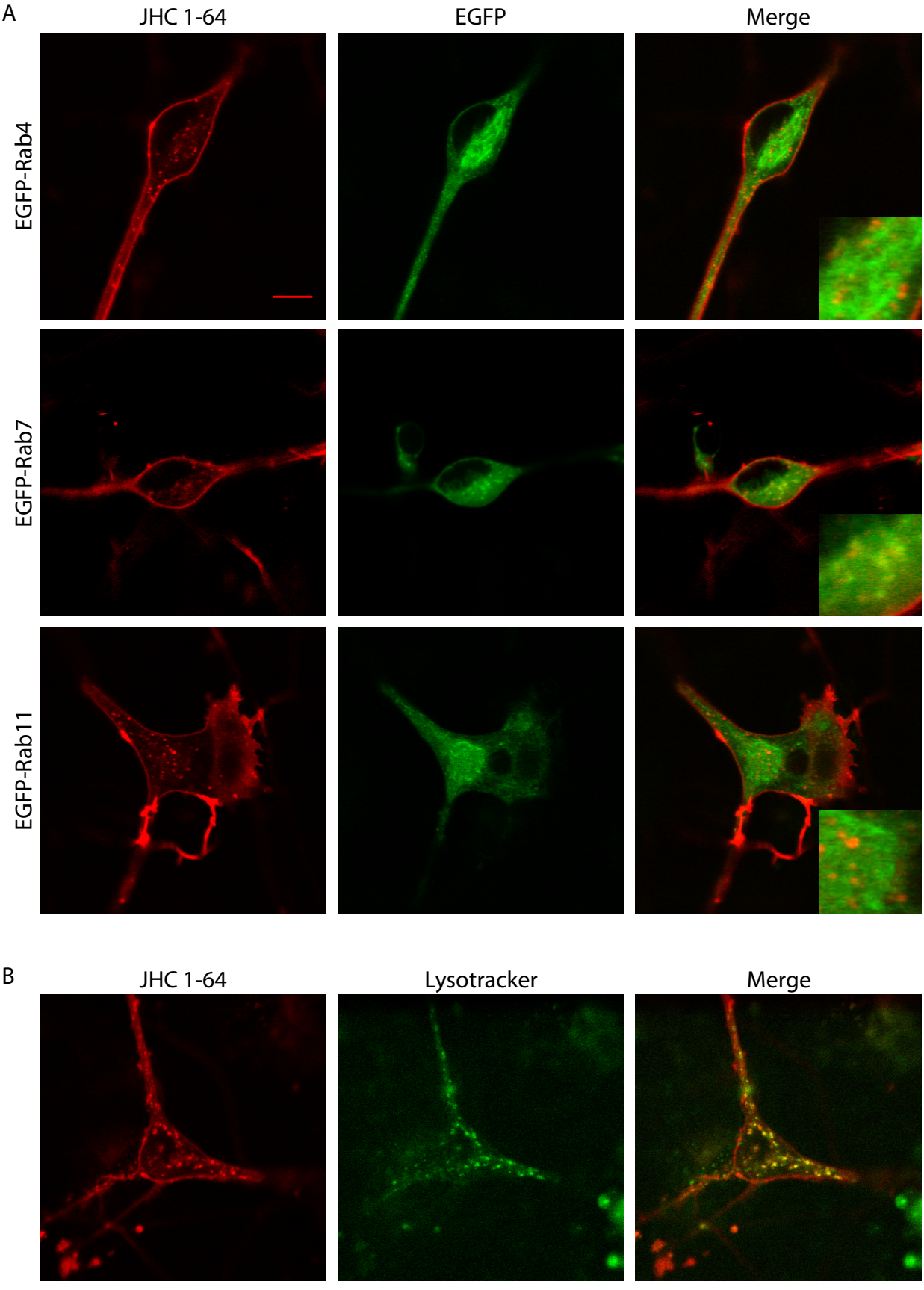
A
JHC 1-64
EGFP
Merge
EGFP-Rab4
EGFP-Rab7
EGFP-Rab11
B
JHC 1-64
Lysotracker
Merge

## Supplementary figures

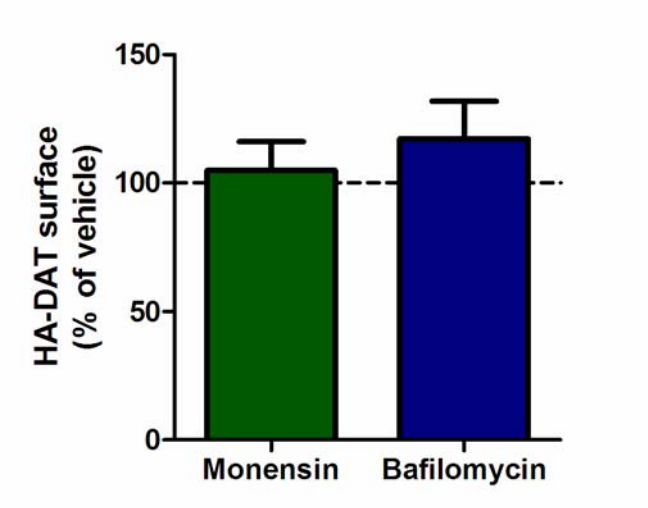


**Figure S1:** HEK293 cells expressing HA-DAT were treated with monensin (25 μM) or bafilomycin (1 μM) for 60 minutes before quantification of HA-DAT surface expression by ELISA. No effect of monensin ($p > 0.05$, paired t-test, n=5) or bafilomycin ($p > 0.05$, paired t-test, n=3) was observed.

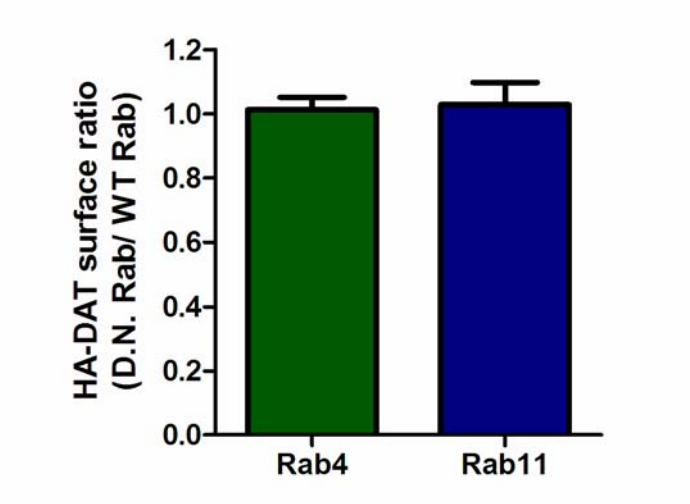


**Figure S2:** Surface expression in HEK293 cells expressing HA-DAT together with either EGFP-tagged Rab4 WT, Rab4 D.N. (S22N), Rab11 or Rab11 D.N. (S25N) by cell surface ELISA. The surface expression was calculated as the ratio between the surface expression of Rab4 D.N. and Rab4 WT and as the ratio between Rab11 D.N. and Rab11 WT. No significant difference was observed between cells expressing HA-DAT + Rab 4WT and cells expressing HA-DAT Rab4 D.N ($p > 0.05$, paired t-test, n=3). Likewise no difference was observed in the surface expression between cells expressing HA-DAT + Rab 4WT and cells expressing HA-DAT Rab4 D.N ($p > 0.05$, paired t-test, n=3).

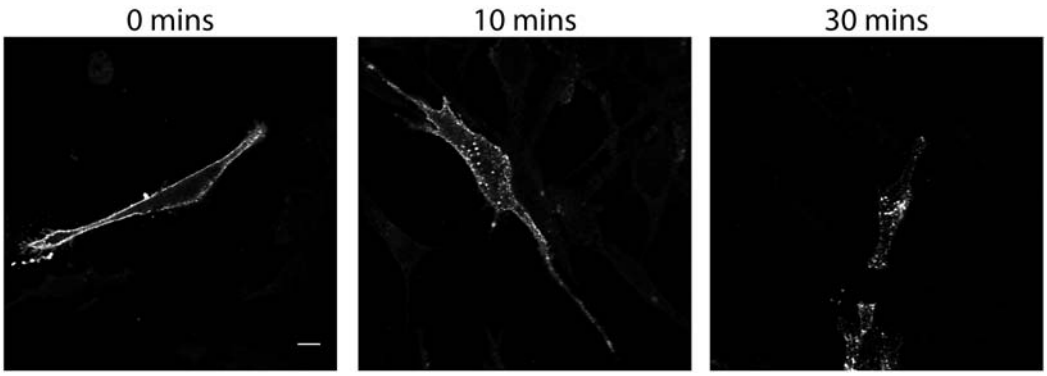


**Figure S3:** 1Rb3An27 cells expressing FLAG-tagged ß$_2$-adrenergic receptor was labelled with M1 antibody and 4 °C, and then incubated with agonist isoproterenol (10 μM) for 0, 10 or 30 minutes. Scale bar 10μm.

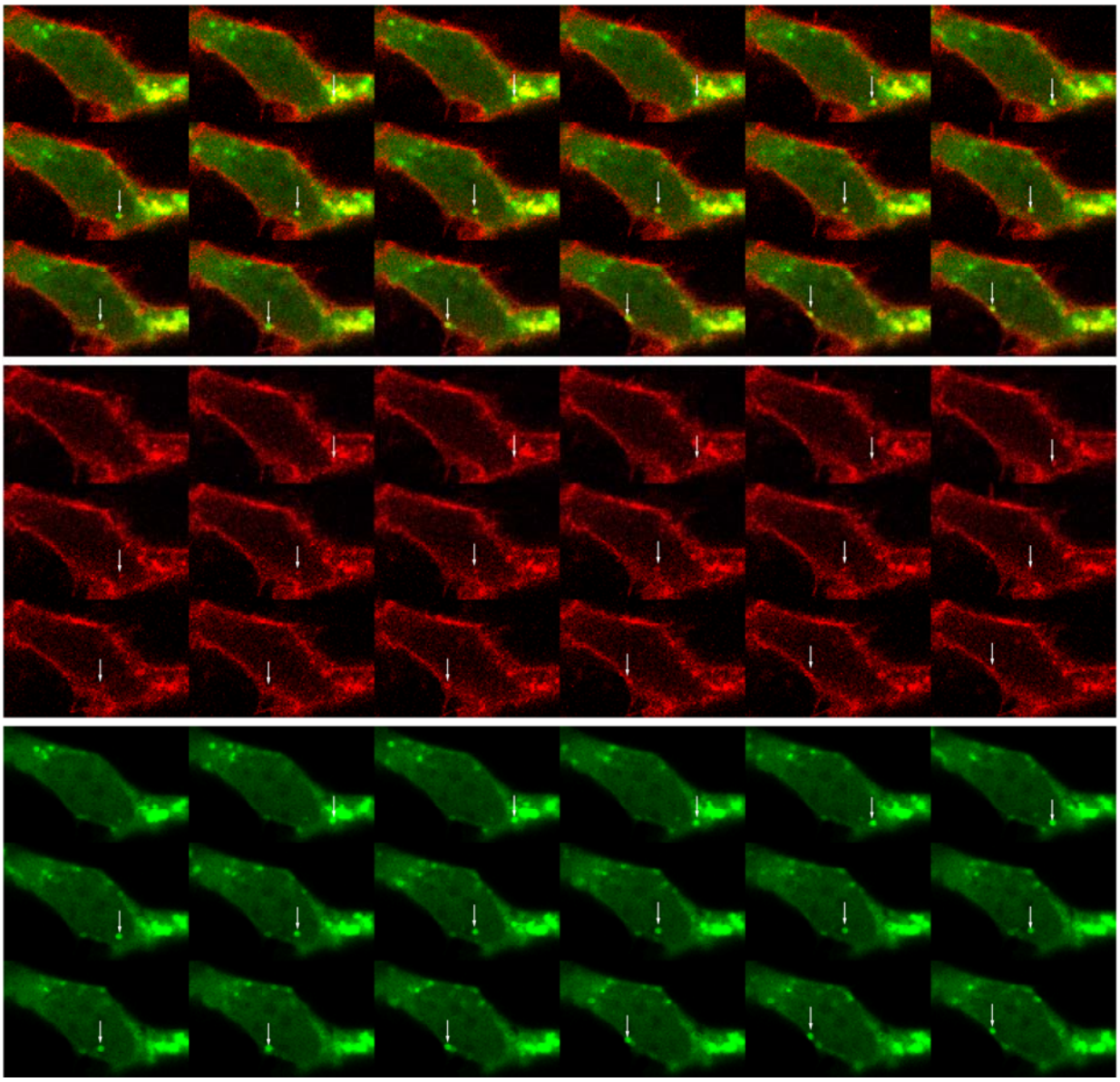

**Figure S4:** 1Rb3An27 cell expressing DAT and EGFP-Rab7 was labelled with JHC 1-64 as described in materials and methods and DAT was allowed to internalize for 1 hour before imaging. Imaging was done at room temperature and each picture repsents a time increment of 8 seconds. Arrow indicates moving vesicle that is both positive for DAT/JHC 1-64 (red channel) and EGFP-Rab7 (green channel).

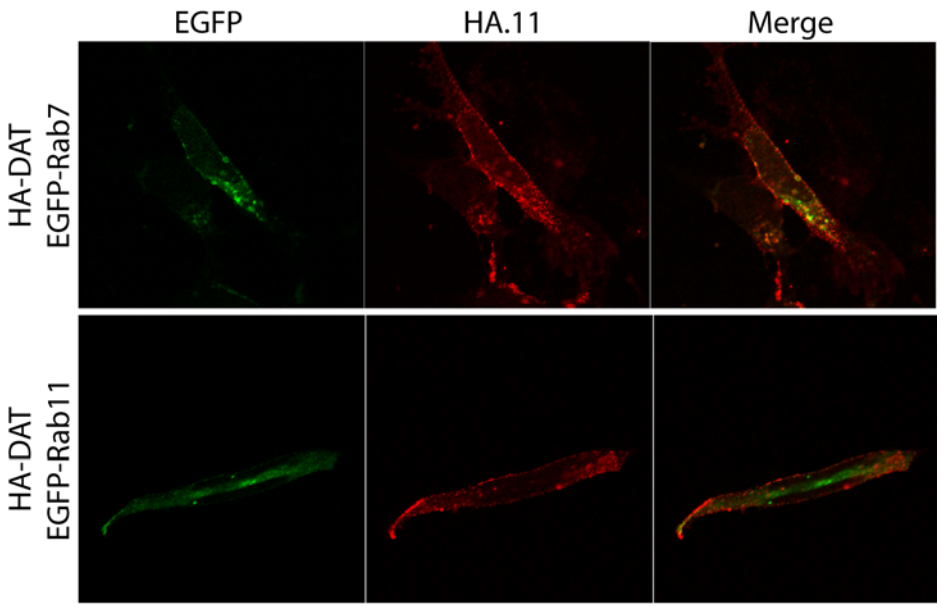


**Figure S5:** 1Rb3An27 cells expressing HA-DAT and EGFP-Rab7 or -Rab11 were incubated HA.11 antibody at 18 °C for 30 minutes to label surface HA-DAT. After labelling the media was replaced and the cells incubated at 37 °C for 1 hour to allow internalization. HA-DAT showed the most colocalization with EGFP-Rab7.

# Paper 3

# Membrane Localization is Critical for Activation of the PICK1 BAR Domain

Traffic 2008; **9:** 1327–1343
Blackwell Munksgaard



doi: 10.1111/j.1600-0854.2008.00761.x

# Membrane Localization is Critical for Activation of the PICK1 BAR Domain

**Kenneth L. Madsen[1], Jacob Eriksen[1], Laura Milan-Lobo[2], Daniel S. Han[3], Masha Y. Niv[3], Ina Ammendrup-Johnsen[1], Ulla Henriksen[1], Vikram K. Bhatia[4], Dimitrios Stamou[4], Harald H. Sitte[2], Harvey T. McMahon[5], Harel Weinstein[3] and Ulrik Gether[1,*]**

*[1]Department of Neuroscience and Pharmacology, Molecular Neuropharmacology Group and Center for Pharmacogenomics, The Panum Institute, University of Copenhagen, DK-2200 Copenhagen N, Denmark*
*[2]Center for Molecular Medicine and Pharmacology, Institute of Pharmacology, Medical University of Vienna, A-1090 Vienna, Austria*
*[3]Department of Physiology and Biophysics, Weill Medical College of Cornell University, New York, NY 10021, USA*
*[4]Bio-nanotechnology Laboratory, Nanoscience Center, University of Copenhagen, DK-2100 Copenhagen, Denmark*
*[5]Laboratory of Molecular Biology, MRC, Hills Road, Cambridge CB2 2QH, UK*
**Corresponding author: Ulrik Gether, gether@sund.ku.dk*

**The PSD-95/Discs-large/ZO-1 homology (PDZ) domain protein, protein interacting with C kinase 1 (PICK1) contains a C-terminal Bin/amphiphysin/Rvs (BAR) domain mediating recognition of curved membranes; however, the molecular mechanisms controlling the activity of this domain are poorly understood. In agreement with negative regulation of the BAR domain by the N-terminal PDZ domain, PICK1 distributed evenly in the cytoplasm, whereas truncation of the PDZ domain caused BAR domain-dependent redistribution to clusters colocalizing with markers of recycling endosomal compartments. A similar clustering was observed both upon truncation of a short putative α-helical segment in the linker between the PDZ and the BAR domains and upon coexpression of PICK1 with a transmembrane PDZ ligand, including the alpha-amino-3-hydroxy-5-methyl-4-isoxazolepropionic acid (AMPA) receptor GluR2 subunit, the GluR2 C-terminus transferred to the single transmembrane protein Tac or the dopamine transporter C-terminus transferred to Tac. In contrast, transfer of the GluR2 C-terminus to cyan fluorescent protein, a cytosolic protein, did not elicit BAR domain-dependent clustering. Instead, localizing PICK1 to the membrane by introducing an N-terminal myristoylation site produced BAR domain-dependent, but ligand-independent, PICK1 clustering. The data support that in the absence of PDZ ligand, the PICK1 BAR domain is inhibited through a PDZ domain-dependent and linker-dependent mechanism. Moreover, they suggest that unmasking of the BAR domain's membrane-binding capacity is not a consequence of ligand binding to the PDZ domain *per se* but results from, and coincides with, recruitment of PICK1 to a membrane compartment.**

**Key words: BAR domains, PDZ domains, protein–lipid interactions, receptors, transporters**

**Received 29 October 2007, revised and accepted for publication 6 May 2008, uncorrected manuscript published online 8 May 2008, published online 29 May 2008**

Protein interacting with C kinase 1 (PICK1) is a dimeric scaffolding protein widely distributed in the central nervous system (CNS) (1). Each protomer in the PICK1 dimer contains a single N-terminal PSD-95/Discs-large/ZO-1 homology (PDZ) domain that was originally found to bind the extreme C-terminus of protein kinase Cα (PKCα) (2) but later was shown to bind also the C-termini of several other proteins (1,3). These include receptor and transporter proteins expressed in the CNS [see data in PDZbase (4)], such as the GluR2/3 subunits of alpha-amino-3-hydroxy-5-methyl-4-isoxazolepropionic acid (AMPA)-type ionotropic glutamate receptors (AMPA receptors), the metabotropic glutamate receptor mGluR7 and various neurotransmitter transporters including the dopamine transporter (DAT), the norepinephrine transporter and the Glt1b glutamate transporter (1,3,5–7). In concordance with these interactions, there is compelling evidence for a critical function of PICK1 in regulation of neuronal signalling (8). A central role for PICK1 in severe psychiatric disorders such as schizophrenia has also been suggested (8). The interaction between PICK1 and AMPA receptors has been demonstrated to be essential for induction of synaptic long-term depression (LTD) (9,10) as well as for a new form of cerebellar synaptic plasticity termed calcium-permeable AMPA receptor plasticity (11). Moreover, induction of neuropathic pain, as well as cocaine sensitization, can be reversed by PICK1-specific peptides, conceivably through disruption of the PICK1/AMPA receptor interaction (12,13).

It is believed that PICK1 fulfils its biological role either by regulating trafficking of its binding partners (5,11,14) or in some cases by recruiting PKCα to facilitate their phosphorylation (6,15,16). For the AMPA receptor, it has been suggested that PICK1 enhances AMPA receptor endocytosis and thereby maintains an intracellular pool of the receptor (14). Observations in mice with targeted disruption of the PICK1 gene suggest that PICK1 might be critical not only for stabilizing an intracellular pool of AMPA receptors but also for mediating the recycling of AMPA receptors back to the plasma membrane – at least in cerebellar stellate cells (11). However, recent results suggest that PICK1 restricts AMPA receptor recycling in hippocampal neurons (17). For other interaction partners such as DAT, PICK1 is unlikely to promote endocytosis but rather seems to stabilize the expression of the binding partner at the cell surface (7,18).

The recent identification of a Bin/amphiphysin/Rvs (BAR) domain in the C-terminal half of PICK1 might shed light on the complex molecular functions of PICK1. BAR domains are homodimeric modules that mediate curvature-dependent recognition and/or tubulation of lipid membranes (19,20). They are present in many proteins involved in cellular trafficking processes and are believed to play a key role as membrane curvature-sensing and curvature-generating modules (19,20). The interaction with lipids has been suggested to be mediated by electrostatic attraction between positive charges on the concave side of the crescent-shaped BAR domain and negative charges on the lipid head groups (19,20). The strongest evidence for a role of the BAR domain in PICK1 function is the demonstration that transfection of wild-type (wt) PICK1 into cerebellar Purkinje cells derived from PICK1 knock-out mice can restore LTD, which was not observed for a PICK1 mutant containing a mutant BAR domain deficient in lipid vesicle binding (21).

Interestingly, the activity of the PICK1 BAR domain has been suggested to be negatively regulated by the PDZ domain, and the lipid-binding capacity was proposed to be activated upon binding of an interaction partner to the N-terminal PDZ domain (22). Such a regulation functionally distinguishes PICK1 from other BAR domain-containing proteins characterized to date. In this study, we have investigated the molecular mechanisms underlying this negative regulation of the PICK1 BAR domain. Our data suggest that the BAR domain activity is indeed inhibited in the absence of PDZ ligand; however, they also support a model in which unmasking of the PICK1 BAR domain activity is not caused by ligand binding to the PDZ domain *per se* but rather by recruitment of PICK1 to a membrane compartment by the interaction partner. We propose that this regulatory mechanism prevents improper BAR domain activity and ensures tight spatial and temporal control of PICK1 function in relation to its several interaction partners.

## Results

### *The PICK1 BAR domain is negatively regulated by the PDZ domain*

It was recently shown that the coiled-coil domain in arfaptin2 is a membrane curvature-recognizing BAR domain (19). This domain is homologous to the coiled-coil domain predicted to be present in PICK1, suggesting that PICK1 also contains a membrane curvature-recognizing BAR domain (19). For arfaptin, the BAR domain was responsible for a characteristic juxtanuclear tubular localization of the protein upon overexpression in heterologous cells such as COS7 cells (19). In contrast to arfaptin2, PICK1 was evenly distributed throughout the cytosol when heterologously expressed in COS7 cells (Figure 1A). Truncation of the N-terminal PDZ domain (PICK1 Δ1–101) caused, however, a significant redistribution of the protein characterized by the presence of multiple distinct vesicle-like clusters (Figure 1A). Truncation of not only the PDZ domain but also the linker between the PDZ domain and the predicted BAR domain (PICK1 Δ1–135) increased the protein clustering at juxtanuclear sites (Figure 1A). Note that the cells expressing PICK1 Δ1–135 actually display a spectrum of clustering phenotypes illustrated in Figure 1B. The cell shown to the right in Figure 1B represents a frequent extreme.

An intriguing explanation for these observations would be that the activity of the BAR domain, as reflected by relocalization to clusters, is inhibited in full-length PICK1 and that removal of the N-terminal PDZ domain allows 'activation' of the BAR domain and thereby clustering. A strikingly similar clustering is seen for full-length BAR domain protein islet cell autoantigen 1, 69 kDa (ICA69) which is very closely related to PICK1 (23). Previous findings by Ziff and coworkers, suggesting a direct interaction between the PDZ domain and the BAR domain of PICK1 that might be responsible for the negative regulation of the BAR domain (22), are in agreement with such a hypothesis.

To interpret the phenotypes observed for the two PICK1 truncations (PICK1 Δ1–135 and PICK1 Δ1–101) in a structural context, we modelled the PICK1 BAR domain-like sequence using the co-ordinates from the crystal structures of known BAR domains, including arfaptin2, amphiphysin and endophilin (Figure 1). In the molecular model, the PICK1 BAR domain exhibited a strong concentration of positive electrostatic potential on the concave side of the crescent shape, similar to that observed for the crystal structure of the BAR domain from Arfaptin2 (19). Positively charged residues generating this potential on the concave side of the BAR domain have been suggested to mediate the electrostatic interaction with negatively charged curved membranes (19). To disrupt the electrostatic interaction, we substituted either three positively charged residues on the concave side of each subunit of the BAR domain (K251E, K252E and K257E; termed 3KE) or two residues (K266E and K268E; termed 2KE) (Figure 1). As shown in Figure 1A, reversing the charges on the concave side of the crescent shape reversed the clustering of both truncated proteins. This observation parallels findings by Lu and Ziff who studied a similar truncation of PICK1 (22). No change in localization was observed when the 2KE and 3KE mutations were introduced in full-length PICK1 (data not shown).

To further substantiate our findings obtained with immunocytochemistry, we employed a biochemical assay in which we separated cytosolic and particulate fractions. PICK1 was distributed equally between the two fractions, suggesting some constitutive membrane association of full-length PICK1 that was not apparent from the confocal imaging. Because the 3KE mutation only slightly reduced association to the particulate fraction, this association was

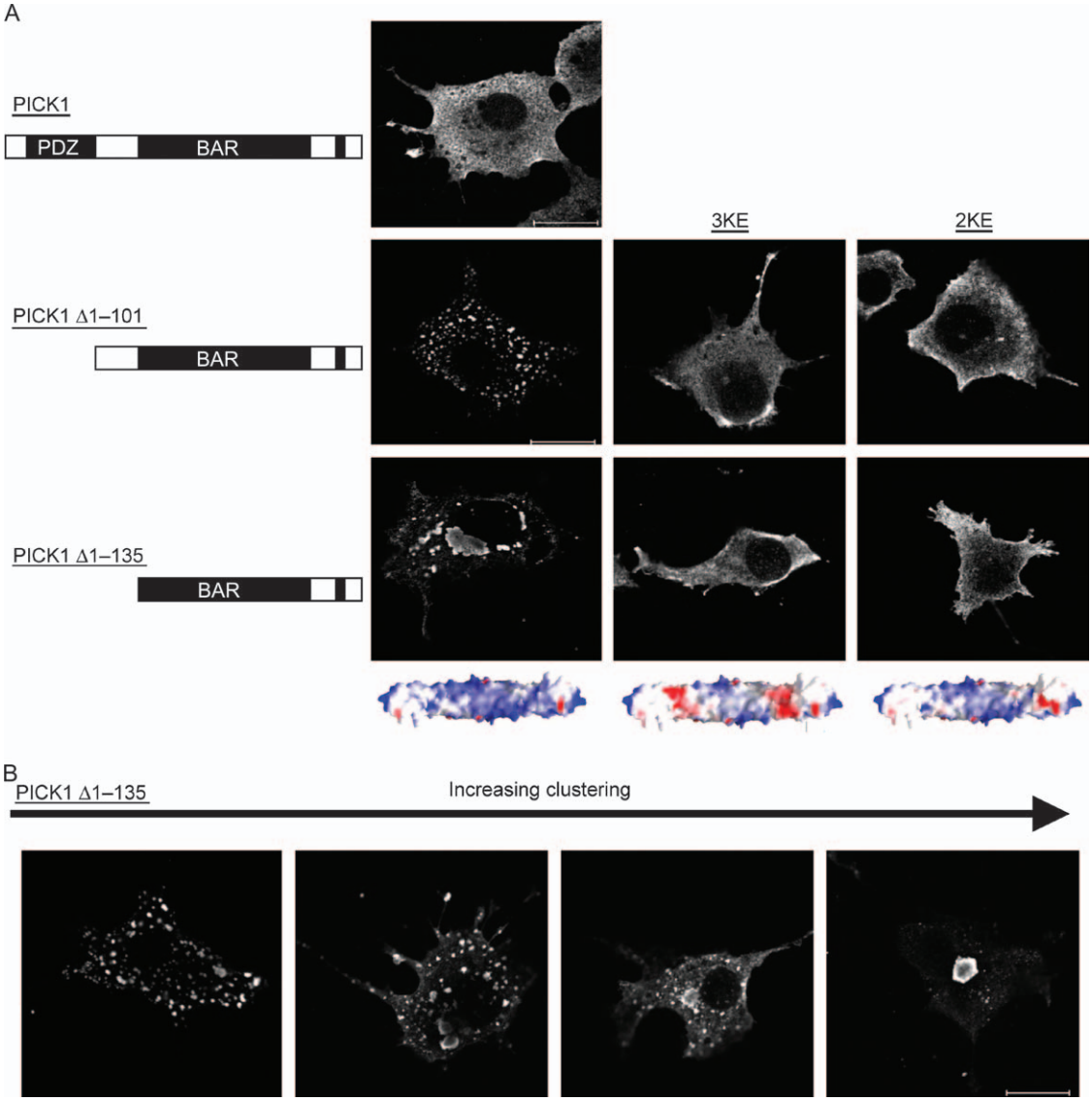


**Figure 1: Activity of the PICK1 BAR domain is inhibited by the N-terminal PDZ domain and the PDZ-BAR linker sequence.** A) COS-7 cells were transiently transfected with indicated myc-tagged PICK1 constructs, immunostained and analysed by confocal microscopy. The diagrams on the left indicate the N-terminal truncations. Left picture panel: representative cells expressing from top mycPICK1, mycPICK1 Δ1–101 or mycPICK1 Δ1–135; middle picture panel: representative cells expressing mycPICK1 Δ1–101 3KE or mycPICK1 Δ1–135 3KE and right picture panel: representative cells expressing mycPICK1 Δ1–101 2KE or mycPICK1 Δ1–135 2KE. The 3KE and 2KE refer to charge-reversing mutations in the BAR domain (3KE, K251E, K252E and K257E) and (2KE, K266E and K268E). Models of the predicted effects of these mutations on the surface charge of the concave side of the PICK1 BAR domain are shown below the pictures (blue, positive and red, negative). B) Four different cells expressing mycPICK1 Δ1–135 and covering the range of phenotypes observed. All white bars = 10 μm. The data shown are representative of more than five similar experiments.

independent of the presence of the positively charged residues on the concave side of the BAR domain. It might, therefore, at least in part reflect the recently reported membrane-interacting capacity of the PDZ domain itself (24).

Importantly, our two deletion mutants (Δ1–101 and Δ1–135) associated to a markedly higher degree to the particulate fraction than to the cytosolic fraction (Figure 2). In agreement with a BAR domain-mediated effect and the confocal imaging data, we found that reversing the charge of lysines 251, 252 and 257 (3KE) in the BAR domain decreased the association with the particulate fraction to the same level as that seen for PICK1 and PICK1 3KE (Figure 2). It should be noted, however, that even though PICK1 and the deletion mutants containing the 3KE mutations display the same degree of association to the particulate fraction, it could very well involve different

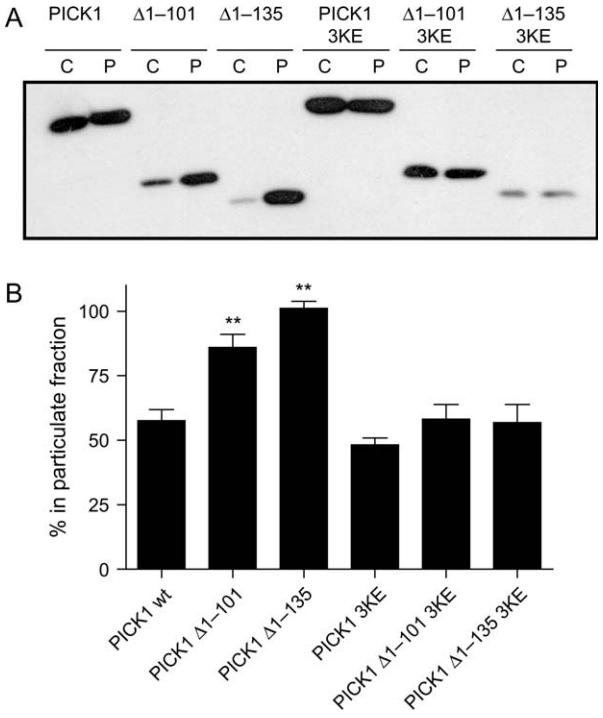


**Figure 2: Association of the PICK1 BAR domain with the particulate fraction is increased in a manner that depends on positively charged residues on the concave side of the domain.** A) Representative immunoblot illustrating distribution of PICK1, PICK1 Δ1–101, PICK1 Δ1–135, PICK1 3KE, PICK1 Δ1–101 3KE and PICK1 Δ1–135 3KE between the cytosolic (C) and the particulate (P) fractions of transiently transfected COS7 cells. B) Densitometry analysis of immunoblots. Data are expressed as percent of total in the particulate fraction for the indicated constructs (mean ± SEM, $^{**}p < 0.01$ compared with PICK1 WT, $n = 3$).

mechanisms, that is, while the PDZ domain might play a role in full-length PICK1, it is possible that in the truncations, the 3KE mutation is insufficient to completely abolish the lipid-binding capacity of the activated BAR domain and thereby association to the particulate fraction.

### *BAR domain-dependent clustering is observed in a neuronal cell line and in hippocampal neurons*

In addition to the immunostainings shown above, we analysed PICK1 fusion constructs with yellow fluorescent protein (YFP). This allowed visualization of the different constructs without antibody staining and cell permeabilization. In both COS7 cells (data not shown) and in 1Rb27AN3 cells (Figure 3), an immortalized dopaminergic cell line (25), we observed results corresponding to those obtained in the immunostainings. However, the clusters seen in the living cells appeared more like distinct vesicles containing enhanced yellow fluorescent protein (eYFP)-tagged PICK1 Δ1–135 or eYFP-tagged PICK1 Δ1–101 (Figure 3A).

We could also reproduce the result in transfected hippocampal neurons [6 days in vitro (DIV)] with clear clustering of eYFP-tagged PICK1 Δ1–135 and eYFP-tagged PICK1 Δ1–101 but not of the corresponding 3KE mutations (Figure 3B).

### *Coexpression of PICK1 with membrane-associated PDZ ligands causes clustering*

The BAR domain-dependent vesicular and juxtanuclear clustering of truncated PICK1 strongly resembles the redistribution of PICK1, which was previously reported to occur upon coexpression of full-length PICK1 with transmembrane proteins that bind to the PICK1 PDZ domain (5,26,27). Congruent with these findings, coexpression of the GluR2 subunit of the AMPA receptor with eYFP–PICK1 caused a marked coclustering of both proteins (Figure 4). However, when GluR2 was coexpressed with eYFP–PICK1 3KE, we did not see this redistribution (Figure 4).

The BAR domain-dependent clustering of PICK1 upon coexpression with a PDZ ligand (GluR2) is consistent with the release of an inhibition of the BAR domain by the binding of an interaction partner to the PDZ domain. To examine whether the C-terminal tail of GluR2, which binds to PICK1, was sufficient to promote clustering, we transferred the 50 C-terminal residues of GluR2 to the single transmembrane protein Tac (the α subunit of interleukin-2 receptor) that has been used previously to study autonomous signal sequences in protein trafficking (28,29). Tac was tagged at the N-terminus with the FLAG tag to obtain FLAG–TacGluR2 C50, which, by itself, localized predominantly to the plasma membrane with some intracellular, vesicular accumulation (Figure 5A). However, upon cotransfection with PICK1, we observed a major relocalization of FLAG–TacGluR2 C50 to clusters where it colocalized with PICK1. This localization mostly resembles the localization of the Δ1–135 PICK1, whereas full-length GluR2 causes a clustering more resembling the Δ1–101 PICK1 or at least the less extreme Δ1–135 PICK1. Importantly, like for full-length GluR2, this clustering was BAR domain dependent because it was abolished by the 3KE mutation (PICK1 3KE) (Figure 5A). We subsequently fused only the 29 C-terminal residues of GluR2 to the C-terminus of Tac. As shown in Figure 5B, this was also sufficient for BAR domain-dependent clustering when PICK1, but not PICK1 3KE, was coexpressed with the ligand (GluR2 C29). This experiment excludes the need for the sequence 843–852 in the GluR2 tail, which was shown previously to mediate direct interaction with the PICK1 BAR domain (30), in forming the clustering phenotype. We also coexpressed FLAG–TacGluR2 C29 with YFP–PICK1 in the neuronally derived 1Rb27AN3 cells and observed clustering similar to that seen in the COS7 cells (data not shown).

Finally, to test whether the clustering was specific to the GluR2 C-terminal sequence, we turned to another interaction partner for PICK1 – the DAT (3). We transferred the C-terminal 24 residues downstream from the putative internalization motif in the DAT C-terminus to Tac. Coexpression of this construct (FLAG–TacDAT C24) with PICK1

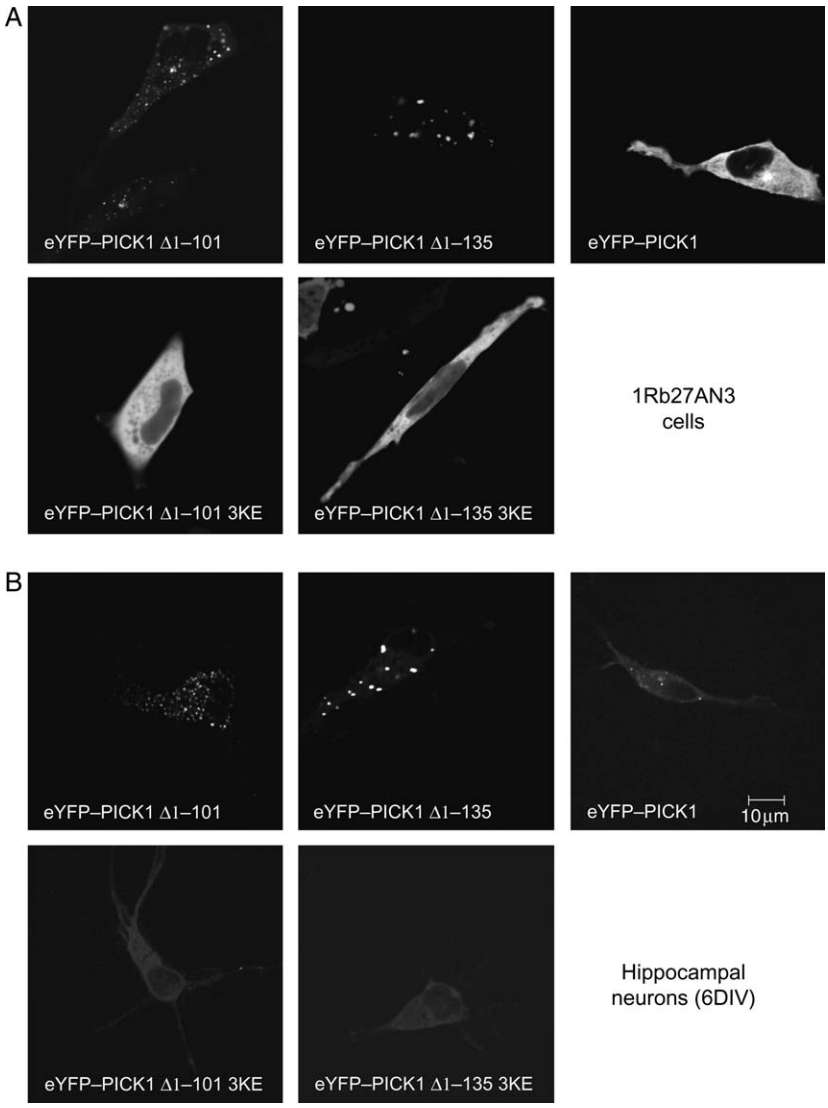


**Figure 3: The BAR domain-dependent clustering is observed in live immortalized dopaminergic neurons and in hippocampal neurons.** A) Immortalized dopaminergic neurons (1Rb27AN3 cells) and B) cultured hippocampal neurons transiently (6 DIV) expressing eYFP–PICK1 Δ1–101, eYFP–PICK1 Δ1–101 3KE, eYFP–PICK1, eYFP–PICK1 Δ1–135 or eYFP–PICK1 Δ1–135 3KE. The transfected cells were analysed by confocal live imaging at 37°C. The data shown are representative of three identical experiments.

induced BAR-dependent clustering just as efficiently as FLAG–TacGluR2 C29 (Figure 5C).

### *Clustering is also seen with partial truncation of the linker between the PDZ domain and the BAR domain*

Our data are consistent with a model in which the PDZ domain in the absence of PDZ ligand is capable of preventing BAR domain-dependent redistribution of PICK1 to clusters. A region that could play a role in this inhibition is the linker between the two domains (residues ∼105 and ∼135). According to a secondary structure prediction of the PICK1 protein, a putative α-helical region was suggested from Ser113 to Val121, whereas the C-terminal half of the linker region was suggested to have little secondary structure. We decided, therefore, to generate two discrete truncation mutations in the linker sequence; one mutation with deletion of the predicted α-helical segment (PICK1 Δ113–121) and another with deletion of the C-terminal part of the linker (PICK1 Δ125–135) (Figure 6A). Interestingly, deletion of the putative α-helical segment (PICK1 Δ113–121) resulted in clustering similar to that seen by expressing the BAR domain alone or together with a transmembrane PDZ ligand (Figure 6B). The PDZ ligand-binding capacity was preserved in the mutant as reflected by relocalization of coexpressed FLAG–TacGluR2 C29 to clusters (Figure 6B). In contrast, PICK1 Δ125–135 did not show constitutive clustering but rather displayed a phenotype similar to PICK1 wt with cytoplasmic distribution in the absence of PDZ ligand and clustering upon coexpression with PDZ ligand (Figure 6).

### *The BAR domain is not activated by a cytosolic ligand*

It was our original hypothesis that ligand binding *per se* to the PDZ domain would unmask the BAR domain activity

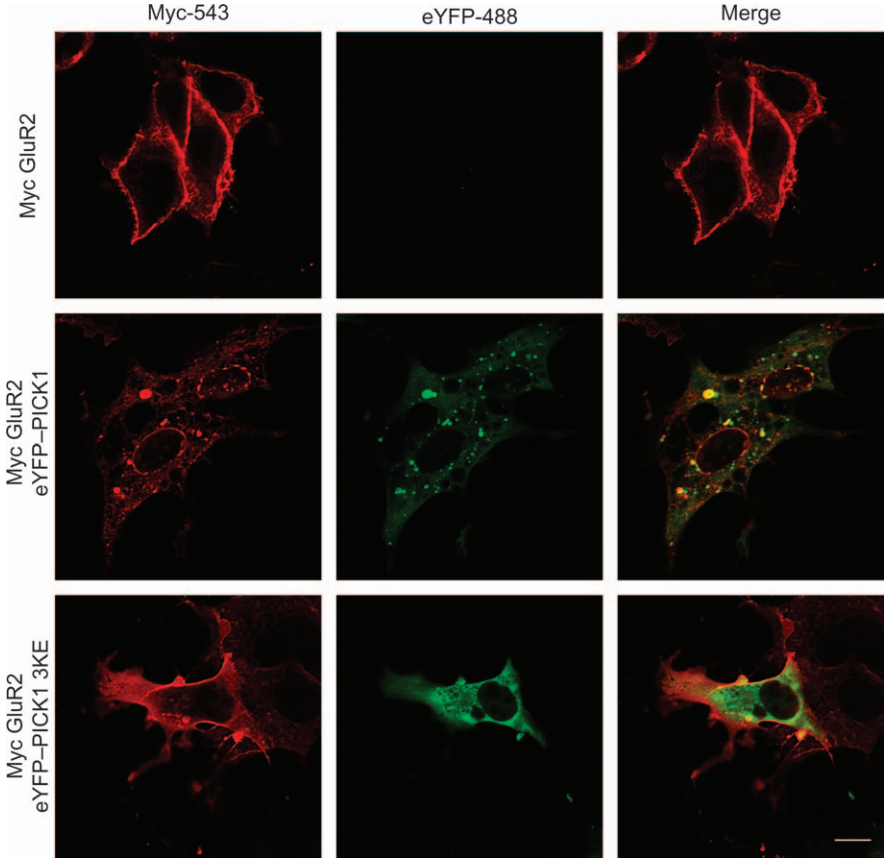


**Figure 4: Coexpression of Myc-tagged GluR2 with eYFP–PICK1 causes BAR domain-dependent co-clustering.** Myc-tagged GluR2 was transiently expressed in COS7 cells alone (upper row), together with eYFP–PICK1 wt (middle row) or together with eYFP–PICK1 3KE (bottom row). Cells were fixed, permeabilized and stained with anti-myc for confocal microscopy. eYFP was visualized by YFP fluorescence. MycGluR2 is shown in red (left column) and eYFP–PICK1 in green (middle column). Right column shows the merged pictures. White bar = 10 μm. The data shown are representative of four experiments.

and thus would not require binding to a transmembrane protein. To test this hypothesis, we transferred the 29 C-terminal residues of GluR2 onto enhanced cyan fluorescent protein (eCFP). This construct localized evenly throughout the cytosol with some tendency to accumulate within the nucleus (Figure 7A), which has previously been reported for enhanced green fluorescent protein (eGFP) itself (31). Upon cotransfection of eCFP–GluR2 C29 with eYFP–PICK1, we observed an entirely even distribution of PICK1 within all cells, suggesting that this cytosolic ligand was unable to cause BAR domain-mediated clustering of PICK1 (Figure 7A). To verify that the eCFP–GluR2 construct was actually bound by the PICK1 PDZ domain, we performed fluorescence resonance energy transfer (FRET) experiments using live cell imaging in an epifluorescence microscopy set up (Figure 7B). In control experiments, we observed substantial energy transfer in an eCFP–YFP fusion protein and we did not see any significant energy transfer when eCPF was coexpressed with YFP–PICK1 (Figure 7C). Importantly, we observed significant energy transfer from eCFP–GluR2 C29 to eYFP–PICK1, and this transfer was essentially abolished by addition of an alanine to the GluR2 C29 sequence (Figure 7C), which is predicted to interfere with the PDZ binding (18). Note that the FRET signal generated by the interaction of eCFP–GluR2 C29 with eYFP–PICK1 was localized evenly throughout the cytosol (Figure 7D), suggesting that the FRET signal is unlikely the result of a small pool of interacting proteins whose membrane localization may not be easily detectable on the background of diffusely localized non-interacting proteins. Note also that eCFP–GluR2 C29 was expressed at markedly higher levels than FLAG–TacGluR2 C29 as estimated from western blots using an antibody directed against the GluR2 C-terminus (Figure 7E). This strongly suggests that the lack of clustering despite significant FRET signal is not the result of reduced expression of ligand (eCFP–GluR2 C29).

To further substantiate that eCFP–GluR2 C29 and PICK1 interact in the cytosol, we performed coimmunoprecipitation experiments. As shown in Figure 7F, PICK1 coimmunoprecipitated with eCFP–GluR2 C29 but not with eCFP–GluR2 C29 + Ala in agreement with the FRET measurements and a PDZ domain-dependent interaction between the two proteins. We used myc-tagged PICK1 in these experiments to have an optimal antibody for the immunoblotting procedure. Of note, myc antibody staining of cells coexpressing eCFP–GluR2 C29 + Ala and myc-tagged PICK1 showed uniform distribution of both proteins in the cytosol identical to that seen for cells coexpressing eCFP–GluR2 C29 and eYFP–PICK1 (data not shown).

Summarized, our FRET and coimmunoprecipitation data provide strong evidence that indeed eCFP–GluR2 C29 and

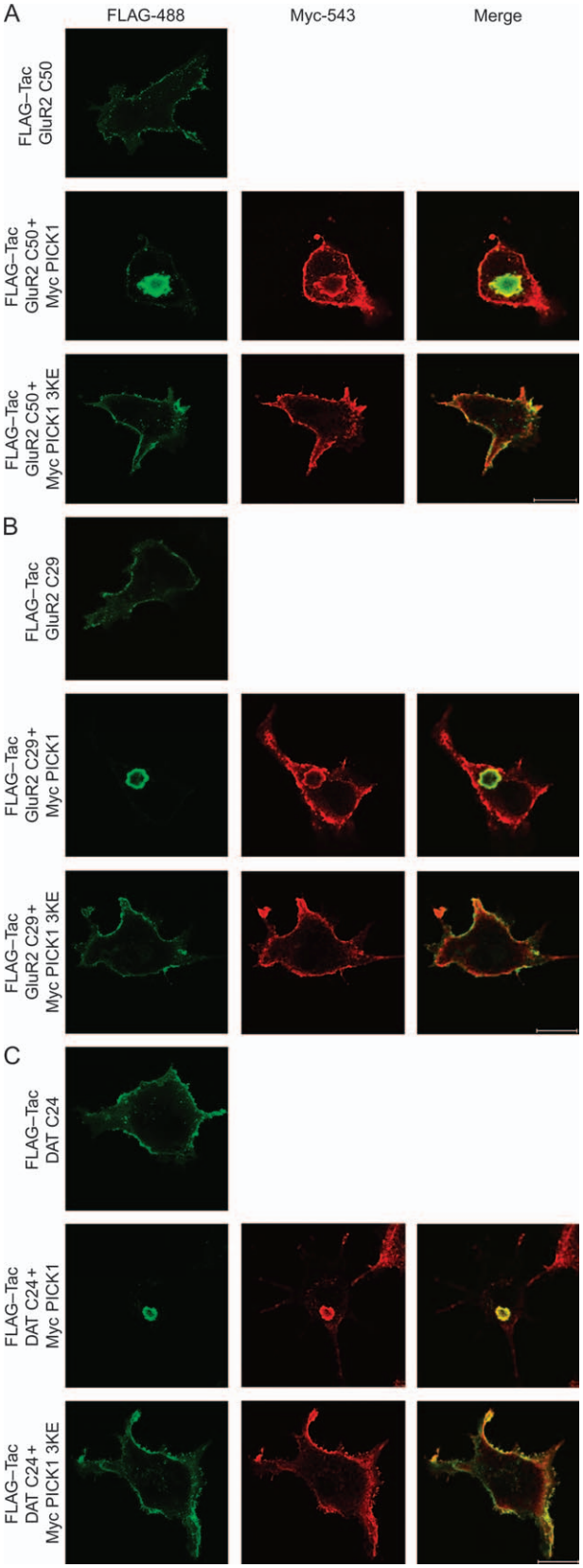


**Figure 5: The C-termini of GluR2 and of DAT fused to the single transmembrane protein Tac are sufficient for BAR domain-dependent coclustering with PICK1.** A) FLAG–Tac-GluR2 C50 and B) FLAG–TacGluR2 C29 transiently expressed in COS7 cells alone (upper row), together with mycPICK1 wt (middle row) or together with mycPICK1 3KE (lower row). C) FLAG–TacDAT C24 transiently expressed in COS7 cells alone (upper row), together with mycPICK1 wt (middle row) or together with mycPICK1 3KE (lower row). Cells were fixed, permeabilized and stained with anti-FLAG and anti-Myc for confocal microscopy. The C-terminal FLAG–Tac fusions are shown in green (left column) and mycPICK1 in red (middle column). Right column shows the merged pictures. White bar = 10 μm. The data shown are representative of four experiments.

eYFP–PICK1 interact, and given that both the PICK1 and the FRET signals are evenly distributed in the cytosol, this suggests that binding of a cytosolic PICK1 ligand does not result in BAR domain activation.

### *The BAR domain is activated by membrane association independent of ligand binding to the PDZ domain*

The inability of a PDZ ligand by itself to activate the BAR domain opened the possibility that activation of BAR domain function in the full-length PICK1 might depend on recruitment of PICK1 to a membrane compartment. To test this hypothesis further, we introduced an N-terminal myristoylation site from the chicken myc protein because N-myristoylation has previously been shown to mediate a relatively weak and reversible plasma membrane localization of numerous proteins (32). The myristoylated PICK1 localized to the plasma membrane as well as to intracellular clusters in COS7 cells (Figure 8A), which resembled the clustering observed for truncated PICK1 and upon cotransfection of PICK1 with transmembrane ligands for the PDZ domain. The clustering appeared to be markedly reduced in the corresponding 3KE mutant (Figure 8A). However, because the effect of the 3KE mutation was less pronounced than the effect seen for truncated PICK1 and PICK1 cotransfected with a transmembrane ligand, we performed a quantification of the clustering. The quantification was done by determining the standard deviation of a line scan through the cells as a measure of clustering (a representative example is shown in Figure 8A). Using 8-bit pixel depth (256 graytones), we observed a mean standard deviation of MyriPICK1 wt profiles of 54.7 ± 1.5 ($n = 64$), whereas the mean standard deviation results for MyriPICK1 3KE profiles was 30.1 ± 1.7 ($n = 63$) (mean ± SEM, $p < 0.0001$, unpaired *t*-test). This is consistent with a significantly higher degree of clustering of MyriPICK1 compared with MyriPICK1 3KE and thus that a part of the clustering phenotype is indeed BAR domain dependent (Figure 8A).

In principle, the observed activation of the BAR domain in MyriPICK1 could be the result of myristoyl-dependent localization of PICK1 to a membrane domain that contains a high concentration of an endogenous PDZ-binding

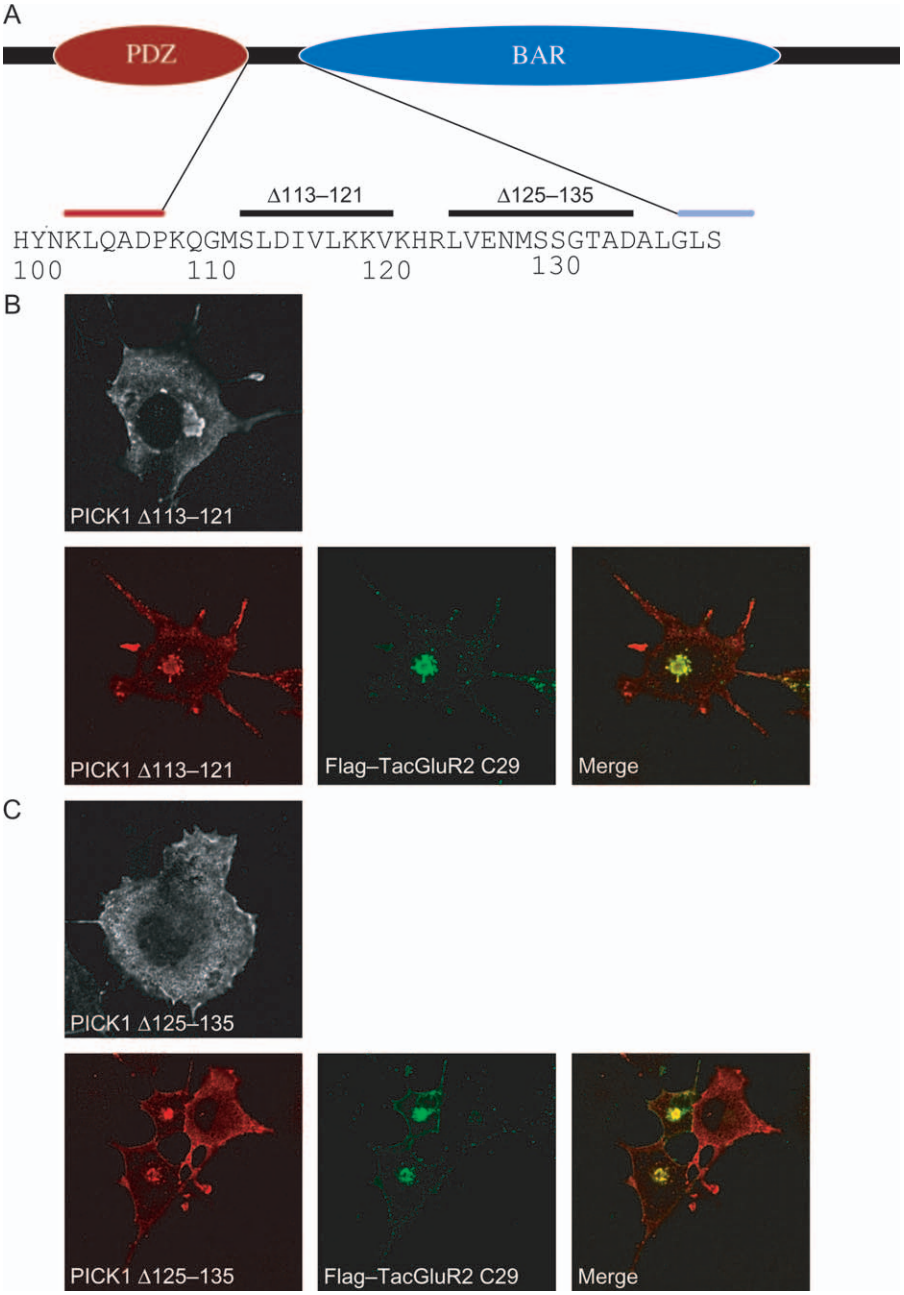


**Figure 6: Deletion of a predicted α-helical region (residues 113–121) in the linker region between the PDZ and the BAR domains causes redistribution of PICK1 to juxtanuclear clusters.** A) Schematic diagram of PICK1 highlighting the linker sequence between the PDZ domain and the BAR domain. According to a secondary structure prediction of the PICK1 protein, the short sequence between residues 113 and 121 was suggested to form an α-helical segment. In contrast, the C-terminal half of the linker was predicted to have a less well-defined structure. To investigate the putative role of the linker in regulation of BAR domain activity, we generated two deletion mutants, one corresponding to residues 113–121 and thus the putative α-helical segment and one corresponding to residues 125–135. B) Expression of myc-tagged PICK1 Δ113–121 alone (upper panel) or together with a PDZ ligand (FLAG–TacGluR2 C29) (lower panels). PICK1 Δ113–121 is shown in red (left picture) and FLAG–TacGluR2 C29 in green (middle picture). The merged pictures are shown on the right. C) Expression of myc-tagged PICK1 Δ125–135 alone (upper panel) or together with a PDZ ligand (FLAG–TacGluR2 C29) (lower panels). PICK1 Δ125–135 is shown in red (left picture) and FLAG–TacGluR2 C29 in green (middle picture). The merged pictures are shown on the right.

partner of PICK1, leading to BAR activation through ligand binding to the PDZ domain. Therefore, we introduced a mutation (A87L) in the binding pocket of the myristoylated PICK1, which we have shown previously to eliminate binding to all tested ligands *in vitro* without compromising the structural integrity of the PDZ domain (3). This mutant of MyriPICK1 displayed the same clustering as observed for MyriPICK1 itself even though the ligand-binding capacity of the PDZ domain was eliminated (Figure 8B). Finally, we wanted to confirm that activation of the PICK1 BAR domain by introduction of the myristoylation site from chicken myc was because of addition of the acyl chain and not an artifact of introducing the sequence itself. Figure 8B shows that mutation of the glycine in position 2 of the chimeric protein, which is the residue modified with the acyl chain, into an alanine completely abolished clustering of the protein.

### *The clusters originate from the plasma membrane*

It is tempting to speculate that the clustering seen upon coexpression of PICK1 with a transmembrane ligand directly reflects the suggested ability of PICK1 to regulate trafficking of its interaction partners. Specifically, the clusters might reflect the suggested ability of PICK1 to generate an intracellular pool of AMPA receptors, which is believed to be essential for induction of LTD (9,10,14).

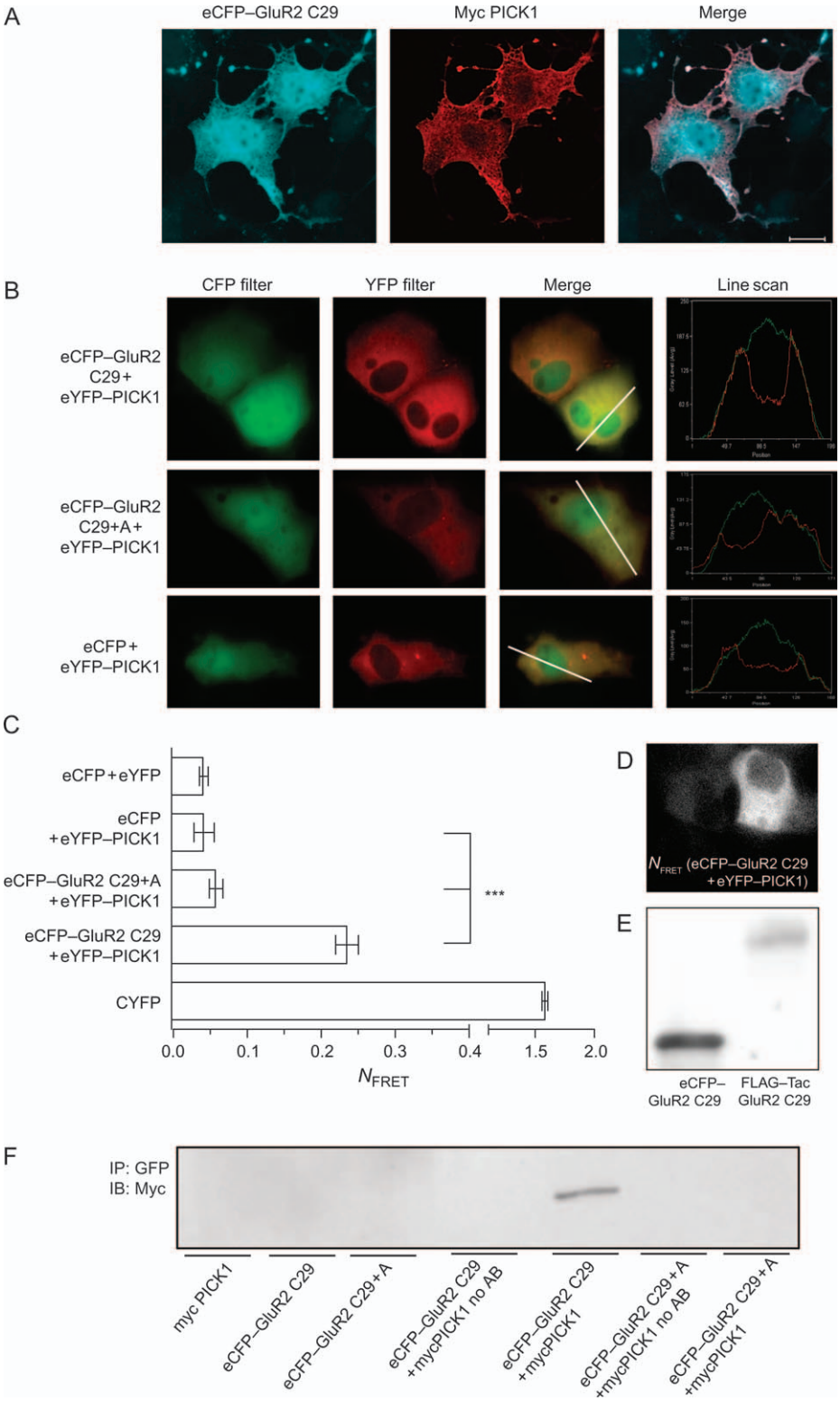


**Figure 7: Legend on next page.**

If the clusters are representative of such an intracellular pool, it would be expected that a transmembrane PDZ ligand coexpressed with PICK1 would be continuously internalized to the observed clusters. To test this, we performed an antibody feeding experiment using FLAG–TacGluR2 C29 as our 'model' construct. Cells expressing FLAG–TacGluR2 C29 with PICK1 were incubated with the M1 antibody at 37°C for 90 min followed by fixation and staining with secondary fluorescent antibody. In agreement with our prediction, we observed clusters containing both PICK1 and FLAG–TacGluR2 C29 (Figure 9). Thus, FLAG–TacGluR2 C29 from the surface was dynamically accumulated in the juxtanuclear clusters. This process was also BAR domain dependent because coexpression of FLAG–TacGluR2 C29 with the PICK1 3KE mutant did not result in accumulation of the two proteins in intracellular clusters (Figure 9).

### *The juxtanuclear clusters represent Rab11-positive endocytic compartments*

We next wanted to investigate the more precise nature of the juxtanuclear clusters. Given that FLAG–TacGluR2 C29 was internalized from the surface, we investigated whether the PICK1 clusters it generated colocalized with any of the small guanosine triphosphatase (GTPase) Rab proteins that characterize distinct endocytic compartments (33–35). Accordingly, FLAG–TacGluR2 C29 and PICK1 were expressed together with eGFP-tagged Rab5, Rab7 or Rab11. As shown in Figure 10A and as expected, the eGFP-tagged Rab proteins displayed distinct expression patterns consistent with localization to different endocytic compartments. The PICK1 clusters generated by FLAG–TacGluR2 C29 showed most prominent colocalization with eGFP–Rab11, a marker of recycling endosomes (33–35), that is, there was a marked overlap between the eGFP–Rab11-positive vesicles and the PICK1-positive juxtanuclear clusters (Figure 10B). This was supported by the quantification of colocalization shown in Figure 10D, showing ∼60% colocalization of PICK1 with eGFP–Rab11. For eGFP–Rab5, which is a marker of the early endosomal compartments (33–35), we also observed overlap, although lower than that with the eGFP–Rab11-positive clusters (∼30%) (Figure 10B,D). In contrast, essentially, no colocalization was observed with eGFP–Rab7, a marker of late endosomes (Figure 10B,D). Finally, we tested the subcellular localization of the PICK1 BAR domain alone (Δ1–135). As seen in Figure 10C,D, we observed clear colocalization with eGFP–Rab11 (∼60%) but very little with eGFP–Rab5 and eGFP–Rab7 (<10%) (Figure 10C,D).

## Discussion

PICK1 is the only protein known to contain a PDZ domain in combination with a BAR domain. Thus, PICK1 has the unique property of having a PDZ domain capable of binding the extreme C-termini of a broad range of proteins critical for neuronal signalling and a BAR domain that can connect these proteins to distinct curved membranes within the cell. Recent studies have documented the critical physiological roles of both domains in PICK1 (21). In this study, we present data providing new insight into the molecular mechanisms controlling the activity of the PICK1 BAR domain and how this might regulate trafficking of transmembrane interaction partners of the PDZ domain.

The presence of a membrane curvature-recognizing BAR domain in PICK1 is a relatively recent insight. PICK1 has long been known to have high sequence identity to the arfaptin2, but it was not until the structure of arfaptin2 was shown to be recapitulated in the BAR domain of amphiphysin that this sequence was realized to be a BAR domain (19). *In vitro* membrane vesicle-binding assays have indicated that the PICK1 BAR domain is indeed capable of binding lipids (21). As shown by Lu and Ziff (22) and in this

**Figure 7: The interaction of PICK1 with a cytosolic ligand does not cause clustering of PICK1.** A) COS7 cells transiently coexpressing eCPF–GluR2 C29 (eCFP with the 29 C-terminal residues of GluR2 fused to the C-terminus) and mycPICK1. Cells were fixed, permeabilized and stained with anti-Myc. eCFP was visualized by CFP fluorescence. eCFP–GluR2 C29 is shown in blue (left column) and mycPICK1 in red (middle column). Right column shows the merged pictures. White bar = 10 μm. The data shown are representative of three experiments. B) COS7 cells expressing eCPF–GluR2 C29 and eYFP–PICK1, eCPF–GluR2 C29 + Ala (non-binding control) and eYFP–PICK1 or eCFP and eYFP–PICK1. The first and second columns from the left show the images obtained with CFP and YFP filter sets, while the third column represents a merged image of CFP and YFP. The fourth column shows line scan histograms illustrating cellular colocalization. The images shown are representative of three independent experiments. C) Normalized FRET efficiency is given for eCFP–GluR2 C29 and eYFP–PICK1 ($n = 29$), eCFP–GluR2 C29 + Ala and YFP–PICK1 ($n = 28$) and eCFP cotransfected with YFP–PICK1 ($n = 22$); as controls, we used CYFP (a covalent fusion of CFP and YFP) ($n = 22$) and cotransfection of CFP and YFP vectors ($n = 20$). All bars represent data from three experimental days (mean ± SEM). Statistical analysis was done using ANOVA, *post hoc* Bonferroni's test for multiple comparisons (***$p < 0.001$). D) Distribution of the FRET signal corrected for bleed-through in COS7 cells expressing eCFP–GluR2 C29 and eYFP–PICK1. E) Western blot of eCFP–GluR2 C29 and FLAG–TacGluR2 C29 transfected in parallel. The two proteins were visualized with an antibody against the C-terminal 20 residues of GluR2 (Santa Cruz). F) Coimmunoprecipitation of myc-tagged PICK1 with eCFP–GluR2 C29 but not with eCFP–GluR2 C29 + Ala in agreement with the FRET measurements and a significant interaction. The experiments were carried out using lysates from COS-7 cells transiently expressing mycPICK1, eCFP–GluR2 C29, eCFP–GluR2 C29 + Ala, eCFP–GluR2 C29 together with mycPICK1 or eCFP–GluR2 C29 + Ala together with mycPICK1. The immunoprecipitations were done with a mouse monoclonal anti-green fluorescent protein antibody and immunoblotting with a rabbit anti-myc antibody. No antibody refers to no antibody in the immunoprecipitate.

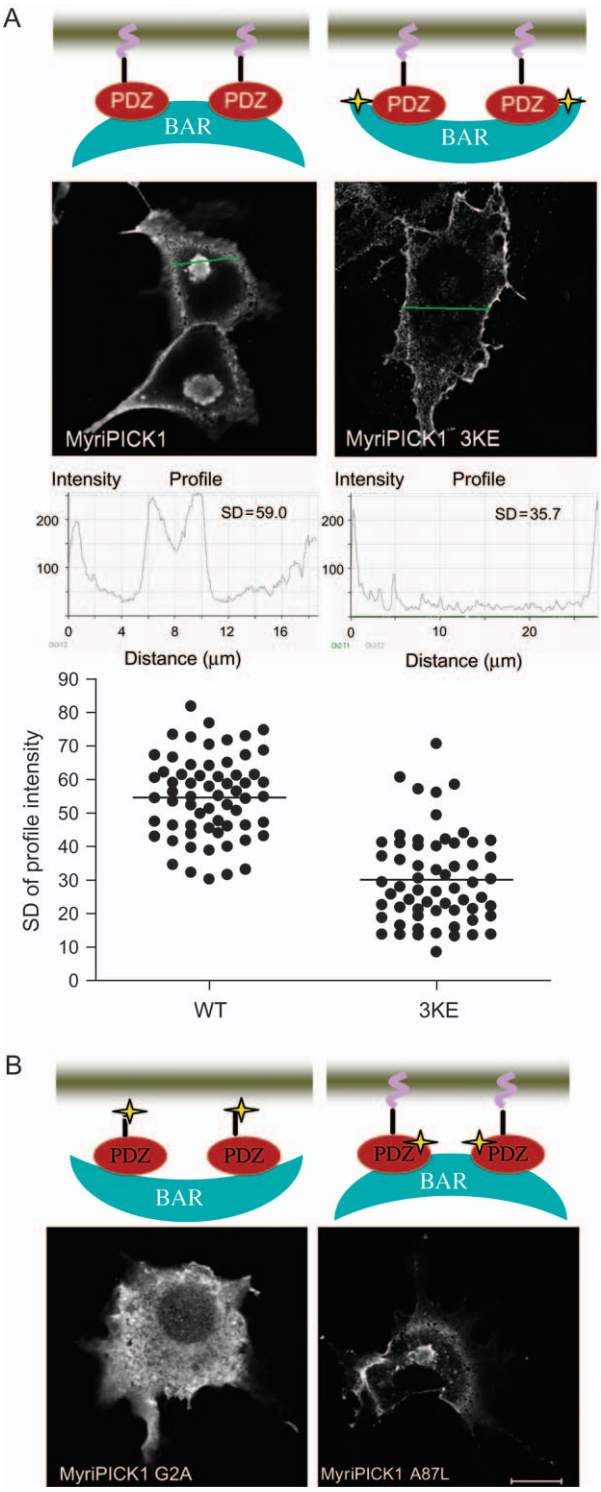


**Figure 8: Evidence for BAR domain activation in PICK1 by membrane localization.** A) COS-7 cells were transiently transfected with PICK1 containing an artificial N-terminal myristoylation site (MyriPICK1) (top left panels) or MyriPICK1 3KE to disrupt the function of the BAR domain (top right panels). The constructs are schematically illustrated above the confocal microscopy pictures of representative cells. The clustering was quantified by determining the standard deviation (SD) of a line scan through the cells as a measure of clustering. Representative line scan along indicated green line is shown below the confocal pictures. The SD for the shown scans were 59.0 for MyriPICK1 and 35.7 for MyriPICK1 3KE. The SD values for 64 cells expressing MyriPICK1 and for 63 cells expressing myriPICK1 3KE are indicated in the lower panel. Mean SD was 54.7 ± 1.5 for myriPICK1 and 30.1 ± 1.7 for myriPICK1 3KE. These values were significantly different ($p < 0.0001$, unpaired *t*-test). B) COS-7 cells expressing MyriPICK1 G2A to prevent myristoylation (left panel) or MyriPICK1 A87L to prevent ligand binding to the PDZ domain (right panel). The mutations are schematically illustrated above the images. Cells were fixed, permeabilized and stained with a C-terminal PICK1 antibody for confocal microscopy. White bar = 10 μm. The PDZ domain is shown in red and the BAR domain in blue. The black bar illustrates the artificial myristoylation sequence, whereas the purple tilde illustrates the myristoyl chain. The stars indicate where mutations are introduced, and the orientation of the BAR domain relative to the PDZ domain suggests whether the BAR domain is activated or not.

study, heterologous expression of the PICK1 BAR domain results in a characteristic clustering that is likely to reflect the vesicle-binding capacity of this type of domain. This juxtanuclear clustering strongly resembles the localization observed for full-length endogenous ICA69 – a closely related BAR domain protein (23).

In a recent study, a series of PICK1 truncation mutants were analysed in an *in vitro* membrane vesicle-binding assay (36). The data suggested that N-terminal deletions decreased vesicle binding, which is in disagreement with both our cellular confocal microscopy data and our data obtained in the cellular fractionation assay. To address this discrepancy, we performed a series of experiments in which we employed a vesicle-binding assay similar to that of Jin et al. (36) using purified PICK1 (Figure S1). In contrast to Jin et al., but in full agreement with our other data, we observed a marked increase in liposome binding upon truncation of the N-terminal PDZ domain (Δ1–135 PICK1). In further agreement with our hypothesis, we did not observe any effect on vesicle binding upon incubation with a peptide ligand (GluR2) (Figure S1). Moreover, we find it reasonable to emphasize that our findings in the vesicle-binding assay are consistent with the results from both our confocal microscopy assays and our cellular fractionation assay. Additionally, the findings by Jin et al. on the PICK1 truncation mutants were not supported by parallel experiments in a cellular system (36).

We have no explanation for the apparent discrepancy between our vesicle-binding data and those of Jin et al. (36). One possibility is that it relates to putative weaknesses and variability of the assay because of the rather high protein concentrations required to perform it; hence, we have reasons to believe based on preliminary experiments that purified PICK1 and Δ1–135 PICK1 are capable not only of binding but also of disrupting liposomes at the concentrations used in the assay (unpublished data). This might affect the results obtained with different PICK1 constructs and thereby potentially contribute to

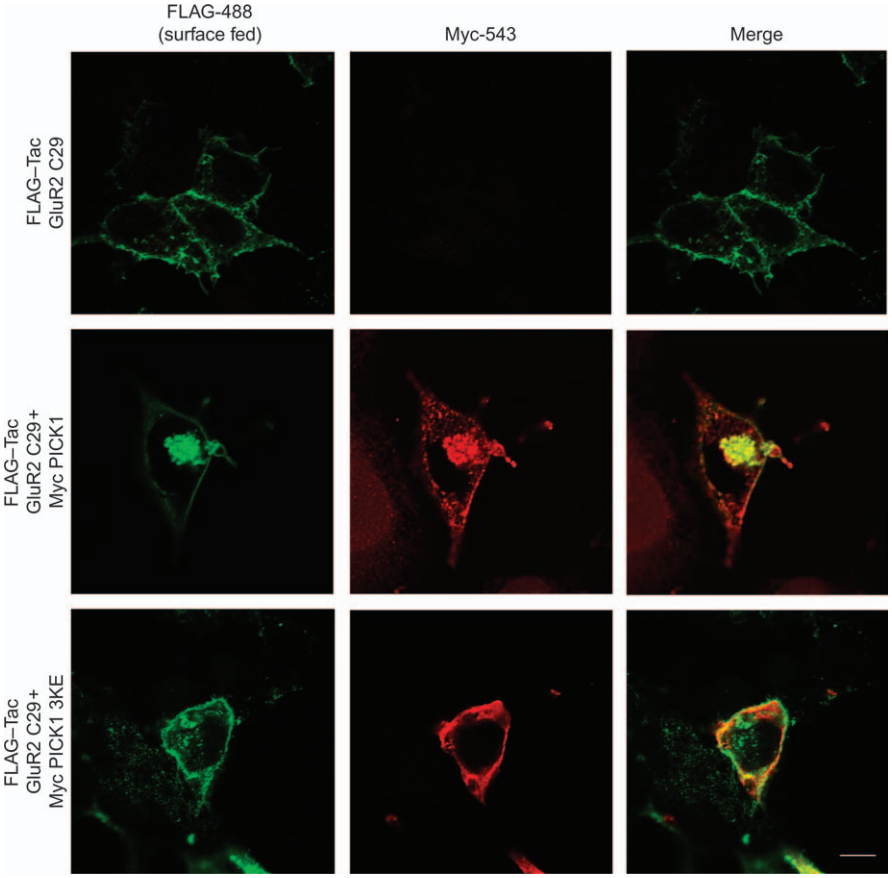


**Figure 9: The transmembrane ligand for PICK1 that coclusters with PICK1 intracellularly originates from the plasma membrane.** Feeding experiments were performed by incubating cells with FLAG-M1 antibody in DMEM for 90 min at 37°C before fixing, permeabilization and staining. FLAG–TacGluR2 C29 transiently expressed with mycPICK1 wt; right column shows the merged pictures. The data shown are representative of four similar experiments.

the discrepancy. It is also possible that, although we both used 100 nm lipid vesicles derived from the brain, even minor differences in the method of preparation could potentially impact the results of the experiments and contribute to differences. An interesting difference between our procedure and that of Jin et al. is that their constructs had glutathione S-transferase (GST) fused to the N-termini of PICK1 and the PICK1 mutants when analysed in the assay, whereas we enzymatically removed the GST before performing the experiments. It is possible that this difference also might affect the results of the experiments.

We were able to cause juxtanuclear clustering of PICK1 not only by deletion of the PDZ domain but also by discrete deletion of a short putative α-helical segment in the linker. This suggests that the linker may also play a critical role in negative regulation of BAR domain activity. The somewhat more pronounced juxtanuclear clustering observed in Δ1–135 PICK1 compared with that of the Δ1–101-PICK1 construct that contains the linker provides additional support for such a functional role. However, it is intriguing to consider as well the data in the context of the suggested direct interaction between the PDZ domain and the BAR domain that was proposed to negatively regulate BAR domain activity (22). Hence, it could be envisioned that the linker is critical for appropriate positioning of the PDZ domains relative to the BAR domain. Notably, in this case, the role of the linker is not a mere consequence of its length because only deletion of the putative α-helical segment (residues 113–121), and not of residues 125–135, resulted in cellular redistribution of the protein.

Initially, we hypothesized that simple ligand binding to the PICK1 PDZ domain was capable of triggering BAR domain activation through conformational changes. Nevertheless, we did not see any sign of BAR domain activation when the interaction took place in the cytosol, that is, when the 29 C-terminal residues of GluR2 were fused to eCFP and coexpressed with PICK1. Conversely, simple membrane recruitment of PICK1 by introduction of an N-terminal myristoyl signal redistributed PICK1 in a BAR domain-dependent manner, suggestive of BAR domain activation. These findings indicate that unmasking of the lipid-binding capacity is not directly elicited by the PDZ ligand but dependent on recruitment of PICK1 to selected membrane compartments.

Certain proteins [e.g. sorting nexin-1 (SNX-1), oligophrenin and centaurin] contain, in addition to a BAR domain, yet another phospholipid-binding domain, such as a pleckstrin homology or a Phox homology (PX) domain (19,37). For SNX-1, mutagenesis studies have shown that the BAR and

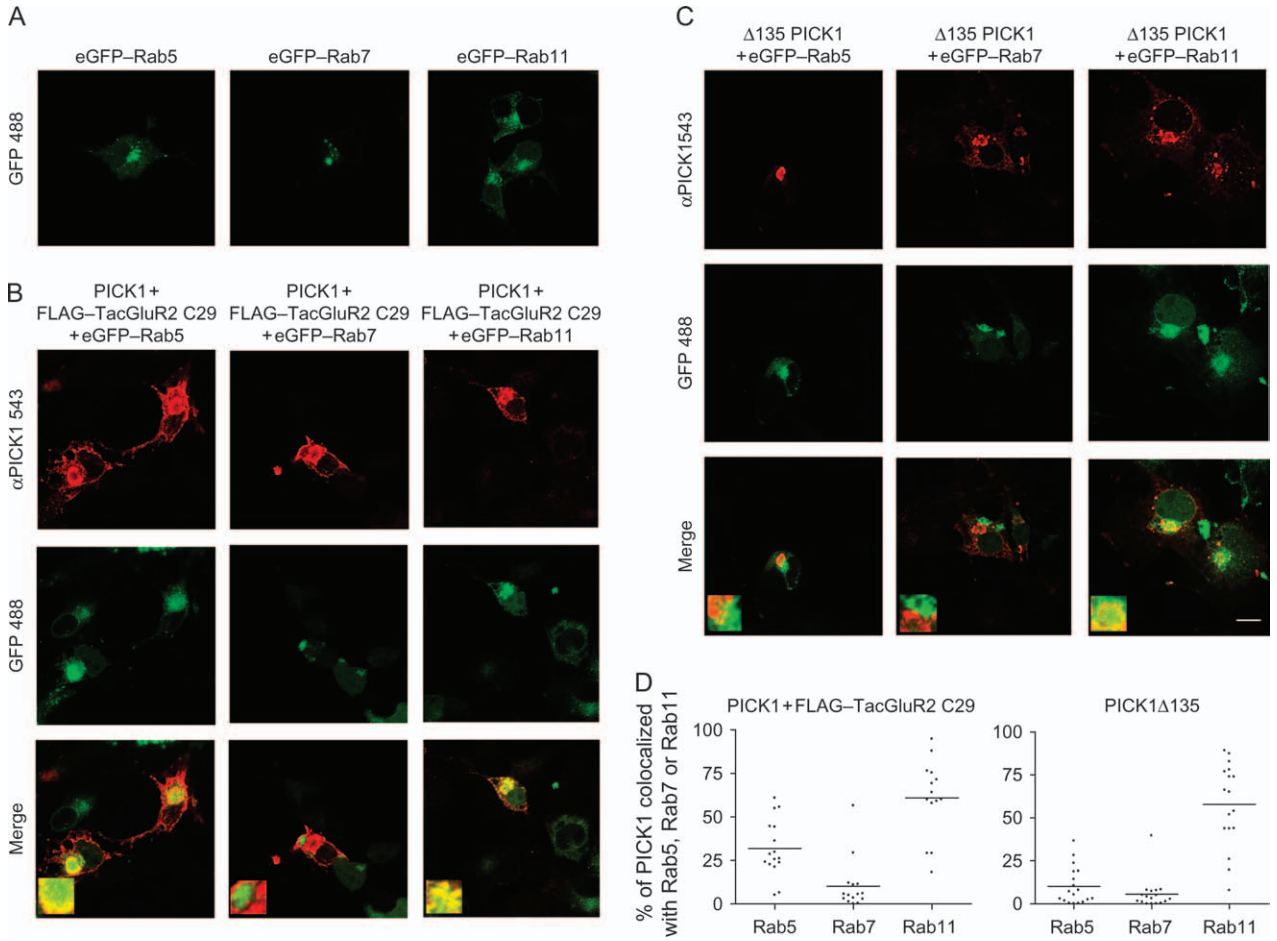


**Figure 10: The juxtanuclear PICK1-positive clusters colocalize primarily with eGFP–Rab11.** A) eGFP-tagged Rab5, Rab7 or Rab11 expressed in COS7 cells as indicated. Cells were fixed before visualization by confocal microscopy. eGFP–Rabs are visualized by eGFP fluorescence. B) Coexpression in COS7 cells of mycPICK1 and FLAG–TacGluR2 C29 with eGFP-tagged Rab5, Rab7 or Rab11 as indicated. Cells were fixed, permeabilized and stained with anti-myc antibody before visualization by confocal microscopy. Staining for mycPICK1 is shown in red (upper row), and eGFP fluorescence is shown in green (middle row). The merged pictures are shown in the lower row. C) Coexpression in COS7 cells of mycPICK1 Δ1–135 with eGFP-tagged Rab5, Rab7 or Rab11 as indicated. Cells were fixed, permeabilized and stained with anti-myc antibody before visualization by confocal microscopy. Staining for mycPICK1 Δ1–135 is shown in red (upper row), and eGFP fluorescence is shown in green (middle row). The merged pictures are shown in the lower row. D) Quantification of colocalization between PICK1 and indicated Rab proteins. The data show percentage of colocalization with data points plotted for all tested cells (a total of >15 cells from three independent experiments for each of the Rab proteins). The quantification was performed according to previously published procedures (46,47).

the PX domains alone were incapable of mediating lipid membrane association. Thus, membrane association required the combined presence of the BAR domain and the intact PX domain (38). This suggests a 'coincidence detection' mechanism in which membrane curvature recognition by the BAR domain coincides with recognition of lipid composition, for example, phosphatidylinositol bisphosphate by the PX domains. Such coincidence detection would be expected to play a critical role in achieving a more precise localization to a given membrane microenvironment with defined curvature and defined lipid composition (20). We note the possibility that while the situation in PICK1 is somewhat different, the mechanism may be analogous. Thus, in PICK1, the BAR domain coexists with a PDZ domain that by virtue of its binding to the C-termini of integral membrane proteins is likely to be brought near the membrane. This would suggest that the PDZ domain may work in conjunction with the BAR domain to ensure localization of the protein complex to the proper microenvironment determined by (i) putative targeting signals inherent to the binding partner of the PDZ domain and (ii) the ability of the BAR domain to recognize specific membrane curvatures. Note, however, that PICK1 differs from SNX by the ability of the BAR domain by itself to mediate lipid membrane binding (19,21,36). Unlike a membrane-binding protein, any uncontrolled binding of the BAR domain is prevented by negative regulation in the full-length molecule. Consequently, it is tempting to

propose for PICK1 a mechanism in which initial recruitment to a specific membrane compartment by the PDZ ligand leads to subsequent unmasking of the BAR domain activity. This unmasking would be facilitated by the avidity generated by the mere proximity of the PICK1 molecule to a lipid membrane and occur when an optimal membrane curvature is available.

Of interest, a recent study has suggested a lipid-binding capacity also for the PDZ domain (24). Specifically, mutation of a 'Cys-Pro-Cys' motif in the PDZ domain diminished coclustering of PICK1 with GluR2 in transfected cells. It is tempting to speculate that this lipid-binding capacity of the PDZ domain might operate in conjunction with that of the activated BAR domain, thereby further enhancing the avidity of the interaction.

It is important, nevertheless, also to note that unmasking of the phospholipid-binding capacity of the BAR domain might involve as well an as yet unknown membrane-localized protein. For example, the BAR domain of arfaptin2, which has the highest homology to the PICK1 BAR domain, was crystallized with a small GTPase in the concavity (39). Additional experiments are required in the future to address these questions; however, the present data clearly support the importance of negatively regulated BAR domain in PICK1 that both might prevent improper BAR domain activity and ensure tight spatial and temporal control of PICK1 function in relation to its interaction partners in the endocytic pathway.

Interestingly, antibody-feeding experiments suggested that transmembrane PDZ ligands coexpressed with PICK1 were internalized from the cell surface to the juxtanuclear clusters within a time frame of $<$90 min in a BAR domain-dependent manner. This supports the notion that the clusters are not static, but highly dynamic entities, and is consistent with a role of PICK1 in regulating trafficking of its transmembrane interaction partners, for example by promoting formation of an intracellular pool of such partners – a possibility that is particularly relevant for the AMPA receptors (9,10,14). A possible weakness of the data could be that the observed clusters represent an artefact resulting from overexpression of PICK1 and that their formation results in general trafficking defects in the cells. To exclude this possibility, we tested internalization and recycling of FLAG-tagged β2 adrenergic receptor in COS7 cells expressing PICK1 Δ135 or PICK1 and GluR2. Our assay followed the principles described by Gage et al. (40) except that we estimated surface expression by enzyme-linked immunosorbent assay instead of by flow cytometry. Importantly, we were unable to detect any significant changes in agonist-induced internalization and subsequent recycling of the receptor when comparing cells expressing the receptor alone and cells expressing the receptor together with either PICK1 Δ135 or PICK1 and GluR2 (data not shown). Thus, PICK1 overexpression together with ligand or overexpression of truncated PICK1 does not cause general trafficking defects despite formation of clusters.

Of further interest is the result of coexpression with eGFP-tagged Rab GTPases, which revealed marked colocalization of the juxtanuclear clusters especially with eGFP–Rab11, and for the FLAG–TacGluR2/PICK1 clusters also with Rab5. Rab5 and Rab11 are associated with early and recycling endosomes, respectively (33–35), and clustered PICK1 has previously been shown to colocalize with Rab5 (41). It is accordingly tempting to suggest that PICK1 associates with its interaction partners during the early stages of the endocytic process conceivably through the combined avidity of the PDZ domain interaction and membrane recognition by the BAR domain. It might even be speculated that the BAR domain is capable of recognizing the high curvature membranes generated during vesicle budding. Given that clustered Δ1–135 PICK1 showed colocalization only with Rab11-positive compartments, it is furthermore tantalizing to propose a role of PICK1 and its BAR domain in the sorting and recycling stages of the endocytic pathways rather than directly in the endocytosis process. This could involve sorting between distinct pathways as suggested for another BAR domain-containing protein, SNX1 (38), or retention of the PDZ domain interaction partner by delaying its recycling as recently suggested for the AMPA receptor (17). Future experimental efforts are required to further address this important issue.

## Materials and Methods

### *Molecular biology*

MycPICK1, mycPICK1 Δ1–101 and mycPICK1 Δ1–135 were amplified by polymerase chain reaction (PCR) of the complementary DNA (cDNA) encoding mPICK1 and inserted into the pCMV vector. The 2KE (K266E and K268E) and 3KE (K251E, K252E and K257E) mutants were made using two-step PCR. The deletions PICK1 Δ112–120 and PICK1 Δ124–134 were generated by using the Quick-Change® strategy (Stratagene). To generate eYFP–PICK1, the cDNA encoding PICK1 was fused at its 5′-end to eYFP in peYFP-C1 (Clontech) by subcloning the entire encoding sequence of rat PICK1 (rPICK1) from eGFP rPICK1 (a kind gift from Dr K. Dev, Switzerland). The eYFP–PICK1 Δ1–101 and eYFP–PICK1 Δ1–135 constructs as well as the corresponding 3KE constructs were obtained by amplification from mycPICK1 and mycPICK1 3KE and ligation into the peYFP-C1 vector. The cDNA encoding Tac was subcloned from a modified pCDM8 vector (kind gift from Dr M. D. Ehlers, North Carolina) into the mammalian expression vector pcDNA3 (Invitrogen). A *Hin*dIII site was removed from pcDNA3, and an N-terminal FLAG tag was introduced downstream from the predicted N-terminal signal sequence of Tac using two-step PCR resulting in pcDNA FLAG-tac. The DNA sequence encoding the C-terminal 50 and 29 residues of hGluR2 as well as the 24 C-terminal residues of the human dopamine transporter were amplified by PCR and ligated in-frame into 3′ of pcDNA FLAG-Tac. To generate eCFP–GluR2 C29, the *Hin*dIII/*Xba*I fragment from FLAG–TacGluR2 C29 was subcloned into peCFP-C1 (Clontech). A C-terminal alanine was introduced using an antisense primer encoding the alanine preceding the stop codon. The peCFP-C1 and peYFP-C1 vectors were used for expressing eCFP and eYFP, respectively, as well as a covalent fusion of the two previously described (42). An N-terminal myristoylation site was introduced into PICK1 (MyriPICK1) using an N-terminal primer encoding the 17 N-terminal residues from chicken c-myc

(43) and a C-terminal primer to amplify mPICK1 (2–416). The PCR product was ligated into pcDNA3.1. MyriPICK1 G2A, 3KE and A87L were made by conventional site-directed mutagenesis. The MycGluR2 was a kind gift from Jonathan Hanley, MRC, Bristol, UK. The eGFP-tagged Rab constructs (pEGFP-C1 Rab5, pEGFP-C1 Rab7, pEGFP-C1 Rab9 and pEGFP-C1 Rab11) were a kind gift from Dr Juan Bonifacino, National Institute of Child Health and Human Development, National Institutes of Health, Bethesda, MD, USA.

### Cell culture

COS-7 and 1Rb27AN3 cells were maintained in DMEM 1965 with Glutamax (L-alanyl-L-glutamine) containing 10% foetal calf serum and 0.01 mg/mL gentamicin (Invitrogen) at 37°C in a humified 5% $CO_2$ atmosphere. Cells were transfected using Lipofectamine 2000 (Invitrogen) and used for experiments after 2 days.

### Preparation and transfection of hippocampal neurons

Hippocampal neurons were prepared from embryonic day (E) 19 Wistar rat embryos as described (44). In short, after a pregnant rat was sacrificed, the hippocampal tissue of the foetuses was dissected in ice-cold modified Krebs–Ringer solution and cleared of blood vessels and meninges. The neurons were crudely homogenized by chopping before trypsin treatment and then washed in the presence of soybean trypsin inhibitor and DNAse 1 (both from Sigma) before plating in Neurobasal medium supplemented with 2% (v/v) B27, 0.4% (w/v) BSA, 20 mM HEPES, 1% (v/v) glutamax, 100 U/mL penicillin and 100 g/mL streptomycin (Invitrogen) (45). Neurons were seeded at a density of 100 000 cells/$cm^2$ in two-well Lab-Tek tissue culture chambers with a growth surface of Permanox plastic (NUNC). For transfection, the neurons were electroporated before plating using a Nucleofector device and a Rat Neuron Nucleofector Kit (Amaxa Inc.) according to the manufacturer's recommendations using program G-13.

### Immunocytochemistry and confocal microscopy

The cells were washed two times in PBS, fixed in 4% paraformaldehyde for 20 min, washed 3× in PBS and permeabilized by incubation for 20 min in PBS containing 5% goat serum and 0.1% Triton-X-100. Primary antibodies rabbit anti-myc 1:1000 (Upstate), mouse anti-haemagglutinin 1:1000 (Nordic Biosite AB), mouse anti-FLAG-M1 1:1000 (Sigma) or chicken anti-PICK1 1:500 (a kind gift from Paul Rosenberg) were added for 1 h followed by incubation with Alexa-conjugated secondary antibodies (1:500) (Molecular Probes) for 30 min prior to mounting. In antibody feeding experiments, M1 anti-FLAG antibody (1:5000) was added to prewarmed serum-free medium and incubated for 90 min at 37°C to allow internalization. The staining procedure was performed as described above except that the primary anti-FLAG antibody was left out from the staining procedure. The stained cells were visualized using a Zeiss LSM 510 confocal laser-scanning microscope using an oil immersion ×63 objective. The Alexa Fluor 488 dye and eYFP were excited with the 488 nm laser line from an argon–krypton laser, and the emitted light was detected using a 505–550 nm bandpass filter, whereas the Alexa Fluor 568 dye was excited at 543 nm with a helium–neon laser, and the emitted light was detected using a 585 nm long-pass filter. The resulting images were combined using IMAGEJ software. Quantification of intracellular clustering of transfected constructs was performed by determining the standard deviation of the pixel intensity of a profile through individual cells (avoiding the nucleus). The profiles were generated using the Zeiss LSM software. Quantification of colocalization with eGPP-tagged Rab5, Rab7 and Rab11 was done using the RG2B colocalization plug-in to IMAGEJ (Rasband W. S., ImageJ, U. S. National Institutes of Health, Bethesda, MD, USA, http://rsb.info.nih.gov/ij/, 1997–2006) as described (46,47). Single cells were defined as regions of interest to avoid noise from untransfected cells and non-specific staining. A minimum threshold pixel intensity of 100 was set for each channel in the 8-bit pictures to focus on clustering, and the minimum ratio for pixel intensity between the two channels was set to 0.5. Results are displayed as percent colocalization as determined by dividing the area of colocalization pixels by the total area over the threshold of the 543 channel reporting PICK1 localization. About 15–16 cells were used for quantification in each condition.

### Molecular modelling

A secondary structure prediction for the PICK1 protein was made using JPRED, a consensus secondary structure prediction server (48). The homology model of a monomer of the PICK1 wt BAR domain (N146–N346) was constructed with MODELLER 8.1 (49) using the sequences and structures of arfaptin2 (1I49), amphiphysin (1URU) and endophilin (1ZWW). An initial model of the PICK1 dimer complex was then obtained by alignment of the monomer on the arfaptin dimer. For refinement, this dimer structure was subjected to a Monte Carlo-minimization scheme in ROSETTADOCK where one of the monomers underwent rigid body displacements, while the side-chain orientations from both monomers were simultaneously optimized (50). The lowest energy structure was then saved as the final dimer complex model. The mutant constructs were obtained by residue replacement and application of SCRWL 3.0, a fast side-chain conformation prediction program (51). The electrostatic potential surfaces were calculated with the program GRASP (52) using the linear Poisson–Boltzmann equation and a probe radius of 2.0 Å.

### Cellular fractionation and western blotting

Cells were fractionated into cytosolic and particulate fractions as previously described with slight modifications (53). Briefly, $1 \times 10^6$ transiently transfected COS7 cells were lysed using 1 mL of hypotonic lysis buffer [20 mM Tris–HCl (pH 7.4), 10 mM potassium acetate, 1.5 mM $MgCl_2$ and protease inhibitor cocktail (Roche)] and douncing (35 strokes). Cell debris and nuclei were pelleted by centrifugation (16 100 × ***g*** for 20 min). The supernatants (the cytosolic fractions) were removed, and the pellet was resuspended in 1.0 mL of the hypotonic buffer described above containing 1% Nonidet P-40 and rotated for 1.5 h at 4°C. The solubilisates were centrifuged 16 100 × ***g*** for 20 min and supernatants (particulate fraction) removed. Equal volumes of cytosolic and particulate fractions were subjected to SDS–PAGE and immunoblotting using primary mouse anti-myc antibody (1:1000) (Sigma) and a secondary horseradish peroxidase (HRP)-conjugated goat α mouse antibody (Pierce). For immunoblotting of Tac–GluR2 and eCFP–GluR2, we used a primary antibody directed towards the 20 C-terminal residues of GluR2 (Santa Cruz) and a secondary HRP-conjugated donkey α goat antibody (Pierce). Quantification was done using QUANTITY ONE (Bio Rad) and GRAPHPAD PRISM 4 (Graphpad Software) for data treatment.

### Coimmunoprecipitations

Lysates from COS7 cells transiently expressing eCFP–GluR2 C29, eCFP–GluR2 C29 + Ala and eYFP–PICK1 alone or in combination were prepared in tris buffered salt (TBS) containing 1% (v/v) Triton-X-100, 5 mM n-ethylmaleimide and a protease inhibitor cocktail (Roche Diagnostics). After 30 min of solubilization, insoluble material was removed by centrifugation at 16 000 × ***g*** for 10 min, and the supernatant (100 μg protein) was diluted to 0.5 mL and precleared for 1 h with 25 μL protein G–agarose (Roche Diagnostics) at 4°C during constant rotation. The supernatant was incubated with rabbit green fluorescent protein antibody (Abcam) for 1 h at 4°C during constant rotation. As controls, samples with only one construct or without antibody were performed in parallel. The mixtures were subsequently centrifuged at 16 000 × ***g*** for 10 min to remove any precipitates before incubation with 25 μL protein A–agarose (Roche Diagnostics) for 60 min at 4°C. The beads were washed three times with TBS containing 0.1% (v/v) Triton-X-100. The bound material was eluted by addition of loading buffer and separated by SDS–PAGE. Precipitated mycPICK1 was detected by immunoblotting using mouse Myc antibody (9E10; Sigma).

### Fluorescence resonance energy transfer

FRET (54) was measured with an epifluorescence microscope (Carl Zeiss TM210) using the 'three-filter method' according to Xia and Liu (55). COS7 cells ($3 \times 10^5$ cells/well) were seeded on to poly-D-lysine-coated glass coverslips (24 mm diameter). Cells were transiently transfected using the calcium phosphate precipitation method. The next day, media were replaced by Krebs–HBS buffer (10 mM HEPES, 120 mM NaCl, 3 mM KCl, 2 mM $CaCl_2$ and 2 mM $MgCl_2$), and images were taken using a ×63 oil objective and a Ludl filter wheel that allows for rapid exchange of filters (less than 100 milliseconds). The system was equipped with the following fluorescence filters: CFP filter ($I_{CFP}$; excitation: 436 nm, dichroic mirror:

455 nm and emission: 480 nm), YFP filter ($I_{YFP}$; excitation: 500 nm, dichroic mirror: 515 nm and emission: 535 nm) and FRET filter ($I_{FRET}$: excitation = 436 nm, dichroic mirror = 455 nm and emission = 535 nm). The acquisition of the images was done with METAMORPH (Meta Imaging; Universal Imaging Corporation, version 4.6). Background fluorescence was subtracted from all images, and fluorescence intensity was measured in cytosolic regions in all images. To calculate a normalized FRET signal ($N_{FRET}$), we used the following equation:

$$N_{FRET} = \frac{I_{FRET} - a \times I_{YFP} - b \times I_{CFP}}{\sqrt{I_{YFP} \times I_{CFP}}},$$

where *a* and *b* represents the bleed-through values for YFP and CFP, respectively.

## Acknowledgments

This study was supported in part by the National Institute of Health grant P01 DA 12408 (U. G. and H. W.), the Lundbeck Foundation (U. G.), the AP Møller Foundation and the Novo Nordic Foundation (U. G.). We thank Donna Czerny for excellent technical assistance. We thank Dr Paul Rosenberg for providing the chicken anti-PICK1 antibody.

## Supplementary Materials

### *Supplementary Materials and Methods*

Protein purification (19)

Liposome pull-down assay

**Figure S1: Liposome pull down of PICK1.** A) Representative liposome pull-down assay showing stronger pelleting of PICK1 Δ135 than of PICK wt. Both constructs show some unspecific pelleting. B) Quantification of the specific pull down from six independent experiments. C) Representative experiment showing the effect of four different peptides on the PICK1 pull down. Peptides are used in a concentration where they have been shown to bind more than 90% of the PICK1 protein. P, pellet; S, supernatant.

Supplemental materials are available as part of the online article at http://www.blackwell-synergy.com

## References

1. Dev KK. PDZ domain protein-protein interactions: a case study with PICK1. Curr Top Med Chem 2007;7:3–20.
2. Staudinger J, Zhou J, Burgess R, Elledge SJ, Olson EN. PICK1: a perinuclear binding protein and substrate for protein kinase C isolated by the yeast two-hybrid system.J Cell Biol 1995;128: 263–271.
3. Madsen KL, Beuming T, Niv MY, Chang CW, Dev KK, Weinstein H, Gether U. Molecular determinants for the complex binding specificity of the PDZ domain in PICK1. J Biol Chem 2005;280:20539–20548.
4. Beuming T, Skrabanek L, Niv MY, Mukherjee P, Weinstein H. PDZBase: a protein-protein interaction database for PDZ-domains. Bioinformatics 2005;21:827–828.
5. Xia J, Zhang X, Staudinger J, Huganir RL. Clustering of AMPA receptors by the synaptic PDZ domain-containing protein PICK1. Neuron 1999; 22:179–187.
6. Dev KK, Nakajima Y, Kitano J, Braithwaite SP, Henley JM, Nakanishi S. PICK1 interacts with and regulates PKC phosphorylation of mGLUR7. J Neurosci 2000;20:7252–7257.
7. Torres GE, Yao WD, Mohn AR, Quan H, Kim KM, Levey AI, Staudinger J, Caron MG. Functional interaction between monoamine plasma membrane transporters and the synaptic PDZ domain-containing protein PICK1. Neuron 2001;30:121–134.
8. Dev KK, Henley JM. The schizophrenic faces of PICK1. Trends Pharmacol Sci 2006;27:574–579.
9. Daw MI, Chittajallu R, Bortolotto ZA, Dev KK, Duprat F, Henley JM, Collingridge GL, Isaac JT. PDZ proteins interacting with C-terminal GluR2/3 are involved in a PKC-dependent regulation of AMPA receptors at hippocampal synapses. Neuron 2000;28:873–886.
10. Xia J, Chung HJ, Wihler C, Huganir RL, Linden DJ. Cerebellar long-term depression requires PKC-regulated interactions between GluR2/3 and PDZ domain-containing proteins. Neuron 2000;28:499–510.
11. Gardner SM, Takamiya K, Xia J, Suh JG, Johnson R, Yu S, Huganir RL. Calcium-permeable AMPA receptor plasticity is mediated by subunit-specific interactions with PICK1 and NSF. Neuron 2005;45: 903–915.
12. Garry EM, Moss A, Rosie R, Delaney A, Mitchell R, Fleetwood-Walker SM. Specific involvement in neuropathic pain of AMPA receptors and adapter proteins for the GluR2 subunit. Mol Cell Neurosci 2003;24:10–22.
13. Bellone C, Luscher C. Cocaine triggered AMPA receptor redistribution is reversed in vivo by mGluR-dependent long-term depression. Nat Neurosci 2006;9:636–641.
14. Hanley JG, Henley JM. PICK1 is a calcium-sensor for NMDA-induced AMPA receptor trafficking. EMBO J 2005;24:3266–3278.
15. Perez JL, Khatri L, Chang C, Srivastava S, Osten P, Ziff EB. PICK1 targets activated protein kinase Calpha to AMPA receptor clusters in spines of hippocampal neurons and reduces surface levels of the AMPA-type glutamate receptor subunit 2. J Neurosci 2001;21:5417–5428.
16. Baron A, Deval E, Salinas M, Lingueglia E, Voilley N, Lazdunski M. Protein kinase C stimulates the acid-sensing ion channel ASIC2a via the PDZ domain-containing protein PICK1. J Biol Chem 2002;277:50463–50468.
17. Lin DT, Huganir RL. PICK1 and phosphorylation of the glutamate receptor 2 (GluR2) AMPA receptor subunit regulates GluR2 recycling after NMDA receptor-induced internalization. J Neurosci 2007;27: 13903–13908.
18. Bjerggaard C, Fog J, Hastrup H, Madsen K, Javitch JA, Gether U. Surface targeting of the dopamine transporter involves discrete epitopes in the distal carboxy terminus but occurs independently of canonical PDZ domain interactions. J Neurosci 2004;24:7024–7036.
19. Peter BJ, Kent HM, Mills IG, Vallis Y, Butler PJ, Evans PR, McMahon HT. BAR domains as sensors of membrane curvature: the amphiphysin BAR structure. Science 2004;303:495–499.
20. McMahon HT, Gallop JL. Membrane curvature and mechanisms of dynamic cell membrane remodelling. Nature 2005;438:590–596.
21. Steinberg JP, Takamiya K, Shen Y, Xia J, Rubio ME, Yu S, Jin W, Thomas GM, Linden DJ, Huganir RL. Targeted in vivo mutations of the AMPA receptor subunit GluR2 and its interacting protein PICK1 eliminate cerebellar long-term depression. Neuron 2006;49: 845–860.
22. Lu W, Ziff EB. PICK1 interacts with ABP/GRIP to regulate AMPA receptor trafficking. Neuron 2005;47:407–421.
23. Spitzenberger F, Pietropaolo S, Verkade P, Habermann B, Lacas-Gervais S, Mziaut H, Pietropaolo M, Solimena M. Islet cell autoantigen of 69 kDa is an arfaptin-related protein associated with the Golgi complex of insulinoma INS-1 cells. J Biol Chem 2003;278:26166–26173.
24. Pan L, Wu H, Shen C, Shi Y, Jin W, Xia J, Zhang M. Clustering and synaptic targeting of PICK1 requires direct interaction between the PDZ domain and lipid membranes. EMBO J 2007;26:4576–4587.

25. Clarkson ED, Rosa FG, Edwards-Prasad J, Weiland DA, Witta SE, Freed CR, Prasad KN. Improvement of neurological deficits in 6-hydroxydopamine-lesioned rats after transplantation with allogeneic simian virus 40 large tumor antigen gene-induced immortalized dopamine cells. Proc Natl Acad Sci U S A 1998;95:1265–1270.
26. Torres R, Firestein BL, Dong H, Staudinger J, Olson EN, Huganir RL, Bredt DS, Gale NW, Yancopoulos GD. PDZ proteins bind, cluster, and synaptically colocalize with Eph receptors and their ephrin ligands. Neuron 1998;21:1453–1463.
27. Dev KK, Nishimune A, Henley JM, Nakanishi S. The protein kinase C alpha binding protein PICK1 interacts with short but not long form alternative splice variants of AMPA receptor subunits. Neuropharmacology 1999;38:635–644.
28. Scott DB, Blanpied TA, Swanson GT, Zhang C, Ehlers MD. An NMDA receptor ER retention signal regulated by phosphorylation and alternative splicing. J Neurosci 2001;21:3063–3072.
29. Loder MK, Melikian HE. The dopamine transporter constitutively internalizes and recycles in a protein kinase C-regulated manner in stably transfected PC12 cell lines. J Biol Chem 2003;278:22168–22174.
30. Hanley JG, Khatri L, Hanson PI, Ziff EB. NSF ATPase and alpha-/beta-SNAPs disassemble the AMPA receptor-PICK1 complex. Neuron 2002;34:53–67.
31. Pines J. GFP in mammalian cells. Trends Genet 1995;11:326–327.
32. Farazi TA, Waksman G, Gordon JI. The biology and enzymology of protein N-myristoylation. J Biol Chem 2001;276:39501–39504.
33. Deneka M, Neeft M, van der Sluijs P. Regulation of membrane transport by rab GTPases. Crit Rev Biochem Mol Biol 2003;38:121–142.
34. Zerial M, McBride H. Rab proteins as membrane organizers. Nat Rev Mol Cell Biol 2001;2:107–117.
35. Lavezzari G, McCallum J, Dewey CM, Roche KW. Subunit-specific regulation of NMDA receptor endocytosis. J Neurosci 2004;24:6383–6391.
36. Jin W, Ge WP, Xu J, Cao M, Peng L, Yung W, Liao D, Duan S, Zhang M, Xia J. Lipid binding regulates synaptic targeting of PICK1, AMPA receptor trafficking, and synaptic plasticity. J Neurosci 2006;26:2380–2390.
37. Zhu G, Chen J, Liu J, Brunzelle JS, Huang B, Wakeham N, Terzyan S, Li X, Rao Z, Li G, Zhang XC. Structure of the APPL1 BAR-PH domain and characterization of its interaction with Rab5. EMBO J 2007;26:3484–3493.
38. Carlton J, Bujny M, Peter BJ, Oorschot VM, Rutherford A, Mellor H, Klumperman J, McMahon HT, Cullen PJ. Sorting nexin-1 mediates tubular endosome-to-TGN transport through coincidence sensing of high-curvature membranes and 3-phosphoinositides. Curr Biol 2004;14:1791–1800.
39. Tarricone C, Xiao B, Justin N, Walker PA, Rittinger K, Gamblin SJ, Smerdon SJ. The structural basis of Arfaptin-mediated cross-talk between Rac and Arf signalling pathways. Nature 2001;411:215–219.
40. Gage RM, Kim KA, Cao TT, von Zastrow M. A transplantable sorting signal that is sufficient to mediate rapid recycling of G protein-coupled receptors. J Biol Chem 2001;276:44712–44720.
41. Sossa KG, Court BL, Carroll RC. NMDA receptors mediate calcium-dependent, bidirectional changes in dendritic PICK1 clustering. Mol Cell Neurosci 2006;31:574–585.
42. Schmid JA, Scholze P, Kudlacek O, Freissmuth M, Singer EA, Sitte HH. Oligomerization of the human serotonin transporter and of the rat GABA transporter 1 visualized by fluorescence resonance energy transfer microscopy in living cells. J Biol Chem 2001;276:3805–3810.
43. Kamikura DM, Khoury H, Maroun C, Naujokas MA, Park M. Enhanced transformation by a plasma membrane-associated met oncoprotein: activation of a phosphoinositide 3′-kinase-dependent autocrine loop involving hyaluronic acid and CD44. Mol Cell Biol 2000;20:3482–3496.
44. Maar TE, Ronn LC, Bock E, Berezin V, Moran J, Pasantes-Morales H, Schousboe A. Characterization of microwell cultures of dissociated brain tissue for studies of cell-cell interactions. J Neurosci Res 1997;47:163–172.
45. Soroka V, Kolkova K, Kastrup JS, Diederichs K, Breed J, Kiselyov VV, Poulsen FM, Larsen IK, Welte W, Berezin V, Bock E, Kasper C. Structure and interactions of NCAM Ig1-2-3 suggest a novel zipper mechanism for homophilic adhesion. Structure 2003;11:1291–1301.
46. Chmelar RS, Nathanson NM. Identification of a novel apical sorting motif and mechanism of targeting of the M2 muscarinic acetylcholine receptor. J Biol Chem 2006;281:35381–35396.
47. Adkins EM, Samuvel DJ, Fog JU, Eriksen J, Jayanthi LD, Vaegter CB, Ramamoorthy S, Gether U. Membrane mobility and microdomain association of the dopamine transporter studied with fluorescence correlation spectroscopy and fluorescence recovery after photobleaching. Biochemistry 2007;46:10484–10497.
48. Cuff JA, Clamp ME, Siddiqui AS, Finlay M, Barton GJ. JPred: a consensus secondary structure prediction server. Bioinformatics 1998;14:892–893.
49. Sali A, Blundell TL. Comparative protein modelling by satisfaction of spatial restraints. J Mol Biol 1993;234:779–815.
50. Gray JJ, Moughon S, Wang C, Schueler-Furman O, Kuhlman B, Rohl CA, Baker D. Protein-protein docking with simultaneous optimization of rigid-body displacement and side-chain conformations. J Mol Biol 2003;331:281–299.
51. Canutescu AA, Shelenkov AA, Dunbrack RL Jr. A graph-theory algorithm for rapid protein side-chain prediction. Protein Sci 2003;12:2001–2014.
52. Nicholls A, Sharp KA, Honig B. Protein folding and association: insights from the interfacial and thermodynamic properties of hydrocarbons. Proteins 1991;11:281–296.
53. Han Y, Meng T, Murray NR, Fields AP, Brasier AR. Interleukin-1-induced nuclear factor-kappaB-IkappaBalpha autoregulatory feedback loop in hepatocytes. A role for protein kinase calpha in post-transcriptional regulation of ikappabalpha resynthesis. J Biol Chem 1999;274:939–947.
54. Schmid JA, Sitte HH. Fluorescence resonance energy transfer in the study of cancer pathways. Curr Opin Oncol 2003;15:55–64.
55. Xia Z, Liu Y. Reliable and global measurement of fluorescence resonance energy transfer using fluorescence microscopes. Biophys J 2001;81:2395–2402.

# Madsen et al - Supplementary Information

## *Supplementary Figure 1*

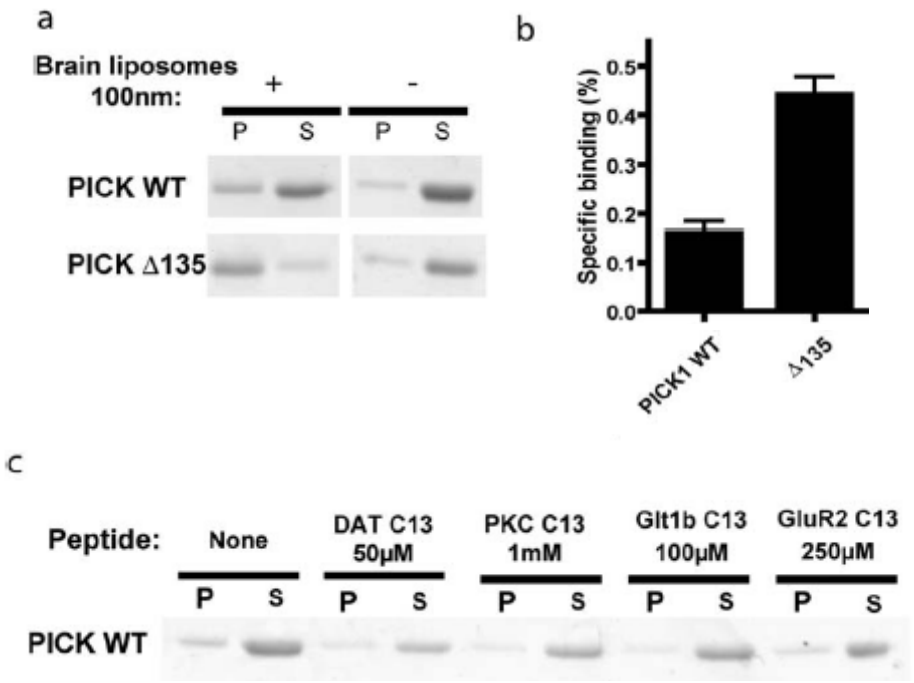


**Fig. S1: Liposome pull-down of PICK1.** (A) Representative liposome pull-down assay showing stronger pelleting of PICK1 Δ135 than of PICK wt. Both constructs show some unspecific pelleting. (B) Quantification of the specific pull down from 6 independent experiments. (C) Representative experiment showing the effect of 4 different peptides on the PICK1 pull-down. Peptides are used in a concentration where they have been shown to bind more than 90% of the PICK1 protein. (P) Pellet, (S) Supernantant.

### Supplementary Material and Methods:

***Protein purification:***

Relevant constructs were inoculated overnight in 50 ml of LB media, diluted into 1 liter of LB media, and grown to A600 1.0 (2–3 h). Expression of the fusion protein was induced with isopropyl-D-thiogalactopyranoside (100 μM) for 3 h at 30°C. Cells were harvested and frozen at -80°C until purification. The pellets were thawed and resuspended in buffer A (50 mM Tris, pH 7.4, 125 mM NaCl, 1%triton X 100, 20 μg/ml DNase I, 1 mM dithiothreitol) and 1x bacterial protease inhibitor mixture (Sigma). The lysate was frozen at -80 °C, thawed and thoroughly triturated to reduce viscosity. The lysate was clarified by centrifugation (rotor SS-34, 18,000 rpm, 48,000 x g, 30 min). The supernatant was incubated with glutathione-Sepharose beads (Amersham Biosciences AB, Uppsala, Sweden) under slow rotation for 90 min at 4 °C. The beads were

pelleted at 1,000 x g for 10 min and washed in buffer B (50 mM Tris, pH 7.4, 125 mM NaCl, 0.01% Triton X-100, 1 mM dithiothreitol) by three batch washes. The protein was separated from the GST domain by cleavage with thrombin protease (Novagen) in buffer B. The protein was eluted on ice until use (usually the same day). Samples of 25 µl were taken from the protein solution for determination of protein concentration and SDS-PAGE. Protein determination was carried out using the BCA Protein Assay Reagent kit (Pierce, Rockford, IL) according to the manufacturer's protocol using bovine serum albumin as standard. Gels were stained with GelCode Blue Stain Reagent (Pierce) to inspect size, integrity, and purity of the protein.

***Liposome Pull Down assay***

The liposome pull-down assay was performed generally as described. Briefly, protein in a final concentration of 5µM in 0.005% TX-100 was incubated with 0.6 mg/ml brain liposomes (Folch fraction I, B1502 from Sigma) extruded 10 times through 100 nm membranes in a total of 100µl for 10 minutes before sedimentation in a Beckmann Airfuge (120,000g) for 15 minutes at 4ºC. Supernatant and pellet was separated and the pellet resuspended in 100µl buffer, before the protein was subjected to SDS-PAGE, Coomassie stained and quantified using the Bio-Rad Quantity One system.

# Paper 4

# The Dopamine Transporter Impairs Dopamine D2 Receptor Surface Expression/Signalling and Reveals Promiscuous Monoamine Transporter/Receptor Interaction

**The dopamine transporter impairs dopamine D2 receptor surface expression/signalling and reveals promiscuous monoamine transporter/receptor interaction**

Jacob Eriksen*, Ib V. Klewe*, Jan Egebjerg, Kenneth V. Christensen and Ulrik Gether

* These authors contributed equally.

**Corresponding author:**

Ulrik Gether, Molecular Neuropharmacology Group

Department of Neuroscience and Pharmacology

University of Copenhagen

The Panum Instutute 18.6, Blegdamsvej 3, DK-2200 Copenhagen N, Denmark

Tel: +45 35327548

Fax: +45 35327610

E-mail: gether@sund.ku.dk

**Abstract**

The dopamine D2 receptor (D2R) is the primary target for anti-psychotic treatment. D2R is among other places expressed as an autoreceptor in dopaminergic neurons where it regulates dopamine release through a negative feedback. Previously it has been shown that D2R directly interacts with the dopamine transporter (DAT). Activation of D2R can upregulate DAT, thereby increasing cellular dopamine uptake capacity and possibly shaping locomotor activity in mice. Here we investigated the effect of DAT as a regulator of D2R signalling. We found that transient over-expression of DAT with D2R in HEK293 cells reduced surface expression of D2R while DAT surface levels remained unaffected. Furthermore ß-Arrestin2 recruitment to D2R was compromised and D2R-mediated inhibition of cAMP accumulation was reduced as a consequence of the reduced surface level expression of D2R. The effects of DAT on D2R surface expression and signalling was not unique for DAT and D2R. Thus, transient co-expression of $ß_2$AR with DAT resulted in reduced surface levels of $ß_2$AR. In addition, co-expression of the serotonin transporter with D2R appeared to modulate the ß-Arrestin2 recruitment to D2R and the D2R-mediated inhibition of cAMP accumulation in a manner similar to co-expression of DAT.

## Introduction

The pre-synaptically expressed dopamine transporter (DAT) and dopamine D2 receptor (D2R) are both expressed in the dopaminergic neurons and both serve to restrain extracellular dopamine signalling (Geracitano *et al.* 2006). Alterations in dopamine signaling is coupled to neurological and psychiatric diseases including schizophrenia, bipolar disorder, ADHD (attention-deficit hyperactivity disorder) and Parkinson's disease (Iversen and Iversen 2007).

DAT exerts its effect by transporting dopamine released to the synapse back into the presynaptic neuron – thereby restricting DA signalling and facilitating the recycling of dopamine. DAT is also the principle target for widely abused psychostimulants, such as cocaine and amphetamine. The transporter belongs to the family of $Na^+/Cl^-$ coupled neurotransmitter transporters (SLC6 gene family) that are characterized by the use of the transmembrane $Na^+$ gradient as a driving force for transport of substrate and co-transport of $Cl^-$ (Torres and Amara 2007; Gether *et al.* 2006; Chen *et al.* 2004).

In the pre-synapse the short splice variant of D2R complements DAT function by acting as a pre-synaptic autoinhibitory receptor that inhibits further dopamine release and increases re-uptake of dopamine (Lee *et al.* 2007; Usiello *et al.* 2000). DAT and D2R were recently reported to interact and that the presence of D2R increased DAT expression in the plasma membrane (Bolan *et al.* 2007; Lee *et al.* 2007). Furthermore the DAT/D2R interaction was proposed to regulate locomotor activity in mice (Lee *et al.* 2007) and recently the interaction has been suggested to be linked to schizophrenia (Lee *et al.* 2009).

It has previously been shown that D2R signalling function can be modulated by other interacting membrane proteins. Expressing D2R with the dopamine D1 receptor that in itself couples to Gs proteins results in a receptor complex that show enlarged Gq/11 mediated increase in intracellular calcium upon dopamine activation (Rashid *et al.* 2007). D2R can also directly interact with the Adenosine A2 receptor (Canals *et al.* 2003) and A2 agonist treatment of striatal membranes decreased agonist affinity for striatal D2R (Ferre *et al.* 1991). Many other GPCR's have been shown to exist in both heteromeric and homomeric complexes and some of these complexes have been shown to alter GPCR signalling (Ferre *et al.* 2007; Fuxe *et al.* 2008; Szidonya *et al.* 2008). An interaction between mGluR2 and 5-$HT_{2A}$ have been shown exist in the rodent cortex in which ligand activation of mGluR2 positively regulates agonist affinity for 5-$HT_{2A}$ while ligand activation of 5-$HT_{2A}$ negatively regulates agonist affinity for mGluR2 in the complex (Gonzalez-Maeso *et al.* 2008) - a phenomenon that may be implicated in psychosis.

In the current work we pursued to further study the interaction between D2Rs and DAT and its consequences. Since previous works have primarily focused on the effect of DAT/D2Rs co-expression on DAT function and expression, we investigated whether DAT expression had any effect on the D2Rs function and expression.

## Materials and Methods

*DNA vectors*

*Transporter constructs*: pCDNA3.1 hSERT (Rasmussen *et al.* 2009), pCDNA3 HA-DAT (Kniazeff *et al.* 2008) have previously been described. pmVenus-SERT was made inserting by hSERT coding sequence into pmVenus-C1 using XbaI and SalI. pmVenus-DAT was made by excising synDAT from the pCDNA3 synDAT vector using *KpnI* and *XbaI* and inserted into pmVenus-C1 using the same restriction enzymes. *Receptor constructs*: pCDNA3.1 sf-$\beta_2$AR was a kind gift from Dr. Mark von Zastrow, pCDNA3.1 sf-$D2_S$ was a kind gift from Jonathan Javitch and sf-$D2_S$-Rluc8 have been described previously (Klewe *et al.* 2008). sf-$\beta_2$AR-Rluc8 were constructed in an analog fashion, i.e. with the same linker sequence separating the coding region of the receptor and the coding region for Rluc8. All receptors were tagged in the N-terminal with signal flag epitope (Cao *et al.* 1999). *Other*: pCDNA3 FLAG-tagged Tac (Madsen *et al.* 2008) and β-Arrestin2(R393E, R395E)-mVenus have been described previously (Klewe *et al.* 2008). TacGlur2-mVenus has mVenus inserted between the Tac sequence and the glutamate receptor 2 C-terminus (the last 29 amino acids of GluR2) in TacGluR2 (Madsen *et al.* 2008).

All constructs have been verified by sequencing.

*Transfections*

Transfections with DNA were done with Lipofectamine 2000 (Invitrogen), according to the manufacturers protocol. The ratio of Lipofectamine 2000 to DNA ratio was 4 (µL to µg). For BRET and cAMP experiments a total of 1000 ng of DNA (where nothing else is stated) was used per 10 $cm^2$ of cells grown to 90-100% confluency at the time of transfection.

*Chemical compounds and vehicle*

All chemical compounds were synthesized by H. Lundbeck A/S, Denmark and dissolved in DMSO to a stock concentration of 10 mM. For BRET measurements compounds were diluted to the appropriate concentration in buffer composed of HBSS with $Ca^{2+}$ and $Mg^{2+}$ (Invitrogen), 0.2 µM ascorbic acid (Sigma-Aldrich) and 5 µM final concentration of coelenterazine *h* (Invitrogen). In saturation BRET experiments control buffer was identical except that 1‰ v/v DMSO (Sigma-Aldrich) was added corresponding to the DMSO carry-over in test solutions with 5 µM compound.

*BRET measurements and calculations*

β-Arrestin2 assay: 48 hours post-transfection cells were harvested by trypsination (250 µL per 10 cm2 for ~45 seconds) (Invitrogen). All subsequent steps were performed at room temperature. Cells were re-suspended in culture medium and centrifuged at 900 *g* for 3 minutes and subsequently re-suspended in HBSS with $Ca^{2+}$ and $Mg^{2+}$ to a density of approximately 100.000-200.000 cells/mL. Cells were left in suspension for 45-60 minutes before incubating with appropriated diluted quinpirole in a buffer with a final concentration of 5 µM coelenterazine h. 10-15 minutes after the addition of compounds luminescence was measured on EnVision multilabel plate reader (Perkin-Elmer, Waltham, MA, USA). Luminescence from each well was measured twice; first through a 520-550 nm band pass filter and then through a 447.5-472.5 nm bandpass-filter (Perkin-Elmer). Within each experiment measurement of each condition was done in duplicate. The BRET ratio was calculated as the long wavelength emission divided by short wave length emission and expressed as the relative change compared to vehicle treated cells (Pfleger *et al.* 2006).

BRET measurements of receptor / monoamine transporter interactions: The essay were essentially done as described above, except cells were transfected directly in 96-well plate with a total of 60 ng DNA per well. BRET donor vector amount was held constant at 3 ng DNA per well, if nothing else is indicated. Measurements were done on ~50-100.000 adherent cells per well and in triplicate.

*cAMP assay*

The receptor / monoamine transporter of interest was co-transfected with the GloSensor plasmid (Promega, Sweden) in the cDNA ratio 1:1:2.5. 48 hours post-transfection cells were harvested by gentle trypsination. Cells were re-suspended to a density of ~1.000.000 cells/mL in HBSS with $Ca^{2+}$ and $Mg^{2+}$ containing 2.5% GloSensor cAMP reagent (Promega) and equilibrated at room temperature for 2 hours. 40 µL cell suspension were mixed with 10 µL appropriately diluted quinpirole and 5 µM forskolin. Total luminescence was measured 15 minutes later on an EnVision multilabel plate reader. The relative decrease in cAMP levels were expressed as the percentage of the relative cAMP level in cells transfected alone with sf-$D2_S$ and GloSensor.

*Cell-based ELISA assay*

HEK293 cells were transfected two days prior to the experiment with equal amounts of HA-DAT/sf-$D2_S$, HA-DAT/mock, sf-$D2_S$/mock, HA-DAT/sf-$ß_2$AR, af-$ß_2$AR/mock (0.5ug/0.5ug + 3ul Lipo2000) all in the pCDNA3 vector. 24h before the experiment the cells were seeded in black 96 well plates (35,000 cells/well) coated with poly-L-ornithine (Sigma). On the day of the experiment the cells were incubated with HEPES buffer (25 mM HEPES, 130 mM NaCl, 5.4 mM KCl, 1.2 mM $CaCl_2$, 1.2 mM $MgSO_4$, 5 mM D-glucose, pH 7.4) +/- 10 µM dopamine, 10 µM amphetamine, 10 µM quinpirole, 10 µM haloperidol for 60 minutes. Then the cells were fixed in 4% paraformaldehyde in phosphate-buffered saline + calcium (PBS) for 10 minutes and subsequently blocked with 5% goat

serum in PBS for 30 minutes. The plates were either incubated with M1 (1:5000; Sigma) or HA.11 (1:1000; Covance) for 1 hour to probe FLAG-tagged receptors or HA-DAT, respectively. After 4 washes the plates were incubated with horseradish peroxidase conjugated goat anti-mouse antibody (1:1000; Pierce) for 30 minutes and again washed 4 times with PBS. Then the plates were incubated with SuperSignal ELISA Pico Chemiluminescent HRP Substrate (Pierce) for 2 minutes and then the luminescence was read using a Wallac Victor2. Background from empty cells was subtracted from raw data and receptor data is represented as percentage of receptor + mock surface expression and HA-DAT data is represented as percentage of DAT + mock surface expression or as percentage of vehicle treatment.

*Statistical analysis and modelling*

Data was analysed with GraphPad Prism 5.0 (GraphPad Software, La Jolla, CA, USA) using the statistical tests indicated in the text. Significance was set to $p < 0.05$.

## Results

*DAT effect on D2R surface expression*

First we tested whether DAT/D2R co-expression affected D2R surface expression as the surface expression of DAT has previously been shown to be modulated by the D2/DAT interaction. We used an HA-tagged DAT and a FLAG-tagged D2R in a cell based ELISA assay to simultaneously determine surface expression of both proteins in transiently co-transfected HEK293 cells (figure 1A). When co-expressing D2R with DAT a reduction in D2Rs surface expression (21% +/-1.6 of D2Rs + mock, t-test, $p < 0.001$) was observed whereas no significant change in DAT surface expression (105% +/-8.5 of HA-DAT + mock, t-test) was seen (figure 1B). To examine whether the effect of DAT was specific for the D2R we conducted a parallel experiment with FLAG-tagged $ß_2$-adrenergic receptor ($ß_2$AR). When co-expressing FLAG-tagged $ß_2$AR and HA-DAT in HEK293 cells a reduction in $ß_2$AR expression (62% +/-7.1 of $ß_2$AR + mock, t-test, $p < 0.001$) was seen compared to expression alone whereas no significant reduction in DAT expression was seen (107% +/-10 of HA-DAT + mock, t-test) (figure 1C).

*ß-Arrestin2 recruitment to D2R*

D2R affects a variety of signalling pathways including inhibition of adenylate cyclase and phosphorylation of a number of kinases including Erk1/2. This happens through canonical G-protein activation and through other protein interactions of which ß-Arrestin2 has been the most investigated (Beaulieu *et al.* 2005; Klewe *et al.* 2008; Lan *et al.* 2009; Masri *et al.* 2008). We examined to which extend D2R signalling pathways is affected by the interaction with DAT in HEK293 cells.

We used a bioluminescence resonance energy transfer (BRET) based ß-Arrestin2 recruitment assay (figure 2H) to establish the effect of DAT on ß-Arrestin2-dependent D2R signalling (Klewe *et al.* 2008). Co-expression of DAT reduces both the efficacy and potency of quinpirole induced ß-Arrestin2 recruitment to the D2R (figure 2A, B, C). Co-expression of DAT with D2R reduced the efficacy to 35 +/- 3% compared to D2R expressed alone (ANOVA, $p < 0.001$, Dunnett's post-hoc). Similarly the potency (Log EC50) was reduced approximately 3-fold from -7.6 +/- 0.1 to -7.0 +/- 0.2 (ANOVA, $p < 0.05$, Dunnett's post-hoc).

To test the specificity of the inhibitory effect of DAT on quinpirole induced ß-Arrestin2 recruitment to the D2R we also co-expressed another monoamine transporter, the serotonin transporter (SERT) as well as the non-homologous single transmembrane protein Tac, a subunit of the interleukin-2 receptor (Waldmann 1991) (figure 2A, B, C). Co-expression of SERT reduced the efficacy to 71 +/- 5% compared to the basal situation and co-expression of Tac to 78 +/- 4% (ANOVA, $p < 0.001$ respectively $p < 0.05$, Dunnett's post-hoc).

*cAMP inhibition*

To detect the effect of DAT on D2R $G_i$-protein mediated signalling, we measured the dose dependent effect of quinpirole on cAMP accumulation in transiently transfected HEK293 cells treated with 1 μM forskolin (figure 2D). Quinpirole did not have any effect on cells not transfected with D2R (data not shown). By co-expressing DAT, SERT and Tac with D2R in HEK293 cells we found that DAT and SERT both resulted in a lower maximal D2R mediated inhibition of cAMP (figure 2E). Co-expression of DAT resulted in a 93 +/-3% maximal inhibition of cAMP production compared to what we observed in cells expressing solely D2R (ANOVA, $p < 0.05$, Dunnett's post-hoc) (figure 2E). SERT co-expression also resulted in a 93 +/- 2% maximal inhibition of cAMP

production (ANOVA, $p < 0.05$, Dunnett's post-hoc) whereas co-expression of Tac did not affect the capacity of D2R to inhibit cAMP production (figure 2E). Co-expression of DAT also shifted the LogIC50 of quinpirole mediated inhibition of cAMP production. With DAT we found the LogIC50 to be -8.6 +/- 0.1 compared to a control value of -9.1 +/- 0.1 (figure 2F). Neither SERT nor Tac significantly affected the IC50 value of quinpirole in the assay (figure 2F). To control for possible effects of variations in the D2 receptor levels imposed by co-expression of another membrane protein we varied the amount of D2R cDNA used for the transfection of HEK293 cells over a 10-fold range and measured the maximal inhibition (cAMP baseline set equal to 1) and LogIC50 for quinpirole. We found that the efficacy values and LogIC50 values obtained from the assay correlated (linear regression, $r^2 \sim 0.58$) (figure 2H). Furthermore we found that the efficacy and LogIC50 values obtained from the assay when co-expressing DAT, SERT and Tac all fell within the 95% prediction band of the correlation (figure 2H), suggesting that the observed effects of DAT and SERT in the assay can be explained by variations in D2R levels.

*Trafficking*

Next we investigated if changes in D2R trafficking might underlie the reduced surface expression, and whether DAT/D2R existed in a stable complex resulting in parallel trafficking patterns. D2R agonists have been reported to induce D2R endocytosis (Ito *et al.* 1999; Iwata *et al.* 1999) and DAT substrates have also in some cases been reported to induce DAT endocytosis (Chi and Reith 2003; Kahlig *et al.* 2004). HEK293 cells expressing DAT and D2R alone as well as cells co-expressing DAT and D2R were incubated with the D2R agonist quinpirole, the D2R antagonist haloperidol, the DAT substrate amphetamine or the endogenous D2R agonist and DAT substrate dopamine. The cells were incubated for 60 minutes with each of the compounds. When expressing D2R alone no significant changes in D2R surface expression was seen for any of the compounds (figure 3A),

however a tendency to a reduced surface expression was seen when incubating with the D2R agonists dopamine and quinpirole. When co-expressing DAT with the D2R a significant reduction in the surface expression of D2R was seen when incubating with the agonists dopamine and quinpirole but no effect was seen with either D2R antagonist haloperidol or DAT substrate amphetamine (Figure 3B). As both dopamine and quinpirole caused a reduction of D2R surface expression the effect is most likely caused by agonist effect on D2R and most likely the increase in effect is caused by the lower expression of D2R when co-expressing DAT. No effect of the compounds was observed on DAT surface expression neither when DAT was expressed alone (figure 3C) or co-expressed with D2R (figure 3D), indicating that neither DAT activity nor ligand activation of D2R affects DAT surface expression in transiently transfected HEK293. The lack of quinpirole and haloperidol effect on DAT was also observed in a native cellular system as we did not see any change in the DAT-mediated dopamine uptake upon D2R agonist or antagonist stimulation in dopaminergic primary cultures (figure S2).

*BRET*

As it was surprising to observe that the functional consequences of DAT expression on ß–Arrestin2 recruitment to the D2R (Figure 2A) and the reduced surface expression of D2R (figure 1B-C) was - even though more pronounced - not unique to DAT co-expression with D2R we decided to investigate the interaction between the GPCRs, D2R and $ß_2$AR, and the monoamine transporters DAT and SERT. For this purpose we conducted what is referred to as type I and type II BRET interaction experiments (James *et al.* 2006). In the type I BRET experiments the BRET donors $D2_S$-Rluc8 and $ß_2$AR-Rluc8 are expressed at a constant level while varying the BRET acceptor mVenus-DAT expression (figure 4A). For the BRET pair $D2_S$-Rluc8 and mVenus-DAT we observed a saturation of the BRET signals at increasing amounts of acceptor as is expected from a specific

interaction (figure 4A). The BRET signal exhibited a parallel saturation for the BRET pair $\beta_2$AR-Rluc8 and mVenus-DAT indicating that the $\beta_2$AR has an affinity for DAT similar to that of D2R. To test whether the interaction depended specifically on DAT we tested the effect of having mVenus-SERT as the BRET acceptor and $D2_S$-Rluc8 and ß$_2$AR-Rluc8 the BRET donors in the type I BRET assay. Again we observed a saturating BRET signal both with $D2_S$-Rluc8 and ß$_2$A-Rluc8 as the donor when increasing the amount of mVenus-SERT (figure 4B). The saturating BRET signal was not only observed between transporters and receptors as the BRET pair $D2_S$-Rluc8 and Tac-Glur2-mVenus yielded a similar saturation curve albeit with a lower maximal BRET signal (figure 4C). BRET pairs with $\beta_2$AR-Rluc8 resulted in a relative higher BRET signal at saturation and BRET pairs with SERT resulted in a relative lower BRET signal at saturation. Finally the BRET signal was the lowest for $D2_S$-Rluc8 and Tac-Glur2-mVenus (figure 4I).

We conducted type II BRET experiments with the described BRET pairs to further substantiate that the interaction between the receptors and the transporters was specific and not a result of random collisions in the membrane. Keeping the vector donor/acceptor ratio constant (1:0.5 ratio of vector DNA) and increasing the total transfected cDNA of the BRET pairs we observed an increase in BRET signal for all the tested donor acceptor pairs that appeared to reach a plateau (figure 4D, E, F). A priori we would have expected a constant BRET signal in an experiment with a constant donor/acceptor ratio if the BRET signal represented a specific interaction and was not the result of random collisions. However, when measuring the relative expression level of the BRET donors by their luminescence signal, we observed that the expression did not linearly depend on the amount of cDNA transfected into the cells. Rather a fast saturation of the donor signal was seen when co-expressing with any of the acceptors (figure 4G). In contrast, the BRET acceptors displayed a clear linear correlation between the amount of transfected cDNA and the expression as measured by

mVenus fluorescence (figure 4H, data from type I experiment). Thus, although keeping the donor/acceptor vector DNA ratio constant, the actual ratio between the expressed BRET donor and BRET acceptor varied between each data point.

Finally, we tested the effects of the ligands and substrates on the receptor / transporter interaction. In a type I BRET interaction experiment with mVenus-DAT and $D2_S$-Rluc8 we tested the effect of the DAT substrate, tyramine, the D2R agonists quinpirole and dopamine (applied for 5 minutes). No significant effect of either of the drugs was seen, however a tendency towards a lower BRET efficacy was observed for the D2R ligands quinpirole and dopamine (figure 5A). Because the signal did not decrease further over time (data not shown) this likely reflects a re-orientation of the receptor and not a receptor/transporter complex dissociation. A similar observations was made with Tac-Glur2-mVenus as the BRET acceptor and $D2_S$-Rluc8 as the BRET donor (figure 5C) and in a parallel experiment using the BRET pair mVenus-DAT and $\beta_2$AR-Rluc8 a tendency for the agonist, isopreteronol to decrease the maximal BRET signal (figure 5B). Seen together this indicates that the tendency towards a lower BRET signal depended on a ligand-activation of the GPCR.

**Discussion**

Initially we made the surprising observation that DAT profoundly affected D2R surface expression. Co-expression of DAT with D2R reduced the surface expression of D2R five-fold without the opposite being true, i.e. we did not observe D2R to affect the surface levels of DAT even though the same expression vector and equal amounts of cDNA was used for both proteins (figure 1B). This curious unidirectional suppressive effect of surface expression led us to test the effect of DAT on the surface expression of the homologous GPCR, $ß_2$AR. From these experiments we observed a similar if not as pronounced reduction in the $ß_2$AR surface expression upon DAT co-expression (figure 1C). We did not observe any increase in the intracellular accumulation of D2R in the presence of DAT when analysing the co-expression of DAT and D2R by confocal microscopy (figure S1) suggesting that the phenotype is not the result of ER retention. We cannot rule out an increased lysosomal or proteasomal degradation as a possible explanation, since this could occur without an increased intracellular accumulation.

Studying the effect of DAT of D2R signalling, we found that co-expression of DAT with D2R resulted in an approximately 3-fold reduction in both efficacy and potency in the agonist-induced (quinpirole) recruitment of ß-arrestin2 to D2R as measured by BRET between D2R and ß-arrestin2 (figure 2A-C). We also tested whether the homologous monoamine transporter, SERT, impaired the ß-arrestin2 recruitment to D2R. SERT co-expression did not have any effect on the potency but exhibited a slight reduction in the efficacy (figure 2A-C). This pattern was also observed with co-expression of the non-homologous single transmembrane protein Tac (figure 2A-C). Because the estimation of the pharmacological parameters of ß-Arrestin2 recruitment to D2R is based on BRET experiments there are a number of potential confounders to the imminent conclusion that DAT inhibits ß-Arrestin2 recruitment to the D2R receptor. First of all BRET is a very sensitive measure

of interaction and both orientation of the dipole moments of the donor and the acceptor as well as the distance between these will affect the maximal obtainable BRET signal. The distance is particular critical as the BRET signal will decrease proportionally with the sixth power of increasing radius (Vogel *et al.* 2006). It is very plausible that D2R interaction with different transmembrane proteins will affect the distance between D2R and ß-Arrestin2. However, in our experiments this is likely not the case because the construct used as the BRET donor, D2S-Rluc8, have been designed with long flexible linker connecting the receptor and Rluc8.

Secondly, the BRET signals are sensitive to changes in the donor/acceptor ratio. However, the response in the ß-Arrestin2 recruitment assay has been shown be stable over a range of BRET donor/acceptor ratios as the maximal BRET signal increases and saturates with an increasing ratio of the BRET acceptor to the BRET donor (Klewe *et al.* 2008). We therefore rule out the possibility that the observed reductions in efficacy and potency in recruiting ß-Arrestin2 to the D2R in the spresence of DAT, SERT and Tac were a consequence reduced levels of the BRET donor $D2_S$-Rluc8.

In summary, our results strongly suggest that DAT inhibits β-Arrestin2 recruitment to D2R and thereby β-Arrestin2 dependent signalling from D2R but due the nature of the BRET based assay this should be explored further before any firm conclusion is drawn.

For a more comprehensive picture of the effects of DAT on D2R signalling, we also investigated the G protein coupled signalling properties of D2R when co-expressing DAT. Studying the D2-mediated inhibition of cellular cAMP accumulation we found that D2R in the presence of DAT, SERT and Tac appeared to have effects on cAMP accumulation reminiscent of our observations with the ß-arrestin assay; e.g activation of D2R with quinpirole resulted in a lower agonist efficay and potency in lowering cAMP accumulation in the presence of DAT and to a smaller degree in the

presence of SERT and Tac (figure 2E, F). Whereas we reasoned that a DAT mediated reduction in D2R surface expression did not negatively affect the BRET signal used to asses ß-Arrestin2 recruitment to the D2R receptor, we predicted that the relative level of D2R expression in the cAMP assay would affect both the efficacy and the IC50 value obtained from the assay. Indeed, we observed a correlation between the efficacy and potency for quinpirole in the assay with varying receptor levels (figure 2G). Because the efficacy and IC50 values obtained from the co-expression experiments with DAT, SERT and Tac did not deviate significantly from this correlation it is unlikely that DAT has any effect on D2/G protein-mediated inhibition of cAMP accumulation other than those stemming from the reduced surface expression of the receptor (figure 2D-G).

As Bolan *et al.* reported that D2R activation increased DAT surface expression (Bolan *et al.* 2007) and as it has been shown that D2R co-traffick as a heterooligomer with both D1R (So *et al.* 2005) and A2AR (Hillion *et al.* 2002) we hypothesized that if DAT/D2R constitutes a stable complex, D2R would in parallel with DAT show an increase the surface expression upon D2R activation. Neither activation of D2R alone, DAT alone nor concomitant activation with dopamine increased D2R surface expression (figure 3A, B). Contrary, we observed a similar reduction of D2R surface expression upon D2R activation alone as well as with simultaneous activation of DAT and D2R indicating that DAT activity does not positively regulate D2R surface expression. None of the compounds affected DAT surface expression (figure 3C, D). This either suggests a flexible complex that segregates upon internalization of the D2R or that D2R and DAT only traffics to and from the plasma membrane when it is not associated with the other.

In contrast to previous observations that D2R activation rapidly increased DAT in the plasma membrane (Bolan *et al.* 2007), we did not observe any changes DAT surface expression upon

agonist stimulation of the D2R in HEK293 cells (figure 2D). We cannot rule out that this discrepancy is due to differences in expression levels and time of agonist treatment. Bolan *et al.* observed that quinpirole treatment increasing DAT surface expression by 30% within 1 minute (Bolan *et al.* 2007). Conversely, we treated our cells with compounds for 1 hour which might abolish an initial effect on DAT insertion into the plasma membrane. In addition, we did not see any effect of quinpirole on DAT mediated dopamine uptake in cultured mesencephalic dopaminergic neurons (figure S2), a system that has previously been shown to be susceptible to D2R agonists (Congar *et al.* 2002; Sulzer *et al.* 1998). Taken together, our experiments support the result from Lee *et al*., where no change in DAT surface expression or DA uptake was seen upon prolonged (30-60 minutes) D2R activation (Lee *et al.* 2007).

Through BRET measurements we established that DAT and D2R interact (figure 4A). However we also observed a specific BRET signal from the following combinations of BRET pairs DAT/ß$_2$AR (figure 4A), SERT/D2R (figure 1B), SERT/ ß$_2$AR (figure 4B), TacGlur2/D2R (figure 4C). To further substantiate our findings and the specificity of the BRET signals we attempted to carry out type II BRET experiments with all the BRET pairs. In this type of experiment the ratio between BRET donor and acceptor is kept constant over a range of expression levels. However due to large perturbations in the ratio between donor:acceptor upon co-expression (figure 4G-H) we were not able to draw a firm conclusion from the type II BRET experiments (figure D-F). It should be noted that the type II experiments have previously been carried out successfully when studying homodimerization - a situation where the ratio between the BRET donor and acceptor is easily controllable (Angers *et al.* 2000; Salahpour and Masri 2007; Fung *et al.* 2009). Our findings suggest that conducting type II experiments for validating interactions between non-homologous interaction partners is a difficult task at best.

Given that all the BRET constructs were equipped with long amino acid regions between the transmembrane segment and the Rluc8 or mVenus (DAT + SERT > 90 a.a.), it is feasible to assume that the fusion exhibits no orientation or distance constraint on neither the donor nor the acceptor. We therefore suggest that the BRET efficacy in the present experiments is likely to represent a quantitative measure of the interaction (figure 4). Following this line of reasoning we propose that DAT has the highest degree of interaction with the GPCRs whereas for SERT the interaction is less and even lower for the non-homologous TacGluR2. A conclusion that mirrors the inhibitory effects of DAT, SERT and TacGlur2 on β-Arrestin2 recruitment to D2R

Further substantiating that the observed interactions are of a specific nature we observed a clear tendency towards a lower BRET signal with ligand-activation of the GPCR (figure 5A-C). This is presumably the result of an intramolecular re-orientation. Such a re-orientation would most likely not interfere with the BRET signal if it was a result of result of random collisions.

Our findings suggest that the previously proposed molecular determinants for the interaction between DAT and D2R might only be part of the interaction interface. Lee *et al*. found, using GST pulldown assays, that the N-terminal portion of DAT interacts with a discrete part the 3$^{rd}$ intracellular loop of D2R (Lee *et al.* 2007). This finding has been challenged by the observation that D2R is capable of increasing cellular DA uptake in cells expressing N-terminally truncated DAT as well as co-immunoprecipitation of this truncated version of DAT (Bolan *et al.* 2007). Although it cannot be excluded that N-terminal of DAT interacts with D2R and plays a functional regulatory role, our findings further suggest that the interaction is mediated by additional molecular components as SERT and DAT are not very homologous in their N-termini (figure S3). If this fact

is co-evaluated by the fact that D2R has a very short C-terminus and long 3rd intracellular loop and ß$_2$AR demonstrate the opposite pattern, the hypothesis immediately materialize that the interaction between the receptors and monoamine transporters is also mediated by interactions between transmembrane helices, where D2R and ß$_2$AR respectively DAT and SERT share a larger degree of homology (Beuming *et al.* 2006). The hypothesis is further substantiated by the surprising finding that D2R also appears to interact with Tac-Glur2.

In this respect, it is interesting to note that D2R has been shown to exist in higher order oligomers in the plasma membrane at physiological expression levels and to be dependent on at least two symmetrical interfaces in the transmembrane regions (transmembrane domains 1 and 4) (Guo *et al.* 2008). Furthermore D2R has been shown to form higher order oligomers with two other GPCRs, the adenosine A2a receptor and the metabotropic glutamate type 5 receptor (Cabello *et al.* 2009). Transporters in the SLC6A gene family including DAT and SERT have also been reported to form homo-oligomers (Hastrup *et al.* 2001; Schmid *et al.* 2001; Sorkina *et al.* 2003; Torres *et al.* 2003) and in the case of DAT the existence of tetrameric homomers with two symmetrical interfaces have been suggested (Hastrup *et al.* 2003). As the homo-oligomerization interfaces for both DAT and D2R have been reported to be in the transmembrane regions, this indicates that both DAT and D2R possess transmembrane parts that are prone to intermolecular interactions. Based on such inherent propensity to in-membrane interactions and the fact that ß$_2$AR (Angers *et al.* 2001; Salahpour *et al.* 2004) also homodimerize it is tempting to suggest that the observed interaction between DAT and D2R is based on intermolecular interactions in the transmembrane domains with no apparent specificity but a shared affinity between transmembrane regions since the interaction is reproduced between unlike partners with pseudo-Kd values that did not significantly differ between the different BRET pairs (Figure S4). This does not rule out that the interaction between D2R and DAT

could have biological consequences. Future studies will have to address this and to what degree the interaction quantitatively differs from other interactions between GPCRs and transporters. In this respect, it would be interesting to pursue experiments that could establish the actual Kd value between interacting pairs of transmembrane proteins expressed at physiological relevant levels in live cells. Such data would perhaps also enable us to decompose interactions into general and specific determinants.

***References***


Angers S., Salahpour A. and Bouvier M. (2001) Biochemical and biophysical demonstration of GPCR oligomerization in mammalian cells. *Life Sci.* **68,** 2243-2250.

Angers S., Salahpour A., Joly E., Hilairet S., Chelsky D., Dennis M. and Bouvier M. (2000) Detection of beta 2-adrenergic receptor dimerization in living cells using bioluminescence resonance energy transfer (BRET). *Proc. Natl. Acad. Sci. U. S. A* **97,** 3684-3689.

Beaulieu J. M., Sotnikova T. D., Marion S., Lefkowitz R. J., Gainetdinov R. R. and Caron M. G. (2005) An Akt/beta-arrestin 2/PP2A signaling complex mediates dopaminergic neurotransmission and behavior. *Cell* **122,** 261-273.

Beuming T., Shi L., Javitch J. A. and Weinstein H. (2006) A Comprehensive Structure-Based Alignment of Prokaryotic and Eukaryotic Neurotransmitter/Na+ Symporters (NSS) Aids in the Use of the LeuT Structure to Probe NSS Structure and Function. *Mol Pharmacol* **70,** 1630-1642.

Bolan E. A., Kivell B., Jaligam V. et al (2007) D2 receptors regulate dopamine transporter function via an extracellular signal-regulated kinases 1 and 2-dependent and phosphoinositide 3 kinase-independent mechanism. *Mol. Pharmacol.* **71,** 1222-1232.

Cabello N., Gandia J., Bertarelli D. C., Watanabe M., Lluis C., Franco R., Ferre S., Lujan R. and Ciruela F. (2009) Metabotropic glutamate type 5, dopamine D2 and adenosine A2a receptors form higher-order oligomers in living cells. *J Neurochem.* **109,** 1497-1507.

Canals M., Marcellino D., Fanelli F. et al (2003) Adenosine A2A-dopamine D2 receptor-receptor heteromerization: qualitative and quantitative assessment by fluorescence and bioluminescence energy transfer. *J Biol. Chem.* **278,** 46741-46749.

Cao T. T., Deacon H. W., Reczek D., Bretscher A. and von Zastrow M. (1999) A kinase-regulated PDZ-domain interaction controls endocytic sorting of the [beta]2-adrenergic receptor. *Nature* **401,** 286-290.

Chen N. H., Reith M. and Quick M. (2004) Synaptic uptake and beyond: the sodium- and chloride-dependent neurotransmitter transporter family SLC6. *Pflügers Archiv European Journal of Physiology* **447,** 519-531.

Chi L. and Reith M. E. A. (2003) Substrate-Induced Trafficking of the Dopamine Transporter in Heterologously Expressing Cells and in Rat Striatal Synaptosomal Preparations. *J Pharmacol Exp Ther* **307,** 729-736.

Congar P., Bergevin A. and Trudeau L. E. (2002) D2 Receptors Inhibit the Secretory Process Downstream From Calcium Influx in Dopaminergic Neurons: Implication of K+ Channels. *J Neurophysiol* **87,** 1046-1056.

Ferre S., Ciruela F., Woods A. S., Lluis C. and Franco R. (2007) Functional relevance of neurotransmitter receptor heteromers in the central nervous system. *Trends Neurosci.* **30,** 440-446.

Ferre S., von E. G., Johansson B., Fredholm B. B. and Fuxe K. (1991) Stimulation of high-affinity adenosine A2 receptors decreases the affinity of dopamine D2 receptors in rat striatal membranes. *Proc. Natl. Acad. Sci. U. S. A* **88,** 7238-7241.

Fung J. J., Deupi X., Pardo L., Yao X. J., Velez-Ruiz G. A., Devree B. T., Sunahara R. K. and Kobilka B. K. (2009) Ligand-regulated oligomerization of beta(2)-adrenoceptors in a model lipid bilayer. *EMBO J.* **28,** 3315-3328.

Fuxe K., Marcellino D., Guidolin D., Woods A. S. and Agnati L. F. (2008) Heterodimers and Receptor Mosaics of Different Types of G-Protein-Coupled Receptors. *Physiology* **23,** 322-332.

Geracitano R., Federici M., Bernardi G. and Mercuri N. B. (2006) On the effects of psychostimulants, antidepressants, and the antiparkinsonian drug levodopa on dopamine neurons. *Ann. N. Y. Acad. Sci.* **1074,** 320-329.

Gether U., Andersen P. H., Larsson O. M. and Schousboe A. (2006) Neurotransmitter transporters: molecular function of important drug targets. *Trends in Pharmacological Sciences* **27,** 375-383.

Gonzalez-Maeso J., Ang R. L., Yuen T. et al (2008) Identification of a serotonin/glutamate receptor complex implicated in psychosis. *Nature* **452,** 93-97.

Guo W., Urizar E., Kralikova M., Mobarec J. C., Shi L., Filizola M. and Javitch J. A. (2008) Dopamine D2 receptors form higher order oligomers at physiological expression levels. *EMBO J* **27,** 2293-2304.

Hastrup H., Karlin A. and Javitch J. A. (2001) Symmetrical dimer of the human dopamine transporter revealed by cross-linking Cys-306 at the extracellular end of the sixth transmembrane segment. *Proc. Natl Acad. Sci U. S. A* **98,** 10055-10060.

Hastrup H., Sen N. and Javitch J. A. (2003) The human dopamine transporter forms a tetramer in the plasma membrane: cross-linking of a cysteine in the fourth transmembrane segment is sensitive to cocaine analogs. *J Biol. Chem.* **278,** 45045-45048.

Hillion J., Canals M., Torvinen M. et al (2002) Coaggregation, cointernalization, and codesensitization of adenosine A2A receptors and dopamine D2 receptors. *J Biol. Chem.* **277,** 18091-18097.

Ito K., Haga T., Lameh J. and Sadee W. (1999) Sequestration of dopamine D2 receptors depends on coexpression of G-protein-coupled receptor kinases 2 or 5. *Eur. J Biochem.* **260,** 112-119.

Iversen S. D. and Iversen L. L. (2007) Dopamine: 50 years in perspective. *Trends Neurosci.* **30,** 188-193.

Iwata K., Ito K., Fukuzaki A., Inaki K. and Haga T. (1999) Dynamin and rab5 regulate GRK2-dependent internalization of dopamine D2 receptors. *Eur. J Biochem.* **263,** 596-602.

James J. R., Oliveira M. I., Carmo A. M., Iaboni A. and Davis S. J. (2006) A rigorous experimental framework for detecting protein oligomerization using bioluminescence resonance energy transfer. *Nat. Methods* **3,** 1001-1006.

Kahlig K. M., Javitch J. A. and Galli A. (2004) Amphetamine regulation of dopamine transport. Combined measurements of transporter currents and transporter imaging support the endocytosis of an active carrier. *J Biol. Chem.* **279,** 8966-8975.

Klewe I. V., Nielsen S. r. M., Tarp° L., Urizar E., Dipace C., Javitch J. A., Gether U., Egebjerg J. and Christensen K. V. (2008) Recruitment of [beta]-arrestin2 to the dopamine D2 receptor: Insights into anti-psychotic and anti-parkinsonian drug receptor signaling. *Neuropharmacology* **54,** 1215-1222.

Kniazeff J., Shi L., Loland C. J., Javitch J. A., Weinstein H. and Gether U. (2008) An Intracellular Interaction Network Regulates Conformational Transitions in the Dopamine Transporter. *J. Biol. Chem.* **283,** 17691-17701.

Lan H., Liu Y., Bell M. I., Gurevich V. V. and Neve K. A. (2009) A dopamine D2 receptor mutant capable of G protein-mediated signaling but deficient in arrestin binding. *Mol. Pharmacol.* **75,** 113-123.

Lee F. J., Pei L. and Liu F. (2009) Disruption of the dopamine transporter-dopamine D2 receptor interaction in schizophrenia. *Synapse* **63,** 710-712.

Lee F. J., Pei L., Moszczynska A., Vukusic B., Fletcher P. J. and Liu F. (2007) Dopamine transporter cell surface localization facilitated by a direct interaction with the dopamine D2 receptor. *EMBO J.* **26,** 2127-2136.

Madsen K. L., Eriksen J., Milan-Lobo L. et al (2008) Membrane localization is critical for activation of the PICK1 BAR domain. *Traffic.* **9,** 1327-1343.

Masri B., Salahpour A., Didriksen M., Ghisi V., Beaulieu J. M., Gainetdinov R. R. and Caron M. G. (2008) Antagonism of dopamine D2 receptor/beta-arrestin 2 interaction is a common property of clinically effective antipsychotics. *Proc. Natl. Acad. Sci. U. S. A* **105,** 13656-13661.

Pfleger K. D., Seeber R. M. and Eidne K. A. (2006) Bioluminescence resonance energy transfer (BRET) for the real-time detection of protein-protein interactions. *Nat. Protoc.* **1,** 337-345.

Rashid A. J., So C. H., Kong M. M., Furtak T., El-Ghundi M., Cheng R., O'Dowd B. F. and George S. R. (2007) D1-D2 dopamine receptor heterooligomers with unique pharmacology are coupled to rapid activation of Gq/11 in the striatum. *Proc. Natl. Acad. Sci. U. S. A* **104,** 654-659.

Rasmussen T. N., Plenge P., Bay T., Egebjerg J. and Gether U. (2009) A single nucleotide polymorphism in the human serotonin transporter introduces a new site for N-linked glycosylation. *Neuropharmacology* **57,** 287-294.

Salahpour A., Angers S., Mercier J. F., Lagace M., Marullo S. and Bouvier M. (2004) Homodimerization of the beta2-adrenergic receptor as a prerequisite for cell surface targeting. *J Biol. Chem.* **279,** 33390-33397.

Salahpour A. and Masri B. (2007) Experimental challenge to a 'rigorous' BRET analysis of GPCR oligomerization. *Nat. Methods* **4,** 599-600.

Schmid J. A., Scholze P., Kudlacek O., Freissmuth M., Singer E. A. and Sitte H. H. (2001) Oligomerization of the human serotonin transporter and of the rat GABA transporter 1 visualized by fluorescence resonance energy transfer microscopy in living cells. *J Biol. Chem.* **276,** 3805-3810.

So C. H., Varghese G., Curley K. J., Kong M. M. C., Alijaniaram M., Ji X., Nguyen T., O'Dowd B. F. and George S. R. (2005) D1 and D2 Dopamine Receptors Form Heterooligomers and Cointernalize after Selective Activation of Either Receptor. *Mol Pharmacol* **68,** 568-578.

Sorkina T., Doolen S., Galperin E., Zahniser N. R. and Sorkin A. (2003) Oligomerization of Dopamine Transporters Visualized in Living Cells by Fluorescence Resonance Energy Transfer Microscopy. *J. Biol. Chem.* **278,** 28274-28283.

Sulzer D., Joyce M. P., Lin L., Geldwert D., Haber S. N., Hattori T. and Rayport S. (1998) Dopamine Neurons Make Glutamatergic Synapses In Vitro. *J. Neurosci.* **18,** 4588-4602.

Szidonya L., Cserzo M. and Hunyady L. (2008) Dimerization and oligomerization of G-protein-coupled receptors: debated structures with established and emerging functions. *J. Endocrinol.* **196,** 435-453.

Torres G. E. and Amara S. G. (2007) Glutamate and monoamine transporters: new visions of form and function. *Current Opinion in Neurobiology* **17,** 304-312.

Torres G. E., Carneiro A., Seamans K., Fiorentini C., Sweeney A., Yao W. D. and Caron M. G. (2003) Oligomerization and Trafficking of the Human Dopamine Transporter. MUTATIONAL ANALYSIS IDENTIFIES CRITICAL DOMAINS IMPORTANT FOR THE FUNCTIONAL EXPRESSION OF THE TRANSPORTER. *J. Biol. Chem.* **278,** 2731-2739.

Usiello A., Baik J. H., Rouge-Pont F., Picetti R., Dierich A., LeMeur M., Piazza P. V. and Borrelli E. (2000) Distinct functions of the two isoforms of dopamine D2 receptors. *Nature* **408,** 199-203.

Vogel S. S., Thaler C. and Koushik S. V. (2006) Fanciful FRET. *Sci. STKE.* **2006,** re2.

Waldmann T. A. (1991) The interleukin-2 receptor. *J. Biol. Chem.* **266,** 2681-2684.

**Figure legends**

*Figure 1:*

DAT suppresses the surface expression of both $D2_SR$ and $ß_2AR$. (**A**) In each batch of transfected cells, the FLAG-$D2_SR$ or FLAG-$ß_2AR$ surface expression was probed with M1 antibody and HA-DAT surface expression with HA.11 antibody. (**B**) HEK293 cells were transfected with equimolar amounts of FLAG-$D2_SR$/mock, HA-DAT/mock or FLAG-$D2_SR$/HA-DAT. Expression of $D2_SR$ (brown bars) together with DAT resulted in a 5-fold reduction in $D2_SR$ surface expression compared to $D2_SR$/mock (21% +/- 1.6, n=4, $p<0.0001$ one sample t-test) whereas no reduction was seen in DAT (orange bars) expression (105% +/- 8.5 of DAT/mock, n=4, p=0.56 one sample t-test). (**C**) As in **B** the surface expression of DAT (orange bars) and $ß_2AR$ (brown bars) was determined in cells transfected with equimolar amounts of FLAG-$ß_2AR$/mock, HA-DAT/mock or FLAG-$ß_2AR$/HA-DAT. Co-expression of DAT and $ß_2AR$ significantly reduced $ß_2AR$ to 63% +/- 7.0 of $ß_2AR$ /mock (n=3, p=0.033 one sample t-test) whereas no change in DAT surface expression was seen (107% +/- 10 of $ß_2AR$ /mock, n=3, t=0.56 one sample t-test).

*Figure 2:*

(**A**) Quinpirole (D2R agonist) dose-response curves of β-Arrestin2 recruitment to D2R in HEK293 cells transiently transfected with the BRET donor $D2_S$-Rluc8 and the BRET acceptor β-Arrestin2(R393E, R395E)-mVenus in combination with either DAT, SERT, Tac or empty vector. The cells were incubated with the indicated concentration of quinpirole and BRET was measured after 10-15 minutes. The BRET signal was normalized to the vehicle condition and expressed as a percentage of the maximal response within the basal assay (donor and acceptor alone). (**B, C**) Quantification of the efficacy and potency of quinpirole in recruiting β-Arrestin2 to D2R in the

presence of DAT, SERT or Tac compared to basal condition were $D2_S$-Rluc8 and β-Arrestin2-mVenus were expressed alone. Mean efficacy and $LogEC_{50}$ +/- s.e.m calculated from three independent experiments (Efficacy: DAT and SERT, $p < 0.001$; Tac, $p < 0.05$. Potency: DAT, $p < 0.01$). (**D**) Quinpirole (D2R agonist) concentration-response curves of forskolin (1 μM) induced cAMP accumulation in HEK293 cells transiently transfected with $D2_S$ and GloSensor in combination with DAT, SERT, Tac or empty vector. The cells were incubated with the indicated concentration of quinpirole and total luminescence was measured after 15-20 minutes. The luminescence signal was normalized to the vehicle condition (forskolin alone) and expressed as a percentage of the maximal and minimal accumulation of the basal assay ($D2_S$ and GloSensor alone). (**E, F**) Quantification of the efficacy and potency of quinpirole in $D2_S$ mediated inhibition of cAMP accumulation in the presence of DAT, SERT or Tac compared to basal condition ($D2_S$ and GloSensor alone). Mean efficacy and $LogIC_{50}$ +/- s.e.m calculated from three independent experiments (Efficacy: DAT and SERT, $p < 0.05$. Potency: DAT, $p < 0.001$). (**G**) The amount of $D2_S$ vector used for transfection in the cAMP assay was varied over a 10-fold range and the maximal inhibition (efficacy) and potency of quinpirole were measured and correlated using linear regression ($r^2 \sim 0.58$, 95% prediction band of the correlation indicated with dashed lines). Data points from cAMP experiments with co-expression of DAT, SERT and Tac are shown but not included in the correlation. (**H**) Diagram describing the basal β-Arrestin2 recruitment setup. Cells expressing $D2_S$-Rluc8 in the plasma membrane recruit cytosolic β-Arrestin2-mVenus upon quinpirole stimulation, which results in an increase in the BRET signal.

*Figure 3:*

D2R agonists reduce D2R surface expression in the presence of DAT in HEK293 cells without affecting DAT surface expression. Surface expression of DAT and GPCRs was determined as

described in Fig. **1A.** HEK293 cells transfected with FLAG-$D2_SR$/mock (**A**), FLAG-$D2_SR$/HA-DAT (**B**, **D**) or HA-DAT/mock (**C**) were treated with either 10μM dopamine (DA), 10 μM amphetamine (Amph), 10 μM quinpirole (Quin) or 10 μM haloperidol (Halo) for 60 minutes and then surface expression of either D2R (**A**, **B**) or DAT (**C**, **D**) was determined. Surface expression was expressed as percentage of vehicle treatment (dashed line). (**A**) No effect of the compounds was seen in cells transfected with $D2_SR$ alone ($D2_SR$/mock: p=0.064), (**B**) whereas a reduction in surface expression was seen after treatment with the D2R agonists, DA and Quin, in cells expressing $D2_SR$/DAT (dopamine: $p < 0.001$ and quinpirole: $p < 0.05$). (**C**, **D**) No effect of the compounds was seen on DAT surface expression in the absence (**C**) (DAT/mock; p= 0.48) or presence of $D2_SR$ (**D**) (DAT/$D2_SR$: p= 0.93). Data represents four independent experiments.

*Figure 4:*

(**A**) Type 1 BRET experiments with the BRET donors $D2_S$-Rluc8 respectively $ß_2$AR -Rluc8 and the BRET acceptor mVenus-DAT. HEK293 cells were transiently co-transfected with the indicated constructs. The amount of BRET donor vector used for the transfections was held constant as was the total amount of DNA while the amount of BRET acceptor vector (DAT-mVenus) was increased (indicated on the ordinal axis as vector DNA ratio). The BRET signal was normalized to the condition were $D2_S$-Rluc8 was expressed alone and calculated as a percentage of the maximal BRET signal between $D2_S$-Rluc8 and mVenus-DAT (mean +/- s.e.m., n = 3, one site binding curve fit). (**B**) As in (A) but using mVenus-SERT as the BRET acceptor. (**C**) As in (A) but using $D2_S$-Rluc8 as BRET donor and Tac-Glur2-mVenus as the BRET acceptor. (**D**) Type 2 BRET experiments with the BRET donors $D2_S$-Rluc8 respectively $ß_2$AR-Rluc8 and the BRET acceptor mVenus-DAT. The BRET donor vector and the BRET acceptor vector used for the transfection was held constant at a ratio of 1 to 0.5 while the combined amount of donor and acceptor DNA was

increased. The total amount of DNA was held constant (mean +/- s.e.m., n = 3, exponential one phase association curve fit). (**E**) As in (D) but using mVenus-SERT as the BRET acceptor. (**F**) As in (D) but using $D2_S$-Rluc8 as BRET donor and Tac-Glur2-mVenus as the BRET acceptor. (**G**) The $D2_S$-Rluc8 expression in the type 2 BRET experiments (D, E, F) was assessed by quantifying the relative total luminescence in each experiment. Luminescence normalized to the transfected condition with the lowest activity. (**H**) The indicated BRET acceptor levels in the type 1 BRET experiments (A, B, C) were assessed by quantifying the relative total fluorescence in the linear range for each experiment. Fluorescence normalized to background. (**I**) Maximal BRET ratio quantified for the indicated BRET pairs. The maximal BRET ratio obtained for $D2_S$-Rluc8/Tac-Glur2-mVenus ($p < 0.01$) as well the BRET donors $D2_S$-Rluc8 ($p < 0.001$) and $ß_2$AR-Rluc8 ($p < 0.001$) expressed alone was significantly lower than the maximal BRET ratio obtained with the BRET pair $D2_S$-Rluc8/mVenus-DAT (ANOVA, Dunnetts post-hoc). Dashed line indicates the maximal BRET ratio level in β-Arrestin2 recruitment assay (agonist induced).

*Figure 5:*

The effect of substrates/agonists in type I BRET experiments. HEK293 cells were transfected with fixed BRET donors and increasing amounts of BRET acceptor as in fig. 4 A and C. (**A**) HEK293 cells transfected with mVenus-DAT and $D2_S$-Rluc8 were incubated for 5 minutes with vehicle (0.1 % DMSO), dopamine (5 µM), quinpirole (5 µM) or tyramine (5 µM) and no significant difference was observed between the 4 saturating curves (mean of $B_{max}$ values obtained from 3 independent experiments, ANOVA). (**B**) HEK293 cells transfected with mVenus-DAT and $ß_2$AR-Rluc8 were incubated for 5 minutes with vehicle (0.1 % DMSO), dopamine (5 µM), isoproterenol (5 µM) or tyramine (5 µM) and no significant difference was observed between the 4 saturating curves (mean of $B_{max}$ values obtained from 3 independent experiments, ANOVA). (**C**) HEK293 cells transfected

with Tac-Glur2-mVenus and $D2_S$-Rluc8 were incubated for 5 minutes with vehicle (0.1 % DMSO), dopamine (5 μM), quinpirole (5 μM) or tyramine (5 μM) and no significant difference was observed between the 4 saturating curves (mean of $B_{max}$ values obtained from 3 independent experiments, ANOVA).

Figure 1

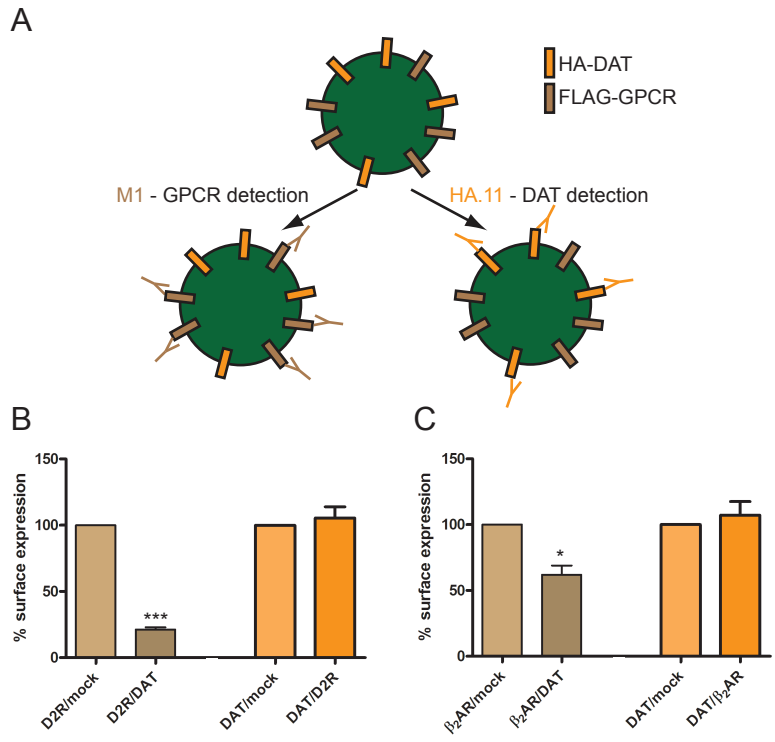
A
HA-DAT
FLAG-GPCR
M1 - GPCR detection
HA.11 - DAT detection
B
% surface expression
150
100
50
0
***
D2R/mock
D2R/DAT
DAT/mock
DAT/D2R
C
% surface expression
150
100
50
0
*
β2AR/mock
β2AR/DAT
DAT/mock
DAT/β2AR

Figure 2

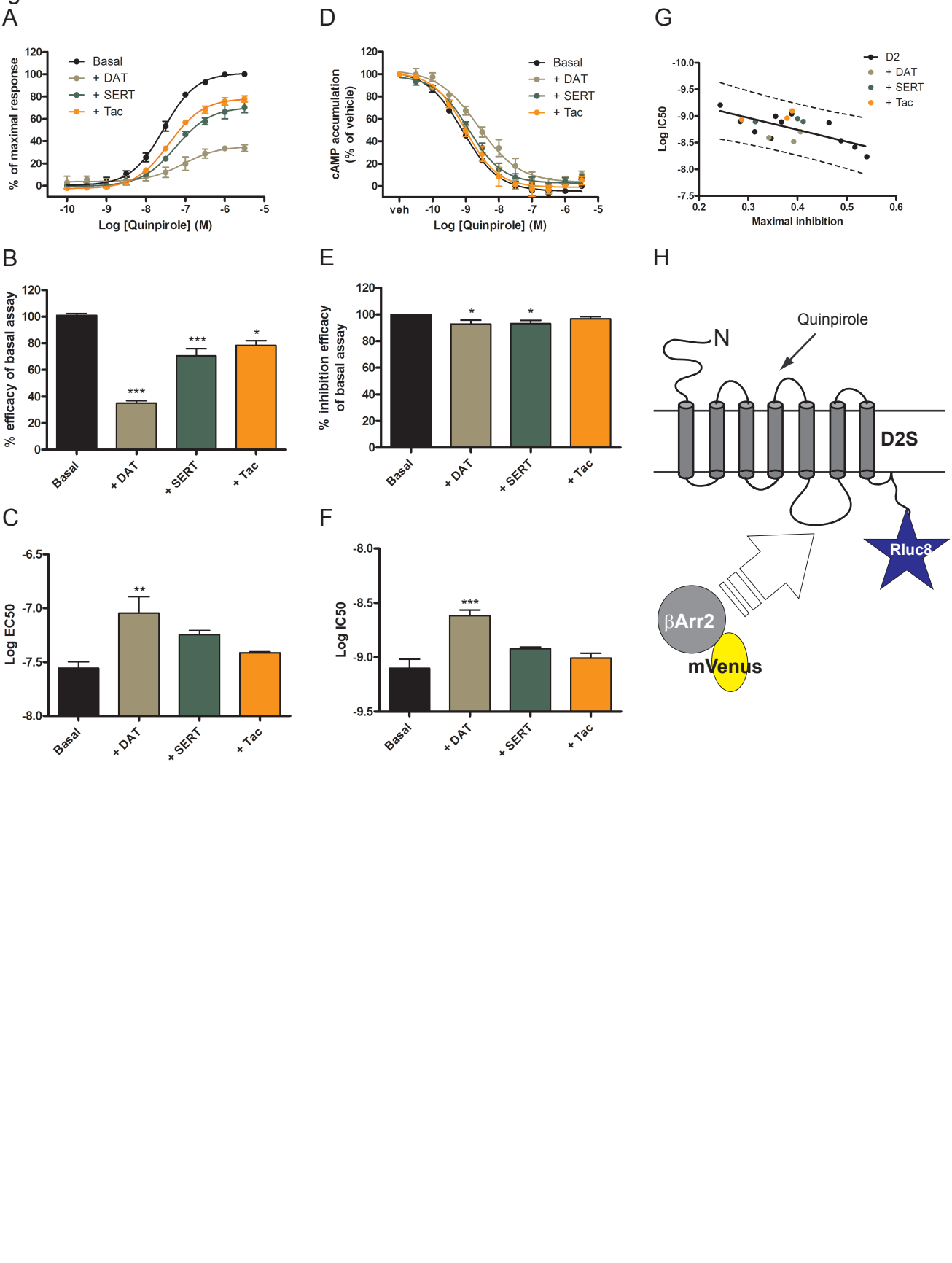
A
% of maximal response
Basal
+ DAT
+ SERT
+ Tac
Log [Quinpirole] (M)
D
cAMP accumulation (% of vehicle)
veh
Log [Quinpirole] (M)
G
Log IC50
D2
+ DAT
+ SERT
+ Tac
Maximal inhibition
B
% efficacy of basal assay
E
% inhibition efficacy of basal assay
H
Quinpirole
N
D2S
Rluc8
βArr2
mVenus
C
Log EC50
F
Log IC50

Figure 3

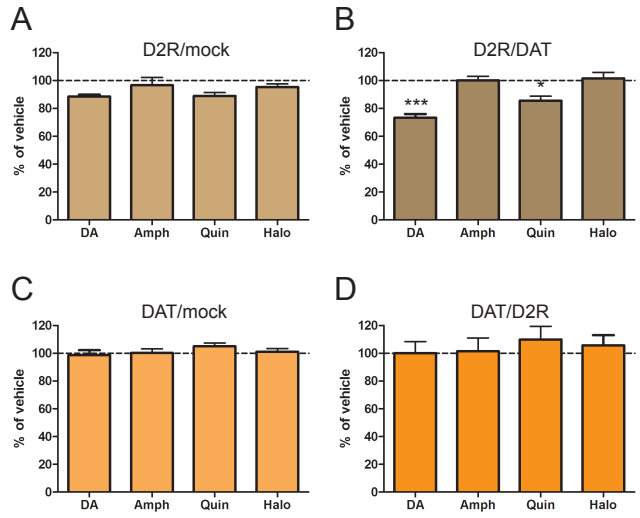
A
D2R/mock
% of vehicle
120
100
80
60
40
20
0
DA
Amph
Quin
Halo
B
D2R/DAT
% of vehicle
***
*
DA
Amph
Quin
Halo
C
DAT/mock
% of vehicle
DA
Amph
Quin
Halo
D
DAT/D2R
% of vehicle
DA
Amph
Quin
Halo

Figure 4

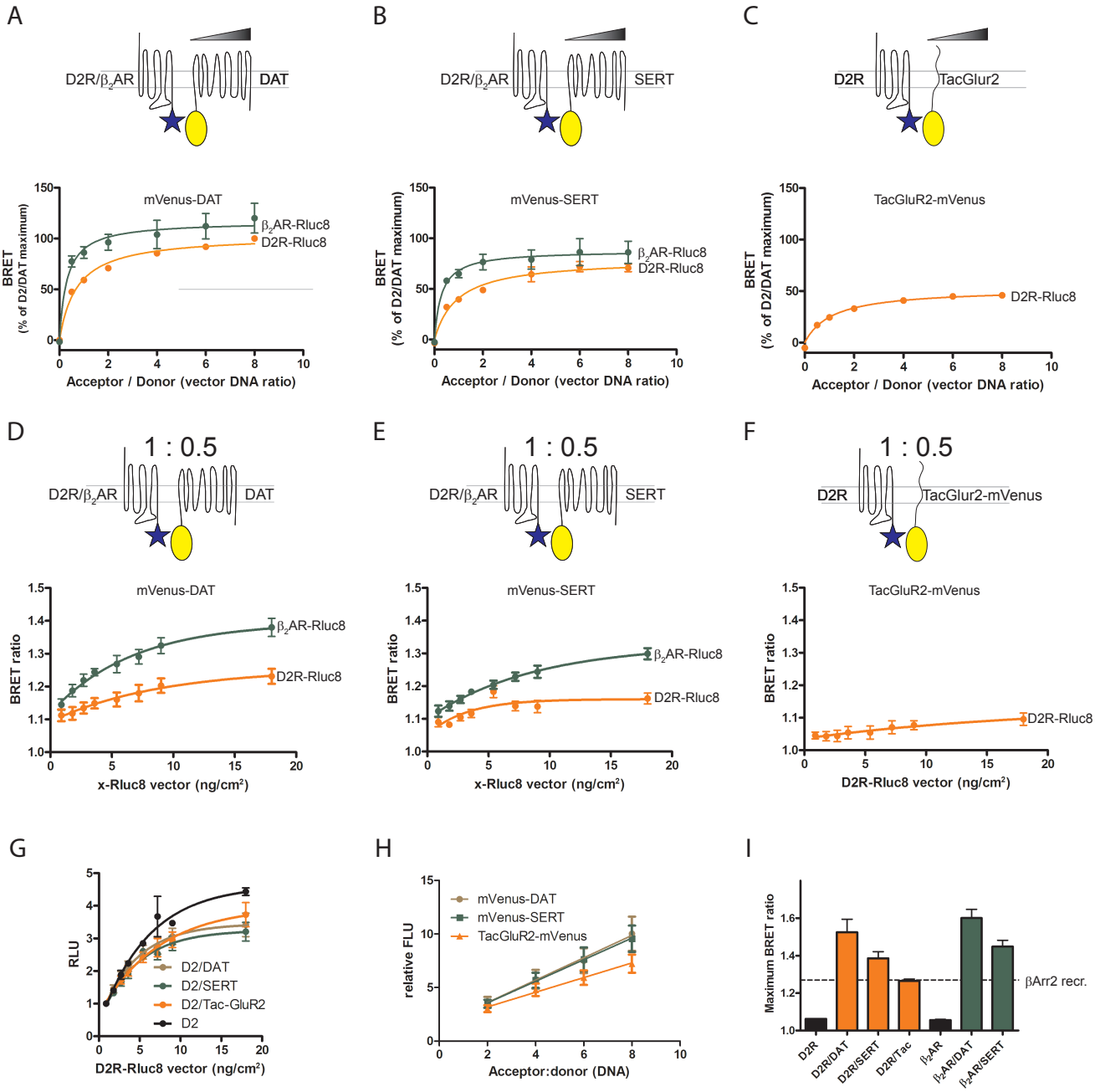
A
D2R/β2AR
DAT
mVenus-DAT
β2AR-Rluc8
D2R-Rluc8
BRET (% of D2/DAT maximum)
Acceptor / Donor (vector DNA ratio)
B
D2R/β2AR
SERT
mVenus-SERT
β2AR-Rluc8
D2R-Rluc8
BRET (% of D2/DAT maximum)
Acceptor / Donor (vector DNA ratio)
C
D2R
TacGlur2
TacGluR2-mVenus
D2R-Rluc8
BRET (% of D2/DAT maximum)
Acceptor / Donor (vector DNA ratio)
D
1 : 0.5
D2R/β2AR
DAT
mVenus-DAT
β2AR-Rluc8
D2R-Rluc8
BRET ratio
x-Rluc8 vector (ng/cm²)
E
1 : 0.5
D2R/β2AR
SERT
mVenus-SERT
β2AR-Rluc8
D2R-Rluc8
BRET ratio
x-Rluc8 vector (ng/cm²)
F
1 : 0.5
D2R
TacGlur2-mVenus
TacGluR2-mVenus
D2R-Rluc8
BRET ratio
D2R-Rluc8 vector (ng/cm²)
G
RLU
D2/DAT
D2/SERT
D2/Tac-GluR2
D2
D2R-Rluc8 vector (ng/cm²)
H
mVenus-DAT
mVenus-SERT
TacGluR2-mVenus
relative FLU
Acceptor:donor (DNA)
I
Maximum BRET ratio
βArr2 recr.
D2R
D2R/DAT
D2R/SERT
D2R/Tac
β2AR
β2AR/DAT
β2AR/SERT

Figure 5

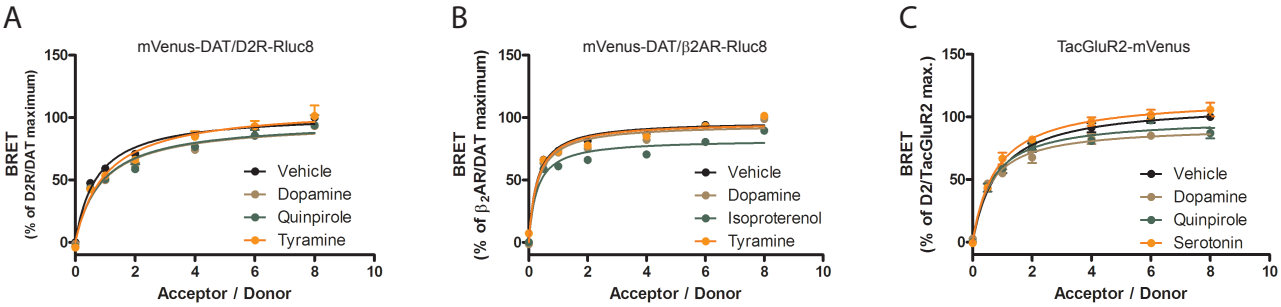
A
mVenus-DAT/D2R-Rluc8
BRET
(% of D2R/DAT maximum)
150
100
50
0
0
2
4
6
8
10
Acceptor / Donor
Vehicle
Dopamine
Quinpirole
Tyramine
B
mVenus-DAT/β2AR-Rluc8
BRET
(% of β2AR/DAT maximum)
Acceptor / Donor
Vehicle
Dopamine
Isoproterenol
Tyramine
C
TacGluR2-mVenus
BRET
(% of D2/TacGluR2 max.)
Acceptor / Donor
Vehicle
Dopamine
Quinpirole
Serotonin

**Supplementary data**

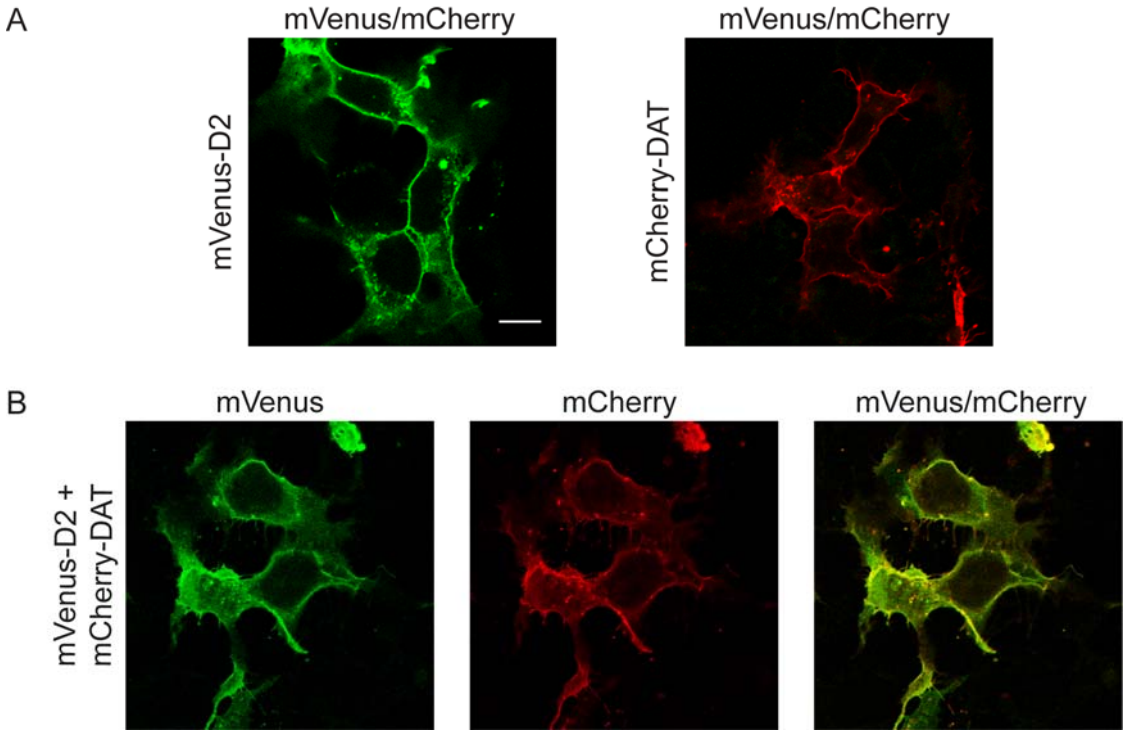


**Figure S1:** Coexpression of mVenus-D2 and mCherryDAT did not affect either DAT or D2 localization. (A) Confocal images of HEK293 cells transfected with mVenus-D2 (left) or mCherry-DAT (right). Both D2 and DAT were expressed primarily at the plasma membrane. (B) HEK293 cell expressing both mVenus-D2 and mCherry-DAT showed no indication of a changed cellular distribution of either DAT or D2 as both were primarily localized to the plasma membrane. Scale bar 10 µm.

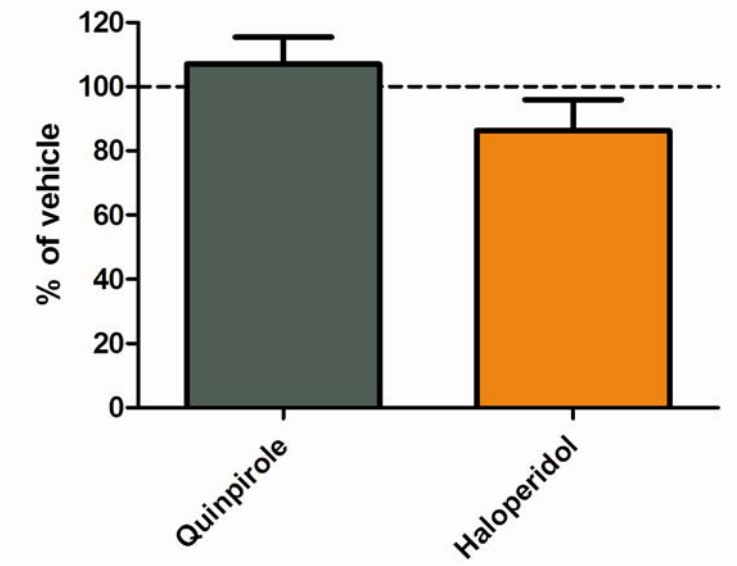


**Figure S2:** No effect of quinpirole and haloperidol on DAT-mediated dopamine uptake. Cultured neurons (13-15 DIV) were incubated for 2 hours in HBS buffer and then 10 uM quinpirole, 10uM haloperidol or 0.1% DMSO (vehicle) was added for 30 minutes. No significant difference was observed between the three conditions (One way ANOVA, paired measurements, n=4, p= 0.1428). Cultures of dopaminergic neurons were prepared and uptake carried out as previously described as previously described (Eriksen *et al.* 2009).

**Intracellular N-terminus**

```
hDAT  .......... .........m skskcsvglm ssvvapakep navgpkevel ilvkeqngvq ltsstltnpr qspveaqdre twgkkidfll svig..
hSERT mettplnsqk qlsacedged cqengvlqkv vptpgdkves gqisngysav pspgagddtr hsipatttl vaelhqgere twgkkvdfll svig..
```

**Intracellular C-terminus**

```
hDAT  .yaaykfcsl pgsfreklay aiapekdrel vdrgevrqftl rhwlkv
hSERT .yiayrliit pgtfkeriik sitpetptei pc.gdirlnav
```

**Figure S3:** Primary sequence alignment of hDAT and hSERT intracellular N and C-termini. Green represents identical amino acid residues, orange similar residues, and solid yellow indicates start and end of transmembrane domain 1 and 12, respectively, as modelled from the LeuT structure (Beuming *et al.* 2006; Yamashita *et al.* 2005). Figure is modified from Torres et al., 2003 and Beuming et al. 2006.

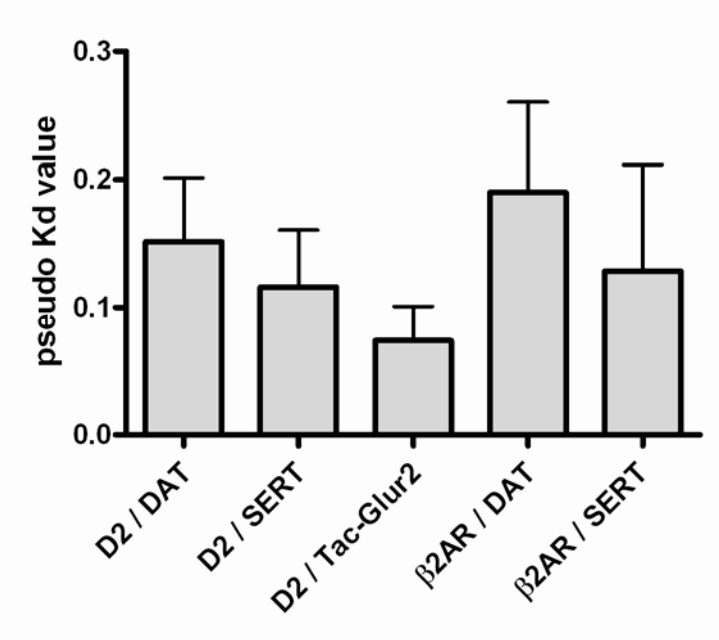


**Figure S4:** No difference between pseudo-Kd values (mean +/- s.e.m from three independent experiments, arbitrary units). Values obtained by modelling the each type I BRET experiments as a ligand binding curve with the BRET signal as "specific binding" and the relative acceptor/donor level (measured as the ratio luminescence/fluorescence) as the "ligand concentration".

Supplementary references

Beuming T., Shi L., Javitch J. A. and Weinstein H. (2006) A Comprehensive Structure-Based Alignment of Prokaryotic and Eukaryotic Neurotransmitter/Na+ Symporters (NSS) Aids in the Use of the LeuT Structure to Probe NSS Structure and Function. *Mol Pharmacol* **70,** 1630-1642.

Eriksen J., Rasmussen S. G. F., Rasmussen T. N., Vaegter C. B., Cha J. H., Zou M. F., Newman A. H. and Gether U. (2009) Visualization of Dopamine Transporter Trafficking in Live Neurons by Use of Fluorescent Cocaine Analogs. *J. Neurosci.* **29,** 6794-6808.

Yamashita A., Singh S. K., Kawate T., Jin Y. and Gouaux E. (2005) Crystal structure of a bacterial homologue of Na+/Cl--dependent neurotransmitter transporters. *Nature* **437,** 215-223.